ΕΛΛΗΝΙΚΗ ΔΗΜΟΚΡΑΤΙΑ
Εθνικόν και Καποδιστριακόν Πανεπιστήμιον Αθηνών
ΙΔΡΥΘΕΝ ΤΟ 1837
Τμήμα Γεωλογίας και Γεωπεριβάλλοντος

Πρόγραμμα Μεταπτυχιακών Σπουδών
Επιστήμες Γης και Περιβάλλον

ΜΟΥΤΖΟΥΡΗΣ ΔΗΜΗΤΡΙΟΣ

22015

Η προέλευση της αμφιβόλου στα υπερμαφικά πετρώματα και ένα νέο θερμόμετρο ανταλλαγής Fe και Mg μεταξύ αμφιβόλου και κλινοπυροξένου για περιδοτιτικές λιθολογίες του μανδύα

Ειδίκευση: Ορυκτοί πόροι – Πετρολογία και Διαχείριση Περιβάλλοντος

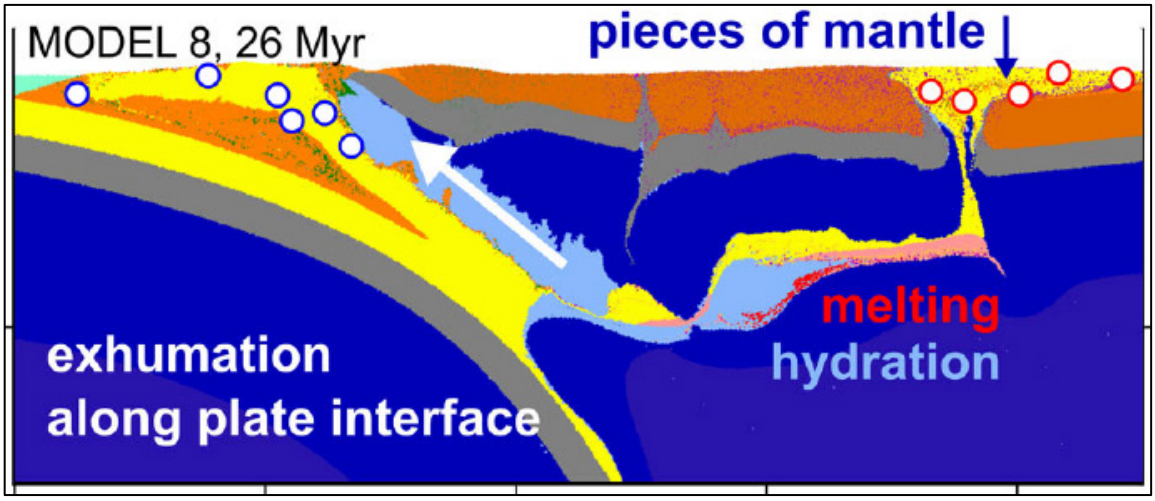

Τριμελής εξεταστική επιτροπή

Αναπλ. Καθηγητής Δημήτριος Κωστόπουλος (Επιβλέπων)

Αναπλ. Καθηγητής Παναγιώτης Πομώνης

Καθηγητής Ευάγγελος Μουλάς

Αθήνα 2023

ΕΛΛΗΝΙΚΗ ΔΗΜΟΚΡΑΤΙΑ
Εθνικόν και Καποδιστριακόν Πανεπιστήμιον Αθηνών
ΙΔΡΥΘΕΝ ΤΟ 1837
Τμήμα Γεωλογίας και Γεωπεριβάλλοντος

Πρόγραμμα Μεταπτυχιακών Σπουδών
Επιστήμες Γης και Περιβάλλον

MOUTZOURIS DIMITRIOS

22015

The origin of amphibole in ultramafic rocks and a new amphibole-clinopyroxene Fe-Mg exchange thermometer for mantle peridotite lithologies

Specialisation: Mineral resources – Petrology and environmental management

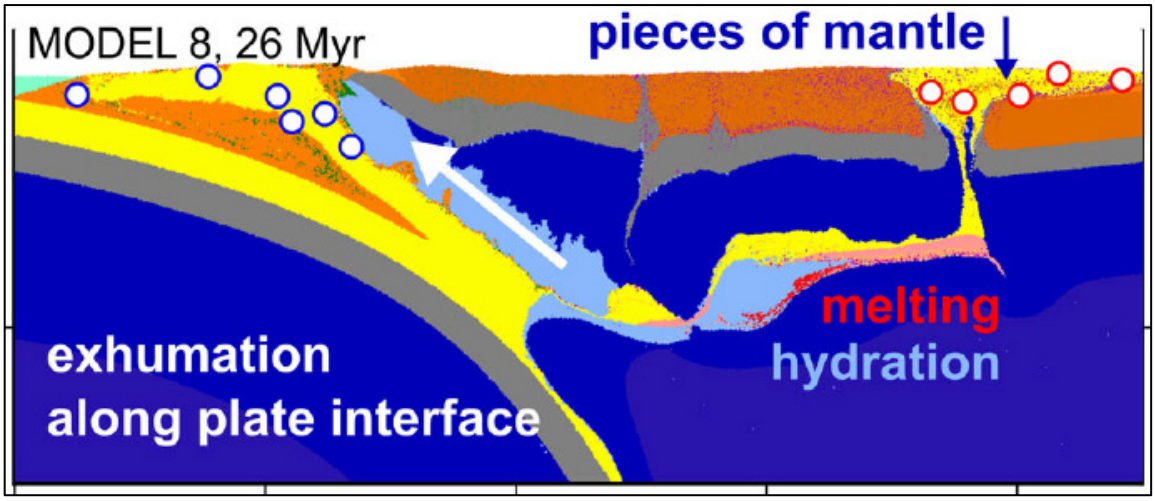

Three-member Committee of Examination

Assoc. Prof. Dimitrios Kostopoulos (Supervisor)

Assoc. Prof. Panagiotis Pomonis

Prof. Evangelos Moulas

Athens 2023

ΔΗΛΩΣΗ ΠΕΡΙ ΜΗ ΠΡΟΣΒΟΛΗΣ ΠΝΕΥΜΑΤΙΚΗΣ ΙΔΙΟΚΤΗΣΙΑΣ

Προσβολή πνευματικής ιδιοκτησίας θεωρείται η ολική ή η μερική αναπαραγωγή του έργου άλλου προσώπου ή η παρουσίαση του έργου κάποιου άλλου ως προσωπικού του γράφοντος. Το Τμήμα Γεωλογίας και Γεωπεριβάλλοντος λαμβάνει πολύ σοβαρά υπόψη και καταδικάζει την προσφυγή σε τέτοιου είδους πρακτικές από τους Μεταπτυχιακούς Φοιτητές. Σε περιπτώσεις πρόδηλης ή εκ προθέσεως προσβολής πνευματικής ιδιοκτησίας, τα αρμόδια όργανα του Τμήματος δύνανται να επιβάλουν ως κύρωση έως και την οριστική διαγραφή από το ΠΜΣ. Κατά την εκπόνηση, υποβολή, εξέταση και δημοσίευση της Διπλωματικής Εργασίας Ειδίκευσης οι Μεταπτυχιακοί Φοιτητές οφείλουν να τηρούν τις ακόλουθες κατευθυντήριες οδηγίες:

1. Η Διπλωματική Εργασία Ειδίκευσης πρέπει να αποτελεί έργο του υποβάλλοντος αυτήν φοιτητή.
2. Η αντιγραφή ή η παράφραση έργου τρίτου προσώπου αποτελεί προσβολή πνευματικής ιδιοκτησίας και συνιστά σοβαρό αδίκημα. Στο αδίκημα αυτό περιλαμβάνεται τόσο η προσβολή πνευματικής ιδιοκτησίας άλλου φοιτητή όσο και η αντιγραφή από δημοσιευμένες πηγές, όπως βιβλία, εισηγήσεις ή επιστημονικά άρθρα. Το υλικό που συνιστά αντικείμενο λογοκλοπής μπορεί να προέρχεται από οποιαδήποτε πηγή. Η αντιγραφή ή χρήση υλικού προερχόμενου από το διαδίκτυο ή από ηλεκτρονική εγκυκλοπαίδεια είναι εξίσου σοβαρή με τη χρήση υλικού προερχόμενου από τυπωμένη πηγή ή βάση δεδομένων.
3. Η χρήση αποσπασμάτων από το έργο τρίτων είναι αποδεκτή εφόσον, αναφέρεται η πηγή του σχετικού αποσπάσματος. Σε περίπτωση αυτολεξεί μεταφοράς αποσπάσματος από το έργο άλλου, η χρήση εισαγωγικών ή σχετικής υποσημείωσης είναι απαραίτητη, ούτως ώστε η πηγή του αποσπάσματος να αναγνωρίζεται.
4. Η παράφραση κειμένου, αποτελεί προσβολή πνευματικής ιδιοκτησίας.
5. Οι πηγές των αποσπασμάτων που χρησιμοποιούνται θα πρέπει να καταγράφονται πλήρως σε πίνακα βιβλιογραφίας στο τέλος της εργασίας.
6. Η προσβολή πνευματικής ιδιοκτησίας επισύρει την επιβολή κυρώσεων. Κατά την απόφαση επί των ενδεδειγμένων κυρώσεων, τα αρμόδια όργανα του Τμήματος θα λαμβάνουν υπόψη παράγοντες όπως το εύρος και το μέγεθος του τμήματος της εργασίας που οφείλεται σε προσβολή πνευματικής ιδιοκτησίας. Οι κυρώσεις θα επιβάλλονται σύμφωνα με το Άρθρο 7 Παράγραφος 7 του Κανονισμού Σπουδών.

Βεβαιώνω ότι η Διπλωματική Εργασία Ειδίκευσης, την οποία υποβάλλω, δεν περιλαμβάνει στοιχεία προσβολής πνευματικής ιδιοκτησίας, όπως αυτά προσδιορίζονται από την παραπάνω δήλωση, τους όρους της οποίας διάβασα και αποδέχομαι.

Παρέχω τη συναίνεσή μου, ώστε ένα ηλεκτρονικό αντίγραφο της διπλωματικής εργασίας μου να υποβληθεί σε ηλεκτρονικό έλεγχο για τον εντοπισμό τυχόν στοιχείων προσβολής πνευματικής ιδιοκτησίας.

Ημερομηνία

25/01/2023

Υπογραφή Υποψηφίου

Acknowledgements

First of all, I would like to thank my supervisor, Prof. Dimitrios Kostopoulos. This work could not have been completed without his enormously precious guidance, advice and support throughout this journey. His never-ending interest on my development as a student but also as a human being, his vision and persistence are only a few characteristics that have inspired me to go further.

I would also like to thank Prof. Evangelos Moulas. Mr. Moulas has drastically influenced the way I view metamorphic rocks. Our conversations have inspired me to further explore the physical laws that govern our planet through a different scope. I am much obliged to Prof. Panagiotis Pomonis for his support and suggestions during the last years.

Cheers to my fellow colleagues Vasilis, Paris, Ioannis, Christina, Vivian, Avgerinos in the university of Athens but also Luca from the university of Ferrara for their insights and discussions.

I am extremely grateful to my friends Aggelos, Telis, Nikos, Elena, Eirini, Konstantina and Giannis that have been with me during both joyful and darker times. I would also like to express my gratitude towards Madalina for her love and the emotional support. The biggest thanks go to my family that has supported me without expecting anything in return and have shaped my morality and my character.

«Εμπρός λοιπόν. Από ‘σένα η άνοιξη εξαρτάται.
Τάχυνε την αστραπή.
Πιάσε το ΠΡΕΠΕΙ από το ιώτα και γδάρε το ίσαμε το πι.»
-Οδυσσέας Ελύτης, 1985, Ο μικρός ναυτίλος

Περίληψη

Η αμφίβολος είναι μια δευτερογενής φάση που συχνά υφίσταται σε υπερμαφικές λιθολογίες (ξενολιθικοί περιδοτίτες του μανδύα, Αλπινότυποι και οφιολιθικοί περιδοτίτες) σε διάφορα περιβάλλοντα όπως μαγματικά τόξα, εσωτερικά πλακών, ρήγματα μετασχηματισμού, ζώνες διάρρηξης και σύγκρουσής. Η δημιουργία της έχει αποδοθεί είτε στην αλληλεπίδραση ρευστών/τηγμάτων με πετρώματα του μανδύα είτε στην απευθείας κρυστάλλωση από ένυδρα τήγματα. Για τον σκοπό της παρούσας εργασίας, συντέθηκε μια εκτενής βιβλιογραφική βάση δεδομένων η οποία περιλαμβάνει τις συστάσεις, σε κύρια στοιχεία, αμφιβόλων που βρίσκονται σε υπερμαφικά πετρώματα σε διαφορετικά γεωτεκτονικά περιβάλλοντα ανά τον κόσμο. Επίσης συμπεριλήφθηκαν γεωχημικά δεδομένα αμφιβόλων από ένα ευρύ φάσμα ηφαιστειακών πετρωμάτων (μαφικά έως φελσικά) τόσο σε φυσικές όσο και σε πειραματικές συνθήκες. Η μελέτη και σύγκριση των προαναφερθέντων συλλογών δεδομένων επέτρεψε την διάκριση διαφόρων τύπων αμφιβόλων καθώς και την κατανόηση της δημιουργίας των αμφιβόλων στον μανδύα. Πιο συγκεκριμένα, οι αμφίβολοι Τύπου-Ι (πλούσιες σε Na και Ti, αλλά φτωχές σε Cr) έχουνε προκύψει από την απευθείας κρυστάλλωση από βασαλτικά, βασανιτικά, ανδεσιτικά, δακιτικά τήγματα και βρίσκονται κυρίως σε ηπειρωτικά τόξα (π.χ. Καμτσάτκα, Ρωσία), περιβάλλοντα εσωτερικά των πλακών (π.χ. Δυτικό Άιφελ, Γερμανία) και ωκεάνια τόξα μετασχηματισμού (π.χ. 15°20' Ζώνη Διάρρηξης, Μέσο-Ατλαντική ράχη). Οι αμφίβολοι Τύπου-ΙΙ είναι πλούσιες σε Cr και περιέχουνε διάφορα ποσοστά σε Ti και αλκάλια. Έχουνε προκύψει από την αντίδραση μεταξύ τηγμάτων και ορυκτών του μανδύα (κυρίως κλινοπυρόξενο και σπινέλιο). Βρίσκονται συνήθως σε μαγματικά κέντρα στο εσωτερικό των πλακών (π.χ. Μασίφ Σαντράλ, Γαλλία) και σε μερικά ηπειρωτικά τόξα (π.χ. Ίτσινομεγκάτα, Ιαπωνία). Οι Τύπου-ΙΙΙ αμφίβολοι αντιπροσωπεύουν την αλληλεπίδραση ένυδρων ρευστών και τηγμάτων με υπερμαφικά πετρώματα σε περιοχές ζωνών υπαγωγής και χαρακτηρίζονται από υψηλά ποσοστά σε Cr και αλκάλια, αλλά μικρό περιεχόμενο σε Ti. Οι Τύπου-ΙΙΙ αμφίβολοι εντοπίζονται σε ωκεάνια τόξα (π.χ. TUBAF, PNG), οφιολίθους (π.χ. Οφιόλιθος της Λυκίας, Τουρκία) αλλά συχνά και σε ηπειρωτικά τόξα. Επιπλέον, στην παρούσα εργασία, δημιουργήθηκε ένα θερμόμετρο ανταλλαγής Fe και Mg μεταξύ αμφιβόλου και κλινοπυροξένου το οποίο βαθμονομήθηκε σύμφωνα με προϋπάρχοντα, πειραματικά δεδομένα σε υπερμαφικές συστάσεις. Το σφάλμα του θερμομέτρου είναι ±34 °C για ένα εύρος πίεσης 0.5-3.7 GPa. Εφαρμόζοντας το θερμόμετρο σε περιδοτιτικούς ξενολίθους, που δείχνουν ενδείξεις χημικής ισορροπίας και ισορροπίας υφών μεταξύ των ορυκτών του μανδύα (π.χ. Δυτικό Άιφελ, Γερμανία; Ανατολική Τρανσυλβανική Λεκάνη, Ρουμανία), προκύπτουν θερμοκρασίες που είναι συγκρίσιμες με τη διπυροξενική θερμομετρία ανταλλαγής Fe και Mg. Το νέο θερμόμετρο μπορεί να χρησιμοποιηθεί για να περιγράψει την θερμοδυναμική ισορροπία της αμφιβόλου και του κλινοπυροξένου στον μανδύα.

Λέξεις κλειδιά: αμφίβολος, κλινοπυρόξενος, μανδύας, ισορροπία, θερμόμετρο

Summary

Amphibole is a secondary phase commonly found in ultramafic lithologies (mantle xenoliths, Alpine-type and ophiolitic peridotites) occurring in diverse environments such as magmatic arcs, plate interiors, transform faults, rifts and collision zones. Its formation has mainly been attributed to fluid-melt/rock interaction or direct crystallisation from melts/fluids. For the purpose of the present thesis, an extensive bibliographical database has been compiled. It involves major-element compositional data of amphibole in ultramafic rocks from various geotectonic settings around the globe. Additionally, amphiboles related to a wide spectrum of melts spanning from felsic to mafic in composition, both natural (rock samples) and synthetic (laboratory experiments) have also been considered. Type-I amphiboles (enriched in Na and Ti but depleted in Cr) are the products of direct crystallisation from basaltic, basanitic, andesitic and dacitic melts and are mostly found in continental arcs (e.g. Kamchatka, Russia), within-plate settings (e.g. West Eifel, Germany) and oceanic transform faults (e.g. 15°20′N Fracture Zone, Mid-Atlantic Ridge). Type-II amphiboles are Cr-rich, contain variable amounts of Ti and alkalis, and form via reaction between the aforementioned melts and primary mantle phases (mostly clinopyroxene and spinel). They are usually found in within-plate magmatic centers (e.g. Massif Central, France) and several localities in continental arcs (e.g. Ichino-megata, Japan). Amphiboles belonging to type-III reflect hydrous fluid/melt-rock interactions above subduction zones. Type-III amphiboles are predominantly encountered in oceanic arcs (e.g. TUBAF seamount, PNG) and ophiolites (Lycian ophiolite, Turkey) but occasionally they also occur in continental-arc settings. We have furthermore calibrated a new Fe-Mg exchange thermometer between amphibole and clinopyroxene based on existing experimental data on ultramafic compositions with an error of ±46°C in the pressure range 0.5–3.7 GPa. Peridotite xenoliths that display good evidence of textural and chemical equilibration among their constituent minerals (e.g. West Eifel, Germany; Eastern Transylvanian Basin, Romania) yield amphibole temperatures comparable to those predicted from two-pyroxene Fe-Mg exchange thermometry.

Keywords: amphibole, clinopyroxene, mantle, equilibrium, thermometer

TABLE OF CONTENTS

CHAPTER 1
Amphiboles: Crystal Structure – Classification / Nomenclature

Introduction

Amphibole is one of the most common and important rock-forming minerals and has been a matter of discussion for decades in the field of geosciences. Its name origin comes from the Greek word "αμφίβολος" meaning "ambiguous". Because of its enormously variable chemical composition, amphibole is abundant in a wide compositional spectrum of rocks. Amphiboles can be found in silica-laden igneous rocks such as dacites, rhyolites and andesites but it also occurs in basic rocks rich in olivine such as basalts and peridotites. In metamorphic rocks, amphibole is an important phase present in greenschist, amphibolite, granulite, blueschist and eclogite facies. This shows that it can be formed and preserved in a wide spectrum of temperatures and pressures. Metamorphosed siliceous dolomites, calcareous metasediments and metamafic to metaultramafic rocks can all contain amphibole given water availability and appropriate P-T conditions (i.e. within the amphibole stability field). Several segments of the metamorphic evolutionary path of many rocks could, therefore, be unlocked by examining the physicochemical processes that led to the formation of amphibole. However, amphibole is a complicated mineral. The number of chemical components that can be incorporated in its crystal structure is very large and this, in turn, creates numerous end-member compositions which will be discussed in the following pages. In fact, Engel & Engel (1962) have referred to amphibole as being a mineralogical "sponge" and Ernst (1968) as a "mineralogical wastebasket". These characteristics, which have been noted since early works, along with the complexity of the crystal structure are the main reasons why amphibole has been and still is a very complicated phase to examine and understand. In order to fully grasp and interpret the processes that are involved in its formation and subsequent evolution one needs to look at petrologic data very carefully and in depth. This introductory chapter aims at summarising some basic and important concepts of amphibole formation and setting the basis for the material that will be laid out in the next chapters.

Amphibole is not an easily identifiable mineral in hand specimen. Colourwise, amphiboles can be white, green, brown, black or blue and they generally present a prismatic or fibrous habit. Although these observations could be of some use, they are

never practical enough to classify an amphibole. Using plain-polarized light microscopy (transmitted light) amphiboles can often be distinguished from other minerals such as pyroxenes as they show two different directions of cleavage that intersect at approximately 56° and 124°. On a few occasions the cleavage is also visible in hand specimen as well. There is no classification scheme that enables the identification of amphibole exclusively from hand specimen observations or microscopy because there are not enough parameters that could be used to discriminate amphiboles with these techniques. The classification is only possible if the chemical composition of amphibole is known.

1.1 The crystal structure of amphibole & site occupancies

The first pioneering study that was devoted on the crystal structure of amphibole was conducted by Warren (1929) on tremolite. This initial work was very influential for scientists to start uncovering more details and gradually a great amount of interest arose about amphiboles. Many studies have been published since that shed ample light on the structure of amphibole with variable composition (see Ernst, 1968 and references therein). The basic characteristics of the amphibole structure that were inferred back then do not have many critical differences with modern works (Hawthorne & Oberti, 2007a). In order to understand the crystal structure of the mineral and how it is related to site occupancies, the general chemical formula of amphibole must be given first.

According to Hawthorne et al. (2012) the general chemical formula of amphibole can be written as $AB_2C_5T_8O_{22}W_2$, where

A = □, Na, K, Ca, Pb, Li
B = Na, Ca, Mn^{+2}, Fe^{+2}, Mg, Li
C = Mg, Fe^{+2}, Mn^{+2}, Al, Fe^{+3}, Mn^{+3}, Cr^{+3}, Ti^{+4}, Li
T = Si, Al, Ti^{+4}, Be
W = (OH), F, Cl, O^{-2}

Sites T and C represent the tetrahedral and octahedral sites, respectively. Site C shows the highest variability as it can be occupied by a greater number of chemical elements compared to the other structural sites. It can additionally contain trace elements such as Zn, Ni^{+2}, Co^{+2}, V^{+3}, Sc and Zr. It is, also, the only site containing Fe^{+3} and Cr^{+3}. Symbol "□" in site A represents vacancies which are very often found in the structure of amphiboles. Hydroxyls, F, Cl and oxygens are all located in W.

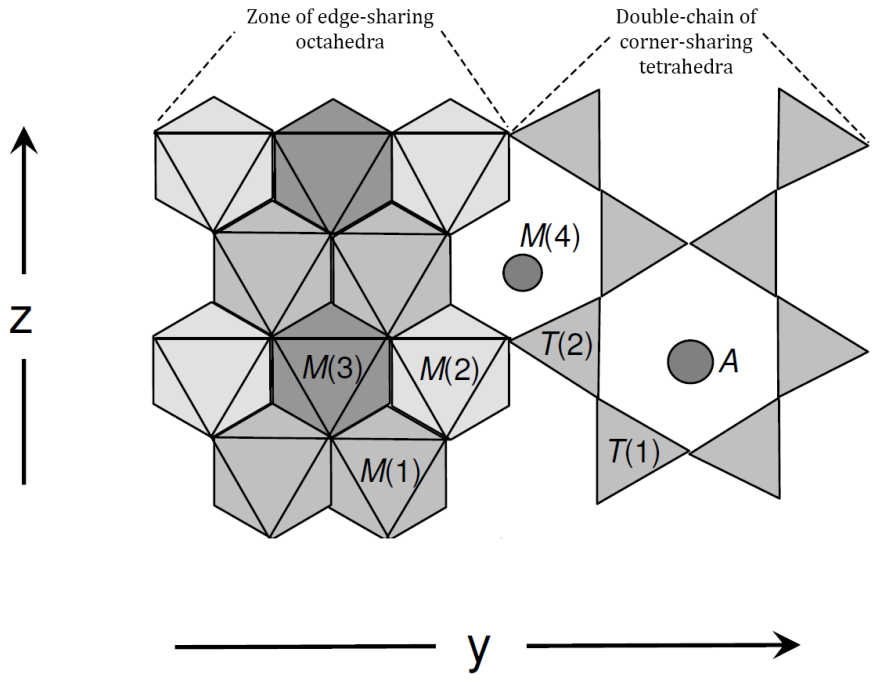

Figure 1: A simplified model showing the crystal structure of amphibole (Hawthorne & Oberti, 2007a)

The amphibole crystal structure can be described by two principal components. A double chain of corner-sharing silica tetrahedra (T-site cations) and zones consisting of edge-sharing octahedra are combined together and are extending parallelly to the c crystallographic direction (Figure 1). The double chain is what makes amphibole belong to the chain silicate minerals. Both tetrahedral and octahedral sites own topologically different areas. Therefore, there must be a distinction between T(1) and T(2) types of tetrahedra and also M(1), M(2), and M(3) types of octahedra based exclusively on their exact location in the crystal structure (Figure 1). Site M(4) defines a free space which lies between the strip of octahedra and the double chain and is occupied exclusively by B cations. Vacancies and cations belonging to A are found at the center of a large cavity in the middle of the double chain. Cations belonging to site C are sharing M(1), M(2) and M(3) sites.

The complexity of the crystal structure of amphibole arises from the existence of multiple types of symmetries. These symmetries are represented by the so-called space groups. Six amphibole space groups have been discovered so far, meaning six different variants of arrangement. The vast majority of calcic, sodic-calcic and alkali amphiboles belong to the C2/m space group. The Mg-Fe-Mn amphiboles can be divided into orthorhombic (this relates them to space groups Pnma or Pnmn) or monoclinic (space groups C2/m or $P2_1/m$). Lithium-bearing amphiboles can also be orthorhombic (space group Pnma) or monoclinic (C2/m). As this study mainly deals

with calcium, sodium-calcium, and magnesium-iron-manganese amphiboles, the most pertinent space groups will be briefly described. A detailed description of all amphibole space groups may be found in the work of Hawthorne & Oberti (2007a).

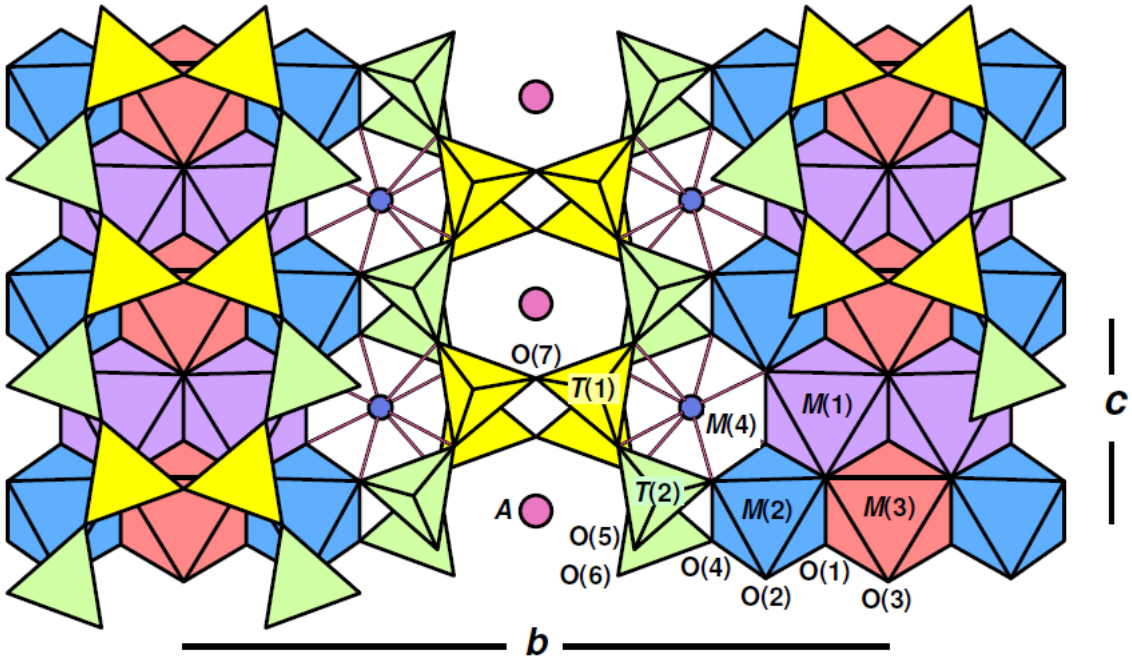

Figure 2: The C2/m structure of amphibole (Hawthorne & Oberti, 2007a).

As it was shown earlier for C2/m amphiboles, the T(1) and T(2) sites form a double chain of corner-sharing tetrahedra. Each site is coordinated by four oxygens as seen in Figure 2. The T(1) tetrahedra form the bridges that tie the double chain together. The octahedral sites M(1), M(2) and M(3) are coordinated by six oxygens each and are sharing edges with each other. The tetrahedral double chain is linked with the octahedral strip by the denoted O(4) oxygens as presented in Figure 2. Site M(4) is located at the empty space in between the double chain and the octahedra and as noted earlier is occupied by B cations. As noted in Hawthorne & Oberti (2007a), this site is very important for the classification of amphiboles as it is responsible for almost all of the compositionally major subgroups of amphiboles but it also defines the different space-group symmetries. Lastly, cations belonging to A are found in the free space in the middle of the double chain and are coordinated by twelve oxygens but they do not always form bonds together.

Space group $P2_1/m$ differs from C2/m in possessing four distinct T sites (T1A, T1B, T2A, T2B) instead of two. These tetrahedral sites link with each other to form two distinct types of double chains which are referred to as A-chain and B-chain.

There are three octahedral sites M(1), M(2), and M(3) which are occupied by cations belonging to C. This time, the octahedron strip is bonding with oxygens of the A-chain from one side and with oxygens from the B-chain on the other side. The M(4) cations (practically B cations), although they are surrounded by eight oxygens, they might not be tied with all of them. Amphiboles that are defined by this symmetry usually have unoccupied A sites which are filled with vacancies. Space group Pnma is very similar to $P2_1/m$ with some minor differences in symmetry. The cavities between the double chains are also occupied by A cations compared to $P2_1/m$ in which they were empty. On the other hand, Pnmn space group shows many similarities with C2/m, having only two tetrahedral sites (T1 and T2) that form a single double chain. It is also defined by three octahedral sites in a similar manner to C2/m but with slightly different symmetries.

What has been presented so far is the main structural unit of amphibole. However, the structural units are repeated in space. Generally, the complete amphibole structure may be thought of as a succession of tetrahedral and octahedral sheets that are stacked together. The stacking sequence depends on the space group that the amphibole belongs to (Hawthorne & Oberti, 2007a).

1.2 Classification schemes

Having clarified the most important aspects of the amphibole crystal structure, the next critical step is to have a classification scheme and name the amphiboles according to their chemical composition. The rapid discovery of new end-member compositions and the improved understanding of amphibole has led to a progressive development of classification nomenclatures that have attempted to thoroughly express the chemical characteristics of amphibole. The first systematic effort on amphibole classification was made by Leake (1968). In that study, almost 2000 major-oxide amphibole analyses of calciferous to sub-calciferous compositions were examined. This led to IMA1978, the International Mineralogical Association meeting that proposed the first nomenclature on the classification of amphiboles in 1978 (Leake, 1978). Subsequent modifications of the original scheme led to IMA1997 and IMA2004 (Leake et al., 1997; Leake et al., 2004) which were aiming to simplify IMA1978 and make the nomenclature more accessible but still detailed and inclusive. These classification schemes received even more revisions by Hawthorne & Oberti (2006, 2007b). This led to the most recent classification that has been proposed by Hawthorne et al. (2012) who tried to encompass new discoveries in the field of amphibole geochemistry (IMA2012). Since IMA2012, even more new end-member

compositions have been identified (e.g. Reznitsky et al., 2018; Hawthorne et al., 2022).

All of the aforementioned classification methods agree on the fact that two major groups of amphiboles exist in nature. Those that are dominated by OH, F and Cl in site W and those in which site W is mostly occupied by O^{-2}. One of the critical differences between IMA2012 and IMA1997-2004 was the consideration, in the former, of amphiboles that contain significant amounts of lithium. Lithium can form a solid solution with sodium in the M(4) site. It was previously pointed out that M(4) is the prime crystallographic site used for the determination of different types of amphibole subgroups. Evidently, a new subgroup had to be considered based on lithium. Moreover, IMA1997 and IMA2004 mainly used cations residing in sites A, B and T to discriminate between different types of amphibole. However Si, which is only found in site T, is invariant and therefore it is not a practical enough element to classify amphiboles. Cations residing in sites A, B and C are much more useful because they can be incorporated in more than one site (Hawthorne et al., 2012). A few other additions of IMA2012 involve the consideration of more detailed prefixes and the decision to use uniform labelling of amphibole subgroups.

For the reasons presented above, IMA2012 will be used throughout this study as it is the most recently approved scheme and considered to be more consistent and complete compared to previous versions. IMA1997, however, has persisted in the literature to this date. In the following section, the nomenclature of IMA2012 will be compared to that of IMA1997 focusing on the amphibole subgroups that will predominantly be used in the present study. It was deemed useful to present both classification schemes so that the reader can thoroughly appreciate the effects of the controlling chemical parameters on amphibole classification. The subgroups that are going to be mostly discussed are the calcium, sodium-calcium, sodium and magnesium-iron-manganese subgroups which all belong to the ^{W}(OH, F, Cl)-dominant group. One specific end-member composition of the $^{W}O^{-2}$-dominant amphiboles will be additionally discussed.

1.2.1 Calcium amphiboles

Calcium amphiboles form one of the most important subgroups and, as it will be shown later, they are the main subject of interest as they occur in rocks of multiple compositions. According to IMA2012, amphiboles that belong to this subgroup, should fulfil the following structural/chemical criteria:

$$^{B}(Ca + \Sigma M^{+2})/ \Sigma B \geq 0.75$$

&

$$^{B}Ca/\Sigma B \geq {}^{B}\Sigma M^{+2}/\Sigma B$$

where $^{B}\Sigma M^{+2}$ refers to the sum of divalent cations in site B and ΣB to the total sum of cations in site B. The main calcium rootnames following IMA2012 are depicted in Figure 3. At this point, it must be noted that a rootname describes a distinct species with a unique chemical composition which can be slightly modified (e.g. pargasite could become ferro-pargasite if divalent iron substitutes for magnesium).

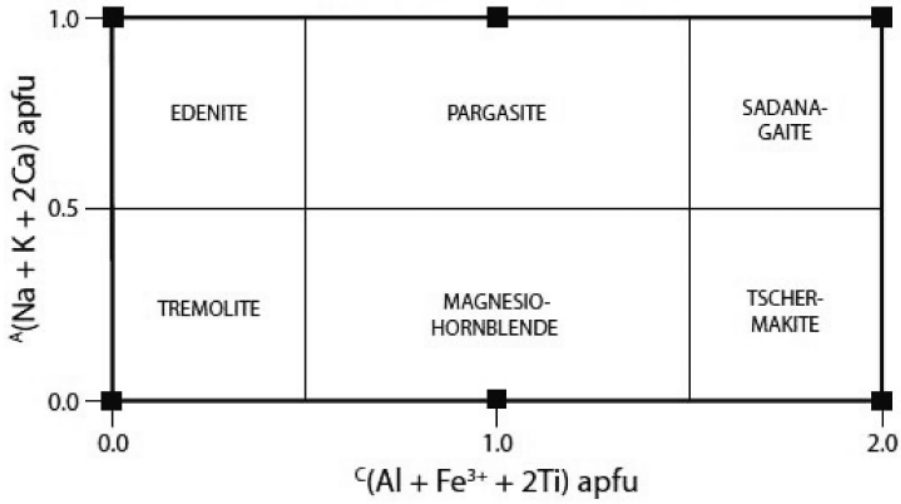

Figure 3: Compositional boundaries that define calcium amphiboles. The heavy solid black lines and the black squares represent the end-member compositions (Hawthorne et al., 2012).

In Figure 3, the x-axis is defined by the (Al + Fe^{+3} + 2Ti) content of amphibole in site C. The y-axis, on the other hand, is defined by the (Na + K + 2Ca) content in site A. Tremolite (□$Ca_2Mg_5Si_8O_{22}(OH)_2$) and edenite ($NaCa_2Mg_5(Si_7Al)O_{22}(OH)_2$) both contain minor or no amounts of ^{C}(Al + Fe^{+3} +2Ti). However, the edenitic rootname contains one atom of Na in site A while tremolite is characterized by a vacancy in site A. Therefore, Na in site A can easily distinguish edenite from tremolite. Likewise, pargasite ($NaCa_2(Mg_4Al)(Si_6Al_2)O_{22}(OH)_2$) and magnesio-hornblende (□$Ca_2(Mg_4Al)(Si_7Al)O_{22}(OH)_2$) are both characterized by identical, intermediate amounts of the x-axis variable but are discriminated by their content of the y-axis variable with pargasite being generally more Al-rich. Sadanagaite ($NaCa_2(Mg_3Al_2)(Si_5Al_3)O_{22}(OH)_2$) and tschermakite (□$Ca_2(Mg_3Al_2)(Si_6Al_2)O_{22}(OH)_2$) are showing the highest contents of ^{C}(Al + Fe^{+3}

+2Ti) but sadanagaite is the more alkali-rich end-member. Evidently, the most Al-poor phases are edenite and tremolite and the most Al-rich calcium amphiboles are

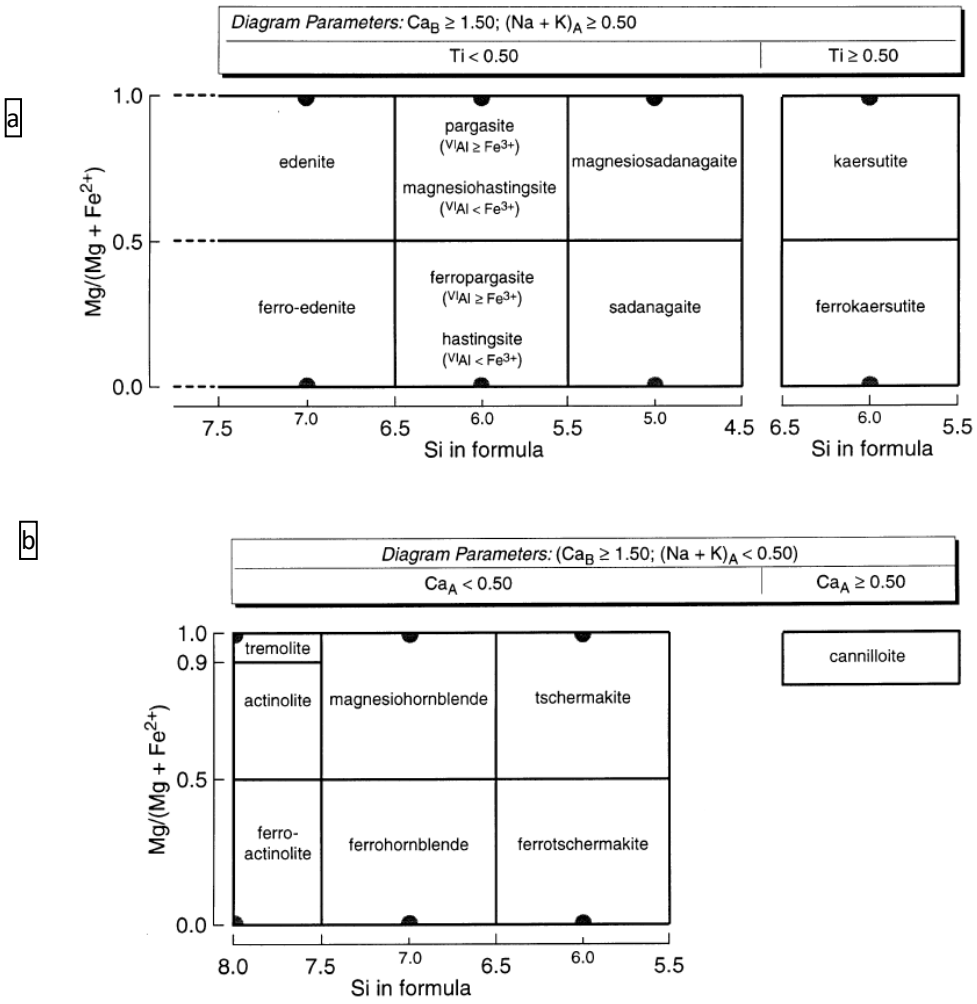

Figure 4: The calcium amphibole classification scheme according to Leake et al. (1997). (a). Calcium amphiboles with $(Na + K)_A \geq 0.5$; (b). Calcium amphiboles with $(Na + K)_A < 0.5$.

sadanagaite and tschermakite. The chemical formulae of all important end-member compositions are tabulated in

Table 1.

Leake et al. (1997) had proposed a completely different method to name calcium amphiboles. According to them, a calcium amphibole is any amphibole with $Ca_B \geq 1.5$. If that criterion is met, then the parameter $(Na + K)_A$ defines whether the amphibole belongs to the edenite-pargasite-hastingsite-sadanagaite-kaersutite or to the actinolite-hornblende-tschermakite-cannilloite group (Figure 4). Kaersutite represents the compositions that contain more than 0.5 atoms of Ti per formula unit. Cannilloite ($CaCa_2(Mg_4Al)(Si_5Al_3)O_{22}(OH)_2$) is defined by $Ca_A > 0.5$ and is plotted on a separate

diagram. Furthermore, IMA1997 used the value of Mg# $\left(\frac{Mg}{(Mg+Fe^{+2})}\right)$ and that of Si in site T to designate the name of amphibole (Figure 4). It is evident that edenite and actinolite/tremolite are the most Si-rich calcium amphiboles while sadanagaite and tschermakite contain relatively low amounts of Si. All of the rootnames in which Fe^{+2} becomes important adopt a ferro- prefix and they are shifted towards compositions with smaller Mg#. Pargasites and ferro-pargasites show Si ranging from 5.5 to 6.5 atoms per formula unit (apfu). Magnesio-hornblendes show Mg# > 0.5 but Si is ranging from 6.5 to 7.5 apfu. According to Figure 4, tremolite is identical to actinolite in terms of Si but they differ in terms of Mg as tremolite is showing Mg# above 0.9.

Calcium amphiboles are defined by eight root compositions which can be additionally described by numerous prefixes and form different end-member compositions. The end-member compositions of amphiboles in the calcium subgroup that will be used in this study are displayed in

Table 1 following Hawthorne et al. (2012). At this point, it is important to note that, based on IMA2012, kaersutite is not regarded as a calcium amphibole but as an oxo-amphibole.

1.2.2 Sodium-calcium amphiboles

Based on Hawthorne et al. (2012), sodium-calcium amphiboles are defined by the following criteria:

$$0.75 > {}^{B}(Ca + \Sigma M^{+2})/\Sigma B > 0.25,\ {}^{B}Ca/\Sigma B \geq {}^{B}\Sigma M^{+2}/\Sigma B$$

and

$$0.75 > {}^{B}(Na + Li)/\ \Sigma B > 0.25,\ {}^{B}Na/\Sigma B \geq {}^{B}Li/\Sigma B$$

Sodium-calcium amphiboles can be distinguished from each other using the same parameters as in the calcium subgroup (Figure 5). The sodium-calcium amphiboles that will mostly be mentioned in this study are richterite ($Na(NaCa)Mg_5Si_8O_{22}(OH)_2$) and katophorite ($Na(NaCa)(Mg_4Al)(Si_7Al)O_{22}(OH)_2$); they are both rich in Na and are plotted in the upper part of Figure 5. Richterite contains insignificant amounts of Al compared to katophorite, therefore, the two can be distinguished on the basis of the ($Al + Fe^{+3} + 2Ti$) parameter on the x-axis. The compositional boundary between calcium and sodium-calcium amphiboles is also indicated in Figure 5.

Following the nomenclature of Leake et al. (1997) sodium-calcium amphiboles are defined by the parameters:

$$(Ca + Na_B) \geq 1.0$$

and

$$0.5 < Na_B < 1.5$$

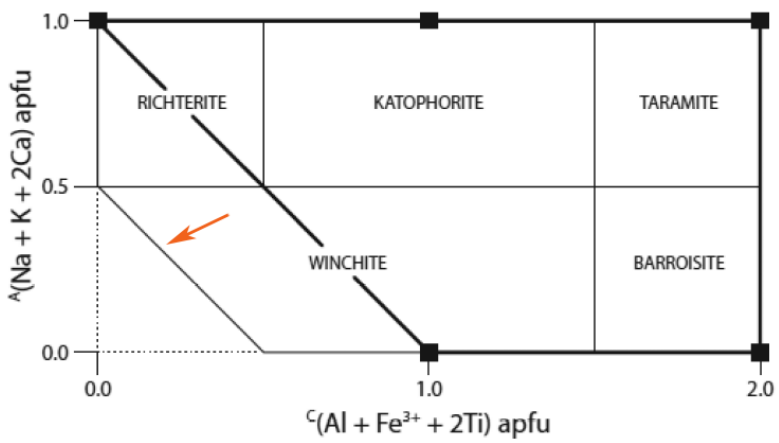

Figure 5: Compositional fields for sodium-calcium amphiboles (Hawthorne et al., 2012). The diagonal line indicated by the red arrow marks the boundary between calcium and sodium-calcium amphiboles.

If $(Na + K)_A$ is equal to 0.5 or higher, the amphibole is plotted in the richterite-katophorite-taramite diagram (Figure 6a). If $(Na + K)_A$ is lower than 0.5, the amphibole is plotted in the winchite-barroisite diagram (Figure 6b). Richterite is more Si-rich compared to katophorite, having values from 7.5 to 8 apfu.

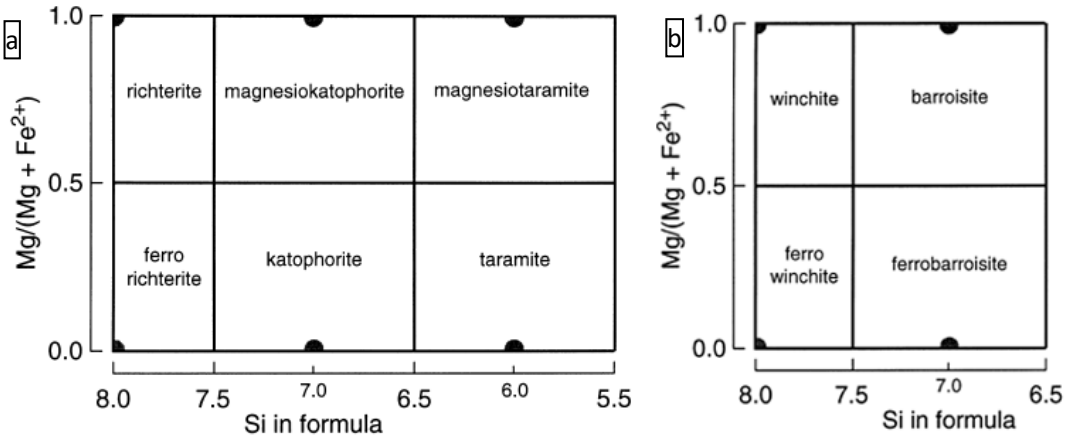

Figure 6: The sodium-calcium amphibole classification scheme according to Leake et al. (1997). (a). Sodium-calcium amphiboles with $(Na + K)_A \geq 0.5$; (b). Sodium-calcium amphiboles with $(Na + K)_A < 0.5$.

1.2.3 Sodium amphiboles

The sodium amphibole end-member compositions that will primarily be discussed in the present study are glaucophane ($\square Na_2(Mg_3Al_2)Si_8O_{22}(OH)_2$) and nybøite ($NaNa_2(Mg_3Al_2)(Si_7Al)O_{22}(OH)_2$) (

Table 1); their compositional fields, according to IMA2012, are depicted in Figure 7. Also, the criteria that should be satisfied by an amphibole to belong to the sodium group are:

$$^{B}(Na + Li)/\Sigma B \geq 0.75$$

and

$$^{B}Na/\Sigma B > {}^{B}Li/\Sigma B$$

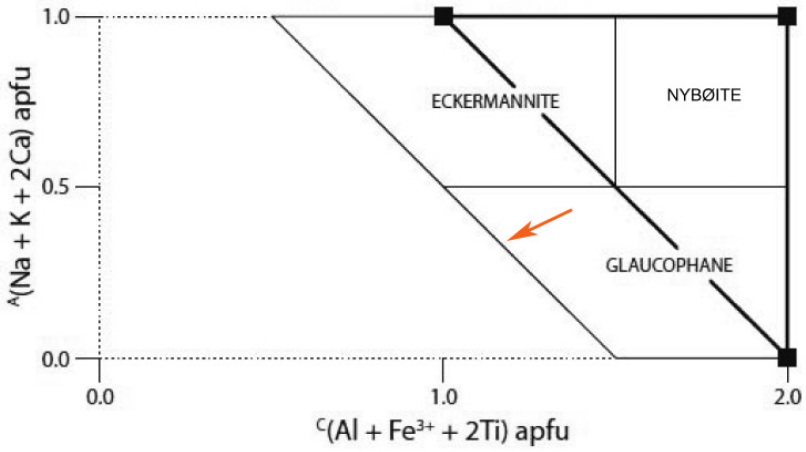

Figure 7: Compositional fields for sodium amphiboles (Hawthorne et al., 2012). The diagonal line indicated by the red arrow shows the boundary between sodium-calcium and sodium amphiboles.

Leake et al. (1997) define sodium amphiboles as those that fulfil the following criteria:

$$Na_B \geq 1.5, (Mg + Fe^{+2} + Mn^{+2}) > 2.5$$

and

$$(Al_T \text{ or } Fe^{+3}) > Mn^{+3}, Li < 0.5, (Mg \text{ or } Fe^{+2}) > Mn^{+2}$$

Comparing Figure 7 and Figure 8, it is evident that nybøite is more Na-rich compared to glaucophane but glaucophane contains far more Si in its crystal structure (7 to 8 apfu Si). The Mg# parameter is similar in both minerals and it cannot be used to discriminate between the two. By using the classification of IMA1997, nybøite can only be distinguished from glaucophane in terms of Si. However, according to IMA2012, nybøite and glaucophane differ both in their Na and Al contents. Both nybøite and glaucophane could carry in their names the ferri- and ferro- prefixes if significant amounts of Fe^{+3} or Fe^{+2} are present, respectively.

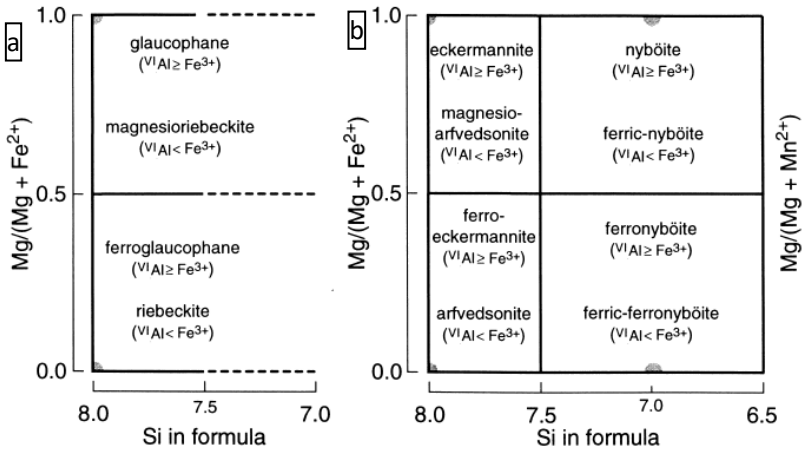

Figure 8: The sodium amphibole classification scheme according to Leake et al. (1997). (a) Sodium amphiboles with $(Na + K)_A < 0.5$; (b) Sodium amphiboles with $(Na + K)_A \geq 0.5$.

1.2.4 Magnesium-iron-manganese amphiboles

The two monoclinic end-members of the magnesium-iron-manganese subgroup that will be discussed in the present work are cummingtonite ($\square Mg_2Mg_5Si_8O_{22}(OH)_2$) and grunerite ($\square Fe_2^{+2}Fe_5^{+2}Si_8O_{22}(OH)_2$). The cation criteria to be satisfied for this subgroup are as follows (IMA2012):

$$^{B}(Ca + \Sigma M^{+2})/\Sigma B \geq 0.75$$

and

$$^{B}\Sigma M^{+2}/\Sigma B > {}^{B}Ca/\Sigma B$$

This time, the IMA2012 diagram that is used to accurately name the different monoclinic magnesium-iron-manganese amphiboles is the ternary plot portrayed in Figure 9, which practically uses Mg, Fe^{+2} and Mn in sites B and C. The end-member compositions are given in

Table 1. Cummingtonite and grunerite both plot at the bottom of the ternary diagram showing a very small content in Mn. Grunerite mostly contains Fe^{+2} and Fe^{+3} in its structure while cummingtonite is the Mg-rich end-member of this subgroup and only minimal amounts of iron are expected to be found.

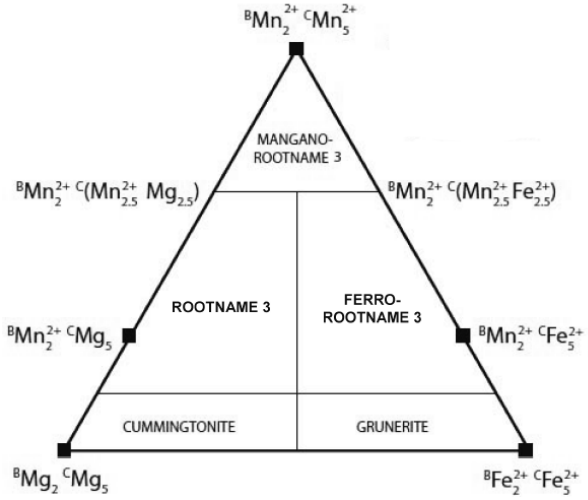

Figure 9: Ternary diagram proposed by IMA2012 to discriminate between monoclinic magnesium-iron-manganese amphiboles (Hawthorne et al., 2012).

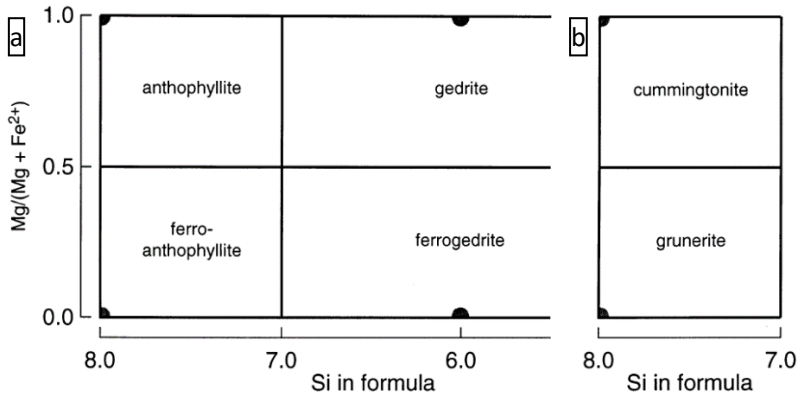

Figure 10: The classification scheme for magnesium-iron-manganese amphiboles according to Leake et al. (1997). (a). Orthorhombic amphiboles; (b). Monoclinic amphiboles.

IMA1997 has proposed the following criteria for magnesium-iron-manganese amphiboles:

$$(Ca + Na_B) < 1,\ (Mg, Fe^{+2}, Mn, Li)_B \geq 1,\ Li_B < 1$$

Leake et al. (1971) have also presented the diagram shown in Figure 10. It is noticeable that cummingtonite and grunerite cannot be distinguished according to Si but only by using the Mg# parameter which exceeds the value of 0.5 in cummingtonite.

1.2.5 Oxo-amphiboles

The last subgroup that will be referred to in this study is the one that involves amphiboles that are dominated by O^{-2} in site W. Although this group contains four root-names, only kaersutite is commonly found in natural rocks and is of petrological interest. As noted by Hawthorne et al. (2012), the occurrence of O^{-2} in site W is accompanied by high-charge (≥3) cations in site C. More specifically, the Ti content is extremely critical and is used to distinguish kaersutite from all other amphiboles. In essence, kaersutite is the amphibole that hosts more than 0.5 apfu Ti in site C. As will be shown in the following pages, Ti is often correlated with O^{-2} in site W and can be used as a relatively good proxy of the oxo-component in amphiboles such as pargasite.

Table 1: Amphibole end-member compositions that will be used in this study. Names in bold represent rootnames. Symbols are from Kretz (1983) and Hawthorne et al. (2012).

End-member name	*Chemical Formula*	*Symbol*
Calcium amphiboles		
Pargasite	$NaCa_2(Mg_4Al)(Si_6Al_2)O_{22}(OH)_2$	Prg
Ferro-pargasite	$NaCa_2(Fe_4^{+2}Al)(Si_6Al_2)O_{22}(OH)_2$	
Magnesio-Hornblende	$\square Ca_2(Mg_4Al)(Si_7Al)O_{22}(OH)_2$	Mhb
Ferro-hornblende	$\square Ca_2(Fe_4^{+2}Al)(Si_7Al)O_{22}(OH)_2$	
Ferro-ferri-hornblende	$\square Ca_2(Fe_4^{+2}Fe^{+3})(Si_7Al)O_{22}(OH)_2$	
Magnesio-ferri-hornblende	$\square Ca_2(Mg_4Fe^{+3})(Si_7Al)O_{22}(OH)_2$	
Hastingsite	$NaCa_2(Fe_4^{+2}Fe^{+3})(Si_6Al_2)O_{22}(OH)_2$	Hs
Magnesio-Hastingsite	$NaCa_2(Mg_4Fe^{+3})(Si_6Al_2)O_{22}(OH)_2$	
Tremolite	$\square Ca_2Mg_5Si_8O_{22}(OH)_2$	Tr
Edenite	$NaCa_2Mg_5(Si_7Al)O_{22}(OH)_2$	Ed
Ferro-edenite	$NaCa_2Fe_5^{+2}(Si_7Al)O_{22}(OH)_2$	
Sadanagaite	$NaCa_2(Mg_3Al_2)(Si_5Al_3)O_{22}(OH)_2$	Sad
Ferro-sadanagaite	$NaCa_2(Fe_3^{+2}Al_2)(Si_5Al_3)O_{22}(OH)_2$	
Ferri-sadanagaite	$NaCa_2(Mg_3Fe_2^{+3})(Si_5Al_3)O_{22}(OH)_2$	
Ferro-ferri-sadanagaite	$NaCa_2(Fe_3^{+2}Fe_2^{+3})(Si_5Al_3)O_{22}(OH)_2$	

Rootname 4	$NaCa_2(Mg_4Ti)(Si_5Al_3)O_{22}(OH)_2$	
Ferro-rootname 4	$NaCa_2(Fe_4^{+2}Ti)(Si_5Al_3)O_{22}(OH)_2$	
Tschermakite	$\square Ca_2(Mg_3Al_2)(Si_6Al_2)O_{22}(OH)_2$	Ts
Ferro-tschermakite	$\square Ca_2(Fe_3^{+2}Al_2)(Si_6Al_2)O_{22}(OH)_2$	
Ferri-tschermakite	$\square Ca_2(Mg_3Fe_2^{+3})(Si_6Al_2)O_{22}(OH)_2$	
Ferro-ferri-tschermakite	$\square Ca_2(Fe_3^{+2}Fe_2^{+3})(Si_6Al_2)O_{22}(OH)_2$	
Cannilloite	$CaCa_2(Mg_4Al)(Si_5Al_3)O_{22}(OH)_2$	Can
Sodium-calcium amphiboles		
Richterite	$Na(NaCa)Mg_5Si_8O_{22}(OH)_2$	Ri
Ferro-richterite	$Na(NaCa)Fe_5^{+2}(Si_8O_{22}(OH)_2$	
Winchite	$\square(NaCa)(Mg_4Al)Si_8O_{22}(OH)_2$	Win
Ferro-winchite	$\square(NaCa)(Fe_4^{+2}Al)Si_8O_{22}(OH)_2$	
Ferri-winchite	$\square(NaCa)(Mg_4Fe^{+3})Si_8O_{22}(OH)_2$	
Ferro-ferri-winchite	$\square(NaCa)(Fe_4^{+2}Fe^{+3})Si_8O_{22}(OH)_2$	
Barroisite	$\square(NaCa)(Mg_3Al_2)(Si_7Al)O_{22}(OH)_2$	Bar
Ferro-barroisite	$\square(NaCa)(Fe_3^{+2}Al_2)(Si_7Al)O_{22}(OH)_2$	
Ferri-barroisite	$\square(NaCa)(Mg_3Fe_2^{+3})(Si_7Al)O_{22}(OH)_2$	
Ferro-ferri-barroisite	$\square(NaCa)(Fe_3^{+2}Fe_2^{+3})(Si_7Al)O_{22}(OH)_2$	
Katophorite	$Na(NaCa)(Mg_4Al)(Si_7Al)O_{22}(OH)_2$	Ktp
Ferro-katophorite	$Na(NaCa)(Fe_4^{+2}Al)(Si_7Al)O_{22}(OH)_2$	
Ferri-katophorite	$Na(NaCa)(Mg_4Fe^{+3})Si_7Al)O_{22}(OH)_2$	
Ferro-ferri-katophorite	$Na(NaCa)(Fe_4^{+2}Fe^{+3})Si_7Al)O_{22}(OH)_2$	
Taramite	$Na(NaCa)(Mg_3Al_2)(Si_6Al_2)O_{22}(OH)_2$	Tar
Ferro-taramite	$Na(NaCa)(Fe_3^{+2}Al_2)(Si_6Al_2)O_{22}(OH)_2$	
Ferri-taramite	$Na(NaCa)(Mg_3Fe_2^{+3})(Si_6Al_2)O_{22}(OH)_2$	
Ferro-ferri-taramite	$Na(NaCa)(Fe_3^{+2}Fe_2^{+3})(Si_6Al_2)O_{22}(OH)_2$	
Sodium amphiboles		
Glauchophane	$\square Na_2(Mg_3Al_2)Si_8O_{22}(OH)_2$	Gln
Ferro-glaucophane	$\square Na_2(Fe_3^{+2}Al_2)Si_8O_{22}(OH)_2$	
Eckermanite	$NaNa_2(Mg_4Al)Si_8O_{22}(OH)_2$	Eck
Ferro-eckermannite	$NaNa_2(Fe_4^{+2}Al)Si_8O_{22}(OH)_2$	
Nybøite	$NaNa_2(Mg_3Al_2)(Si_7Al)O_{22}(OH)_2$	Nyb
Ferro-nybøite	$NaNa_2(Fe_3^{+2}Al_2)(Si_7Al)O_{22}(OH)_2$	
Ferri-nybøite	$NaNa_2(Mg_3Fe_2^{+3})(Si_7Al)O_{22}(OH)_2$	
Ferro-ferri-nybøite	$NaNa_2(Fe_3^{+2}Fe_2^{+3})(Si_7Al)O_{22}(OH)_2$	
Arfvedsonite	$NaNa_2(Fe_4^{+2}Fe^{+3})Si_8O_{22}(OH)_2$	Arf
Magnesio-arfvedsonite	$NaNa_2(Mg_4\ Fe^{+3})Si_8O_{22}(OH)_2$	
Monoclinic magnesium-iron-manganese amphiboles		
Cummingtonite	$\square Mg_2Mg_5Si_8O_{22}(OH)_2$	Cum
Grunerite	$\square Fe_2^{+2}Fe_5^{+2}Si_8O_{22}(OH)_2$	Gru
Oxo-amphiboles		
Kaersutite	$NaCa_2(Mg_3Ti^{+4}Al)(Si_6Al_2)O_{22}O_2$	Krs
Ferro-kaersutite	$NaCa_2(Fe_3^{+2}Ti^{+4}Al)(Si_6Al_2)O_{22}O_2$	
Ferri-kaersutite	$NaCa_2(Mg_3Ti^{+4}\ Fe^{+3})(Si_6Al_2)O_{22}O_2$	

Ferro-ferri-kaersutite $NaCa_2(Fe_3^{+2}Ti^{+4}Fe^{+3})(Si_6Al_2)O_{22}O_2$

1.3 Calculation of the amphibole chemical formula

One of the biggest issues in mineral analysis with the use of the Electron Probe Micro-Analyser (EPMA) has been the determination of the valence state of iron (Droop, 1987; Dyar et al., 1989; Canil et al., 1994; Quinn et al., 2016; Masci et al., 2019). Especially with amphibole, knowing the Fe^{+3}/Fe^{+2} ratio plays a major role not only in the mineral classification and nomenclature but also in its use in fugacity and temperature calculations (Popp et al., 1995, 2006; Lamb & Popp, 2009; Hunt & Lamb, 2019). There are two ways to quantify the amounts of Fe^{+2} and Fe^{+3} present in amphibole; one is to measure it employing sophisticated analytical techniques, the other being to calculate it using stoichiometry arguments.

1.3.1 Analytical versus Empirical techniques for the determination of Fe^{+3}

Analytical techniques involve Electron Energy-Loss Spectroscopy (EELS) and Mössbauer spectroscopy (e.g. Bancroft & Brown, 1975; Enders et al., 2000) which can measure the $Fe^{+3}/(Fe^{+2} + Fe^{+3})$ ratio in minerals quite accurately. The electron-beam intensity in EELS, however, should be carefully controlled so that there is no damage on the analyzed minerals. Both of them are relatively money-efficient and can be routinely used by scientists that are interested in calculating the exact amounts of Fe in amphibole. More expensive techniques involve the X-ray Photoelectron Spectroscopy (XPS) and the X-ray Absorption Near-Edge Structure spectroscopy (XANES) (e.g. Dyar et al., 2002) which can measure the $Fe^{+3}/(Fe^{+2} + Fe^{+3})$ ratio at a scale of $\geq 40\mu m$.

Stoichiometric methods of determining Fe^{+3} are entirely empirical. These methods are based on the assumptions that the anhydrous oxygen content of amphibole is known (usually 23 oxygen ions) and that certain cations are restricted to specific structural sites (Schumacher, 2007). Many different empirical techniques devoted to the calculation of Fe^{+3} in amphibole have been proposed (Stout, 1972; Robinson et al., 1982; Droop, 1987; Jacobson, 1989; Schumacher, 1991; Holland & Blundy. 1994; Leake et al., 1997; Schumacher, 2007). Methods such as those of Schumacher (2007) and Leake et al. (1997) are additionally constrained by the all-ferrous (i.e. $Fe^{+3} = 0$) and all-ferric (i.e. $Fe^{+2} = 0$) chemical limits.

Hawthorne et al. (2012) have proposed a new method of determining $Fe^{+3}/(Fe^{+2} + Fe^{+3})$. Their technique was solely based on site-occupancy limitations

and the electroneutrality principle. According to these authors, an amphibole chemical formula should be calculated based on 24(O, OH, F, Cl) with (OH, F, Cl) = 2 apfu. This procedure enables the derivation of H_2O, therefore yielding more accurate results. Then, the $Fe^{+3}/(Fe^{+2} + Fe^{+3})$ ratio can be calculated by *"constraining the sum of a set of cations to a particular value and adjusting* $Fe^{+3}/(Fe^{+2} + Fe^{+3})$ *for electroneutrality"* (Hawthorne et al., 2012). This is referred to as the electroneutrality principle. Although these empirical methods are still not as accurate as analytical techniques in measuring Fe^{+3}, (Hawthorne et al., 2012; Schumacher, 2007), they are considered to be far better than assuming that $Fe^{+3}/(Fe^{+2} + Fe^{+3}) = 0$ (Hawthorne, 1983).

In the past fifteen years, several computer codes have been developed for the calculation of amphibole formulae using the aforementioned empirical techniques and classification schemes (e.g. Yavuz, 2007; Esawi, 2011). Oberti et al. (2012) have developed the AMPH2012 program which enables the calculation of amphibole formulae based on IMA2012. However, AMPH2012 requires the already calculated cations as an input. For that reason, Locock (2014) developed a new Microsoft Excel spreadsheet to convert compositional data (wt.%) to apfu. His empirical calculation technique follows the Hawthorne et al. (2012) nomenclature and is based on 24 anions (O, OH, F, Cl). The spreadsheet enables the control of a series of parameters which can be significant and can affect the chemical formula of amphibole. For example, the entrance of Ti into the amphibole structure is commonly accompanied by the replacement of OH^{-1} by O^{-2} in site W (i.e. $Ti^{+4} + O^{-2} \leftrightarrow 2\ OH^{-1}$). The spreadsheet allows the option to estimate (OH, F, Cl) = 2-2Ti and from this ^{W}O = 2Ti apfu, so as to handle the anion content at the W site. The spreadsheet also enables the determination of Fe^{+3} according to the electroneutrality principle discussed earlier. To summarise, the spreadsheet developed by Locock (2014) is a program that enables the calculation of amphibole formulae according to the most recent classification scheme.

Ridolfi et al. (2018) have developed a multivariate least-squares analysis method to study the relationship between mass concentration and unit formula of Li-free amphiboles. They have used 114 major-element oxide analyses of calcium and sodium-calcium amphiboles, both synthetic and natural, and 75 analyses of Li-free and Mn-free amphiboles belonging to the C2/m space group that have been fully crystallochemically characterised. Their method enables the calculation of the Fe^{+3} content of amphibole with high precision. Their work suggests that the particular technique provides much more reliable results compared to previous methods.

Recently, a new study has been published in which machine-learning methods have been adopted (Li et al., 2020). In this work, a dataset consisting of 173 Li-free

and 66 Li-bearing amphibole analyses has been compiled. These analyses were carefully selected so that they cover a large compositional range. Only amphiboles that have measured values of $Fe^{+3}/(Fe^{+2} + Fe^{+3})$ by Mössbauer or XANES have been included in order to calibrate the method precisely. This dataset has been used in a machine-learning algorithm which is referred to as principal components regression (PCR) to develop the new calculation method. According to this method, the user has to provide a routine electron-microprobe analysis as an input. The linear regression algorithm then finds the best fitting amphibole from the dataset that is compositionally similar to the analysis that has been entered. Then the algorithm calculates the most possible distribution of atoms in the different sites of amphibole based on the original dataset and from this the most possible value of Fe^{+3}.

1.3.2 Comparison between the available calculation methods

Estimating the minimum (all-ferrous) and maximum (all-ferric) content of Fe^{+3} in amphibole yields a range of possible chemical formulae. For that reason, techniques like those proposed by Leake et al. (1997) and Schumacher (2007) will not be adopted in the present study although they can be useful on certain occasions where samples have been extremely oxidized.

The most recently proposed amphibole nomenclature - that of IMA2012 - requires an overall site assignment of cations that reside on different sites. Some of these cations are very important in the determination of the amphibole subgroup and type. For example, Fe^{+2} and Mg^{+2} must necessarily be distributed between B and/or C sites. Ridolfi et al. (2018) have restricted the distribution of Mg^{+2} and Fe^{+2} exclusively to site C which is a major limitation. This issue has also been pointed out by Li et al. (2020). Although the method proposed by Ridolfi et al. (2018) is very accurate in estimating Fe^{+3}, its use was not deemed appropriate for the purposes of the present work.

Li et al. (2020) presented another rationale for correct cation assignment and accurate determination of Fe^{+3} in amphibole. Their method was tested on our extensive database which comprises 8844 natural and experimental amphibole compositions culled from the literature (). Nearly 140 amphibole entries could not be assigned to any of the available end-member compositions; instead an “error” message was displayed. The stoichiometry of the calculated amphibole formulae was also investigated. An arbitrary error of ± 0.2 was chosen to check the sum of cations in each site. About 650 amphibole entries were returned as non-stoichiometric (Figure 11). The same cation-check procedure was followed in the calculation of amphibole

formulae using the spreadsheet of Locock (2014). This time, only 85 amphiboles were found to be non-stoichiometric. It is possible that the discrepancy between the two methods is due to the rather limited number of amphibole compositions used by Li et al. (2020) in their machine-learning training set.

As Ridolfi et al. (2018) have noted, the method of Locock (2014) underestimates Fe^{+3} when the $^{W}O^{-2}$ calculation is not applied. However, by ignoring $^{W}O^{-2}$, kaersutites (which are oxo-amphiboles) cannot be distinguished from calcium amphiboles. Therefore a kaersutite could be confused with a rootname 4 composition (

Table 1). On the other hand, if the $^{W}O^{-2}$ estimation is applied, kaersutites are easily identifiable. Ridolfi et al. (2018) have also shown that consideration of $^{W}O^{-2}$ in the method of Locock (2014) causes a large overestimation of Fe^{+3}. As a result, many pargasites could erroneously be classified as hastingsites. For the purposes of the present study, it was decided that the $^{W}O^{-2}$ estimation should only be applied to kaersutites. In other words it should only be applied to amphiboles with more than 4.5 wt.% TiO_2 (or more than 0.5 Ti apfu as IMA2012 has also suggested).

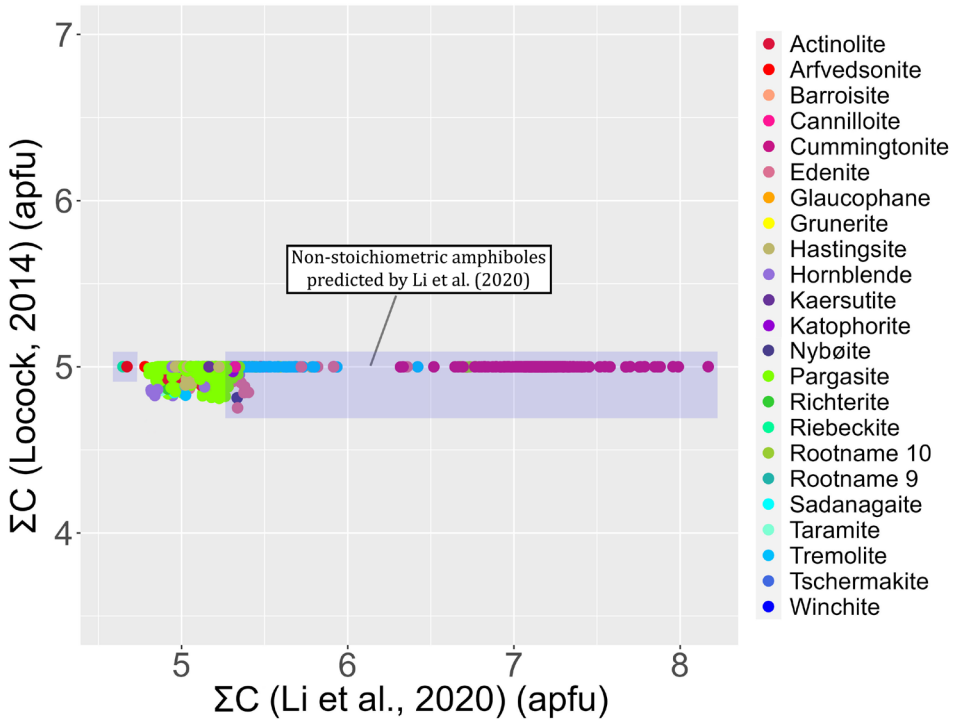

Figure 11: Comparison of ΣC between Li et al. (2020) and Locock (2014). Hornblende is not displayed as magnesio-hornblende as all of the possible compositions are considered.

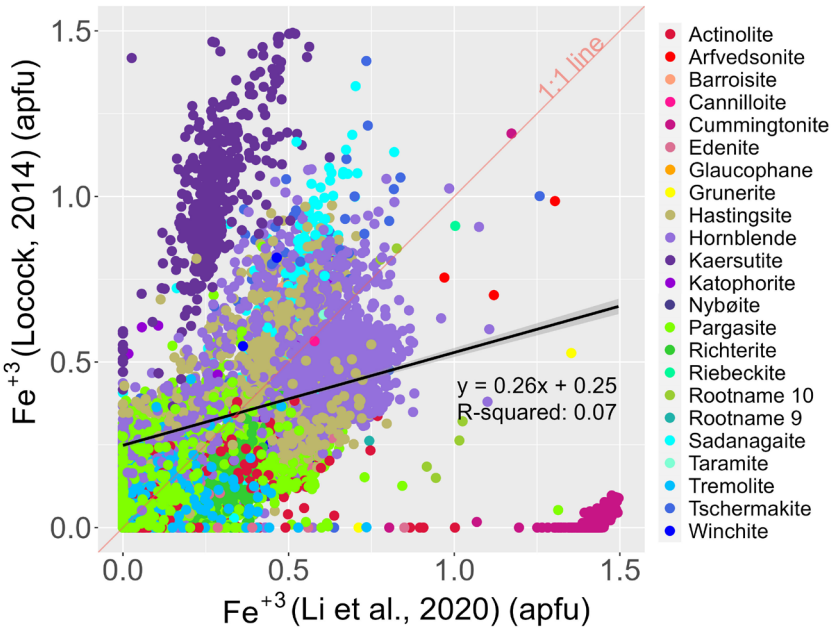

Figure 12: Comparison of Fe^{+3} calculated for the amphiboles of our database using the methods proposed by Locock (2014) and Li et al. (2020). Colors indicate different amphibole root-names. The trendline is represented by a black solid line. Oxygen in site W has only been calculated for kaersutites.

The influence of $^{W}O^{-2}$ in calculating Fe^{+3} is portrayed very vividly in Figure 12 where Fe^{+3} calculated by the methods of Locock (2014) and Li et al. (2020) is presented. Kaersutites are standing out compared to the remainder of the amphiboles because of the Fe^{+3} overestimation mentioned earlier. Pargasites, hornblendes, sadanagaites and hastingsites, to which no $^{W}O^{-2}$ calculation has been applied, seem to be well correlated in terms of Fe^{+3} between the two methods. The method of Locock (2014) slightly overestimates Fe^{+3} in sadanagaites and underestimates Fe^{+3} in tremolites. It is also fairly noticeable that the method of Li et al. (2020) largely overstimates Fe^{+3} in cummingtonite. More than 1 Fe^{+3} apfu is predicted in the chemical formula of the mineral causing all cummingonites to deviate from stoichiometry. This happens because cummingtonitic compositions have not been employed in the training set of the machine-learning algorithm by Li et al. (2020).

Cations in other structural sites show a satisfactory correlation between the two methods (Figure 13). The only important divergence is displayed by the Fe^{+2} content in site C of kaersutites which is clearly understimated by the method of Locock (2014). This, once again, reflects the impact of the $^{W}O^{-2}$ calculation discussed above.

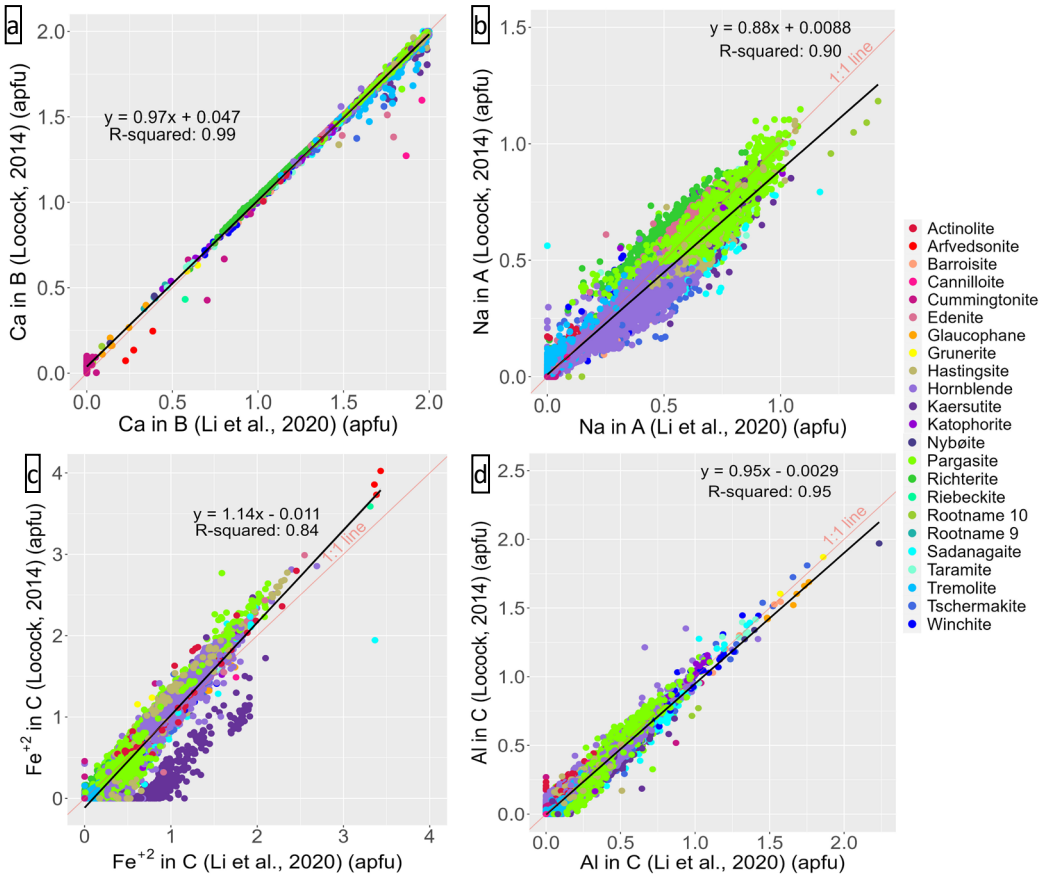

Figure 13: Cation plots for the amphiboles of our database calculated using the methods of Locock (2014) and Li et al. (2020). (a). Ca in B; (b). Na in A; (c). Fe^{+2} in C; (d). Al in C.

In conclusion, machine-learning methods might be at a very premature stage to be fully reliable. This has also been pointed out in other scientific fields as well (e.g. Seifert & Rasp, 2020). The database of this study was constructed using amphiboles from multiple geotectonic settings with an extremely wide compositional range. The method of Li et al. (2020) has compositional limitations and should only be used for amphiboles that strictly fall in its calibration range. For reasons presented earlier, the method of Locock (2014) has been chosen as the most useful and accurate without any compositional dependencies. However, it should be used with caution as Fe^{+3} could either be underestimated or overestimated depending on the choices of the user. Amphiboles that turned out to be non-stoichiometric by the method of Locock (2014) were completely excluded from this study.

References

1. Bancroft G.M., Brown J.R., 1975, A Mössbauer Study of Coexisting Hornblendes and Biotites: Quantitative Fe^{+3}/Fe^{+2} Ratios, American Mineralogist, vol. 60, pp. 265-272.
2. Canil D., O'Neill H.St.C., Pearson D.G., Rudnick R.L., McDonough W.F., Carswell D.A., 1994, Ferric iron in peridotites and mantle oxidation states, Earth and Planetary Science Letters, vol. 123, pp. 205-220.

3. Droop G.T.R., 1987, A general equation for estimating Fe^{+3} concentrations in ferromagnesian silicates and oxides from microprobe analyses, using stoichiometric criteria, Mineralogical Magazine, vol. 51, pp. 431-435.
4. Dyar M.D., McGuire A.V., Ziegler R.D., 1989, Redox equilibria and crystal chemistry of coexisting minerals from spinel lherzolite mantle xenoliths, American Mineralogist, vol. 74, pp. 969-980.
5. Dyar M.D., Lowe E.W., Guidotti C.V., Delaney J.S., 2002, Fe3+ and Fe2+ partitioning among silicates in metapelites: A synchrotron micro-XANES study, American Mineralogist, vol. 87, pp. 514-522
6. Enders M., Speer D., Maresch W.V., McCammon C.A., 2000, Ferric/ferrous iron ratios in sodic amphiboles: Mössbauer analysis, stoichiometry-based model calculations and the high-resolution microanalytical flank method, Contributions to Mineralogy and Petrology, vol. 140, pp. 135-147.
7. Engel A.E.J., Engel C.G., 1962, Hornblendes formed during progressive metamorphism of amphibolites, northwest Adirondack Mountains, Geological Society of America Bulletin, vol. 73, pp. 1499-1514.
8. Ernst W.G., 1968, Amphiboles, Crystal Chemistry, Phase Relations and Occurrence, in Minerals, Rocks and Inorganic Materials, edited by Engelhardt W., Roy R., Winchester J.W., Springer-Verlag New York Inc., vol.1.
9. Esawi E.K., 2011, Calculations of amphibole chemical parameters and implementation of the 2004 recommendations of the IMA classification of nomenclature of amphiboles, Journal of Mineralogical and Petrological Sciences, vol. 106, pp. 123-129.
10. Hawthorne F.C., 1983, The crystal chemistry of the amphiboles, The Canadian Mineralogist, vol. 21, pp. 173-480.
11. Hawthorne F.C., Oberti R., 2006, On the classification of amphiboles, The Canadian Mineralogist, vol. 44, pp. 1-21.
12. Hawthorne F.C., Oberti R., 2007a, Amphiboles: Crystal Chemistry, Reviews in Mineralogy & Geochemistry, vol. 67, pp. 1-54.
13. Hawthorne F.C., Oberti R., 2007b, Classification of the Amphiboles, Reviews in Mineralogy & Geochemistry, vol. 67, pp. 55-88.
14. Hawthorne F.C., Oberti R., Harlow G.E., Maresch W.V., Martin R.F., Schumacher J.C., Welch M.D., 2012, Nomenclature of the amphibole supergroup, American Mineralogist, vol. 97, pp. 2031-2048.
15. Hawthorne F.C., Day M.C., Fayek M., Linthout K., Lustenhouwer W.J., Oberti R., 2022, Ferro-papikeite, ideally $NaFe_2^{+2}(Fe_3^{+2}Al_2)(Si_5Al_3)O_{22}(OH)_2$, a new orthorhombic amphibole from Nordmark (Western Bergslagen), Sweden: Description and crystal structure, American Mineralogist, vol. 107, pp. 306-312.
16. Holland T., Blundy J., 1994, Non-ideal interactions in calcic amphiboles and their bearing on amphibole-plagioclase thermometry, Contributions to Mineralogy and Petrology, vol. 116, pp. 433-447.
17. Hunt L.E., Lamb W.M., 2019, Application of mineral equilibria to estimate fugacities of H_2O, H_2 and O_2 in mantle xenoliths from the southwestern U.S.A., vol. 104, pp. 333-347.
18. Jacobson C.E., 1989, Estimation of Fe^{+3+} from electron microprobe analyses: observations on calcic amphibole and chlorite, Journal of Metamorphic Geology, vol. 7, pp. 507-513.
19. Kretz R. (1983), Symbols for rock-forming minerals, American Mineralogist, vol. 68, pp. 277-279.
20. Lamb W.M., Popp R.K., 2009, Amphibole equilibria in mantle rocks: Determining values of mantle α_{H_2O} and implications for mantle H_2O contents, American Mineralogist, vol. 94, pp. 41-52.
21. Leake B.E., 1968, A catalog of analyzed calciferous and subcalciferous amphiboles together with their nomenclature and associated minerals, Special Papers- Geological Society of America, vol. 98, pp. 1-44.

22. Leake B.E., 1978, Nomenclature of amphiboles, Mineralogical Magazine, vol. 42, pp. 533-563.
23. Leake B.E., Woolley A.R., Arps C.E.S., Bitch W.D., Gilbert M.C., Grice J.D., Hawthorne F.C., Kato A., Kisch H.J., Krivovichev V.G., Linthout K., Laird J., Mandarino J.A., Maresch W.V., Nickel E.H., Rock N.M.S., Schumacher J.C., Smith D.C., Stephenson N.C.N., Ungaretti L., Whittaker E.J.W., Youzhi G., 1997, Nomenclature of amphiboles, report of the subcommittee on amphiboles of the International Mineralogical Association, Commission on new minerals and mineral names, The Canadian Mineralogist, vol. 35, pp. 219-246.
24. Leake B.E., Woolley A.R., Birch W.D., Burke E.A.J., Ferraris G., Grice J.D., Hawthorne F.C., Kisch H.J., Krivovichev V.D., Schumacher J.C., Stephenson N.C.N., Whittaker J.W., 2004, Nomenclature of amphiboles: Additions and revisions to the International Mineralogical Association's 1997 recommendations, The Canadian Mineralogist, vol. 41, pp. 1355-1362.
25. Li X., Zhang C., Behrens H., Holtz F., 2020, Calculating amphibole formula from electron microprobe analysis data using a machine learning method based on principal components regression, Lithos, vol. 362-363, 105469.
26. Locock A.J., 2014, An Excel spreadsheet to classify chemical analyses of amphiboles following the IMA 2012 recommendations, Computers & Geosciences, vol. 62, pp. 1-11.
27. Masci L., Dubacq B., Verlaguet A., Chopin C., De Andrade V., Herviou C., 2019, A XANES and EPMA study of Fe^{3+} in chlorite: Importance of oxychlorite and implications for cation site distribution and Thermobarometry, American Mineralogist, vol. 104, pp. 403-417.
28. Oberti R., Cannillo E., Toscani G., 2012, How to name amphiboles after the IMA2012 report: rules of thumb and a new PC program for monoclinic amphiboles, Periodico di Mineralogia, vol. 81, pp. 257-267.
29. Popp R.K. Virgo D., Yoder H.S., Hoering T.C., Phillips M.W., 1995, An experimental study of phase equilibria and Fe oxy-component in kaersutitic amphibole: Implications for the f_{H_2} and α_{H_2O} in the upper mantle, American Mineralogist, vol. 80, pp. 534-548.
30. Quinn R.J., Valley J.W., Page F.Z., Fournelle J.H., 2016, Accurate determination of ferric iron in garnets, American Mineralogist, vol. 101, pp. 1704-1707.
31. Reznitsky L.Z., Sklyarov E.V., Cametti G., Suvorova L.F., Ushchapovskaya Z.F., Barash I.G., 2018, Vanadio-pargasite $NaCa_2(Mg_4V)(Si_6Al_2)O_{22}(OH)_2$: A New Mineral of the Amphibole Supergroup, Geology of Ore Deposits, vol. 60, pp. 607-615.
32. Ridolfi F., Zanetti A., Renzulli A., Perugini D., Holtz F., Oberti R., 2018, AMFORM, a new mass-based model for the calculation of the unit formula of amphiboles from electron microprobe analyses, American Mineralogist, vol. 103, pp. 1112-1125.
33. Robinson P.R., Hollocher K.T., Tracy R.J., Dietsch C.W., 1982, High grade Arcadian regional metamorphism in south-central Massachusetts, in Guidebook for Fieldtrips in Connecticut and South-Central Massachusetts, edited by Joesten R. & Quarrier S.S., pp. 289-339.
34. Schumacher J.C., 1991, Empirical Ferric Iron Corrections: Necessity, Assumptions, and Effects on Selected Geothermobarometers, Mineralogical Magazine, vol. 55, pp. 3-18.
35. Schumacher J.C., 2007, Metamorphic Amphiboles: Composition and Coexistence, Reviews in Mineralogy & Geochemistry, vol. 67, pp. 359-416.
36. Seifert A., Rasp S., 2020, Potential and Limitations of Machine Learning for Modeling Warm-Rain Cloud Microphysical Processes, Journal of Advances in Modeling Earth Systems, vol. 12, e2020MS002301.
37. Stout J.H., 1972, Phase Petrology and Mineral Chemistry of Coexisting Amphiboles from Telemark, Norway, Journal of Petrology, vol. 13, pp. 99-145 .
38. Warren B.E., 1929, The structure of tremolite, Zeitschrift fur Kristallographie, vol. 72, pp. 42-57.
39. Yavuz F., 2007, WinAmphcal: A Windows program for the IMA-04 amphibole classification, Geochemistry, Geophysics, Geosystems, vol. 8, Q01004.

CHAPTER 2
Geotectonic settings related to amphibole-bearing ultramafic rocks

Amphibole is found in ultramafic rocks in the vast majority of geotectonic settings around the globe. From mantle xenoliths to peridotitic massifs, the presence of amphibole signifies the operation of some major processes that are responsible for its formation in the upper mantle. In the following section, the most important characteristics of the geotectonic settings in which amphibole is observed in ultramafic rocks will be briefly discussed. This is going to enable a terminology clarification that will facilitate the discussion later on in the study.

2.1 Mantle xenoliths

Mantle xenoliths represent lithospheric chunks picked up by magmas en route to the surface. It was until the pioneering work of Fermor (1913) and Wagner (1914) that xenoliths started being recognized as coming from the lithospheric mantle. Because they are rapidly carried to the surface, their geochemical and mineralogical characteristics remain basically unaltered. However, in certain occasions they appear to have been infiltrated by fluids/melts or to have reacted with their carrier magma. These processes alter their chemical/mineralogical composition. Nonetheless, mantle xenoliths represent “frozen” samples of the interior of the planet and as such they provide critical information on the chemical and physical characteristics of the upper mantle. This, in turn, provides insights into the thermal state and the properties of the lithosphere (crust and upper mantle).

Mantle xenoliths are nodule-shaped ranging in size from a few millimeters to even 1 meter across. Their host rocks are mostly alkali olivine basalts/basanites, tholeiitic basalts, and calc-alkaline effusives (e.g. andesites to dacites) depending on the geotectonic setting. Basanites are basalts with porphyritic texture (large crystals in a fine-grained matrix) that contain calcic plagioclase, clinopyroxene, olivine, nepheline, leucite and on several occasions analcime. Kimberlites can also be important carriers of mantle xenoliths as will be discussed later. These rocks are thought to transfer peridotitic samples from greater depths than those of basaltic compositions. Single, coarse-grained amphibole crystals can also be transported by the host melts individually. These crystals represent a unique type of mantle xenoliths (amphibole megacrysts).

2.1.1 Mantle xenoliths in intra-cratonic settings

Intra-cratonic settings are often accompanied with the occurrence of kimberlitic rocks that contain amphibole-bearing mantle xenoliths. Cratons are old continental regions that are tectonically and magmatically inactive. They represent the nucleus of continents. Kimberlites are complex, volatile-rich, potassic ultramafic rocks generated at great depths, beyond the graphite-diamond transition, that mostly contain olivine, ilmenite, garnet, clinopyroxene, phlogopite, orthopyroxene and chromite. Kimberlite-borne mantle xenoliths have been divided into two distinct groups: a low-temperature group with coarse-grained texture and a high-temperature group with fine-grained texture due to shearing deformation.

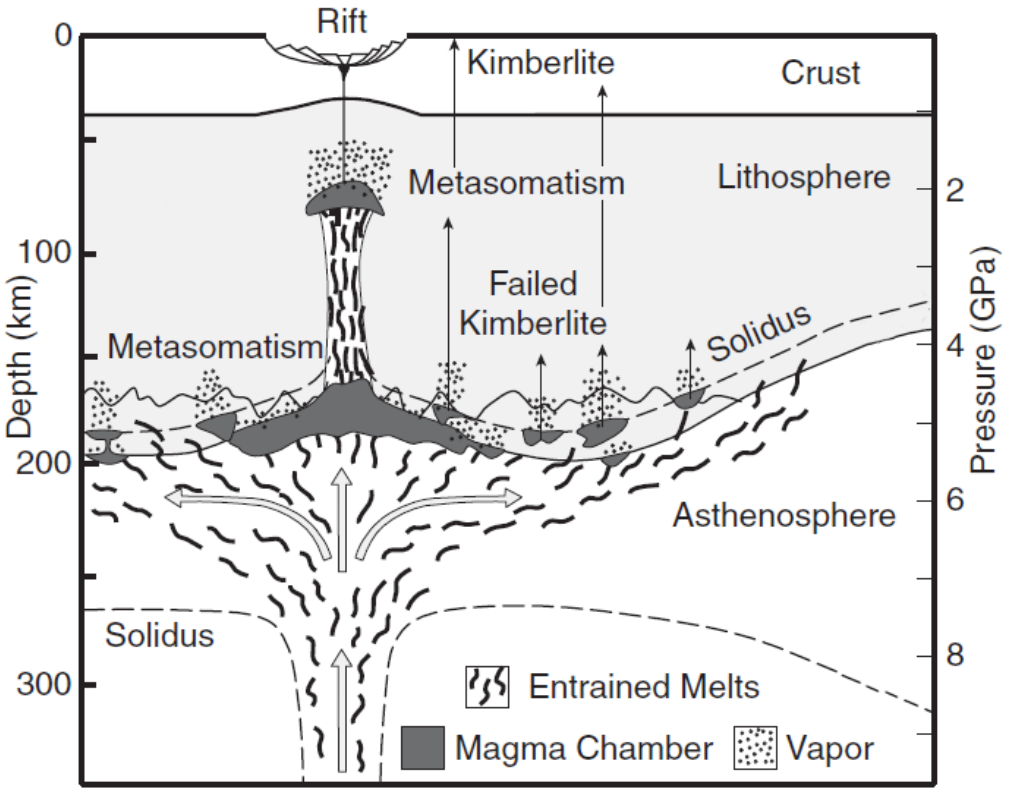

Figure 2.1: Sketch showing a mantle plume impinging upon the base of the continental lithosphere and causing rifting along with the generation of kimberlitic melts. Modified after Wyllie (1988a) and Wyllie et al. (1990). Notice that some kimberlitic melts fail to reach the crust.

As kimberlites ascent in intra-cratonic regions, they often sample parts of the subcontinental lithospheric mantle (Figure 2.1) which could also be diamondiferous. The Jagersfontein pipe in the Kaapvaal craton, South Africa, is an example of kimberlitic magmatism that has transported mantle xenoliths from great depths

(Haggerty & Sautter, 1990; Winterburn et al., 1990; Sautter et al., 1991). The calculated equilibrium pressure for the Jagersfontein mantle xenoliths is ~4.5 GPa (Winterburn et al., 1990), equivalent to more than 150km depth. Other Kaapvaal pipes such as Kimberley and Lesotho contain amphibole-bearing xenoliths (Simon et al., 2007). A peculiar type of xenolith in cratonic regions is the so-called MARID suite (Dawson & Smith, 1977). The most well-studied MARID xenoliths are located in South African kimberlites from Bultfontein, Wesselton, De Beers and Kamfersdam (Dawson & Smith, 1977; Fitzpayne et al., 2018). A MARID xenolith is a rock composed of mica, amphibole, rutile, ilmenite and diopside. In terms of composition, it is an ultramafic to ultrapotassic rock with K_2O ranging from 4.0 to 9.5 wt%.

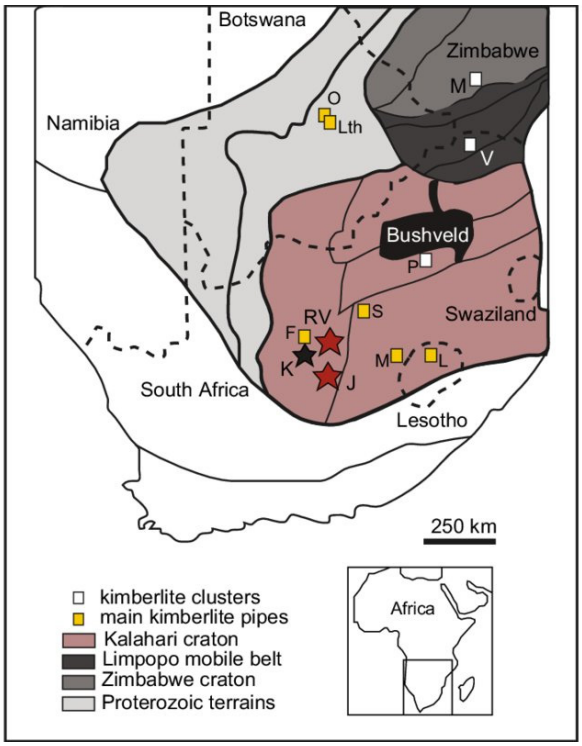

Figure 2.2: Kimberlitic localities in South Africa. K. Kimberly cluster; P. Premier/Cullinan cluster; M. Murowa/Sese kimberlite; V. Venetia kimberlite cluster; RV. Roberts Victor mine; F. Finsch; J. Jagersfontein mine; S. Star; L. Letseng; M. Monastery; O. Orapa; Lth. Letlhakane

2.1.2 Mantle xenoliths in continental rift-related settings

Rift-related regions in intra-plate settings are dominated by spinel-lherzolite (olivine + orthopyroxene + clinopyroxene + spinel) mantle xenoliths which are usually hosted in basanitic, tholeiitic or alkali-basaltic rocks. Spinel lherzolites often carry hydrous minerals such as amphibole, phlogopite and, rarely, apatite. The East African Rift system was amongst the first locales where the concept of continental rifting was applied. The rifting of continental lithosphere may be the result of

complex tectonic processes that usually have acted during the recent geological past. Rifting could occur at locations where incipient plate divergence is taking place (e.g. eastern Africa). Continent-continent post-collision or post-subduction processes could also result in the generation of a rift system as exemplified by the Rhine Graben, Germany. Under such extensional settings small localized volcanic centers dominated by alkali-rich melts are generated. These magmas sample the subcontinental mantle from depths ranging between 35 and 80km, by transporting xenoliths to the surface. However, tholeiitic basalts in rift-related regions are not uncommon and they are usually accompanied by voluminous magmatic activity that is most likely related to a mantle plume (flood basalts).

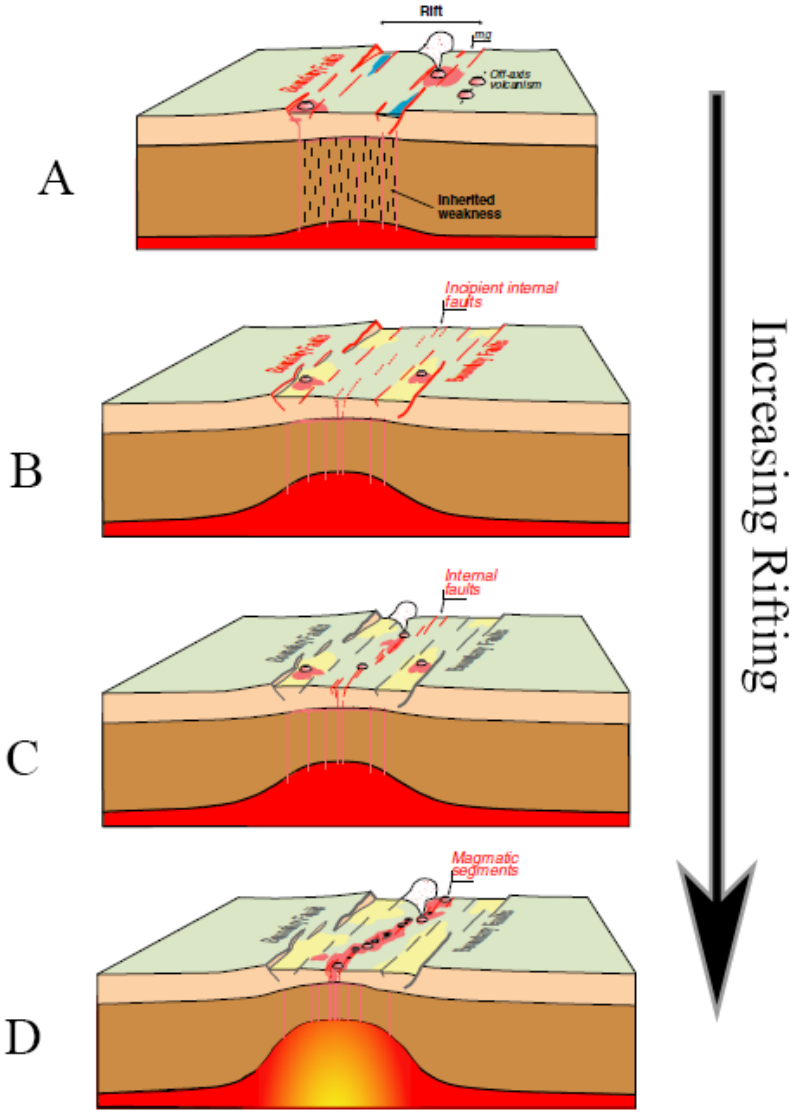

Figure 2.3: Results of numerical modelling aiming to describe the continental rifting of the Main Ethiopian Rift (modified after Corti, 2011). Notice the progressive upwelling of the mantle and the thinning of the continental lithosphere.

But what exactly causes continental rifting? This is a problem that shows many complications (e.g. Armitage et al., 2010). Generally, there are two types of continental rifting, active and passive. During active rifting, extensional stresses are generated from the upwelling and expansion of mantle material (e.g. mantle plume) which is impinging upon the base of the continental lithosphere (Figure 2.1 & Figure 2.3). The rising asthenosphere delaminates the base of the lithosphere due to heat convection. Passive rifting is defined by extensional stresses that are generated by plate tectonics at plate boundaries (i.e. plate-related far-field forces). On many occasions such as the East African Rift system, the two aforementioned processes contribute together to form the appropriate continental rifting conditions. Similarly, the Massif Central volcanic field, France, is believed to have experienced both active and passive rifting (Michon & Merle, 2001). The West Eifel volcanic field, on the other hand, is thought to lie directly above a region of diapirically upwelling mantle (mantle plume) according to Keyser et al. (2002) and Ritter et al. (2001).

Some of the most well studied rift-related, amphibole-bearing mantle xenoliths are those from Nushan, China (Xu et al., 1997; Xu et al., 1998; Xu & Bodinier, 2004), West Eifel, Germany (Witt-Eickchen & Harte, 1994; Shaw & Klugel, 2002; Ban et al., 2005; Shaw et al., 2005; Hecker et al., 2020), Victoria, Australia (Stolz & Davies, 1988; Sutherland & Hollis, 1982; O'Reilly et al., 1991; Griffin et al., 1984; Powell et al., 2004; Bonadiman et al., 2021) and Grand Canyon, United States of America (Best, 1970; Best, 1974; Best, 1975; Alibert, 1994; Hunt & Lamb, 2019). Some other less noticed rift-related xenoliths are exposed in Cerro Gordo in Spain (Villaseca et al. 2020), Massif Central in France (Uenver-Thiele et al., 2014), Wilcza Góra in Poland (Matusiak-Malek, 2017), Nograd-Gomor, Szigliget and Szentbekalla in Hungary (Liptai et al., 2017; Ntaflos et al., 2017; Bali et al., 2018), Marsabit in Kenya (Kaeser et al., 2007), Teria in Algeria (Kaczmarek et al., 2016), Jabel El Arab in Syria (Ismail et al., 2008), Spitsbergen in Norway (Ionov et al., 2002), Foster crater in Antarctica (Gamble et al., 1988), Injibara in Ethiopia (Ferrando et al., 2008; Frezzotti et al., 2010) and Damara in Namibia (Baumgartner et al., 2000). It is noted that some of these localities (e.g. Nushan and Cerro Gordo) show evidence of subduction-related processes in the past but they are presently lying on intra-continental regions of thinned lithosphere.

2.1.3 Mantle xenoliths in oceanic volcanic rocks

The suboceanic lithospheric mantle is usually investigated via the geochemistry of its partial melts. However, ultramafic amphibole-bearing mantle xenoliths are rarely found in oceanic volcanic rocks and are useful when no other piece of information is available. In the Hawaiian volcanic chain, which is an active

hotspot, mantle xenoliths are often hosted in basaltic rocks but rarely contain amphibole. On the contrary, xenoliths from Malaita (Solomon Islands) are amphibole-bearing and are thought to sample the mantle lithosphere beneath the Ontong-Java oceanic plateau. Malaitan xenoliths are showing some unique characteristics and have been explained with the involvement of a mantle plume (Neal, 1988). Mantle xenoliths from the Kerguelen Islands involve another locality where the suboceanic lithospheric mantle is sampled by intraplate volcanic rocks related to a mantle plume (Grégoire et al., 2000; Moine et al., 2001 and references therein).

2.1.4 Mantle xenoliths in subduction zones

Amphibole-bearing ultramafic xenoliths can also be found in subduction zone settings where oceanic lithosphere dives under continental (continental arc/active continental margin) or oceanic (oceanic arc) lithosphere. In such settings, the subducting slab is dehydrated due to the increasing P-T conditions. The generated fluids hydrate the overlying mantle wedge which then partially melts. During their ascent towards the surface, the melts are sampling peridotitic xenoliths from the mantle wedge. Amphibole-bearing xenoliths from continental arcs, for example, have been extensively studied in Kamchatka peninsula, Russia (Kepezhinskas et al., 1995; Ishimaru, 2007; Ishimaru & Arai, 2008; Ionov, 2010; Bénard & Ionov, 2013; Siegrist et al., 2019) and in the Adak Island, Aleutian arc (e.g. Debari et al., 1987). The continental arc is not the only region where magmatism occurs in this geotectonic setting. Xenolithic localities from the western United States of America (e.g. Dish Hill, Cima, Deadman Lake) are currently lying in a suprasubduction-zone position and show the influence of the subduction zone (Luffi et al., 2009). Therefore, they are also considered to belong to the same category of mantle xenoliths. However, according to Luffi et al. (2009), the back-arc region of this subduction-zone system is experiencing extension which results to a magmatism with different geochemical characteristics and isotopic signatures. This extension has been explained by the slab breakoff of the Farallon oceanic lithosphere (Figure 2.4) which generated a rifting domain on the overlying North American slab. Another occasion of a continental back-arc is located in Gobernador Gregores, Southern Patagonia (e.g. Laurora et al., 2001). On the other hand, amphibole-bearing xenoliths from intraoceanic arcs have been observed and widely investigated in the Luzon arc of Philippines (Gregoire et al., 2008; Yoshikawa et al., 2016; Payot et al., 2018; Valera et al., 2019) and Papua New Guinea (Gregoire et al., 2001; McInnes et al., 2001; Franz et al., 2002; Bénard et al. 2021).

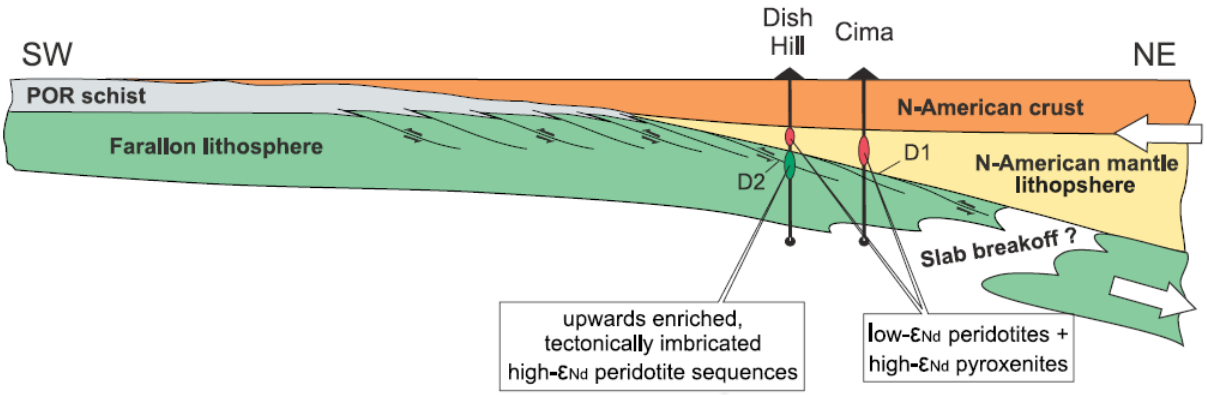

Figure 2.4: The subducting system of the western United states where the oceanic Farallon slab is subducting under the North American lithosphere (Luffi et al., 2009).

2.2 Ophiolites

Ophiolites represent slivers of ancient oceanic lithosphere obducted on top of continental or oceanic crust (Nicolas & Boudier, 2003). Amphibole is often found in the mantle section of ophiolites, mostly in harzburgites, and it is usually of tremolitic to actinolitic composition as will be shown later. Some examples involve the Xigaze ophiolite in Tibet (Tian et al., 2022), the Lycian, Kizilirmak and Küre ophiolites in Turkey (Celik et al., 2018; Pan et al., 2022), Mt. Kalnik in Croatia (Slovenec & Segvic, 2018), the Oeyama and Ohsa-yama ophiolites in Japan (Nozaka & Shibata, 1995; Nozaka, 2014), the Hagar Dungash and the Gerf ophiolites in Egypt (Abdel-Karim et al., 2016; Moussa et al., 2022) and the Yungbwa Ophiolite in Tibet (Liu et al., 2010). Amphibole inclusions in chromite from ophiolitic chromitites have been noticed in many important ophiolites around the world such as the Lycian and Kop ophiolites in Turkey (Uysal et al., 2007; Pan et al., 2022), the Semail Ophiolite in Oman (Borisova et al., 2012) and the Tiebaghi ophiolite in New Caledonia (Johan et al., 2017; Cluzel et al., 2022). Amphiboles have, additionally, been found in ophiolitic dunites from the Semail ophiolite in Oman (Rospabé et al., 2018).

2.3 Alpine-type peridotites

Orogenic peridotite massifs or Alpine-type peridotites represent large bodies of ultramafic composition that have been equilibrated in the garnet-, spinel- or plagioclase-peridotite stability fields. They do not represent ophiolites as they lack of the complete ophiolitic sequence or any characteristics that could indicate that origin. Instead, they are considered as 'tectonically emplaced' mantle rocks that occur as dispersed bodies of a few meters to kilometers in metamorphic rocks, in suture zones and mountain belts. This theory started emerging at the end of the 1950s (De

Roever, 1957; Dietz, 1963; Hess, 1962). Alpine-type peridotites are now widely thought to be remnants of the subcontinental lithospheric mantle that have been exhumed to the surface during orogeny. They are often affected by deformation and recrystallization processes and on several occasions, they have experienced UHP metamorphism. However, there is still a lot of controversy about their original geotectonic setting and the processes that have led to their exhumation. This uncertainty is a major disadvantage compared to mantle xenoliths.

Alpine-type peridotites are dominated by garnet- or spinel- lherzolites that contain more than 10 % clinopyroxene and show variable amounts of serpentinization. Subordinate harzburgites and mafic layers may also be present but only in minor amounts compared to the main lherzolitic bodies. Finero in the Italian Alps is, however, an exception as it is mainly comprised of phlogopite- and amphibole-rich harzburgites. Dunites, hornblendites, glimmerites (mica + clinopyroxene) and pyroxenites are also evident as dikes or veins in some Alpine-type peridotites and they usually have a melt/fluid-rock interaction origin (e.g. Gysi et al., 2011; Mazzucchelli et al., 2009). Several Alpine-type bodies have been intruded by shallow volcanic rocks which are thought to represent an embryonic oceanic crust. This type of orogenic peridotites is considered to belong to a transitional lherzolitic category (Müntener et al., 2005).

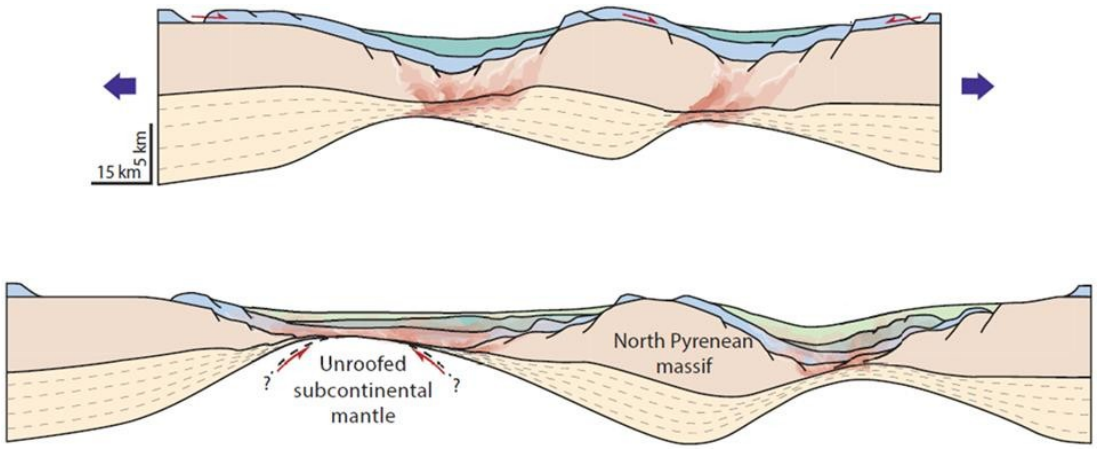

Figure 2.5: The exhumation of the Pyrenean subcontinental lithospheric mantle due to the weakening and continuous thinning of the continental crust (Clerc er al., 2015).

Alpine-type peridotites can be divided into two major groups based on the tectonic processes that are responsible for their exhumation on the surface. The exhumation of peridotites such as those in the Pyrenean orogenic belt (e.g. Lherz and Caussou), have been explained by the initial weaking and thinning of the continental crust and the subsequent exposure of the subcontinental lithospheric mantle (Clerc et al., 2015). A schematic representation of this process is presented in Figure 2.5. On the other hand, the exhumation of Alpine-type peridotites from the Italian and the

Swiss Alps, China and the Norwegian Caledonides has been a subject of constant debate. These peridotites show evidence of equilibration at mantle conditions followed by a progressive decrease in temperature and pressure (Brueckner, 2017 and references therein). One of the most accepted models involves active subduction and subsequent continental convergence. The geometrical configuration of the subduction zone enables the entrainment of peridotitic fragments from the mantle wedge into the continental subducting slab (Figure 2.6). Then, the continental slab containing the peridotitic inclusions is exhumed towards the surface due to complicated tectonic processes and is found along the orogenic suture zone. Recently, a new theory has been proposed to explain the ultra-high pressure mantle rocks from the Bohemian Massif of Central Europe (Maierova et al., 2021). The authors predicted the initial, deep subduction of continental crust which was later exhumed as a partially molten lithospheric diapir as depicted in Figure 2.7.

Bodinier & Godard (2003) have subdivided Alpine-type peridotites into three main categories. The High-Pressure (HP) and Ultra-High-Pressure (UHP) resemble garnet peridotites and are mostly found in Central Alps (Alpe Arami, Cima di Gagnone, Ulten), China (Dabie and Su-Lu peridotites, North Qaidam), the Western Gneiss Region in Norway and the European Variscan belt (e.g. Bohemian Massif). These peridotites are often surrounded by eclogites. They show evidence of equilibration at great depths. However, the geotectonic setting of formation along with the maximum depth of equilibration for these peridotites is still a matter of debate.

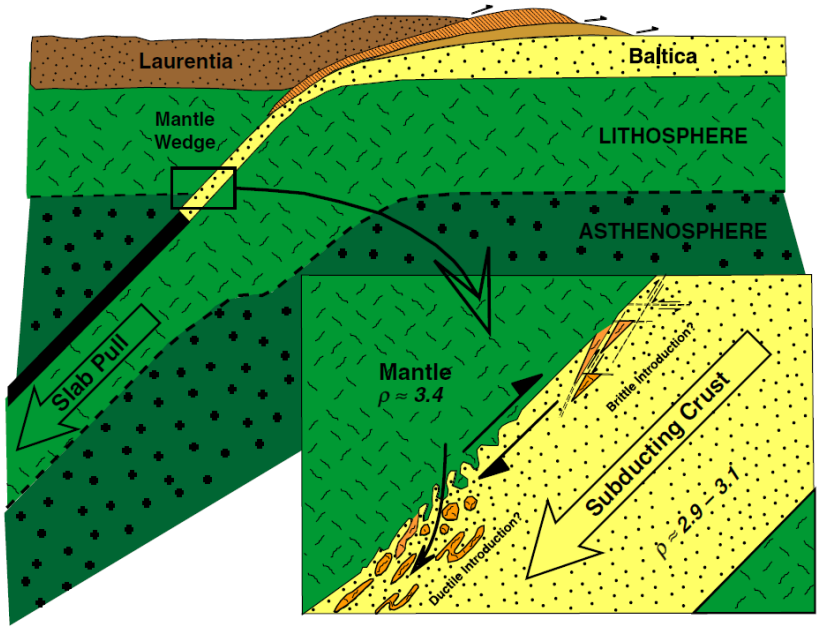

Figure 2.6: Schematic model presenting a possible solution to the exhumation of the Norwegian Caledonides (Brueckner, 2017).

From the aforementioned localities, Alpe Arami has attracted the most attention. Interpretations began with Grubenmann (1908) and Dal Vesco (1953) who suggested that Alpe Arami represents an ultramafic melt that intruded the continental crust. Ernst (1977, 1981) stressed the fact that Alpe Arami has been derived from the upper mantle and has been tectonically inserted in the lithospheric crust. From 1997 and onwards a series of papers were published supporting an ultra-deep origin for Alpe Arami from the subcontinental lithospheric mantle (>300 kms) (Green et al., 1997; Dobrzhinetskaya et al., 1999; Bozhilov et al., 1999; Green et al., 2010; Das & Basu, 2019). However, the validity of their arguments was questioned by Ulmer & Trommsdorff (1997), Risold et al. (1997), Arlt et al. (2000), Paquin (2001) and Nimis & Trommsdorff (2001) who positioned Alpe Arami at a considerably shallower depth (~150 kms) using mostly experimental petrology and thermodynamic arguments. From this discussion, it is fairly evident how controversial the origin of UHP Alpine-type peridotites can be.

Intermediate-Pressure (IP) peridotites are several massifs that have equilibrated in the spinel stability field. Their derivation from the subcontinental mantle is less debatable than the UHP peridotites. Examples of these massifs include Ronda and Beni Bousera in Morocco, several Pyrenean localities and the Ivrea localities in the Italian Alps. In the Pyrenees, the Lherz spinel lherzolite has been a matter of extensive study throughout the years (Bodinier & Godard, 2003 and references therein). Baldissero, Balmuccia and Finero are several well-known

examples of IP peridotites in the Alps and are considered to represent asthenospheric mantle that was emplaced in the continental crust during late Paleozoic or early Mesozoic (Quick et al., 1995).

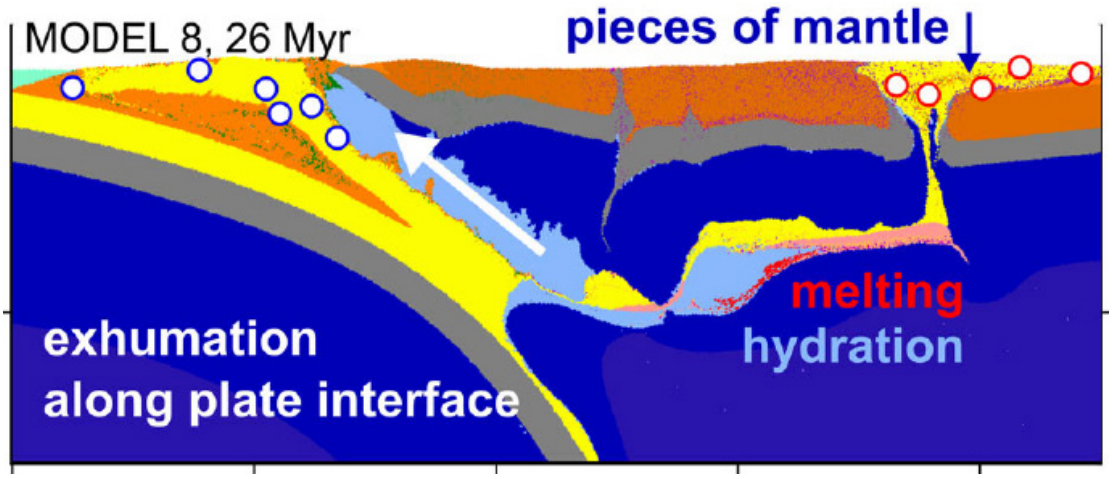

Figure 2.7: Numerical model representing a possible process for the exhumation of UHP (Ultra-High-Pressure) rocks (Maierova et al., 2021).

Many Low-Pressure (LP) peridotitic massifs can be found at the suture zone between the Southern Alpine and European plates. It is thought that they represent ultramafic bodies that were exhumed during the early stages of a continental rifting event and were exposed along continental passive margins (Bodinier & Godard, 2003 and references therein). It is predicted that they were later involved in the Alpine orogenesis. Therefore, they could generally be classified as continental margin ophiolites (CM). Some typical localities involve the Val Malenco, Mt. Avic, the external Ligurides and the Lanzo peridotites. Spinel- and plagioclase-peridotites that are found in these massifs are often intruded by small bodies of gabbroic, acidic rocks and basaltic dikes with a MORB affinity (e.g. Kaczmarek et al., 2008; Rampone & Borghini, 2008; Piccardo & Guarnieri, 2011). However, LP peridotites do not show a clear ophiolitic sequence and they display characteristics intermediate between Alpine-type peridotites and ophiolites. Considering the interplay of both oceanic and continental processes, the absence of a continuous basaltic crust overlying the peridotites and the fertile composition of the peridotites, both Lanzo and the external Ligurides ultramafic bodies are considered as Alpine-type peridotites which is a broader and less strict characterization. However, it is noted that this distinction is somewhat arbitrary.

Amphibole-, plagioclase- and spinel-bearing peridotites are hosted in crustal granulitic rocks at the Zabargad island. Zabargad is located at a very unique position in the middle of the Red Sea. It is therefore directly related to continental rifting

processes and the formation of a new oceanic basin. As it is clear, it does not belong to Alpine-type peridotites because it has not been part of an orogenetic episode. However, as most Alpine-type peridotites, it is widely considered a sample of the subcontinental lithospheric mantle (Brueckner et al., 1988; Dupuy et al., 1991; Piccardo et al., 1988, 1993) although other theories have also been proposed (e.g. Nicolas et al., 1987). The location of the Zabargad peridotites near a passive continental margin (Martinez & Cochran, 1988), its exhumation history, the reequilibration in the plagioclase stability field and the existence of MORB and doleritic dikes (e.g. Petrini et al., 1988) have led Bodinier & Godard (2003) to include Zabargad in the LP peridotites. This classification will also be adopted in the present study.

Amphibole is found in all of the previously mentioned categories of Alpine-type peridotites. For example, amphibole has been widely discussed in UHP garnet-lherzolites and pyroxenites from Su-Lu and Raobazhai in China (Yang & Hahn, 2000; Yang, 2003; Zhao et al., 2007; Chen et al., 2009; Ye et al., 2009; Zhang et al., 2011; Yan et al., 2021; Liu et al., 2022), peridotitic massifs in Switzerland such as Alpe Arami, Cima di Gagnone and Monte Duria (Green et al., 1997; Nimis & Trommsdorff, 2001; Paquin & Altherr, 2001; Hermann et al., 2006, Scambelluri et al., 2014; Pellegrino et al., 2020), North Qaidam in Tibet (Song et al., 2005; Chen et al., 2017), multiple localities in Western Gneiss Region of Norway (Carswell et al., 1983; Beyer et al., 2006; Vrijmoed et al., 2013) and Nove Dvory in Czech Republic (Muriuki et al., 2020). Amphibole is also present in IP peridotitic massifs such as Beni Bousera in Morocco (El Atrassi et al., 2014), Lherz and Caussou in the Pyrenees (Conquéré, 1971; Fabriès et al., 1989) and Balmuccia, Finero and Baldissero in Italy (Cawthorn, 1974; Zanetti et al., 1999; Mazzucchelli et al., 2009; Mazzucchelli et al., 2010; Corvò et al., 2020; Hecker et al., 2020). Finally, examples of LP amphibole-bearing peridotite massifs involve the external Ligurides (Hidas et al., 2021) and Lanzo in Italy (Kaczmarek & Müntener, 2008; Duarte et al., 2020). It is, therefore, evident that amphibole is an important phase in Alpine-type peridotites.

2.4 Oceanic Core Complexes

According to Whitney et al. (2013), a core complex is "*a domal or arched geologic structure composed of ductilely deformed rocks and associated intrusions underlying a ductile-to-brittle high-strain zone that experienced tens of kilometers of normal-sense displacement in response to lithospheric extension"*. The concept of core complexes started in order to explain continental rocks bounded by low-angle faults in the North American Cordillera (e.g. Davis & Coney, 1979). The low-angle

faults (also known as detachment faults) were thought to be related with extensional tectonics that led to the exhumation of those rocks to the surface. Oceanic Core Complexes (OCCs) are similar structures that were firstly identified in Mid-Atlantic Ridges (e.g. Cann et al., 1997) (Figure 2.8). Although the logistics of investigating OCCs is an important problem, many of them have been explored in the Mid-Atlantic Ridge (e.g. St. Paul rocks), the Southwest Indian Ridge and also at back-arc positions such as in the Godzilla and Mado Megamullion (Philippine Sea). The exhumed rocks in OCCs are usually mantle-derived. Therefore, OCCS display unique opportunities to understand processes related to the suboceanic mantle from oceanic environments around the globe.

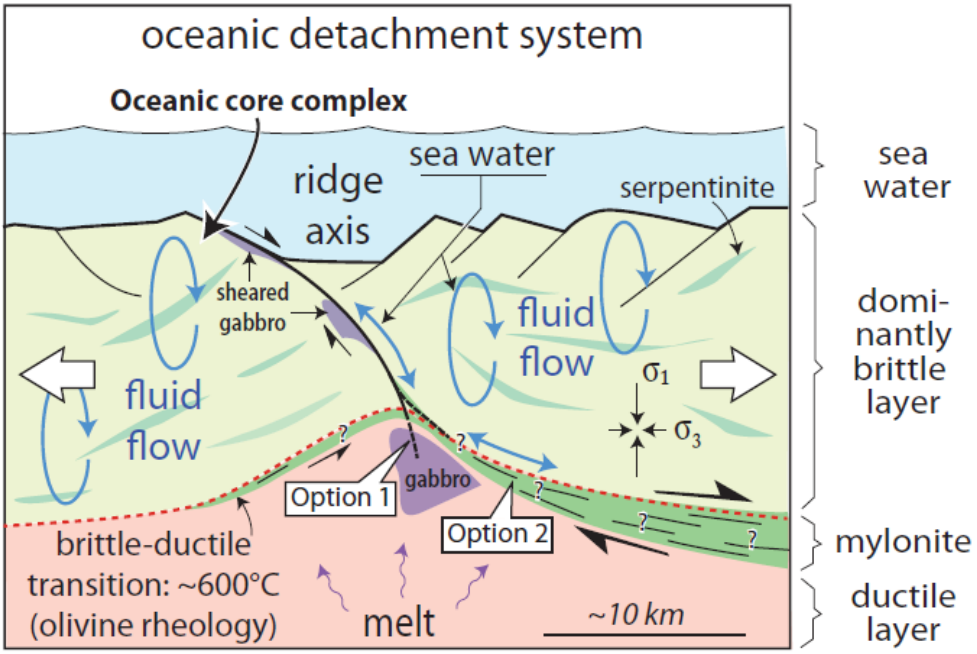

Figure 2.8: Sketch depicting the main characteristics of an Oceanic Core Complex (after Whitney et al., 2013).

An Oceanic Core Complex is defined by the existence of a detachment fault. In turn, this detachment fault consists of a hanging-wall and a footwall (Figure 2.8). The detachment fault usually serves as a conduit for fluids to hydrothermally alter the hanging-wall. (e.g. McCaig & Harris, 2012). The detachment fault consists of two zones principally: one which is defined by brittle deformation (<200 m thick according to Escartín et al., 2003) and an underlying one which shows evident signs of ductile deformation which may or may not be overprinted by brittle textures (Schroeder & John, 2004). Ductile zones are characterized by peridotitic mylonites which are fine-grained rocks that have recrystallized because of the high-stress conditions. Shallow parts of the detachment zone may also be extensively hydrated and could contain talc, amphibole, chlorite and serpentine. The footwalls of OCCs are mostly comprised of variably altered gabbroic and ultramafic rocks which often

exhibit sings of mylonitic deformation. The footwall is practically the part of the OCC that contains all of the important mantle rocks that have been exposed to the surface and give us information about the suboceanic mantle.

Significant amounts of amphibole are found in peridotitic rocks from OCCs around the globe. The Atlantis and Saint Paul OCCs are two particularly well-studied localities in which amphibole has been found in mylonitic peridotites (Tilley & Long, 1967; Melson et al., 1972; Tamura et al., 2008; Tamura et al., 2014). Albers et al. (2019) and Cannat & Seyler (1995) have also investigated amphibole-bearing ultramafic rocks from the footwalls of the 15°20'N Fracture Zone and the Vema Transform Fault in Mid-Atlantic Ridge, respectively. The Mado Megamullion in the Shikoku Basin is a great example of an OCC that is related to an extensional tectonic regime at a back-arc position. Amphibole in Mado Megamullion was found in serpentinized mantle peridotites that exhibited extensive deformation from Sen et al. (2021). Finally, the Hess Deep represents a < 1 Ma oceanic lithosphere in the East Pacific Rise which was exposed after the activation of a detachment zone. The Hess Deep, is comprised of highly serpentinized, amphibole-bearing harzburgites but dunites are also present (Kodolanyi et al., 2011).

2.5 The Pechenga ultramafic rocks

A particularly interesting and unique occurrence of ultramafic rocks is that of the Pechenga Greenstone Belt. The ultramafic rocks are found in the Pilgüjarvi Volcanic and Sedimentary Formations as well as in the Nyasyukka dyke complex. The Pilgüjarvi Volcanic Formation mainly consists of tholeiites and intrusive ferropicrites. Picrites are igneous intrusive rocks of ultramafic composition that contain olivine, clinopyroxene and often plagioclase, hornblende and biotite. In the Pechenga Greenstone Belt, the ferropicrites contain more than 14 wt % FeO_{tot} and almost 15 wt % MgO. Effort has been made to understand the petrology and origin of the Pechenga ferropicrites (e.g. Brügmann et al., 2000). The Sm-Nd and Pb-Pb isotopic results of Hanski et al. (1990) and Hanski (1992) demonstrated that the Pechenga ferropicrites are derived from a mantle source but the contamination with ancient upper-crust material is also evident.

Fiorentini et al. (2008) investigated amphiboles that are contained in the ultramafic rocks of the Pechenga Greenstone belt. More specifically, the aforementioned amphiboles are found in a wehrlite-olivinite zone that is part of the Pilgüjarvi layered intrusion. Olivinite is a term that is used to describe a magnetite-bearing dunite. The wehrlite-olivinite zone is made of pyroxenites, wehrlites and pyroxene-bearing olivinites. Amphibole is also present in layered ultramafic sills in

the Ortoaivi, Kotselvaara and Kammikivi localities which are hosted in sulfur-poor phyllites. The ultramafic sills are mostly cumulates that contain olivine, chrome-spinel and amphibole. Additionally, amphiboles were examined from ferropicritic layered lava flows and peridotites from the Nyasyukka dyke complex. These peridotites are thought to be cumulative in origin and contain medium- to coarse-grained olivine, amphibole, plagioclase and clinopyroxene. Fiorentini et al. (2008) proposed that the Pechenga ferropicrites could be derived either from a volatile-rich subcontinental mantle or a mantle plume. Additionally, they disregarded the fact that amphiboles in intrusive rocks are related to crustal contamination.

The Pechenga magmatic activity has been previously related to intra-cratonic rifting owing many similarities with the Ethiopian rift (e.g. Kremenetsky & Ovchinnikov, 1986; Sharkov, 1984; Barbey et al., 1984). However, Marker (1985) has proposed a geotectonic evolution from continental rifting to a subduction zone to an arc-continent collision event but this model was later questioned (e.g. Hanski & Smolkin, 1989). According to Pharaoh et al. (1987), the Pechenga volcanics had been erupted at a continental arc but this is contrast with their within-plate geochemical signature (Hanski & Smolkin, 1989). It is profound that the formation of the Pechenga ultramafic rocks is a very complex subject which has not been resolved yet. Therefore, it is fairly evident that the Pechenga rocks form a separate type of ultramafic rocks and have to be distinguished from the previous ones.

References

1. Abdel-Karim A.-A. M., Ali S., Helmy H.M., El-Shafei S.A., 2016, A fore-arc setting of the Gerf ophiolite, Eastern Desert, Egypt: Evidence from mineral chemistry and geochemistry of ultramafites, Lithos, vol. 263, pp. 52-65

2. Albers E., Schroeder T., Bach W., 2019, Melt Impregnation of Mantle Peridotite Facilitates High-Temperature Hydration and Mechanical Weakening: Implications for Oceanic Detachment Faults, Geochemistry, Geophysics, Geosystems, vol. 20, pp. 84-108

3. Alibert C., 1994, Peridotite xenoliths from western Grand Canyon and the Thumb: A probe into the subcontinental mantle of the Colorado Plateau, Journal of Geophysical Research, vol. 99, pp. 605-621
4. Arlt T., Kunz M., Stolz J., Armbruster T, Angel R.J., 2000, P-T-X data on P2/c-clinopyroxenes and their displacive phase transitions, Contributions to Mineralogy and Petrology, vol. 138, pp. 35-45
5. Armitage J.J., Collier J.S., Minshull T.A., 2010, The importance of rift history for volcanic margin formation, Nature, vol. 465, pp. 913-917
6. Bali E., Hidas K., Guðfinnsson G.H., Kovács Z., Török K., Román-Alpiste M.J., 2018, Zircon and apatite-bearing pyroxene hornblendite mantle xenolith from Hungary, Carpathian-Pannonian region, Lithos, vol. 316-317, pp. 19-32

7. Ban M., Witt-Eickschen G., Klein M., Seck H.A., 2005, The origin of glasses in hydrous mantle xenoliths from the West Eifel, Germany: incongruent break down of amphibole, Contributions to Mineralogy and Petrology, vol. 148, pp. 511-523
8. Barbey P., Convert J., Moreau B., Capdevila R., Hameurt J., 1984, Petrogenesis and evolution of an early Proterozoic collisional orogenic belt: The granulite belt of Lapland and the Belomorides (Fennoscandia) , Bulletin of The Geological Society of Finland, vol. 56, pp. 161-188
9. Baumgartner M.C., le Roex A.P., Gurney J.J., 2000, Mantle and crustal xenoliths from the Okenyenya lamprophyre diatreme: constraints on the upper mantle and lower crust beneath the Damara Belt, northwestern Namibia, Communications of the Geological Survey of Namibia, vol. 12, pp. 315-327
10. Bénard A., Ionov D.A., 2013, Melt- and Fluid-Rock Interaction in Supra-Subduction Lithospheric Mantle: Evidence from Andesite-hosted Veined Peridotite Xenoliths
11. Bénard A., Müntener O., Pilet S., Arculus R.J., Nebel O., 2021, Silica-rich spinel harzburgite residues formed by fractional hybridization-melting of the intra-oceanic supra-subduction zone mantle: New evidence from TUBAF seamount peridotites, Geochimica et Cosmochimica Acta, vol. 293, pp. 477-506
12. Best M.G., 1970, Kaersutite-Peridotite Inclusions and Kindred Megacrysts in Basanitic Lavas, Grand Canyon, Arizona, Contributions to Mineralogy and Petrology, vol. 27, pp. 25-44
13. Best M.G., 1974, Contrasting types of chromium-spinel peridotite xenoliths in basanitic lavas, western Grand Canyon, Arizona, Earth and Planetary Science Letters, vol. 23, pp. 229-237
14. Best M.G., 1975, Amphibole-bearing Cumulate Inclusions, Grand Canyon, Arizona and their bearing on Silica-Undersaturated Hydrous Magmas in the Upper Mantle, Journal of Petrology, vol. 16, pp. 212-236
15. Beyer E.E., Griffin W.L., O'Reilly S.Y., 2006, Transformation of Archaean Lithospheric Mantle by Refertilization: Evidence from Exposed Peridotites in the Western Gneiss Region, Norway, Journal of Petrology, vol. 47, pp. 1611-1636
16. Bodinier J.-L., Godard M., 2003, Orogenic, ophiolitic, and abyssal peridotites, In: Treatise on Geochemistry, edited by Carlson R.W., Holland H.D., Turekian K.K., vol. 2, pp. 103-170
17. Bonadiman C., Brombin V., Andreozzi G.B., Benna P., Coltorti M., Curetti N., Faccini B., Merli M., Pelorosso B., Stagno V., Tesauro M., Pavese A., 2021, Phlogopite-pargasite coexistence in an oxygen reduced spinel-peridotite ambient, Scientific Reports, vol. 11, no. 11829
18. Borisova A.Y., Ceuleneer G., Kamenetsky V.S., Arai S., Bejina F., Abily B., Bindeman I.N., Polvé M., De Parseval P., Aigouy T., Pokrovski G.S., 2012, A new View on the Petrogenesis of the Oman Ophiolite Chromitites from Microanalyses of Chromite-hosted Inclusions, Journal of Petrology, vol. 53, pp. 2411-2440
19. Bozhilov K.N., Green H.W., Dobrzhinetskaya L., 1999, Clinoenstatite in Alpe Arami Peridotite: Additional Evidence of Very High Pressure, Science, vol. 284, pp. 128
20. Brueckner H.K., Zindler A., Seyler M., Bonatti F., 1988, Zabargad and the isotopic evolution of the sub-Red Sea mantle crust, Tectonophysics, vol. 150, pp. 163-176.
21. Brueckner H.K., 2017, The great eclogite debate of the Western Gneiss Region, Norwegian Caledonies: The in situ crustal v. exotic mantle origin controversy, Journal of Metamorphic Geology, vol. 36, pp. 517-527.
22. Brügmann G.E., Hanski E.J., Naldrett A.J., Smolkin V.F., 2000, Sulphide Segregation in Ferropicrites from the Pechenga Complex, Kola Peninsula, Russia, vol. 41, pp. 1721-1742
23. Cannat M., Seyler M., 1995, Transform tectonics, metamorphic plagioclase and amphibolitization in ultramafic rocks of the Vema transform fault (Atlantic Ocean), Earth and Planetary Science Letters, vol. 133, pp. 283-298
24. Cann J.R., Blackman D.K., Smith D.K., McAllister E., Janssen J., Mello S., Avgerinos E., Pascoe A.R., Escartin J., 1997, Corrugated slip surfaces formed at North Atlantic ridge-transform intersections, Nature, vol. 385, pp. 329-332

25. Carswell D.A., Harvey M.A., Al-Samman A., 1983, The petrogenesis of contrasting Fe-Ti and Mg-Cr garnet peridotite types in the high grade gneiss complex of Western Norway, Bulletin de Minéralogie, vol. 106, pp. 727-750
26. Cawthorn R.G., 1974, The Amphibole Peridotite-Metagabbro Complex, Finero, Northern Italy, The Journal of Geology, vol. 83, pp. 437-454
27. Çelik O.F., Marzoli A., Marschik R., Chiaradia M., Mathur R., 2018, Geochemical, mineralogical and Re-Os isotopic constraints on the origin of Tethyan oceanic mantle and crustal rocks from the Central Pontides, northern Turkey, Mineralogy and Petrology, vol. 112, pp. 25-44
28. Chen S., Yang J., Li T., 2009, Petrological investigation of the Ganyu peridotite in the Sulu ultrahigh-pressure terrane, eastern China, Tectonophysics, vol. 475, pp. 383-395
29. Chen R.-X., Li H.Y., Zheng Y.F., Zhang L., Gong B., Hu Z., Yang Y., 2017, Crust-Mantle Interaction in a Continental Subduction Channel: Evidence from Orogenic Peridotites in North Qaidam, Northern Tibet, Journal of Petrology, vol. 58, pp. 191-226
30. Clerc C., Lahfid A., Monie P., Lagabrielle Y., Chopin C., Poujol M., Boulvais P., J.-C. Ringenbach, Masini E., de St Blanquat M., 2015, High-temperature metamorphism during extreme thinning of the continental crust: a reappraisal of the North Pyrenean passive paleomargin, Solid Earth, vol. 6, pp. 643=668.
31. Cluzel D., Aitchison J.C., Zhou R., Ireland T., Heizler M., Patias D., Lesimple S., Maurizot P., Teyssier C., 2022, Direct dating of podiform Chromitite: U-Pb (Zircon, Rutile) and $^{40}Ar/^{39}Ar$ (Pargasite) evidence from Tiebaghi Cr deposit (New Caledonia), Ore Geology Reviews, vol. 145, Issue 104873
32. Conquéré F., 1971, La lherzolite à amphibole du gisement de Caussou (Ariége, France), Contributions to Mineralogy and Petrology, vol. 30, pp. 296-313
33. Corti G., 2011, Evolution and characteristics of continental rifting: Analog modeling-inspired view and comparison with examples from the East African Rift System, Tectonophysics, vol. 522-523, pp. 1-33
34. Corvò S., Langone A., Padròn-Navarta J.A., Tommasi A., Zanetti A., 2020, Porphyroclasts: Source and Sink of Major and Trace Elements During Deformation-Induced Metasomatism (Finero, Ivrea-Verbano Zone, Italy), Geosciences, vol. 10, 196
35. Dal Vesco E., 1953, Genesi e metamorfosi delle rocce basiche e ultrabasiche nell'ambiante mesozonale dell'orogene Pennidico, Schwizerische Mineralogische und Petrographische Mitteilungen, vol. 51, pp. 329-348
36. Das S., Basu A.R., 2019, Evidence of majoritic garnet from the mantle transition zone in the Alpe Arami garnet peridotite, International Geology Review
37. Davis G.H., Coney P.J., 1979, Geologic development of the Cordilleran metamorphic core complexes, Geology, vol. 7, pp. 120-124
38. Dawson J.B., Smith J.V., 1977, The MARID (mica-amphibole-rutile-ilmenite-diopside) suite of xenoliths in kimberlite, Geochimica et Cosmochimica Acta, vol. 41, pp. 309-310
39. Debari S., Kay S.M., Kay R.W., 1987, Ultramafic xenoliths from Adagdak volcano, Adak, Aleutian islands, Alaska: Deformed igneous cumulates from the MOHO of an island arc, Journal of Geology, vol. 95, pp. 329-341.
40. De Roever W.P., 1957, Sind die alpinotypen peridotitmassen vielleicht teknosch verfachtete bruchtücke der Peridotitschale?, Geologische Rundschau, vol. 46, pp. 137-146
41. Dietz R.S., 1963, Alpine serpentinites as oceanic rind segments, Geological Society of America Bulletin, vol. 74, pp. 947-952
42. Dobrzhinetskaya L., Bozhilov K.N., Green H.W., 1999, The solubility of TiO in olivine: implications for the mantle wedge environment, Chemical Geology, vol. 163, pp. 325-338
43. Duarte J.F.V., Kaczmarek M.-A., Vonlanthen P., Putlitz B., Müntener O., 2020, Hydration of a Mantle Shear Zone Beyond Serpentine Stability: A possible Link to Microseismicity Along Ultraslow Spreading Ridges?, Journal of Geophysical Research: Solid Earth, vol. 125, Issue 10

44. Dupuy C., Mevel C., Bodinier J.-L., Savoyant L., 1991 , The Zabargad peridotite: Evidence for multi-stage metasomatism during Red Sea rifting, Geology, vol. 19, pp. 722-725
45. El Atrassi F., Chazot G., Brunet F., Chopin C., Bouybaouene M., 2014, Amphibole genesis in pyroxenites from the Beni Bousera peridotite massif (Rif, Morocco): Evidence for two different metasomatic episodes, Lithos, vol. 208-209, pp. 67-80
46. Ernst W.G., 1977, Mineralogic Study of Eclogitic Rocks from Alpe Arami, Lepontine Alps, Southern Switzerland, Journal of Petrology, vol. 18, pp. 371-398
47. Ernst W.G., 1981, Petrogenesis of eclogites and peridotites from the Western and Ligurian Alps, American Mineralogist, vol. 66, pp. 443-472
48. Fabriès J., Bodinier J.-L., Dupuy C., Lorand J.-P., Benkerrou C., 1989, Evidence for Modal Metasomatism in the Orogenic Spinel Lherzolite Body from Caussou (Northeastern Pyrenees, France), Journal of Petrology, vol. 30, pp. 199-228
49. Fermor L.L., 1913, Preliminary note on garnet as a geological barometer and on an intra-plutonic zone in the Earth's crust, Geological Survey of India, vol. 43, pp. 41-47
50. Ferrando S., Frezzotti M.L., Neumann E.-R., De Astis G., Peccerillo A., Dereje A., Gezahegn Y., Teklewold A., 2008, Composition and thermal structure of the lithosphere beneath the Ethiopian plateau: evidence from mantle xenoliths in basanites, Injibara, Lake Tana Province, Mineralogy and Petrology, vol. 93, pp. 47-78
51. Fiorentini M.L., Beresford S.W., Deloule E., Hanski E., Stone W.E., Pearson N.J., 2008, The role of mantle-derived volatiles in the petrogenesis of Paleoproterozoic ferropicrites in the Pechenga Greenstone Belt, northwestern Russia: Insights from in-situ microbeam and nanobeam analysis of hydromagmatic amphibole, Earth and Planetary Science Letters, vol. 268, pp. 2-14
52. Fitzpayne A., Giuliani A., Hergt J., Phillips D., Janney P., 2018, New geochemical constrains on the origins of MARID and PIC rocks: Implications for mantle metasomatism and mantle-derived potassic magmatism, Lithos, vol. 318-319, pp. 478-493
53. Franz L., Becker K.-P., Kramer W., Herzig P.M., 2002, Metasomatic Mantle Xenoliths from the Bismarck Microplate (Papua New Guinea)-Thermal Evolution, Geochemistry and extent of Slab-induced Metasomatism, Journal of Petrology, vol. 43, pp. 315-343
54. Frezzotti M.L., Ferrando S., Peccerillo A., Petrelli M., Tecce F., Perucchi A., 2010, Chlorine-rich metasomatic H_2O-CO_2 fluids in amphibole-bearing peridotites from Injibara (Lake Tana region, Ethiopian plateau): Nature and evolution of volatiles in the mantle of a region of continental flood basalts, Geochimica et Cosmochimica Acta, vol. 74, pp. 3023-3039
55. Gamble J.A., McGibbon F., Kyle P.R., Menzies M.A., Kirsch I., 1988, Metasomatized Xenoliths from Foster Crater, Antarctica: Implications for Lithospheric Structure and Processes beneath the Transantarctic Mountain Front, Journal of Petrology, Special Lithosphere Issue, pp. 109-138
56. Green H.W., Dobrzhinetskaya L., Riggs E.M., Jin Z.-M., 1997, Alpe Arami: a peridotite massif from the Mantle Transition Zone?, Tectonophysics, vol.279, pp. 1-21
57. Green H.W., Dobrzhinetskaya L., Bozhilov K.N., 2010, The Alpe Arami Story: Triumph of Data over Prejudice, Journal of Earth Science, vol. 21, pp. 731-743
58. Grégoire M., Lorand J.P., O'Reilly S.Y., Cottin J.Y., 2000, Armacolite-bearing, Ti-rich metasomatic assemblages in harzburgitic xenoliths from the Kerguelen Islands: Implications for the oceanic mantle budget of high-field strength elements, Geochimica et Cosmochimica Acta, vol. 64, pp. 673-694
59. Grégoire M., McInnes B.I.A., O'Reilly S.Y., 2001, Hydrous metasomatism of oceanic sub-arc mantle, Lihit, Papua New Guinea. Part 2. Trace element characteristics of slab-derived fluids, Lithos, vol. 59, pp. 91-108
60. Grégoire M., Jego S., Maury R.C., Polve M., Payot B., Tamayo R.A., Yumul Jr. G.P., 2008, Metasomatic interactions between slab-derived melts and depleted mantle: Insights from xenoliths within Monglo adakite (Luzon arc, Philippines), Lithos, vol. 103, pp. 415-430

61. Griffin W.L., Wass S.Y., Hollis J.D., 1984, Ultramafic Xenoliths from Bullenmerri and Gnotuk Maars, Victoria, Australia: Petrology of a Sub-Continental Crust-Mantle Transition, Journal of Petrology, vol. 25, pp. 53-87
62. Grubenmann U., 1908, Der Granatolivinfels des Gordunatales und seine Begleitgesteine, Vierteljahresschrift der Naturforschenden Gesellschaft Zurich, vol. 53, pp. 129-153
63. Gysi A.P., Jagoutz O., Schmidt M.W., Targuisti K., 2011, Petrogenesis of pyroxenites and melt infiltrations in the ultramafic complex of Beni Bousera, northern Morocco, Journal of Petrology, vol. 52, pp. 1679-1735
64. Haggerty S.E., Sautter V., 1990, Ultradeep (greater than 300 kilometers), ultramafic upper mantle xenoliths, Science, vol. 248, pp. 993-996
65. Hanski E. Smolkin V.F., 1989, Pechenga Ferropicrites and other Early Proterozoic Picrites in the Eastern Part of the Baltic Shield, Precambrian Research, vol. 45, pp. 63-82
66. Hanski E., Huhma H., Smolkin V.F., Vaasjoki M., 1990, The age of the ferropicritic volcanics and comagmatic Ni-bearing intrusions at Pechenga, Kola Peninsula, U.S.S.R., Bulletin of the Geological Society of Finland, vol. 62, pp. 123-133
67. Hanski E., 1992, Petrology of the Pechenga Ferropicrites and Cogenetic Ni-bearing Wehrlite Intrusions, Kola Peninsula, Russia, Geological Survey of Finland, vol. 367, pp. 192
68. Hecker J.G., Marks M.A.W., Wenzel T., Markl G., 2020, Halogens in amphibole and mica from mantle xenoliths: Implications for the halogen distribution and halogen budget of the metasomatized continental lithosphere, American Mineralogist, vol. 105, pp. 781-794
69. Hermann J., Rubatto D., Trommsdorff V., 2006, Sub-solidus Oligocene zircon formation in garnet peridotite during fast decompression and fluid infiltration (Duria, Central Alps), Mineralogy and Petrology, vol. 88, pp. 181-206
70. Hess H.H., 1962, History of ocean basins, In: Petrologic Studies: A volume in Honor of A.F. Buddington, edited by Engle A.E.J., James H.L., Leonard B.L., New York: Geological Society of America, pp. 599-620
71. Hidas K., Borghini G., Tommasi A., Zanetti A., Rampone E., 2021, Interplay between melt infiltration and deformation in the deep lithospheric mantle (External Liguride ophiolite, North Italy), Lithos, vol. 380-381, Issue 105855
72. Hunt L.E., Lamb W.M., 2019, Application of mineral equilibria to estimate fugacities of H_2O, H_2 and O_2 in mantle xenoliths from the southwestern U.S.A., American Mineralogist, vol. 104, pp. 333-347
73. Ionov D.A., Bodinier J.-L., Mukasa S.B., Zanetti A., 2002, Mechanisms and Sources of Mantle Metasomatism: Major and Trace Element Compositions of Peridotite Xenoliths from Spitsbergen in the Context of Numerical Modelling, Journal of Petrology, vol. 43, pp. 2219-2259
74. Ionov D.A., 2010, Petrology of Mantle Wedge Lithosphere: New Data on Supra-Subduction Zone Peridotite Xenoliths from the Andesitic Avacha Volcano, Kamchatka, Journal of Petrology, vol. 51, pp. 327-361
75. Ishimaru S., Arai S., Ishida Y., Shirasaka M., Okrugin V.M., 2007, Melting and Multi-stage Metasomatism in the Mantle Wedge beneath a Frontal Arc Inferred from Highly Depleted Peridotite Xenoliths from the Avacha Volcano, Southern Kamchatka, Journal of Petrology, vol. 48, pp. 395-433
76. Ishimaru S., Arai S., 2008, Calcic amphiboles in peridotite xenoliths from Avacha volcano, Kamchatka, and their implications for metasomatic conditions in the mantle wedge, From: Coltorti M., Grégoire M., Metasomatism in Oceanic and Continental Lithospheric Mantle, Geological Society, London, Special Publications, vol. 293, pp. 35-55
77. Ismail M., Delpech G., Cottin J.-Y., Grégoire M., Moine B.N., Bilal A., 2008, Petrological and geochemical constraints on the composition of the lithospheric mantle beneath the Syrian rift, northern part of the Arabian plate, From: Coltorti M., Grégoire M., Metasomatism in Oceanic and Continental Lithospheric Mantle, Geological Society, London, Special Publications, vol. 293, pp. 223-251

78. Jarrard R. D., 1986, Relations among subduction parameters, *Reviews of Geophysics., vol 24*, 217–283

79. Johan Z., Martin R.F., Ettler V., 2017, Fluids are bound to be involved in the formation of ophiolitic chromite deposits, European Journal of Mineralogy, vol. 29, pp. 543-555
80. Kaczmarek M.-A., Muntener O., 2008, Juxtaposition of melt impregnation and high-temperature shear zones in the upper mantle; field and petrological constraints from the Lanzo peridotite (Northern Italy), Journal of Petrology, vol. 49, pp. 2187-2220
81. Kaczmarek M.-A., Bodinier J.-L., Bosch D., Tommasi A., Dautria J.-M., Kechid S.A., 2016, Metasomatized Mantle Xenoliths as a Record of Lithospheric Mantle Evolution of the Northern Edge of the Ahaggar Swell, In Teria (Algeria), Journal of Petrology, vol. 57, 345-382
82. Kaeser B., Kalt A., Pettke T., 2007, Crystallization and Breakdown of Metasomatic Phases in Graphite-bearing Peridotite Xenoliths from Marsabit (Kenya), Journal of Petrology, vol. 48, pp. 1725-1760
83. Kepezhinskas P.K., Defant M.J., Drummond M.S., 1995, Na Metasomatism in the Island-Arc Mantle by Slab Melt-Peridotite Interaction: Evidence from Mantle Xenoliths in the North Kamchatka Arc, Journal of Petrology, vol. 36, pp. 1505-1527
84. Keyser M., Ritter J.R.R., Jordan M., 2002, 3D shear-wave velocity structure of the Eifel plume, Germany, Earth and Planetary Science Letters, vol. 203, pp. 59-82
85. Klimm K., Blundy J.D., Green T.H., 2008, Trace Element Partitioning and Accessory Phase Saturation during H_2O-Satureated Melting of Basalt with Implications for Subduction Zone Chemical Fluxes, Journal of Petrology, vol. 49, pp. 523-553
86. Kodolányi J., Pettke T., Spandler C., Kamber B.S., Gméling K., 2011, Geochemistry of Ocean Floor and Fore-arc Serpentinites: Constraints on the Ultramafic Input to Subduction Zones, Journal of Petrology, vol. 53, pp. 235-270
87. Kremenetsky A.A., Ovchinnikov L.N., 1986, Geochemistry of Deep Rocks, Nauka, Moscow, pp. 262.
88. Laurora A., Mazzucchelli M., Rivalenti G., Vannucci R., Zanetti A., Barbieri M.A., Cingolani C.A., 2001, Metasomatism and Melting in Carbonated Peridotite Xenoliths from the Mantle Wedge: The Gobernador Gregores Case (Southern Patagonia), Journal of Petrology, vol. 42, pp. 69-87.
89. Liptai N., Patkó L., Kovács I.J., Hidas K., Pintér Z., Jeffries T., Zajacz Z., O'Reilly S.Y., Griffin W.L., Pearson N.J., Szabó C., 2017, Multiple Metasomatism beneath the Nógrád-Gömör Volcanic Field (Northern Pannonian Basin) Revealed by Upper Mantle Peridotite Xenoliths, Journal of Petrology, vol. 58- pp. 1107-1144
90. Liu C.-Z., Wu F.-Y., Wilde S.A., Yu L.-J., Li J.-L., 2010, Anorthitic plagioclase and pargasitic amphibole in mantle peridotites from the Yungbwa ophiolite (southwestern Tibetan Plateau) formed by hydrous melt metasomatism, Lithos, vol. 114, pp. 413-422

91. Liu J., Wang J., Hattori K., Wang Z., 2022, Petrogenesis of Garnet Clinopyroxenite and Associated Dunite in Hujialin, Sulu Orogenic Belt, Eastern China, Minerals, vol. 12, pp. 162

92. Luffi P., Saleeby J.B., Lee C.-T. A., Ducea M.N., 2009, Lithospheric mantle duplex beneath the central Mojave Desert revealed by xenoliths from Dish Hill, California, Journal of Geophysical Research, vol. 114, Issue B3
93. Maierova P., Schulmann K., Stipska P., Gerya T., Lexa O., 2021, Trans-lithospheric diapirism explains the presence of ultra-high pressure rocks in the European Variscides, Communications Earth & Environment, 2, 56.
94. Marker M., 1985, Early Proterozoic (c. 2000-1900 Ma) crustal structure of the northeaster Baltic Shield: tectonic division and tectogenesis, Norwegian Journal of Geology, vol. 403, pp. 55-74
95. Martinez F., Cochran J.R., 1988, Structure and tectonics of the northern Red Sea: Catching a continental margin between rifting and drifting, Tectono physics, vol. 150, pp. 1-32

96. Matusiak-Malek M., Puziewicz J., Ntaflos T., Grégoire M., Kukula A., Wojtulek P. M., 2017, Origin and evolution of rare amphibole-bearing mantle peridotites from Wilcza Góra (SW Polang), Central Europe, vol. 286-287, pp. 302-323
97. Mazzucchelli M., Rivalenti G., Brunelli D., Zanetti A., Boari E., 2009, Formation of highly refractory dunite by focused percolation of pyroxenite-derived melt in the Balmuccia peridotite massif (Italy), Journal of Petrology, vol. 50, pp. 1205-1233
98. Mazzucchelli M., Zanetti A., Rivalenti G., Vannucci R., Correia C.T., Tassinari C.C.G., 2010, Age and geochemistry of mantle peridotites and diorite dykes from the Baldissero body: Insights into the Paleozoic-Mesozoic evolution of the Southern Alps, Lithos, vol. 119, pp. 485-500
99. McCaig A.M., Harris M., 2012, Hydrothermal circulation and the dike-gabbro transition in the detachment mode of slow seafloor spreading, Geology, vol. 40, pp. 367-370
100. McInnes B.I.A., Grégoire M., Raymond A.B., Herzig P.M., Hannington M.D., 2001, Hydrous metasomatism of oceanic sub-arc mantle, Lihir, Papua New Guinea: petrology and geochemistry of fluid-metasomatized mantle wedge xenoliths, Earth and Planetary Science Letters, vol. 188, pp. 169-183
101. Merle O., Michon L., 2001, The formation of the West European Rift; a new model as exemplified by the Massif Central area, Bulletin de la Societe Geologique de France, vol. 172, pp. 213-221
102. Melson W.G., Hart S.R., Thompson G., 1972, St.Paul's Rocks, Equatorial Atlantic: Petrogenesis, Radiometric Ages, and Implications on Sea-Floor Spreading, In: Studies in Earth and Space Sciences, edited by Shagam R., Hargraves R.B., Morgan W.J., Van Houten F.B., Burk C.A., Holland H.D., Hollister L.C., vol. 132, pp. 241-272
103. Moine B.N., Grégoire M., O'Reilly S.Y., Sheppard S.M.F., Cottin J.Y., 2001, High Field Strength Element Fractionation in the Upper Mantle: Evidence from Amphibole-Rich Composite Mantle Xenoliths from the Kerguelen Islands (Indian Ocean), Journal of Petrology, vol. 42, pp. 2145-2167
104. Moussa H.E., Mubarak H.S., Azer M.K., Surour A.A., Asimow P.D., Kabesh M.M.L., 2022, Multistage petrogenetic evolution of Neoproterozoic serpentinized ultramafic rocks and podiform chromitites at Hagar Dungash, Eastern Desert of Egypt, Precambrian Research, vol. 369, no. 106507
105. Müntener O., Piccardo G.B., Polino R., Zanetti A., 2005, Revisiting the Lanzo peridotite (NW-Italy): 'Asthenospherization' of ancient mantle lithosphere, Ofioliti, vol. 30, pp. 111-124
106. Muriuki J., Nakamura D., Hirajima T., Svojtka M., 2020, Mineralogical heterogeneity of UHP garnet peridotite in the Moldanubian Zone of the Bohemian Massif (Nové Dvory, Czech Republic), Journal of Mineralogical and Petrological Sciences, vol. 115, pp. 1-20
107. Neal C.R., 1988, The Origin and Composition of Metasomatic Fluids and Amphiboles beneath Malaita, Solomon Islands, Journal of Petrology, vol. 29, pp. 149-179
108. Newman S., Stolper E., Stern R. J., 2000, H2O and CO2 in magmas from the Mariana arc and back arc systems, *Geochemistry, Geophysics, Geosystems., vol. 1*, issue 5
109. Nicolas A., Boudier F., Montigny R., 1987, Structure of Zabargad Island and early rifting of the Red Sea, Journal of Geophysical Research, vol. 92, pp. 461-474
110. Nicolas A., Boudier F., 2003, Where ophiolites come from and what they tell us, Special Paper of the Geological Society of America, vol. 373, pp. 137-152
111. Nimis P., Trommsdorff V., 2001, Revised Thermobarometry of Alpe Arami and other Garnet Peridotites from the Central Alps, Journal of Petrology, vol. 42, pp. 103-115
112. Nozaka T., Shibata T., 1995, Mineral paragenesis in thermally metamorphosed serpentinites, Ohsa-yama, Okayama Prefecture, Earth Science Reports, vol.. 2, pp. 1-12
113. Nozaka T., 2014, Metasomatic hydration of the Oeyama forearc peridotites: Tectonic implications, Lithos, vol. 184-187, pp. 346-360

114. Ntaflos T., Bizimis M., Abart R., 2017, Mantle xenoliths from Szentbékálla, Balaton: Geochemical and petrological constraints on the evolution of the lithospheric mantle underneath Pannonian Basin, Hungary, Lithos, vol. 276, pp. 30-44
115. O'Reilly S.Y., Griffin W.L., Ryan C.G., 1991, Residence of trace elements in metasomatized spinel lherzolite xenoliths: a proton-microprobe study, Contributions to Mineralogy and Petrology, vol. 109, pp. 98-113
116. Pan Q.-Q., Xiao Y., Su B.-X., Liu X., Robinson P.T., Cui M.-M., Wang J., Uysal I., 2022, Fingerprinting stealth metasomatism in ophiolitic peridotites, vol. 424-425, 106755
117. Paquin J., Altherr R., 2001, New Constraints on the P-T Evolution of the Alpe Arami Garnet Peridotite Body (Central Alps, Switzerland), Journal of Petrology, vol.42, pp. 1119-1140
118. Payot B.D., Arai S., Yoshikawa M., Tamura A., Okuno M., Rivera D.J.V., 2018, Mantle Evolution from Ocean to Arc: The Record in Spinel Peridotite Xenoliths in Mt. Pinatubo, Philippines, Minerals, vol. 8, pp. 515
119. Peacock S.M., 2001, Are the lower planes of double seismic zones caused by serpentine dehydration in subducting oceanic mantle?, Geology, vol. 29, pp. 299-302
120. Pellegrino L., Malaspina N., Zanchetta S., Langone A., Tumiati S., 2020, High pressure melting of eclogites and metasomatism of garnet peridotites from Monte Duria Area (Central Alps, N Italy): A proxy for melt-rock reaction during subduction, Lithos, vol. 358-359, Issue 105391
121. Petrini R., Joron J.-L., Ottonello G., Bonatti E., Seyler M., 1988, Basaltic dykes from Zabargad Island, Red Sea: Petrology and geochemistry, Tectonophysics, vol. 150, pp. 229-248
122. Piccardo G.B., Rampone E., Scambelluri M., 1988, The Alpine evolution of the Erro-Tobbio Peridotites (Voltri Massif-Ligurian Alps): Some field and petrographic constraints, Ofioliti, vol. 13, pp. 169-174
123. Pharaoh T.C., Warren A., Walsh N.J., 1987, Early Proterozoic metavolcanic suites of the northernmost part of the Baltic Shield, In: Geochemistry and Mineralization of Proterozoic Volcanic Suites, edited by Pharaoh T.C., Beckinsale R.D., Rickard D., Geological Society, London, Special Publications, vol. 33, pp. 41-58
124. Piccardo G.B., Guarnieri L., 2011, Gabbro-norite cumulates from strongly depleted MORB melts in the Alpine-Apennine ophiolites, Lithos, vol. 124, pp. 200-214
125. Powell W., Zhang M., O'Reilly S.Y., Tiepolo M., 2004, Mantle amphibole trace-element and isotopic signatures trace multiple metasomatic episodes in lithospheric mantle, western Victoria, Australia, Lithos, vol. 75, pp. 141-171
126. Quick J.E., Sinigoi S., Mayer A., 1995, Emplacement of mantle peridotite in the lower continental crust, Ivrea-Verbano Zone, Northwest Italy, Geology, vol. 23, pp. 739-742
127. Rampone E., Borghini G., 2008, Melt migration and intrusion in the Erro-Tobbio peridotites (Ligurian Alps, Italy): Insights on magmatic processes in extending lithospheric mantle, European Journal of Mineralogy, vol. 20, pp. 573-585
128. Risold A.C., Trommsdorff V., Reusser E, Ulmer P., 1997, Genesis of $FeTiO_3$ inclusions in garnet peridotites from the central Alps, Terra Nova 9, Abstract Supplement, vol. 1, pp. 28-29
129. Ritter J.R.R., Jordan M., Christensen U.R., Achauer U., 2001, A mantle plume below the Eifel volcanic fields, Germany, Earth and Planetary Science Letters, vol. 186, pp. 7-14
130. Rospabé M., Benoit M., Ceuleneer G., Hodel F., Kaczmarek M.-A., 2018, Extreme geochemical variability through the dunitic transition zone of the Oman ophiolite: Implications for melt/fluid-rock reactions at Moho level beneath oceanic spreading centers, Geochimica et Cosmochimica Acta, vol. 234, pp. 1-23
131. Sautter V., Haggerty S., Field S., 1991, Ultradeep (>300 Kilometers) Ultramafic Xenoliths: Petrological Evidence from the Transition Zone, Science, vol. 252, pp. 827-830
132. Scambelluri M., Pettke T., Rampone E., Godard M., Reusser E., 2014, Petrology and Trace Element Budgets of High-pressure Peridotites Indicate Subduction Dehydration of Serpentinized Mantle (Cima di Gagnone, Central Alps, Switzerland), Journal of Petrology, vol. 55, pp. 459-498

133. Schroeder T., John B.E., 2004, Strain localization on an oceanic detachment fault system, Atlantis Massif , 30°N, Mid-Atlantic Ridge, Geochemistry, Geophysics, Geosystems, vol. 5, Q11007
134. Sen A., Snow J.E., Ohara Y., Hirauchi K., Kouketsu Y., Sanfilippo A., Basch V., Harigane Y., Fujii M., Okino K., Akizawa N., 2021, Melting and Evolution of Amphibole-Rich Back-Arc Abyssal Peridotites at the Mado Megamullion, Shikoku Basin, Geochemistry, Geophysics, Geosystems, vol. 22, Issue 12
135. Sharkov E.V., 1984, Continental rift magmatism of the Lower Proterozoic of the Karelian-Kola region, Geotectonika, vol. 2, pp. 37-50
136. Shaw C.S.J., Klügel A., 2002, The pressure and temperature conditions and timing of glass formation in mantle-derived xenoliths from Baarley, West Eifel, Germany: the case for amphibole breakdown, lava infiltration and mineral-melt reaction, Mineralogy and Petrology, vol. 74, pp. 163-187
137. Shaw C.S.J., Eyzaguirre J., Fryer B., Gagnon J., 2005, Regional Variations in the Mineralogy of Metasomatic Assemblages in Mantle xenoliths from the West Eifel Volcanic Fiend, Germany, Journal of Petrology, vol. 46, pp. 945-972
138. Siegrist M., Yogodzinski G., Bizimis M., Fournelle J., Churikova T., Dektor C., Mobley R., 2019, Fragments of Metasomatized Forearc: Origin and Implications of Mafic and Ultramafic Xenoliths From Kharchinsky Volcano, Kamchatka, Geochemistry, Geophysics, Geosystems, vol. 20, pp. 4426-4456
139. Simon N.S.C., Carlson R.W., Pearson D.G., Davies G.R., 2007, The Origin and Evolution of the Kaapvaal Cratonic Lithospheric Mantle, Journal of Petrology, vol. 48, pp. 589-625
140. Slovenec D., Šegvić B., 2018, The first record of ultramafic cumulates from the Mt. Kalnik ophiolite mélange in the SW part of the Zagorje-Mid-Transdanubian Zone (NW Croatia): mineralogy, petrology, geochemistry and tectono-magmatic affinity, Geologia Croatica, vol. 71, pp. 185-197
141. Song S., Zhang L., Chen J., Liou J.G., Niu Y., 2005, Sodic amphibole exsolutions in garnet from garnet-peridotite, North Qaidam UHPM belt, NW China: Implications for ultradeep-origin and hydroxyl defects in mantle garnets, American Mineralogist, vol. 90, pp. 814-820
142. Stern R.J., 2002, Subduction Zones, Reviews of Geophysics, vol. 40, Issue 4
143. Stolz A.J., Davies G.R., 1988, Chemical and Isotopic Evidence from Spinel Lherzolite Xenoliths for Episodic Metasomatism of the Upper Mantle beneath Southeast Australia, Journal of Petrology, Special Lithosphere Issue, pp. 303-330
144. Sutherland F.L., Hollis J.D., 1982, Mantle-Lower crust petrology from Inclusions in basaltic rocks in Eastern Australia- an outline, Journal of Volcanology and Geothermal Research, vol. 14, pp. 1-29
145. Tamura A., Arai S., Ishimaru S., Andal E.S., 2008, Petrology and geochemistry of peridotites from IODP Site U1309 at Atlantis Massif, MAR 30°N: micro- and macro-scale melt penetrations into peridotites, Contributions to Mineralogy and Petrology, vol. 155, pp. 491-509
146. Tamura A., Morishita T., Ishimaru S., Arai S., 2014, Geochemistry of spinel-hosted amphibole inclusions in abyssal peridotite: insight into secondary melt formation in melt-peridotite reaction, Contributions to Mineralogy and Petrology, vol. 167, pp. 974
147. Tian L.-R., Zheng J.-P., Xiong Q., Zhou X., Liang H., Dai H.-K., 2022, Xigaze ophiolite (South Tibet) records complex melt-fluid-peridotite interaction in the crust-mantle transition zone beneath oceanic slow-ultraslow spreading centers, Lithos, vol. 414-415, Issue 106623
148. Tilley C.E., Long J.V.P., 1967, The porphyroclast Minerals of the Peridotite-Mylonites of St.Paul's Rocks (Atlantic), Geological Magazine, vol. 104, no. 1
149. Uenver-Thiele L., Woodland A.B., Downes H., Altherr R., 2014, Oxidation State of the Lithospheric Mantle below the Massif Central, France, Journal of Petrology, vol. 55, pp. 2457-2480

150. Uyeda S., Kanamori H., 1979, Back-Arc Opening and the Mode of Subduction, Journal of Geophysical Research, vol. 84, no. B3
151. Uysal I., Tarkian M., Sadiklar M.B., Sen C., 2007, Platinum-group-element geochemistry and mineralogy of ophiolitic chromitites from the Kop Mountains, Northeastern Turkey, The Canadian Mineralogist, vol. 45, pp. 355-377
152. Valera G.T.V., Payot B.D., Arai S., Takeuchi M., Ishimaru S., Tamura A., 2019, Petrologic nature of the active subarc crust-mantle boundary: Mixed magmatic-metasomatic processes recorded in xenoliths from Sabtang island, Luzon arc, Journal of Volcanology and Geothermal Research, vol. 374, pp. 80-99
153. Villaseca C., Serrano J.G., Pérez-Soba C., 2020, Subduction-related metasomatism in the lithospheric mantle beneath the Calatrava volcanic field (central Spain): constraints from lherzolite xenoliths of the Cerro Gordo volcano, International Geology Review, vol. 64, pp. 469-488
154. Vrijmoed J.C., Austrheim H., John T., Hin R.C., Corfu F., Davies G.R., 2013, Metasomatism in the Ultrahigh-pressure Svartberget Garnet-peridotite (Western Gneiss Region, Norway): Implications for the Transport of Crust-derived Fluids with the Mantle, Journal of Petrology, vol. 54, pp. 1815-1848
155. Wagner P.A., 1914, The Diamond Fields of Southern Africa, Johannesburg: Transvaal Leader, pp. 347
156. Whitney D.L., Teyssier C., Rey P.F., Buck R., 2013, Continental and oceanic core complexes, Geological Society of America Bulletin, vol. 125, pp. 273-298
157. Winterburn P.A., Harte B., Gurney J.J., 1990, Peridotite xenoliths from the Jagersfontein kimberlite pipe: I. Primary and primary-metasomatic mineralogy, Geochimica et Cosmochimica Acta, vol. 54, pp. 329-341
158. Witt-Eickschen G., Harte B., 1994, Distribution of trace elements between amphibole and clinopyroxene from mantle peridotites of the Eifel (western Germany): An ion-microprobe study, Chemical Geology, vol. 117, pp. 235-250
159. Xu Y., Mercier J.C., Chuanyong L., 1997, Amphibole-Bearing Peridotite Xenoliths from Nushan, Anhui Province: Evidence for Melt Percolation Process in the Upper Mantle and Lithospheric Uplift, Chinese Journal of Geochemistry, vol. 16, no. 3
160. Xu X., O'Reilly S.Y., Griffin W.L., Zhou X., Huang X., 1998, The Nature of the Cenozoic Lithosphere at Nushan, Eastern China, Mantle Dynamics and Plate Interactions in East Asia Geodynamics, vol. 27
161. Xu Y.-G., Bodinier J.-L., 2004, Contrasting Enrichments in High- and Low-Temperature Mantle Xenoliths from Nushan, Eastern China: Results of a Single Metasomatic Event during Lithospheric Accretion?, Journal of Petrology, vol. 45, pp. 321-341
162. Ulmer P., Trommsdorff V., 1997, Titanium content of mantle olivine: an experimental study to 10GPa, Terra Nova 9, Abstract Supplement, vol. 1, pp. 39
163. Yan F.C., Liu Q., Ma X.Y., He M., 2021, Metamorphic P-T-t path and tectonic implication of garnet pyroxenite from Raobazhai, North Dabie Complex, central-eastern China, Acta Petrologica Sinica, vol. 37, pp. 2579-2598
164. Yang J.-J., Jahn B.-M., 2000, Deep subduction of mantle-derived garnet peridotites from the Su-Lu UHP metamorphic terrane in China, Journal of Metamorphic Geology, vol. 18, pp. 167-180
165. Yang J.-J., 2003, Relict edenite in a garnet lherzolite from the Chinese Su-Lu UHP metamorphic terrane: Implications for metamorphic history, American Mineralogist, vol. 88, pp. 180-188
166. Ye K., Song Y. R., Chen Yi., Xu H. J., Liu J. B., Sun M., 2009, Multistage metamorphism of orogenic garnet-lherzolite from Zhimafang, Sulu UHP terrane, E. China: Implications for mantle wedge convection during progressive oceanic and continental subduction, vol. 109, pp. 155-175

167. Yoshikawa M., Tamura A., Arai S., Kawamoto T., Payot B.D., Rivera D.J., Bariso E.B., Mirabueno M.H.T., Okuno M., Kobayashi T., 2016, Aqueous fluids and sedimentary melts as agents for mantle wedge metasomatism, as inferred from peridotite xenoliths at Pinatubo and Iraya volcanoes, Luzon arc, Philippines, Lithos, vol. 262, pp. 355-368
168. Zanetti A., Mazzucchelli M., Rivalenti G., Vannucci R., 1999, The Finero phlogopite-peridotite massif: an example of subduction-related metasomatism, Contributions to Mineralogy and Petrology, vol. 134, pp. 107-122
169. Zhang R.Y., Liou J.G., Huberty J.M., Xu H., Maki K., Jahn B.-M., Iizuka Y., 2011, Origin and Metamorphic Evolution of Garnet Clinopyroxenite from the Sulu UPP Terrane, China: Evidence from Mineral Chemistry and Microstructures, In: Ultrahigh-Pressure Metamorphism, 25th Years After The Discovery Of Coesite And Diamond, Edited by Dobrzhinetskaya L.F., Faryad S.W., Wallis S., Cuthbert S., pp. 151-185
170. Zhao R., Liou J. G., Tsujimori T., Zhang R.Y., 2007, Petrology and U-Pb SHRIMP Geochronology of a Garnet Peridotite, Sulu UHP Terrane, East-Central China, vol. 49, pp. 732-752

CHAPTER 3
Amphibole Textures and Modes of Formation

Introduction

Water is hosted in two types of solid phases in ultramafic rocks. The first type involves the nominally anhydrous minerals (NAMs) such as olivine, pyroxene and garnet that can carry tens to hundreds of parts per million (ppm) of hydrogen in the defects of their crystal structure. The discovery of NAMs is attributed to two scientific groups (Beran, 1976; Rossman, 1988). Since then, continued research has shown that the solubility of hydrogen in NAMs is increasing with increasing pressure (e.g. Ohtani et al., 2018). Therefore, it is predicted that they can contain measurable amounts of water only in greater depths. For this reason, NAMs have become a subject undergoing intense studying as they could shed light to the evolution of the planet or give insights on the rheological properties of the mantle. Moreover, NAMs could serve as an extremely important repository of water in the deeper parts of the mantle. They could also explain magmatism that occurs directly above the Mantle Transition Zone (MTZ) at around 410 kms (e.g. Andrault & Bolfan-Casanova, 2022).

Hydrous mineral phases that are formed from metasomatic processes are also extremely important hosts of water in the mantle. Metasomatism occurs when a rock is compositionally and/or mineralogically altered by the so-called metasomatic fluids. These metasomatic agents involve H_2O-rich fluids or silicate melts of variable composition that are important carriers of fluid-mobile elements such as Na and K. Two distinct types of metasomatism exist· modal and cryptic. Modal metasomatism (Harte, 1983) is defined by the formation of new minerals. On the other hand, enrichment in trace elements without any visible modal or textural modifications may also occur from the interaction of metasomatic fluids with a rock. This is referred to as cryptic metasomatism (Dawson, 1984). Hydrous minerals, such as amphibole and phlogopite, are stable at far shallower mantle depths compared to water-bearing NAMs. During their formation, they store critical amounts of water in their crystal structure. At subduction zones these minerals are experiencing conditions of elevating temperatures and pressures. Therefore, hydrous minerals are gradually dehydrated and release their constituent water to the system. A fraction of the released water is transported to the mantle wedge (see 2.1.4) or to deeper parts of the mantle where it is stored in NAMs.

The presence of amphibole (and phlogopite) in ultramafic rocks that are related to a wide variety of different geotectonic settings has been widely related to metasomatic processes (e.g. Mengel & Green, 1989). This chapter will review the majority of the possible amphibole-related textures in ultramafic rocks. It will additionally provide the suggested modes of formation of amphibole for each texture according to the literature.

3.1 The texture of ultramafic rocks

Ultramafic rocks can show both metamorphic and igneous textures. Some of the most used textural nomenclatures for ultramafic rocks are those of Mercier & Nicolas (1975), Pike & Schwarzman (1977) and Harte (1977). Many of the later-developed modifications were very subjective and therefore they had little practical use (Swan & Sandilands, 1995). This is the reason that the three aforementioned nomenclatures are still widely used in the literature. Recently, Tabor & Downes (2019) have developed a new quantitative method to classify ultramafic rocks. They have proposed that the methods of whole slide scanning and thin-section skeleton images analysis (see Tabor et al., 2010) are more than enough to describe ultramafic textures.

According to Pike & Schwarzman (1977) igneous textures in ultramafic rocks are not rare but it is often hard to recognize them. Zoning and twinning in pyroxenes, euhedral grain shapes and inclusions of spinel in coarse-grained silicate minerals are several criteria that might indicate an igneous texture. The most easily identifiable igneous texture is the existence of veins or dikes of pyroxenites in ultramafic rocks. Exsolution lamellae is very usual texture both in igneous and metamorphic rocks, therefore it cannot be used as a safe criterion to distinguish between the two origins. Moreover, Pike & Schwarzman (1977) have described the so-called pyrometamorphic textures. Pyrometamorphism occurs when a partial melt locally solidifies in an ultramafic rock. The solidification is defined by the formation of glass which usually contains quenched crystals of olivine, augite and plagioclase. Spongy borders of pyroxene may indicate locations where the partial melt was generated. Additionally, on a few occasions igneous cumulate textures may also be evident. Cumulate textures result from the accumulation of crystals either by gravitational settling or by floating within a body of magma. Cumulus olivine enclosed by post-cumulus orthopyroxene is an igneous texture that is found in several ultramafic rocks.

Following the nomenclature of Mercier & Nicolas (1975), metamorphic textures of ultramafic rocks can be divided into three types: protogranular, porphyroclastic and equigranular. The protogranular texture is defined by coarse-grained (~4 mm) olivine and orthopyroxene and smaller (~1 mm) grains of clinopyroxene and spinel. Olivine in the protogranular texture often displays kink bands. Kink bands are parts of crystals that underwent slight degrees of rotation, with respect to the unkinked parts of crystals, as a result of localized, compressional deformation. Clinopyroxene and spinel are often in direct contact with large orthopyroxene grains. The porphyroclastic texture is very usual in ultramafic rocks. It can be described by the existence of large, strained crystals of olivine and enstatite (porphyroclasts) that exist in a matrix of fine-grained, polygonal and strain-free olivines, orthopyroxenes and clinopyroxenes (neoblasts). This indicates the presence of two distinct generations of minerals. Finally, the equigranular type is defined by fine-grained minerals (~0.7 mm) with even dimensions. However, a few relics of porphyroclasts may be visible. It is thought that the protogranular texture is caused by an initial recrystallization process. With increasing degrees of plastic flow and deformation, the protogranular texture is replaced by the porphyroclastic one. Then, the equigranular texture is thought to derive from the complete recrystallization of the porphyroclastic texture.

3.2 Interstitial amphibole

Interstitial amphibole is one of the most common textures of the mineral in ultramafic rocks. Interstitial amphiboles fill the interstices (free spaces) between earlier-formed minerals. They are usually anhedral to subhedral in shape but they can also be found as fine-grained euhedral crystals in narrow zones among primary minerals. Interstitial amphiboles do not show a clear textural relationship with other silicate minerals (e.g. intergrowths, inclusions, replacement textures or mantles around primary minerals). Additionally, they are present in almost every type of ultramafic rock (harzburgites, lherzolites, dunites, websterites, wehrlites, pyroxenites) from all the possible geotectonic settings.

Examples of interstitial amphiboles are presented in Figure 3.1. Interstitial amphibole from the Cerro-Gordo volcanic field in Spain (Figure 3.1a) displays the most important characteristics of this texture. Notice how the irregularly-shaped amphibole crystals exist in the spaces between the earlier-formed protogranular olivine and pyroxenes. In Figure 3.1b, a completely anhedral and large interstitial amphibole is present in a dunite belonging to the Lycian Ophiolite in Turkey (Pan et

al., 2022). This time, the amphibole has filled the interstice between chromite and olivine and its shape reflects the geometry of the pre-existing space in which amphibole was formed. An example of a fine-grained, elongated interstitial amphibole is present in Figure 3.1c and is found in a mantle xenolith from the Nógrád-Gömor volcanic field (Liptai et al., 2017). Ionov (2010) noticed that some of the amphiboles in the Avacha ultramafic xenoliths exist in interstitial pockets with empty vesicles such as the one depicted in Figure 3.1d. They show relatively euhedral shapes although some of them that are in contact with spinel are entirely anhedral.

According to the literature, interstitial amphiboles are products of direct crystallization from melts or fluids. For example, interstitial amphibole from xenolithic peridotites in the Kharchinsky volcanic rocks (Kamchatka) are considered to represent a late step in the evolution of the xenoliths. Based on geochemical criteria, Siegrist et al. (2019) proposed that they are of igneous origin and that they were directly crystallized from magmas. The authors completely disregarded an origin from fluids or fluid-rock interactions. Fabriès et al. (1989) noticed that interstitial amphiboles along narrow planar zones in the Caussou peridotites (Pyrenees) are compositionally identical to amphiboles from alkali-basalts. Therefore, they could be direct precipitates from similar melts. However, variations in the K/Na ratio have additionally led them to conclude that the alkali-basaltic melts must have coexisted with an aqueous, CO_2-rich fluid. Late-stage interstitial amphiboles are also present in the Barombi and Nyos xenoliths (Cameroon). Pintér et al. (2015), based on textural characteristics and geochemical evidence of cryptic metasomatism, predicted that they are the result of precipitation from melts and fluids that percolated along grain boundaries. According to Ionov (2010), prior to the transport of xenoliths to the surface, tectonic processes have fractured the mantle rocks under the Avacha volcano. Subsequent infiltration of hydrous fluids were responsible for the precipitation of interstitial amphibole. Interstitial amphibole from Lightning Peak (British Columbia) is showing a crystallization origin from a metasomatic fluid that percolated along grain boundaries in the lherzolitic xenoliths (Brearley & Scarfe, 1984). Generally, the metasomatic melts or fluids that percolate in the ultramafic rocks may or may not have reacted with the wall-rocks. Therefore, their composition could be slightly modified compared to the original one. For this reason, the chemical composition of the precipitative, interstitial amphibole could also be affected from the evolution of the melt.

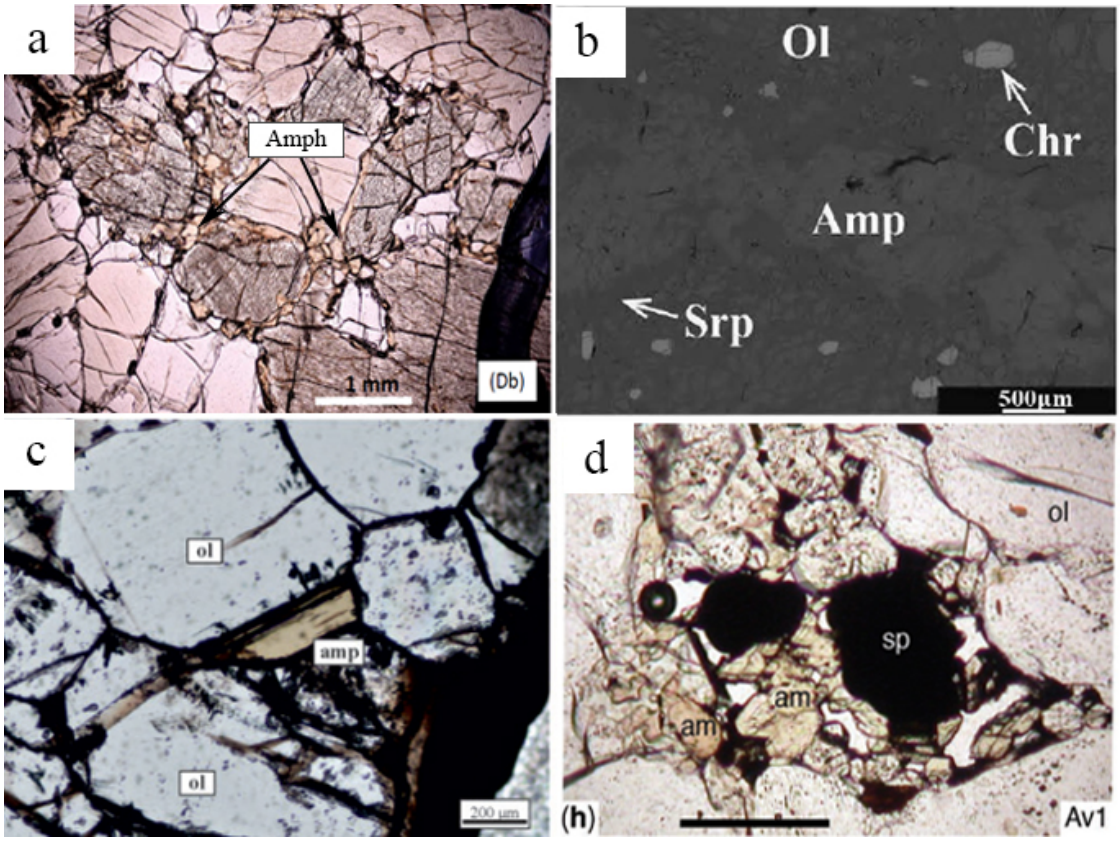

Figure 3.1: Photomicrographs of interstitial amphiboles from different ultramafic rocks (see text for more details). a Villaseca et al., 2020; b. Pan et al., 2022; c. Liptai et al., 2017; d. Ionov, 2010.

3.3 Matrix amphibole

Matrix amphiboles display entirely different features compared to interstitial ones. They are found as isolated and disseminated crystals in ultramafic rocks. They are usually euhedral and polygonal in shape, devoid of mineral inclusions and show sharp boundaries with the surrounding minerals. Moreover, they display little or no evidence of deformation. Amphiboles of this texture are part, along with other minerals, in the matrix of the porphyroclastic, protogranular or equigranular texture. They show sizes which are comparable to those of the other matrix phases (e.g. olivine and pyroxenes) from hundreds of µm to a few mm. According to our dataset matrix amphiboles are mostly found in Alpine-type peridotites and xenoliths from intra-continental settings and continental arcs. On a few occasions, matrix amphiboles are present in ultramafic rocks from oceanic settings (e.g. Neal, 1988).

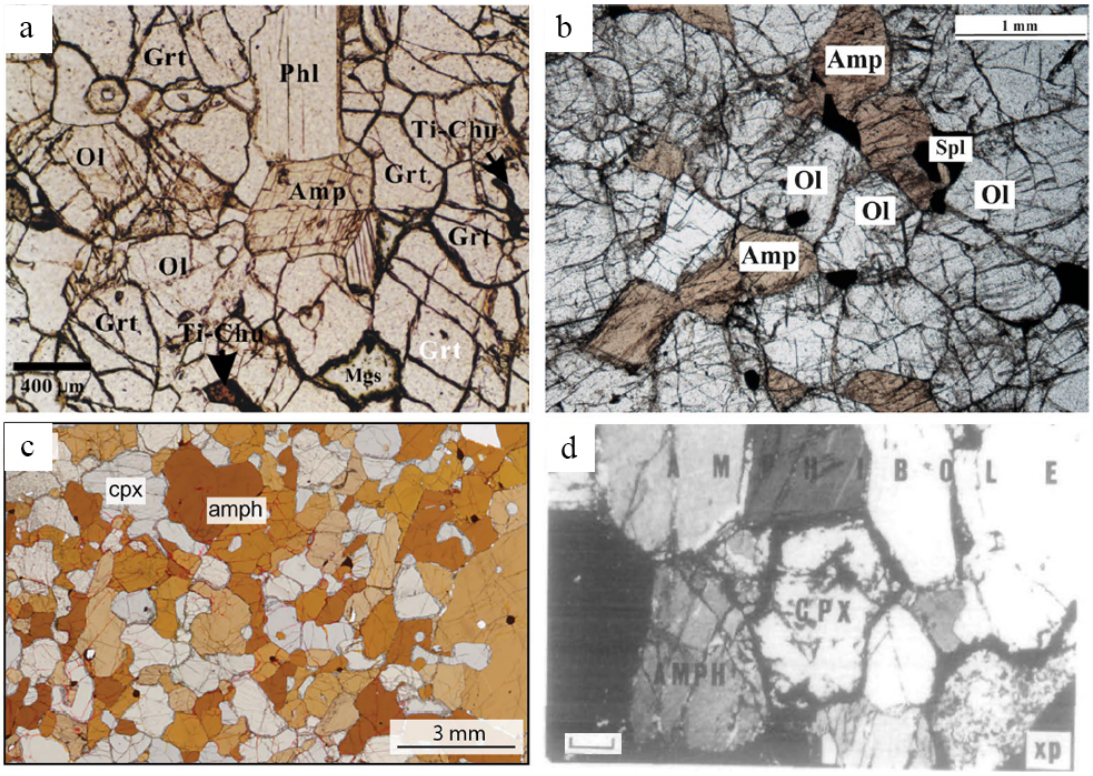

Figure 3.2: Photomicrographs of polygonal matrix amphiboles from different ultramafic rocks. a. Garnet lherzolite from the Su-Lu ultramafic body (Ye et al., 2009); b. Pyroxene-bearing peridotite from the Ivrea-Verbano Zone (Berno et al., 2020); c. Hornblendite from Spitsbergen (Hecker et al., 2020); d. Peridotite xenolith from Malaita (Neal, 1988).

Matrix amphiboles in ultramafic rocks, such as those depicted in Figure 3.2, are characterized by sharp boundaries with the coexisting minerals (garnet, olivine, spinel and pyroxenes). This feature has been widely used as evidence of textural equilibrium. It is considered that matrix amphiboles have been recrystallized and/or equilibrated (to some extent) in the same conditions with the rest of the matrix phases. This implies that their original textural characteristics have been completely eliminated. For this reason, matrix amphiboles require a thorough investigation to discover whether they have originally been crystallized directly from melts or fluids or if they are the result of fluid-melt/rock interactions.

For the reasons presented earlier, the origin of matrix amphiboles is a relatively not well-discovered topic to this day. However, the metasomatic agent that is involved in their formation is something which can often be derived from geochemical evidence. For example, matrix amphiboles from the Zhimafang garnet lherzolite (Su-Lu) have been related to metasomatic fluids or melts that were probably generated from the country UHP crustal rocks (Zhang et al., 2011; Ye et al., 2009). However, it is unknown whether the metasomatic fluids originally precipitated amphibole or reacted with the host peridotite. Similarly, the development of amphibole which is in textural equilibrium with other matrix minerals in the Ulten

peridotites, was also postulated to form from crustal fluids or SiO_2-rich melts. Rampone & Morten (2001) predicted the existence of H_2O-CO_2 fluids that modally metasomatized the Ulten peridotites. The fluids were probably generated from the partial melting of the host gneisses. Gudelius et al. (2019) have also concluded that all amphiboles from the Ulten peridotites (along with matrix amphiboles) resulted from the hydration of peridotites from crustal aqueous fluids. It is evident for matrix amphiboles, that it is particularly difficult to assess the processes that were involved at the time of their initial formation especially if they are part of peridotites. In other cases where an igneous origin is expected, the exact process of formation may be possible. For example, matrix amphiboles in xenolithic hornblendites from Khibiny (Russia) seem to own a cumulative origin from hydrous magmas according to Hecker et al. (2020).

3.4 Amphibole growing at the expense of other minerals

Amphiboles growing at the expense of other minerals is the most common and characteristic texture in ultramafic rocks. Clinopyroxene, orthopyroxene and spinel are by far the most usual minerals that are being replaced by amphiboles. Less often, amphiboles are part of coronas around garnet. A few demonstrative examples can be seen in Figure 3.3. Amphibole is usually developed as mantles around the boundaries of pyroxenes and spinel and it is completely anhedral in shape. Rarely, amphibole may be recrystallized forming small neoblasts around the replaced mineral phase. Frequently, amphibole is extremely pervasive and seems to have replaced a large portion of the volume of the pre-existing anhydrous phase such as in Figure 3.3a. On different occasions, amphiboles seem to be intruding orthopyroxene along cleavage planes (Figure 3.3b). In Figure 3.3c, a matrix clinopyroxene is surrounded by a thin mantle of amphibole and in Figure 3.3d, a large orthopyroxene has been extensively replaced by Mg-hornblende. Similarly, amphibole can occur as a thin zone around spinel (Figure 3.3e). In Figure 3.3f, amphibole has replaced a large fraction of spinel.

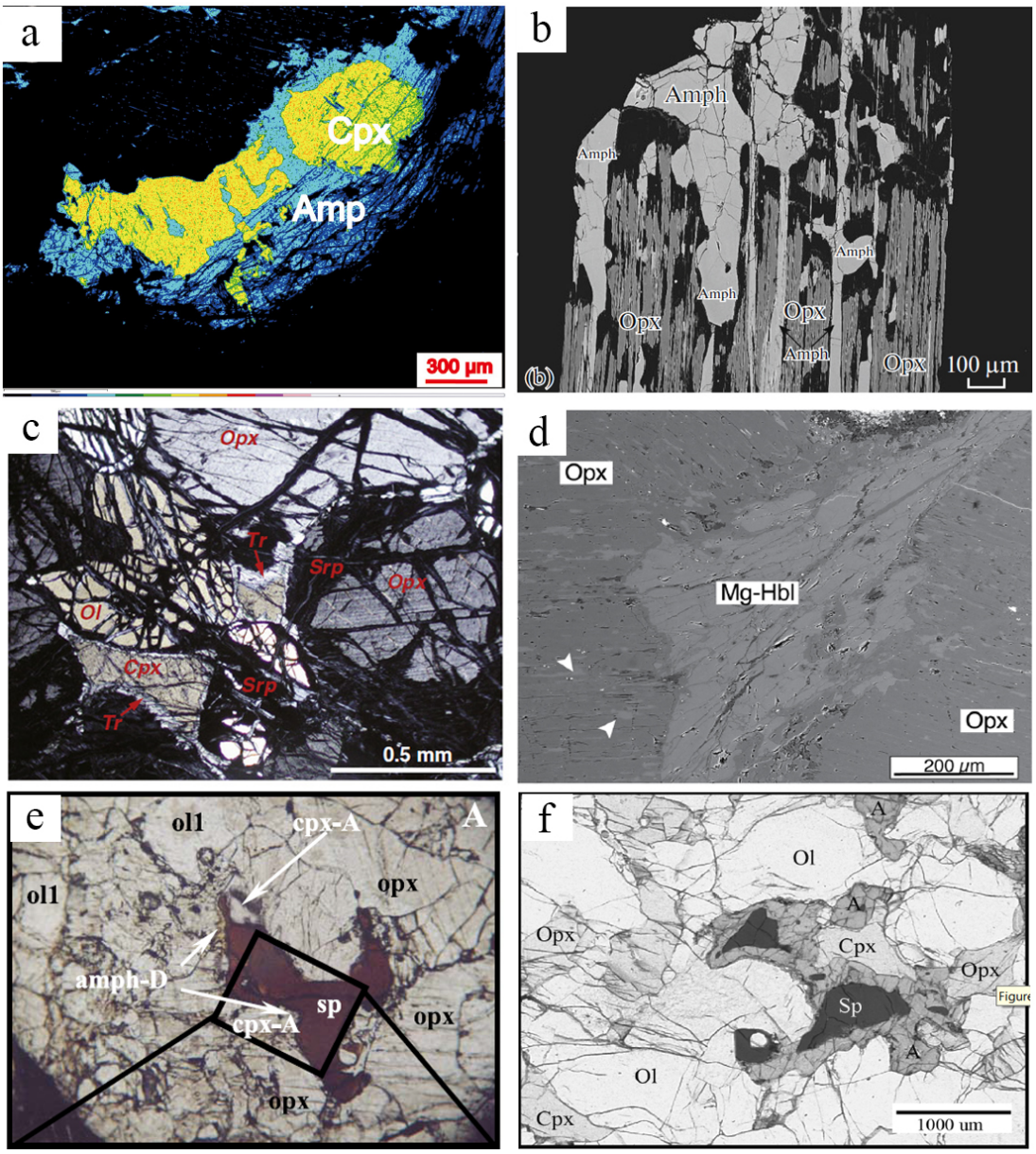

Figure 3.3: Photomicrographs of amphiboles replacing pyroxenes from different ultramafic rocks. a. Harzburgite from the Xigaze (Tian et al., 2022); b. Xenolithic peridotite from the Birekte Terrane in Siberia (Solov'eva et al., 2017); c. Peridotite from the Oeyama ophiolite in Japan (Nozaka, 2014); d. Mylonitic lherzolite from the Lanzo Massif in Italy (Vieira Duarte et al., 2020); e. Xenolithic peridotite from Victoria Land in Antarctica (Coltorti et al., 2004); Xenolithic peridotite from Dish Hill in California (Hunt & Lamb, 2019).

Reaction between metasomatizing melts or fluids and pre-existing mineral phases (e.g. pyroxenes and spinel) has been proposed to explain this characteristic texture. This reaction had firstly received two fundamental forms:

$$\text{Diopside} + \text{Spinel} + \text{Water} = \text{Amphibole} \quad \text{(Conquéré, 1971)} \qquad (1)$$

$$\text{Garnet} + \text{Diopside} + \text{Water} = \text{Amphibole} \quad \text{(Boyd, 1971)} \qquad (2)$$

Reaction (1) shows that both clinopyroxene and spinel interact with an H_2O-rich fluid or melt to form amphibole.

Boyd (1971) observed intergrowths of spinel and amphibole around garnet in harzburgites from Wesselton (South Africa). This led him to propose reaction (2). In fact, amphibole is usually found as an accessory mineral of kelyphitic coronas around garnets. Kelyphites are intergrowths that consist of orthopyroxene, spinel (± clinopyroxene ± amphibole) (for more details see Godard & Martin, 2000; Obata & Ozawa, 2011). On very rare occasions, amphibole is the only mineral mantling garnet (e.g. Janák et al., 2006). Kelyphites are thought to result from reactions of the following form:

$$\text{Garnet} + \text{Olivine} = \text{Orthopyroxene} + \text{Clinopyroxene} + \text{Spinel} + \text{Amphibole} \quad (3)$$

Subsequently, based on textural data, Best (1974) has proposed the following reaction:

$$\text{Cr-Spinel} + \text{Diopside} + \text{Fluid} = \text{Amphibole} \quad (4)$$

Reaction (4) is important because it shows that amphibole can incorporate Cr from spinel. Francis (1976) attempted to balance the reaction of Best (1974). He found out that although the involvement of a compositionally very complex fluid can give good results, it is not a very realistic option. For this reason he considered that orthopyroxene must necessarily be a reactant to balance the reaction:

$$\text{Fluid} + 28\ \text{Orthopyroxene} + 54\ \text{Clinopyroxene} + 71\ \text{Spinel} = 57\ \text{Chromite} + 100\ \text{Amphibole} \quad (5)$$

Francis (1976) has also pointed out that as reaction (5) progresses, amphibole is incorporating increasing amounts of Cr in its crystal structure. Neal (1988) has proposed a modification of (5) in which olivine is present as a product:

$$24\ \text{Cr-Spinel} + 16\ \text{Clinopyroxene} + 14\ \text{Orthopyroxene} + \text{Na-rich Fluid} = 8\ \text{Pargasite} + 12\ \text{Chromite} + 12\ \text{Olivine} \quad (6)$$

Neal (1988) has additionally proposed a reaction in which spinel is completely consumed and is not present as a product:

$$6\ \text{Spinel} + 8\ \text{Clinopyroxene} + 7\ \text{Orthopyroxene} + \text{Na-rich Fluid} = 4\ \text{Pargasite} + 6\ \text{Olivine} \quad (7)$$

Very often amphibole is found pervasive along the cleavage planes of clinopyroxene (Figure 3.4). In optical microscopy, this could be confused with a two-pyroxene exsolution lamellae. For this reason, the term “lamellae” has been extensively used in the literature in order to describe the texture. Amphibole lamellae in clinopyroxene has been observed in multiple localities around the globe (e.g. Yamaguchi et al., 1978; Neal, 1988; Franz et al., 2002; Chen & Xu, 2005; Ye et al., 2009). Although many processes have been proposed to explain amphibole lamellae, only two of them seem to be the most satisfactory. The first one involves reactions, similar to those that were previously given, in which metasomatic agents react with clinopyroxene along the cleavage planes and replace it with amphibole (e.g. Nakajima & Hafner, 1980; Isaacs et al., 1981). The second process involves the exsolution of amphibole from pyroxene as originally proposed by Desnoyers (1975). This hypothesis has also been envisaged by Smith (1977) and Yamaguchi (1978). In fact, Yamaguchi suggested that amphibole lamellae in Alpe Arami (Switzerland) occurred due to the decreasing solubility of Na, Al and Cr in clinopyroxene. Recently, Chen et al. (2019), have observed the existence of amphibole exsolution lamellae in chromites from the Semail Ophiolite.

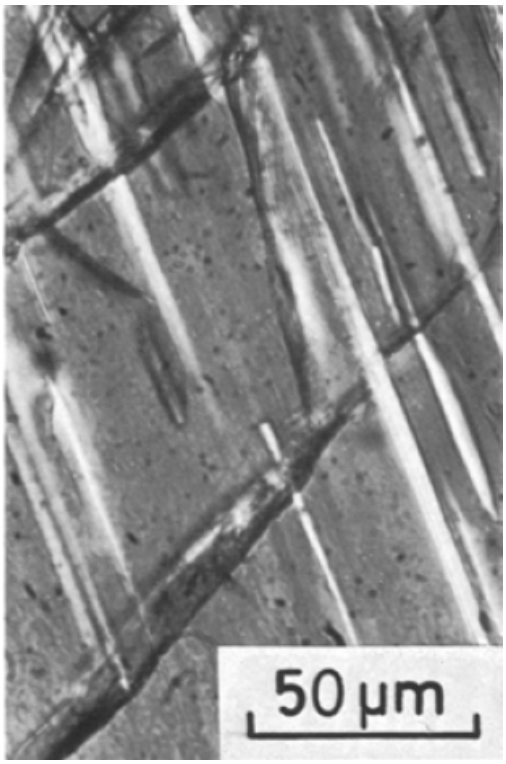

Figure 3.4: Amphibole present along the cleavage planes of clinopyroxene from the Alpe Arami peridotite (Yamaguchi et al., 1978)

Another puzzling texture is observed in several ultramafic rocks in which amphibole is overgrown by secondary clinopyroxene. For example, Matusiak-Malek

et al. (2017) have observed that coarse-grained matrix amphibole grains in the Wilcza Góra mantle xenoliths have been partially replaced by a late-stage generation of clinopyroxene. Clinopyroxene is euhedral and related to a glassy, spinel-bearing matrix (Figure 3.5). Shaw & Klügel (2002) and Ban et al. (2005) proposed that glass, clinopyroxene, spinel and olivine that grow at the expense of pre-existing amphibole may result from rapid heating and decompression. The disequilibrium experiments of Shaw (2009) at 1.2 GPa and 1000 °C, showed that the breakdown of amphibole generates pockets of glass, amphibole, clinopyroxene and olivine that occur within amphibole. With an increase of 50 °C, the volume of glass rapidly increases and a secondary amphibole is formed that contains olivine inclusions and is mantled by clinopyroxene. These experiments managed to prove that the breakdown of amphibole is more than enough to explain clinopyroxene, glass and spinel growing around amphibole such as the texture depicted in Figure 3.5.

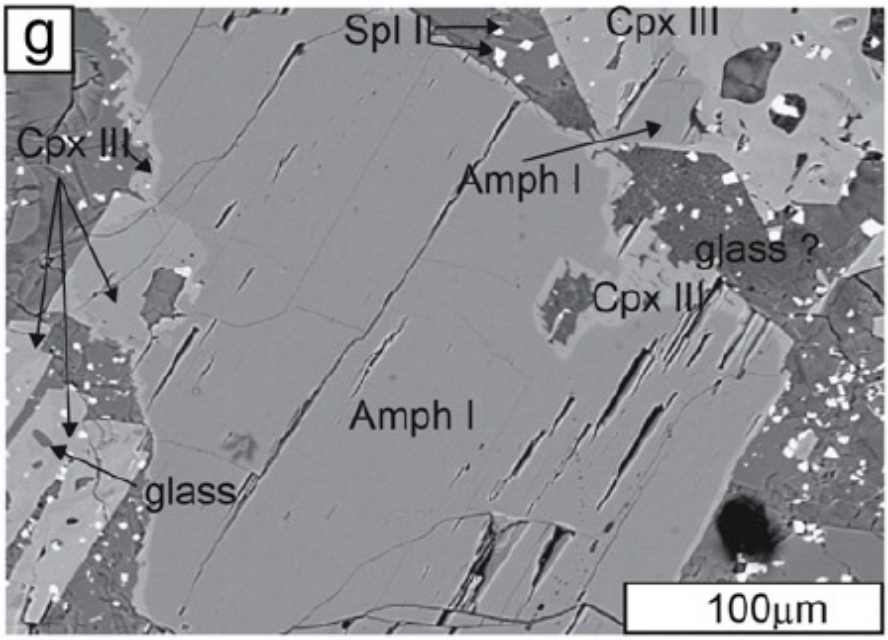

Figure 3.5: Photomicrograph of a coarse-grained matrix amphibole that is partially replaced by euhedral clinopyroxene (Matusiak-Malek et al., 2017).

3.5 Amphibole in veins

Amphiboles may occur in late-stage veins or veinlets that intrude and traverse ultramafic rocks. The veins can be monomineralic (amphibole only) or polymineralic (made of amphibole, pyroxene, spinel and apatite). Amphiboles in veins can be anhedral to euhedral in shape and constitute individual grains. Very often veins have been present at ambient mantle conditions for long enough time to equilibrate with

their host rocks (e.g. Ghent et al., 2019). Figure 3.6a depicts a thin (~500 μm thick) vein that shows acicular orthopyroxene at its boundaries with the host-rock and euhedral, prismatic amphibole and orthopyroxene at its center. It is predicted that amphiboles which formed at the center of veins are probably direct crystallization products from melts and fluids (e.g. Witt-Eickschen et al., 1994; Ghent et al., 2019; Siegrist et al., 2019). In Figure 3.6b, neoblastic amphibole and anhedral clinopyroxene have been formed at the contact between the vein and the wall-rock and are practically grown upon olivine. This may indicate a reactive origin for both minerals. The presence of sulfides along with metasomatic minerals may indicate that the metasomatizing agent was a sulfide-bearing silicate melt (Figure 3.6b). Therefore, amphiboles in veins that occur in contact with their host-rocks might indicate a reactive origin. Geochemical and textural data must be combined to confirm this hypothesis.

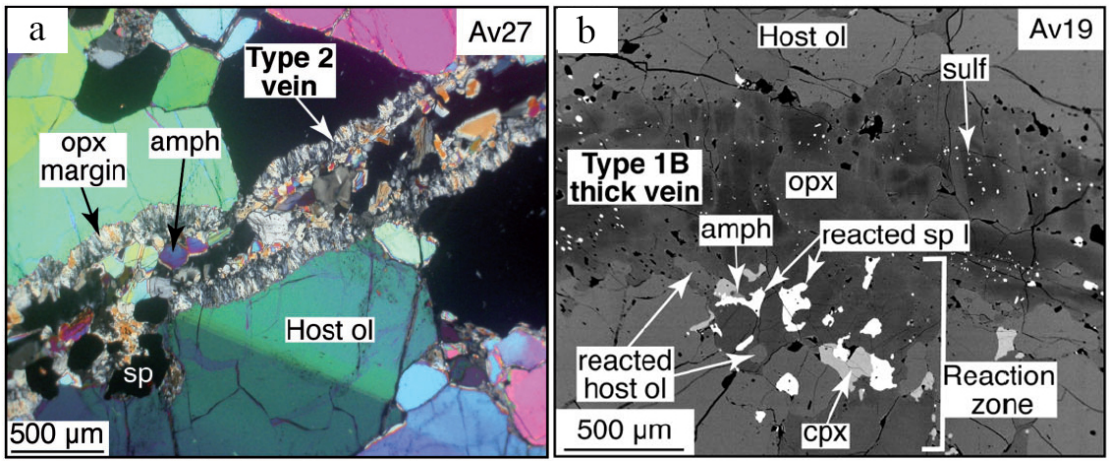

Figure 3.6: Amphiboles occurring in veins in xenoliths from the Avacha Volcano (Kamchatka) (Bénard & Ionov, 2013).

3.6 Amphibole porphyroclasts

Amphibole porphyroclasts are relatively usual in mantle xenoliths from continental rifting regions but also in Alpine-type peridotites (e.g. Piccardo et al., 1988; Xu & Bodinier, 2004; Sapienza et al., 2009; Nozaka, 2014; Czertowicz et al., 2016; Gudelius et al., 2019; Corvò et al., 2020; Pellegrino et al., 2020). They are large and tectonically deformed grains that are set in a fine-grained matrix that generally consists of olivine, clinopyroxene, orthopyroxene and other accessory minerals. They can be equidimensional or own a slightly elongated shape such as in Figure 3.7. Furthermore, in most cases the contacts with the matrix minerals are sharp and no coronas or reaction rims are evident.

Amphibole porphyroclasts are thought to represent a relic structure of an older and originally coarse-grained generation of minerals. Czertowicz et al. (2016) predicted that Mg-hornblende and edenite porphyroclasts from the Anita peridotite predate the rest of the metasomatic minerals found in the rocks. Similarly, Pellegrino et al. (2020) proposed that porphyroclastic amphiboles from Monte Duria (Switzerland) are in equilibrium with garnet and clinopyroxene porphyroclasts and they have all formed during peak-metamorphism in the garnet-peridotite stability field. After reaching peak conditions, amphibole porphyroclasts that are rich in Ti may exsolve ilmenite during pressure decrease and retrogression (e.g. Chen & Xu, 2005). From the discussion above it is profound that porphyroclastic amphiboles predate matrix phases. They were formed at an earlier metasomatic episode but the metamorphic evolution of the rock (re-equilibration, recrystallization etc.) have eliminated their original texture and characteristics. Therefore, similarly to matrix minerals, it is difficult to infer the processes that were involved during their original formation.

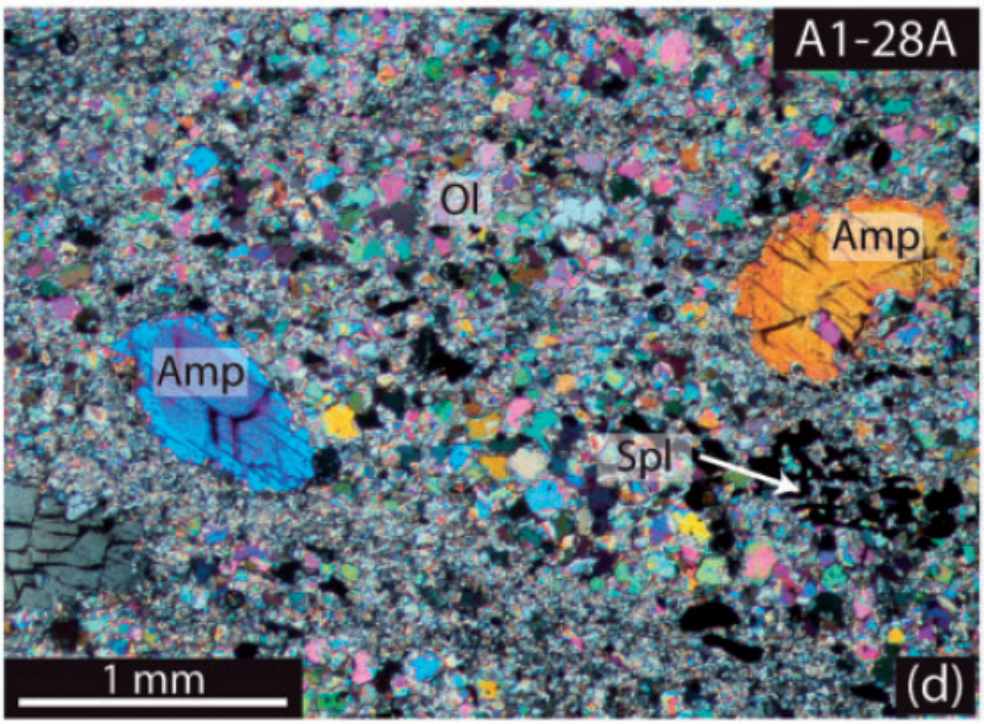

Figure 3.7: Amphibole porphyroclasts from the Anita peridotite (Czertowicz et al., 2016).

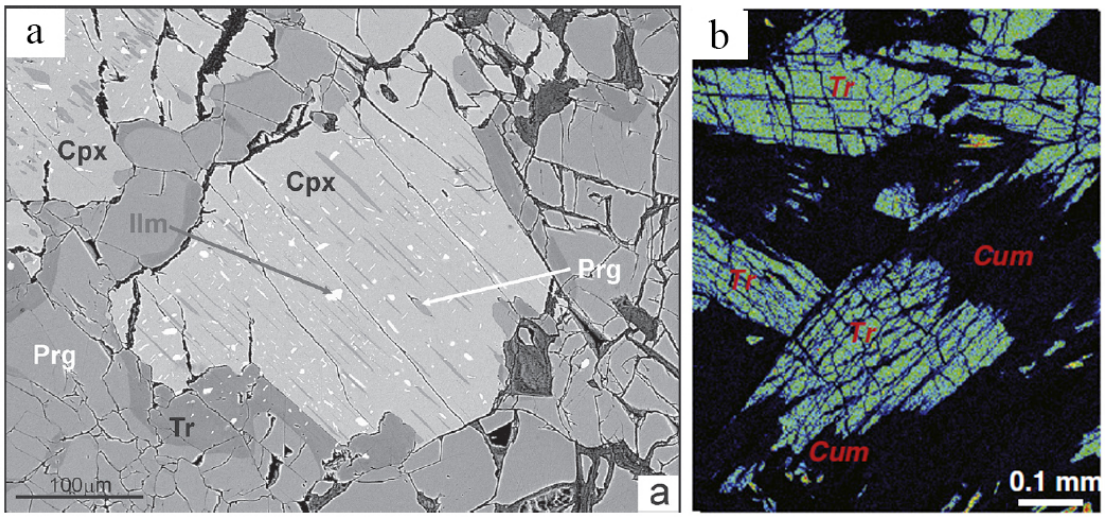

Figure 3.8: a. Tremolite replacing pargasite from the Pohorje garnet peridotite (Slovenia) (Vrabec, 2010); b. Cummingtonite replacing tremolite in the Oeyama ophiolite (Japan) (Nozaka, 2014)

3.7 Replacive amphiboles

Late-stage amphibole may replace amphibole that was formed in an older metasomatic episode. Two examples of this texture can be seen in Figure 3.8. A matrix clinopyroxene from the Pohorje garnet peridotite is mostly surrounded by pargasite which has been partly replaced by tremolite (Figure 3.8a). This clinopyroxene is also showing amphibole lamellae. Because pargasitic amphibole is stable at higher pressures, Vrabec (2010) considered that tremolite has replaced pargasite at the lower pressures and temperatures during a retrogression stage. In the Oeyama ophiolitic peridotites, cummingtonitic amphibole replaces tremolite (Figure 3.8b). According to Nozaka (2014) both cummingtonite and tremolite have been formed from metasomatic fluids in the temperature range of 650-750 °C. Similar textures have been observed in other localities (e.g. Albers et al., 2019; Pellegrino et al., 2020; Cluzel et al., 2022). However, the exact mechanism that leads to this texture is still not well discovered. It is generally thought that the late-stage amphibole is replacing the older generation during retrogression and cooling events.

3.8 Amphibole Inclusions

Amphibole may occur as round, irregular or polygonal inclusions in clinopyroxene, orthopyroxene, garnet and spinel in ultramafic rocks of all the

geotectonic settings. For example, amphibole inclusions in garnets from the Su-Lu garnet-lherzolite are pargasitic in composition and seem to be associated with chlorite but also with fractures that have penetrated the host mineral (Figure 3.9a). Clinopyroxenes, from Su-Lu, contain edenite inclusions that are in contact with phlogopite and seem to predate fractures (Figure 3.9b). In Figure 3.9c, a pargasite inclusion in spinel has been partially replaced by tremolite indicating that amphibole inclusions may be affected by processes similar to those that were discussed in 3.7.

Different genetic models, either metamorphic or igneous, have been proposed in the literature to explain amphibole inclusions. They have mostly been interpreted as relic phases that were crystallized at an earlier metamorphic/metasomatic stage than their host-phase (e.g. Carswell et al., 1983; Alibert, 1994; Yang, 2003). Sebsequent recrystallization of the rock has led to the formation of the host-mineral that enclosed amphibole. In contrast to this process, Yang & Hahn (2000) have observed aligned amphibole inclusions in porphyroblastic garnets from the Su-Lu garnet-lherzolite. From textural and geochemical charateristics they have concluded that the inclusions have been formed prior to the UHP metamorphism but later than the formation of garnets. They have also anticipated that metasomatic fluids infiltrated and reacted with the fractured garnets to form amphibole (fracture healing).

Based on trace-element data, Tamura et al. (2014) have predicted that pargasite inclusions in spinel from harzburgites in the Atlantis Massif oceanic core complex have been formed by secondary melts that were trapped and crystallized in spinel. Recently, numerous studies have shown that a similar, igneous origin may be postulated for amphibole inclusions in chromites of ophiolitic chromitites, dunites and harzburgites (Borisova et al., 2012; Johan et al., 2017; Rospabé et al., 2017; Rospabé et al., 2020; Pan et al., 2022). According to these studies, amphibole inclusions in chromites could be crystallized by hydrous melts. However, on many occasions, fluids may also be important factors in their formation. For example, Pan et al. (2022) have expected that amphibole inclusions in chromite (Figure 3.9d) have been derived from reactions between hydrous fluids and silicate melts. Rospabé et al. (2020) have also predicted that amphiboles in dunitic chromite may have precipitated from a hydrous and silica-rich melt or fluid. Borisova et al. (2012) have calculated that inclusions in chromites of the Oman ophiolitic chromitites may have formed between 950 and 1050 °C at 200 MPa from MORB melts.

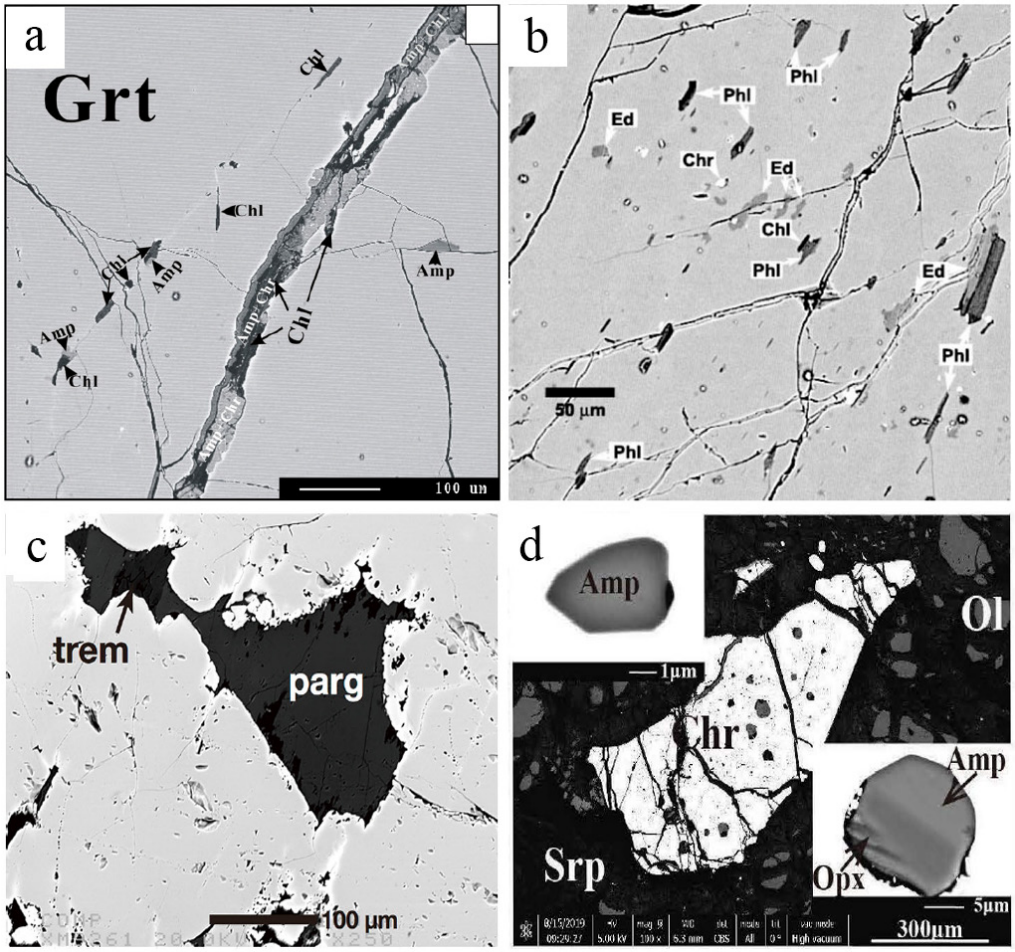

Figure 3.9: Inclusions of amphibole in: a. Garnet from the Su-Lu garnet-lherzolite (Ye et al., 2009); b. Clinopyroxene from the Su-Lu garnet lherzolite (Yang, 2003); c. Spinel in harzburgite from the IODP Site U1309 (Atlantis Massif) (Tamura et al., 2014); d. Chromite in harzburgite from the Lycian Ophiolite (Pan et al., 2022).

Conclusions

Bonatti et al. (1986) emphasized on the fact that different types of amphiboles are related to different evolutionary stages. Therefore, we can use amphiboles to obtain more information about each evolutionary stage. However, this is not always possible. In this chapter, it was shown that amphiboles can be divided into two major categories· those that directly precipitate from melts and fluids (precipitative amphiboles) and those that result from melt/fluid-rock interactions (reactive amphiboles). For the present study, interstitial amphiboles and some of the amphiboles that are found as inclusions or in veins will be considered precipitative. Amphiboles that are growing at the expense of other minerals or that are present in coronas around garnets belong to the reactive category. Another, less usual category,

involves amphiboles that replace preexisting ones (replacive). Finally, on many occasions it is extremely difficult to predict how the amphibole was formed because re-equilibration and recrystallization processes have acted on the rock. For this reason, a separate category must exist that is comprised of the matrix and porphyroclastic textures.

References

1. Albers E., Schroeder T., Bach W., 2019, Melt Impregnation of Mantle Peridotite Facilitates High-Temperature Hydration and Mechanical Weakening: Implications for Oceanic Detachment Faults, Geochemistry, Geophysics, Geosystems, vol. 20, pp. 84-108
2. Alibert C., 1994, Peridotite xenoliths from western Grand Canyon and the Thumb: A probe into the subcontinental mantle of the Colorado Plateau, Journal of Geophysical Research, vol. 99, pp. 605-621
3. Andrault D., Bolfan-Casanova N., 2022, Mantle rain toward the Earth's surface: A model for the internal cycle of water, Physics of the Earth and Planetary Interiors, vol. 322, 106815
4. Ban M., Witt-Eickschen G., Klein M., Seck H.A., 2005, The origin of glasses in hydrous mantle xenoliths from the West Eifel, Germany: incongruent break down of amphibole, Contributions to Mineralogy and Petrology, vol. 148, pp. 511-523
5. Bénard A., Ionov D.A., 2013, Melt- and Fluid-Rock Interaction in Supra-Subduction Lithospheric Mantle: Evidence from Andesite-hosted Veined Peridotite Xenoliths
6. Beran A., 1976, Messung des Ultrarot-Pleochroismus von Mineralen. XIV. Der Pleochroismus der OH-Streckfrequenz in Diopsid., Tschermaks Mineralogische und Petrographische Mitteilungen, vol. 23, pp. 79-85
7. Berno D., Tribuzio R., Zanetti A., Hémond C., 2020, Evolution of mantle melts intruding the lowermost continental crust: constraints from the Monte Capio-Alpe Cevia mafic-ultramafic sequences (Ivrea-Verbano Zone, northern Italy), Contributions to Mineralogy and Petrology, vol. 175, Issue 2
8. Best M.G., 1974, Contrasting types of chromium-spinel peridotite xenoliths in basanitic lavas, western Grand Canyon, Arizona, Earth and Planetary Science Letters, vol. 23, pp. 229-237
9. Bonatti E., Ottonello G., Hamlyn P.R., 1986, Peridotites from the island of Zabargad (St. John), Red Sea: Petrology and Geochemistry, Journal of Geophysical Research, vol. 91, pp. 599-631
10. Borisova A.Y., Ceuleneer G., Kamenetsky V.S., Arai S., Bejina F., Abily B., Bindeman I.N., Polvé M., De Parseval P., Aigouy T., Pokrovski G.S., 2012, A new View on the Petrogenesis of the Oman Ophiolite Chromitites from Microanalyses of Chromite-hosted Inclusions, Journal of Petrology, vol. 53, pp. 2411-2440
11. Boyd F.R., 1971, Pargasite-spinel peridotite xenolith from the Wesselton Mine, Yb. Carnegie Instn. Wash., vol. 70, pp. 138-42
12. Brearley M., Scarfe C.M., 1984, Amphibole in a spinel lherzolite xenolith: evidence for volatiles and partial melting in the upper mantle beneath southern British Columbia, Experimental Petrology Laboratory, Publication 80
13. Carswell D.A., Harvey M.A., Al-Samman A., 1983, The petrogenesis of contrasting Fe-Ti and Mg-Cr garnet peridotite types in the high grade gneiss complex of Western Norway, Bulletin de Minéralogie, vol. 106, pp. 727-750

14. Chen J., Xu Z.-Q., 2005, Pargasite and ilmenite exsolution texture in clinopyroxenes from the Hujialing garnet-pyroxenite, Su-Lu UHP terrane, Central China: a geodynamic implication, European Journal of Mineralogy, vol. 17, pp. 895-903
15. Chen T., Jin Z., Zhang J., Wang L., 2019, Calcium amphibole exsolution lamellae in chromite from the Semail ophiolite: Evidence for a high-pressure origin, Lithos, vol. 334-335, pp. 273-280
16. Cluzel D., Aitchison J.C., Zhou R., Ireland T., Heizler M., Patias D., Lesimple S., Maurizot P., Teyssier C., 2022, Direct dating of podiform Chromitite: U-Pb (Zircon, Rutile) and $^{40}Ar/^{39}Ar$ (Pargasite) evidence from Tiebaghi Cr deposit (New Caledonia), Ore Geology Reviews, vol. 145, Issue 104873
17. Coltorti M., Beccaluva L., Bonadiman C., Faccini B., Ntaflos T., Siena F., 2004, Amphibole genesis via metasomatic reaction with clinopyroxene in mantle xenoliths from Victoria Land, Antarctica, Lithos, vol. 75, pp. 115-139
18. Conquére F., 1971, La lherzolite à amphibole du gisement de Caussou (Ariège, France), Contributions to Mineralogy and Petrology, vol. 30, pp. 296-313
19. Corvò S., Langone A., Padròn-Navarta J.A., Tommasi A., Zanetti A., 2020, Porphyroclasts: Source and Sink of Major and Trace Elements During Deformation-Induced Metasomatism (Finero, Ivrea-Verbano Zone, Italy), Geosciences, vol. 10, 196
20. Czertowicz T.A., Scott J.M., Waight T.E., Palin J.M., Van der Meer Q.H.A., Le Roux P., Münker C., Piazolo S., 2016, The Anita Peridotite, New Zealand: Ultra-depletion and Subtle Enrichment in Sub-arc Mantle, Journal of Petrology, vol. 57, pp. 717-750
21. Dawson J.B., 1984, Contrasting types of upper mantle metasomatism?, In: Kimberlites II: The Mantle and Crust-Mantle Relations, edited by Kornprobst J., Amsterdam: Elsevier, pp. 277-287
22. Desnoyers C., 1975, Exsolutions d'amphibole, de grenat et de spinelle dans les pyroxènes des roches ultrabasiques: pèridotite et pyroxènolites, Bulletin de la Société francaise de Minéralogie et de Cristallographie, vol. 98, pp. 65-77
23. Duarte Vieira J.F., Kaczmarek M.-A., Vonlanthen P., Putlitz B., Müntener O., 2020, Hydration of a Mantle Shear Zone Beyond Serpentine Stability: A possible Link to Microseismicity Along Ultraslow Spreading Ridges?, Journal of Geophysical Research: Solid Earth, vol. 125, Issue 10
24. Fabriès J., Bodinier J.-L., Dupuy C., Lorand J.-P., Benkerrou C., 1989, Evidence for Modal Metasomatism in the Orogenic Spinel Lherzolite Body from Caussou (Northeastern Pyrenees, France), Journal of Petrology, vol. 30, pp. 199-228
25. Francis D.M., 1976, The Origin of Amphibole in Lherzolite Xenoliths from Nunivak Island, Alaska, Journal of Petrology, vol. 17, pp. 357-378
26. Franz L., Becker K.-P., Kramer W., Herzig P.M., 2002, Metasomatic Mantle Xenoliths from the Bismarck Microplate (Papua New Guinea)-Thermal Evolution, Geochemistry and extent of Slab-induced Metasomatism, Journal of Petrology, vol. 43, pp. 315-343
27. Ghent E.D., Edwards B.R., Russel J.K., 2019, Pargasite-bearing vein in spinel lherzolite from the mantle lithosphere of the North America Cordillera, Canadian Journal of Earth Sciences, vol. 56, Issue 8
28. Godard G., Martin S., 2000, Petrogenesis of kelyphites in garnet peridotites: a case study from the Ulten zone, Italian Alps, Journal of Geodynamics, vol. 30, pp. 117-145
29. Gudelius D., Aulbach S., Braga R., Höfer H.E., Woodland A.B., Gerdes A., 2019, Element Transfer and Redox Conditions in Continental Subduction Zones: New Insights from Peridotites of the Ulten Zone, North Italy, Journal of Petrology, vol. 60, pp. 231-268
30. Harte B., 1977, Rock Nomenclature with Particular Relation to Deformation and Recrystallisation Textures in Olivine-Bearing Xenoliths, Journal of Geology, vol. 85, pp. 279-288

31. Harte B., 1983, Mantle peridotites and processes-the kimberlite samples, In: Continental basalts and mantle xenoliths, edited by Hawkesworth C.J., Norry M.J., Shiva Publishing Ltd., Nantwich, Cheshire, UK, pp. 46-91
32. Hecker J.G., Marks M.A.W., Wenzel T., Markl G., 2020, Halogens in amphibole and mica from mantle xenoliths: Implications for the halogen distribution and halogen budget of the metasomatized continental lithosphere, American Mineralogist, vol. 105, pp. 781-794
33. Hunt L.E., Lamb W.M., 2019, Application of mineral equilibria to estimate fugacities of H_2O, H_2 and O_2 in mantle xenoliths from the southwestern U.S.A., American Mineralogist, vol. 104, pp. 333-347
34. Ionov D.A., 2010, Petrology of Mantle Wedge Lithosphere: New Data on Supra-Subduction Zone Peridotite Xenoliths from the Andesitic Avacha Volcano, Kamchatka, Journal of Petrology, vol. 51, pp. 327-361
35. Isaacs A.M., Brown P.E., Valley J.W., Essene E.J., Peacor D.R., 1981, An analytical Electron Microscopic Study of a Pyroxene-Amphibole Intergrowth, Contributions to Mineralogy and Petrology, vol. 77, pp. 115-120
36. Janàk M., Froitzheim N., Vrabec M., Krogh Ravna E.J., de Hoog J.C.M., 2006, Ultrahigh-pressure metamorphism and exhumation of garnet peridotite in Pohorje, Eastern Alps, Journal of Metamorphic Geology, vol. 24, pp. 19-31
37. Johan Z., Martin R.F., Ettler V., 2017, Fluids are bound to be involved in the formation of ophiolitic chromite deposits, European Journal of Mineralogy, vol. 29, pp. 543-555
38. Liptai N., Patkó L., Kovács I.J., Hidas K., Pintér Z., Jeffries T., Zajacz Z., O'Reilly S.Y., Griffin W.L., Pearson N.J., Szabó C., 2017, Multiple Metasomatism beneath the Nógrád-Gömör Volcanic Field (Northern Pannonian Basin) Revealed by Upper Mantle Peridotite Xenoliths, Journal of Petrology, vol. 58- pp. 1107-1144
39. Matusiak-Malek M., Puziewicz J., Ntaflos T., Grégoire M., Kukula A., Wojtulek P. M., 2017, Origin and evolution of rare amphibole-bearing mantle peridotites from Wilcza Góra (SW Polang), Central Europe, vol. 286-287, pp. 302-323
40. Mengel K., Green D.H., 1989, Stability of amphibole and phlogopite in metasomatized peridotite under water-saturated and water-undersaturated conditions, Fourth International Kimberlite Conference, Perth. Geol. Soc. Aust. Spec. Publ., vol. 14, pp. 571-581
41. Mercier J.-C. C., Nicolas A., 1975, Textures and Fabrics of Upper-Mantle Peridotites as Illustrated by Xenoliths from Basalts, Journal of Petrology, vol. 16, pp. 454-487
42. Nakajima Y., Hafner S.S., 1980, Exsolution in Augite From the Skaergaard Intrusion, Contributions to Mineralogy and Petrology, vol. 72, pp. 101-110
43. Neal C.R., 1988, The Origin and Composition of Metasomatic Fluids and Amphiboles beneath Malaita, Solomon Islands, Journal of Petrology, vol. 29, pp. 149-179
44. Nozaka T., 2014, Metasomatic hydration of the Oeyama forearc peridotites: Tectonic implications, Lithos, vol. 184-187, pp. 346-360
45. Obata M., Ozawa K., 2011, Topotaxic relationships between spinel and pyroxene in kelyphite after garnet in mantle-derived peridotites and their implications to reaction mechanism and kinetics, Mineralogy and Petrology, vol. 101, pp. 217-224
46. Ohtani E., Yuan L., Ohira I., Shatskiy A., Litasov K., 2018, Fate of water transported into the deep mantle by slab subduction, Journal of Asian Earth Sciences, vol. 167, pp. 2-10
47. Pan Q.-Q., Xiao Y., Su B.-X., Liu X., Robinson P.T., Cui M.-M., Wang J., Uysal I., 2022, Fingerprinting stealth metasomatism in ophiolitic peridotites, vol. 424-425, 106755
48. Pellegrino L., Malaspina N., Zanchetta S., Langone A., Tumiati S., 2020, High pressure melting of eclogites and metasomatism of garnet peridotites from Monte Duria Area (Central Alps, N Italy): A proxy for melt-rock reaction during subduction, Lithos, vol. 358-359, Issue 105391
49. Piccardo G.B., Rampone E., Scambelluri M., 1988, The Alpine evolution of the Erro-Tobbio Peridotites (Voltri Massif-Ligurian Alps): Some field and petrographic constraints, Ofioliti, vol. 13, pp. 169-174

50. Pike J.E.N., Schwarzman E.C., 1977, Classification of textures in ultramafic xenoliths, Journal of Geology, vol. 85, pp. 49-61
51. Pintér Z., Patkó L., Djoukam J.F.T., Kovács I., Tchouankoue J.P., Falus G., Konc Z., Tommasi A., Barou F., Mihály J., Németh C., Jeffries T., 2015, Characterization of the sub-continental lithospheric mantle beneath the Cameroon volcanic line inferred from alkaline basalt hosted peridotite xenoliths from Barombi Mbo and Nyos Lakes, Journal of African Earth Sciences, vol. 111, pp. 170-193
52. Rampone E., Morten L., 2001, Records of Crustal Metasomatism in the Garnet Peridotites of the Ulten Zone (Upper Austroalpine, Eastern Alps), Journal of Petrology, vol. 42, pp. 207-219
53. Rospabé M., Ceuleneer G., Benoit M., Abily B., Pinet P., 2017, Origin of the dunitic mantle-crust transition zone in the Oman ophiolite: The interplay between percolating magmas and high-temperature hydrous fluids, Geology, vol. 45, PP. 471-474
54. Rospabé M., Ceuleneer G., Benoit M., Kaczmarek M.-A., 2020, Composition gradients in silicate inclusions in chromites from the dunitic mantle-crust transition (Oman ophiolite) reveal high temperature fluid-melt-rock interaction controlled by faulting, Ofioliti, Edizioni ETS, vol. 45, pp. 103-114
55. Rossman G.R., 1988, Vibrational Spectroscopy of Hydrous Components. In: Spectroscopic Methods in Mineralogy, edited by Hawthorne F.C., Reviews in Mineralogy, vol. 18, pp. 193-206
56. Sapienza G.T., Scambelluri M., Braga R., 2009, Dolomite-bearing orogenic garnet peridotites witness fluid-mediated carbon recycling in a mantle wedge (Ulten Zone, Eastern Alps, Italy), Contributions to Mineralogy and Petrology, vol. 158, pp. 401-420
57. Shaw C.S.J., Klügel A., 2002, The pressure and temperature conditions and timing of glass formation in mantle-derived xenoliths from Baarley, West Eifel, Germany: the case for amphibole breakdown, lava infiltration and mineral-melt reaction, Mineralogy and Petrology, vol. 74, pp. 163-187
58. Shaw C.S.J., 2009, Textural development of amphibole during breakdown reactions in a synthetic peridotite, Lithos, vol. 110, pp. 215-228
59. Siegrist M., Yogodzinski G., Bizimis M., Fournelle J., Churikova T., Dektor C., Mobley R., 2019, Fragments of Metasomatized Forearc: Origin and Implications of Mafic and Ultramafic Xenoliths From Kharchinsky Volcano, Kamchatka, Geochemistry, Geophysics, Geosystems, vol. 20, pp. 4426-4456
60. Smith D., 1977, The origin and interpretation of spinel-pyroxene clusters in peridotite, Journal of Geology, vol. 85, pp. 476-482
61. Solov'eva L.V., Kalashnikova T.V., Kostrovitsky S.I., Ivanov A.V., Matsuk S.S., Suvorova L.F., 2017, Phlogopite and Phlogopite-Amphibole Parageneses in the Lithospheric Mantle of the Birekte Terrane (Siberian Craton), Doklady Earth Sciences, vol. 475, pp. 822-827
62. Swan A.R.H., Sandilands M., 1995, Introduction to Geological Data Analysis, Blackwell Science, Oxford
63. Tabor F.A., Tabor B.E., Downes H., 2010, Quantitative characterization of textures in mantle spinel peridotite xenoliths. In: Petrological Evolution of the European Lithospheric Mantle, Geological Society, London, Special Publications, vol. 337, pp. 195-211
64. Tabor B.E., Downes H., 2019, Textures of mantle peridotite rocks revisited, Lithos, vol. 348-349, 105203
65. Tamura A., Morishita T., Ishimaru S., Arai S., 2014, Geochemistry of spinel-hosted amphibole inclusions in abyssal peridotite: insight into secondary melt formation in melt-peridotite reaction, Contributions to Mineralogy and Petrology, vol. 167, pp. 974
66. Tian L.-R., Zheng J.-P., Xiong Q., Zhou X., Liang H., Dai H.-K., 2022, Xigaze ophiolite (South Tibet) records complex melt-fluid-peridotite interaction in the crust-mantle transition zone beneath oceanic slow-ultraslow spreading centers, Lithos, vol. 414-415, Issue 106623
67. Villaseca C., Serrano J.G., Pérez-Soba C., 2020, Subduction-related metasomatism in the lithospheric mantle beneath the Calatrava volcanic field (central Spain): constraints from

lherzolite xenoliths of the Cerro Gordo volcano, International Geology Review, vol. 64, pp. 469-488

68. Vrabec M., 2010, Garnet peridotites from Pohorje: Petrography, geothermobarometry and metamorphic evolution, Geologija, vol. 53, pp. 21-36
69. Witt-Eickschen G., Harte B., 1994, Distribution of trace elements between amphibole and clinopyroxene from mantle peridotites of the Eifel (western Germany): An ion-microprobe study, Chemical Geology, vol. 117, pp. 235-250
70. Xu Y.-G., Bodinier J.-L., 2004, Contrasting Enrichments in High- and Low-Temperature Mantle Xenoliths from Nushan, Eastern China: Results of a Single Metasomatic Event during Lithospheric Accretion?, Journal of Petrology, vol. 45, pp. 321-341
71. Yamaguchi Y., Akai J., Tomita K., 1978, Clinoamphibole Lamellae in Diopside of Garnet Lherzolite From Alpe Arami, Bellinzona, Switzerland, Contributions to Mineralogy and Petrology, vol. 66, pp. 263-270
72. Yang J.-J., 2003, Relict edenite in a garnet lherzolite from the Chinese Su-Lu UHP metamorphic terrane: Implications for metamorphic history, American Mineralogist, vol. 88, pp. 180-188
73. Yang J.-J., Hahn B.-M., 2000, Deep subduction of mantle-derived garnet peridotites from the Su-Lu UHP metamorphic terrane in China, Journal of Metamorphic Geology, vol. 18, pp. 167-180
74. Ye K., Song Y. R., Chen Yi., Xu H. J., Liu J. B., Sun M., 2009, Multistage metamorphism of orogenic garnet-lherzolite from Zhimafang, Sulu UHP terrane, E. China: Implications for mantle wedge convection during progressive oceanic and continental subduction, vol. 109, pp. 155-175
75. Zhang R.Y., Liou J.G., Huberty J.M., Xu H., Maki K., Jahn B.-M., Iizuka Y., 2011, Origin and Metamorphic Evolution of Garnet Clinopyroxenite from the Sulu UPP Terrane, China: Evidence from Mineral Chemistry and Microstructures, In: Ultrahigh-Pressure Metamorphism, 25th Years After The Discovery Of Coesite And Diamond, Edited by Dobrzhinetskaya L.F., Faryad S.W., Wallis S., Cuthbert S., pp. 151-185

CHAPTER 4
A new amphibole-clinopyroxene Fe+2–Mg exchange thermometer for ultramafic rocks

Introduction

The partitioning of Fe^{+2} and Mg between coexisting ferromagnesian minerals has been widely used as a geothermometer, as it is mainly a function of temperature. Iron-magnesium exchange reactions are characterized by minimum volume changes ($\Delta V_{reaction}$) hence, the pressure dependence of such reactions is insignificant. However, the partitioning of Fe^{+2} and Mg may be influenced by the concentrations of other components present (e.g., Graham & Powell, 1984). This behavior is related to non-ideal mixing in multi-component solid solutions such as garnet, pyroxene, and amphibole. Consequently, in thermometric expressions, the inclusion of compositional parameters that describe non-ideal behavior is important.

In ultramafic rocks, some of the most well-established and used Fe^{+2}–Mg exchange thermometers are those between garnet and orthopyroxene (Harley, 1984; Lee & Ganguly, 1988; Nimis & Grütter, 2010), garnet and clinopyroxene (Ellis & Green, 1979; Powell, 1985; Krogh, 1988; Ai, 1993; Nakamura, 2009), garnet and olivine (O'Neill & Wood, 1979; Wu & Zhao, 2007), and orthopyroxene and olivine (Seckendorff & O'Neill, 1993). Two-pyroxene geothermometry is different as it is based on the miscibility gap between clinopyroxene and orthopyroxene, which is temperature-dependent. Exchange of the enstatite component between the two pyroxenes is the most common formulation method (Wells, 1977; Bertrand & Mercier, 1985; Brey & Köhler, 1990; Taylor, 1998).

Iron-magnesium exchange geothermometers involving amphibole have been proposed only for felsic to mafic composition rocks. Wells (1979) was the first to construct an empirical garnet-hornblende calibration. However, it was based on limited data, exclusively on eclogitic rock compositions, and its application was questioned. Graham & Powell (1984) and Powell (1985) devised an empirical equation using garnet-hornblende pairs from natural amphibolites, granulites, and experimental basalts with applications to metamorphic rocks of andesitic to basaltic composition. Krogh Ravna (2000) published the latest garnet-amphibole, Fe^{+2}–Mg exchange thermometer along with a method to estimate Fe^{+3} in both amphibole and

garnet. His thermometer has been proven to be more precise, but it is only applicable to amphibolites and hornblende-metapelites of intermediate to basic composition.

Niida & Green (1999) have proposed a method to calculate the temperature and pressure of amphibole formation in ultramafic rocks based on the sodium content of amphibole according to their experimental results. Mandler & Grove (2016) suggested an empirical amphibole geothermobarometer based entirely on their experimental data as well. Recently, new geothermobarometric methods have been proposed, but they are focused on magmatic amphiboles in equilibrium with mafic to felsic melts (e.g., Ridolfi, 2021; Higgins et al., 2022). A thorough and inclusive geothermometric formulation for amphiboles in ultramafic rocks has not yet been considered. In this chapter, a new Fe^{+2}–Mg exchange thermometer between amphibole and clinopyroxene will be presented that makes use of all available experimental data on ultramafic compositions. Because amphibole is a metasomatic mineral that is incorporated in ultramafic rocks at some point during their evolution, the amphibole-clinopyroxene thermometer aims to explore the degree of equilibration of amphibole with the primary mantle phases.

4.1 P-T-X controls on amphibole formation

The presence of amphibole in the mantle is crucial in petrological studies. Amphibole, as well as other metasomatic minerals such as phlogopite, influence partial melting processes occurring in the mantle and thus the generation of basaltic melts. Therefore, the stability of amphibole in the mantle is a very important topic that has troubled petrologists throughout the years. It was first discussed by Oxburgh (1964), Ringwood (1962), and Kushiro (1968), but in these works, no experimental amphiboles were investigated.

Mysen & Boettcher (1975) have observed that the stability of amphibole in peridotite is highly dependent on bulk composition with higher peridotite Mg# $\left(\frac{Mg}{Mg+Fe_{tot}}\right)$ stabilizing amphibole at higher pressure. Wallace & Green (1991) demonstrated that alkali-rich peridotitic compositions stabilize amphibole at higher P–T conditions. This was also supported by Niida & Green (1999) who observed that the stability field of pargasite may be isobarically expanded from 1025 to 1150°C with increasing alkali (Na and K) content of the starting bulk-rock composition. This idea was also supported by Fumagalli et al. (2009) and Mandler & Grove (2016). Amphibole stability is also highly dependent on the H_2O content of the rock. This was observed in several experimental studies on water-saturated compositions (e.g.,

Millhollen et al., 1974; Grove et al., 2006). It was found that large, but non-realistic, amounts of H_2O decrease the P-T stability of amphibole in mantle rocks. However, even 1 wt.% of H_2O is enough to decrease the stability of amphibole as Green et al. (2014) have shown. Therefore, free H_2O may destabilize amphibole by leaching alkalis into the fluid phase (Mandler & Grove, 2016).

Some of the first, experimentally produced, amphiboles were synthesized by Green (1973) by adding variable amounts of H_2O to a pyrolite mantle composition. Pyrolite is a model composition proposed by Ringwood (1962) to simulate the MORB-source mantle. Pyrolite is comprised of one part of tholeiitic basalt and three parts of dunite. In every experimental run of Green (1973), approximately 40 vol. i % of olivine was removed from the original pyrolite to reduce the dominance of olivine and to facilitate the detection of minor phases. This method was also used in subsequent studies (e.g., Wallace & Green, 1991; Niida & Green, 1999; Fumagalli et al. 2009). Olivine subtraction increases the relative abundance of all oxides in the starting material except MgO. For example, in Green (1973), CaO has been shifted from 3.1 to 5.1 wt.% and Na_2O from 0.6 to 0.95 wt.%. The relative increase in oxide weights enhances the experimental composition in terms of alkalis which, as discussed earlier, are important for the stabilization of amphibole. Mandler & Grove (2016) have pointed out that olivine subtraction may introduce errors and uncertainty due to the assumptions made about the composition of olivine. According to these authors, olivine subtraction leads to higher Cr/Al, Al/Mg, and Na/Si ratios, but lower Fe/Mg ratios in residual phases.

Millhollen et al. (1974) adopted a different experimental approach. Instead of using a pyrolite mantle composition and removing olivine from the starting material, they have used a natural spinel-bearing peridotite from the St. Paul's Rocks. The peridotite was already rich in pargasite and contained 5.7 wt.% H_2O bound in hydrous minerals. Likewise, Mysen & Boettcher (1975) used natural peridotites of variable composition. In their experiments, amphibole was scarce in the peridotitic compositions with the lowest alkalis and abundant in alkali-rich experimental runs. On other occasions, the metasomatic component was added in the form of phlogopite which provided the needed alkalis and H_2O to the experimental system. For example, Mengel & Green (1989) have added an equivalent of 1.5 wt.% phlogopite in an anhydrous peridotitic composition to account for the metasomatic component. Mandler & Grove (2016) have also introduced 1 wt.% of a metasomatic component made of 65 wt.% H_2O, 30 wt.% Na_2O and 5 wt.% K_2O to simulate slab-derived fluids/melts.

In many recent experimental studies, the starting materials were constructed by mixing pure synthetic oxide powders and carbonates (e.g., Adam & Green, 2006; Grove et al., 2006; Green et al., 2014; Mallik et al., 2015; Pintér et al., 2021; Wang et al., 2021). In Mallik et al. (2015) and Wang et al. (2021), experimentally synthesized peridotites, representing unmodified compositions, were fluxed and reacted with model, hydrous rhyolitic or basaltic melts. In these experiments, the melts provided the required H_2O and probably alkalis to the system to generate amphibole. Once the reaction occurred, the samples were allowed to equilibrate. In the remaining studies, H_2O was introduced either via a microsyringe or in the form of brucite [$Mg(OH)_2$].

As noted in previous chapters, amphibole is a metasomatic mineral which is related either to melts or fluids of variable composition. These metasomatic agents penetrate the ultramafic rocks and then directly crystallize amphibole or react with pre-existing minerals like pyroxene, spinel, and garnet. Therefore, amphibole is not a primary mantle phase, which means that it does not naturally form under ambient mantle conditions because these anhydrous conditions do not favor its crystallization. Amphibole is a secondary mineral, and its formation requires the existence of an external hydrous metasomatic agent that is rich in alkalis. This metasomatic agent has been approximated by several different methods in ultramafic composition experiments.

4.2 Construction of the thermometer

4.2.1 Collection of experimental data

A total of 84 amphibole-clinopyroxene equilibrium pairs on ultramafic compositions were culled from the literature. During the initial inspection of the data, one pair from Gorbachev et al. (2020) and two pairs from Green (1973) were suspected of disequilibrium and excluded outright. All amphibole-clinopyroxene pairs from Shaw (2009) were also excluded from the data set, as the attainment of equilibrium was not the primary goal of the experimental work. Unfortunately, the compositions of the experimental run products of Millhollen et al. (1974) and Mysen & Boettcher (1975) were not given in their publications.

Table 4.2: Experimental amphibole-clinopyroxene pairs from ultramafic compositions used.

Reference (in chronological order)	No. of pairs (before calibration)	No. of pairs (after calibration)
Mengel & Green, 1989	4	3
Wallace & Green, 1991	3	3
Niida & Green, 1999	18	15
Adam & Green, 2006	2	1
Grove et al., 2006	1	1
Fumagalli et al., 2009	5	4
Green et al., 2010	1	1
Green et al., 2014	17	12
Mallik et al., 2015	3	2
Mandler & Grove, 2016	19	18
Corgne et al., 2018	2	0
Pinter et al., 2021	2	2
Wang et al., 2021	7	2
Total	84	64

4.2.2 P-X and T-X diagrams

The variation in the chemical composition of amphibole and clinopyroxene with experimental temperature and pressure is shown in Figures 4.1–4.3. According to Niida & Green (1999), total Al in amphibole increases with increasing temperature. This, however, was not observed in our data set (Figure 4.1a). On the other hand, there is a significant negative correlation between total Al and pressure (Figure 4.1b). The difference between our study and Niida & Green (1999) is possibly due to the wider and more inclusive compositional range of our database. Tetrahedral Al and total Ca in amphibole, also display a negative trend with pressure but no relation to temperature (Figure 4.1c-f). Total Na, and Na in site A increase with increasing temperature and pressure (Figure 4.1a-d). This is in good agreement with the observations of Niida & Green (1999) and Mandler & Grove (2016). However, pressure affects the Na content of amphibole in a much more profound and significant way compared to temperature. This is indicated by the much higher R^2 values and the more precise linear fitting (Figure 4.1a-d). Finally, Ti in experimental amphibole shows no significant relation with either temperature or pressure (Figure 4.2e-f).

Most of the compositional changes discussed above are related to ionic substitutions in the amphibole crystal lattice. Generally, as pressure and temperature increase, pargasitic amphiboles become gradually enriched in the edenite, richterite

and magnesio-katophorite components. The most important substitutions that define these transformations, as noted by Mandler & Grove (2016), may be written as:

Richterite substitution: $Ca^{+2} + (Al, Fe, Cr)^{+3} + 2\ Al^{+3} \Leftrightarrow Na + Mg^{+2} + 2\ Si^{+4}$
Magnesio-katophorite substitution: $Ca^{+2} + Al^{+3} \Leftrightarrow Na^{+} + Si^{+4}$
Edenite substitution: $(Al, Fe, Cr)^{+3} + Al^{+3} \Leftrightarrow Mg^{+2} + Si^{+4}$

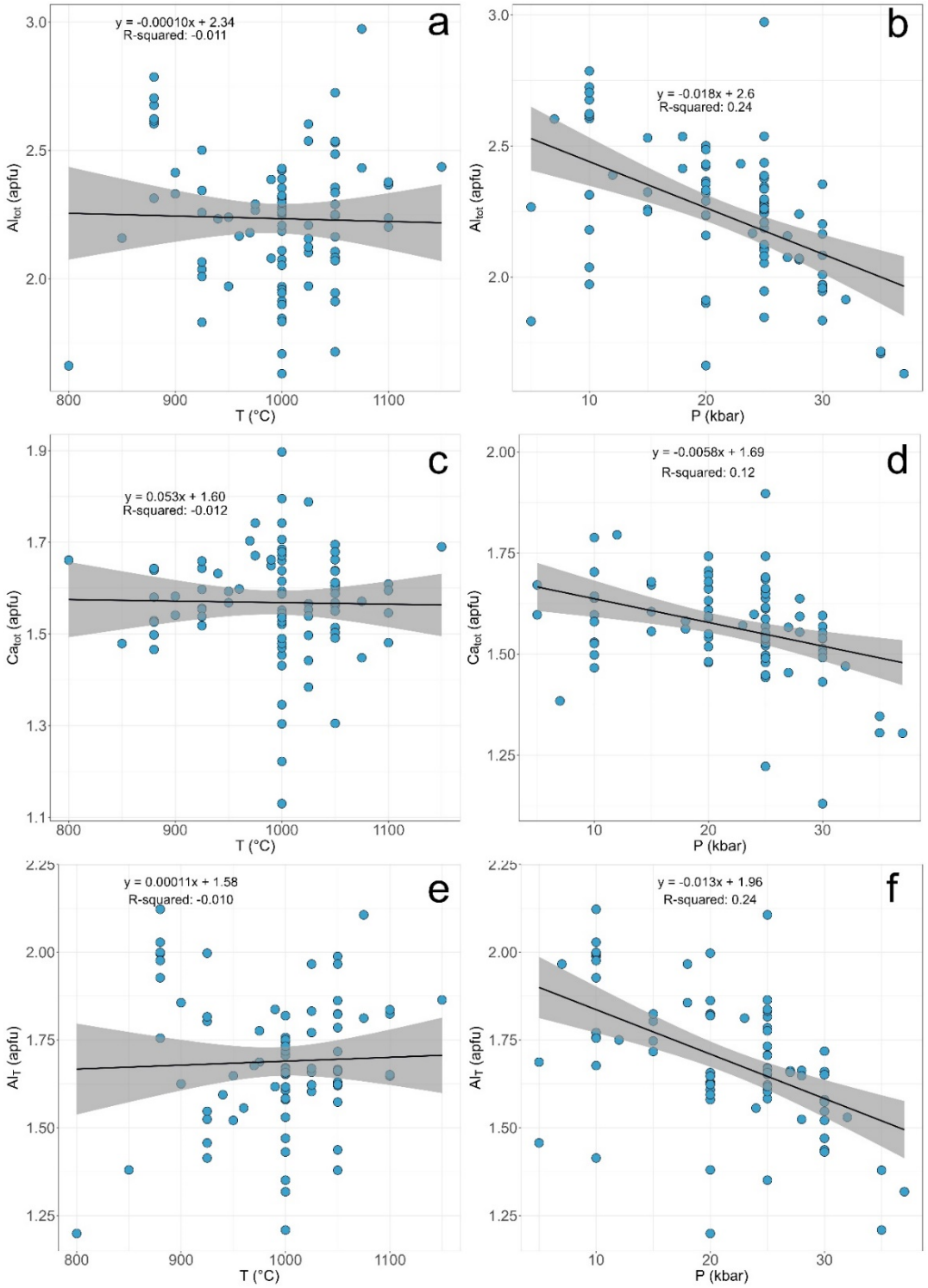

Figure 4.1: Al_{tot}, Al_T and Ca_{tot} in amphibole (a.p.f.u.) against experimental temperature (a, c, e) and pressure (b, d, f). The shaded area represents the 95% confidence level interval.

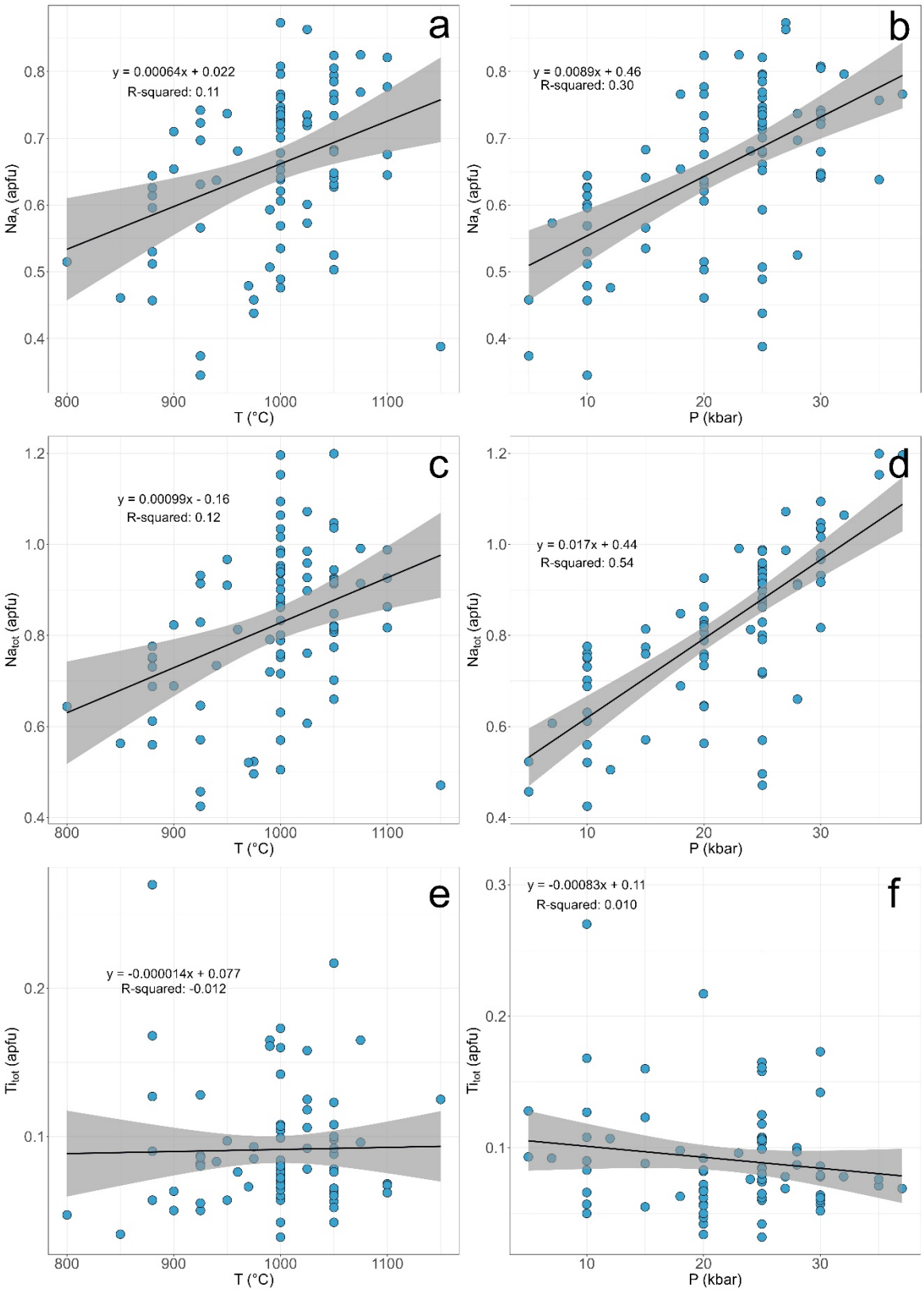

Figure 4.2: Na_A, Na_{tot} and Ti_{tot} in amphibole (a.p.f.u.) against experimental temperature (a, c, e) and pressure (b, d, f). The shaded area represents the 95% confidence level interval.

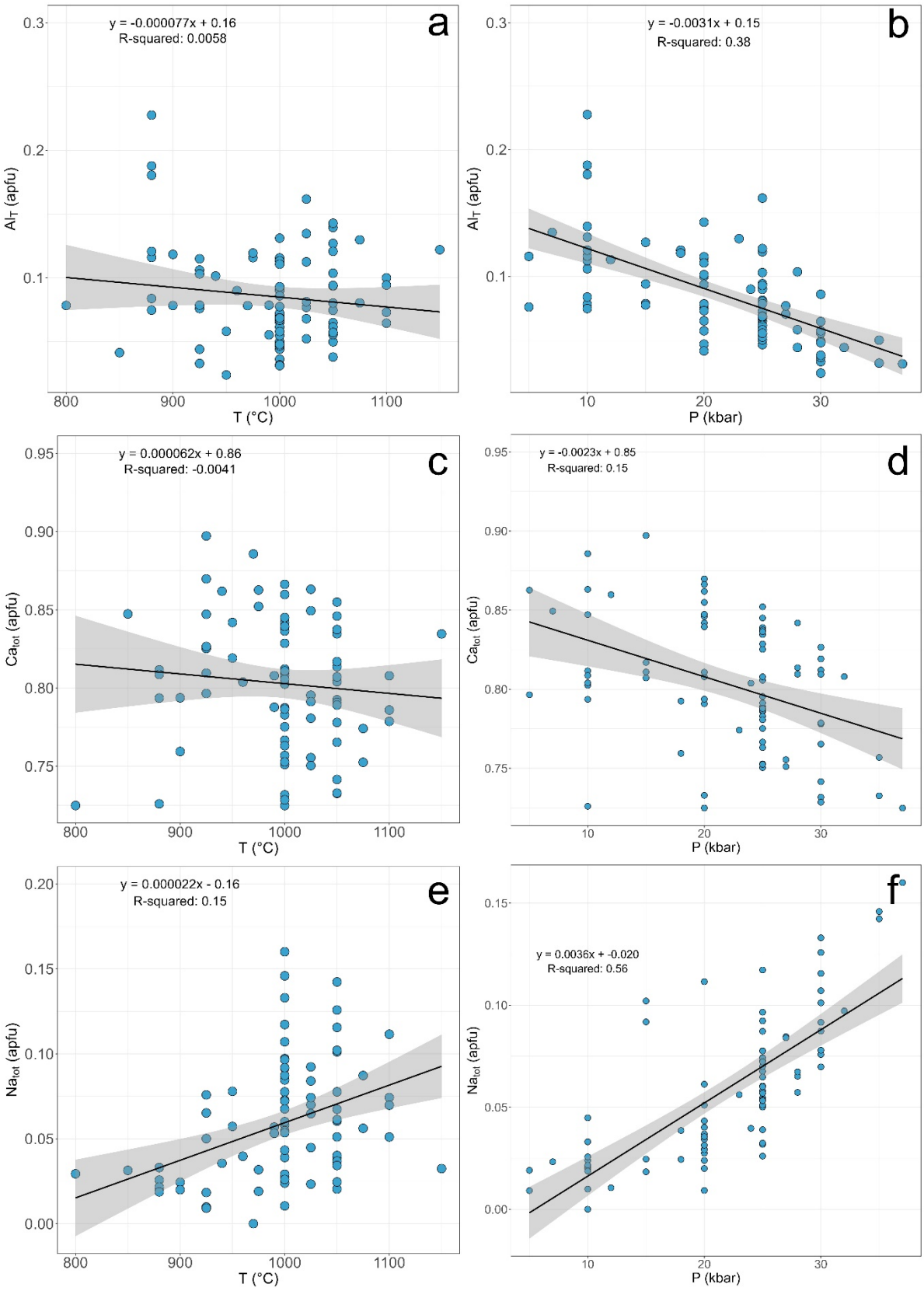

Figure 4.3: Al_T, Ca_{tot} and Na_{tot} in clinopyroxene (a.p.f.u.) against experimental temperature (a, c, e) and pressure (b, d, f). The shaded area represents the 95% confidence level interval.

Tetrahedral Al and total Ca in clinopyroxene seem to be unaffected by temperature but show a systematic dependence on pressure (negative trend, Figure 4.3a-d). On the other hand, total Al is unrelated to pressure but slightly affected by temperature (not shown). As in amphibole, total Na in clinopyroxene increases with both temperature and pressure (Figure 4.3e-f). However, the pressure influence is much more important.

4.2.3 Thermodynamic formulation

The exchange of Mg and Fe^{+2} between amphibole and clinopyroxene may be expressed by the following reaction:

$$\tfrac{1}{4}\,NaCa_2Mg_4Al_3Si_6O_{22}(OH)_2 \text{ (pargasite)} + FeCaSi_2O_6 \text{ (hedenbergite)} \rightarrow \tfrac{1}{4}\,NaCa_2Fe_4Al_3Si_6O_{22}(OH)_2 \text{ (Fe-pargasite)} + MgCaSi_2O_6 \text{ (diopside)} \quad (4.8)$$

The equilibrium constant of this reaction may be written as:

$$K = \left(\frac{\alpha_{Fe-Prg}^{1/4} \cdot a_{Di}}{\alpha_{Prg}^{1/4} \cdot a_{Hd}} \right) \quad (4.2)$$

where α represents the activities of each constituent phase that are defined as follows:

$$a_{Fe-Prg} = \left(X_{Fe-Prg} \cdot \gamma_{Fe-Prg}\right)^{1/4} \quad (4.3)$$

$$a_{Prg} = \left(X_{Prg} \cdot \gamma_{Prg}\right)^{1/4} \quad (4.4)$$

$$a_{Di} = X_{Di} \cdot \gamma_{Di} \quad (4.5)$$

$$a_{Hd} = X_{Hd} \cdot \gamma_{Hd} \quad (4.6)$$

X_j is the mole fraction of each endmember (j) in amphibole or clinopyroxene whereas γ is the activity coefficient. Substituting equations (4.3) – (4.6) in equation (4.2) and rearranging we obtain:

$$K = \left(\frac{X_{Fe-parg} \cdot X_{di}}{X_{parg} \cdot X_{hed}}\right) \cdot \left(\frac{\gamma_{Fe-parg} \cdot \gamma_{di}}{\gamma_{parg} \cdot \gamma_{hed}}\right) = K_D \cdot K_\gamma \quad (4.7)$$

where K_D is usually referred to as the distribution coefficient and describes the partitioning of Fe^{2+} and Mg between amphibole and clinopyroxene. Kγ is the ratio of the products of the respective activity coefficients (products over reactants). In the case of all participating phases forming ideal solutions, the activity coefficients become equal to unity and therefore:

$$K = K_D = \left(\frac{X_{Fe}^{amph} \cdot X_{Mg}^{cpx}}{X_{Mg}^{amph} \cdot X_{Fe}^{cpx}}\right) = \frac{\left(\frac{Fe}{Fe+Mg}\right)_{amph}\left(\frac{Mg}{Fe+Mg+Ca+Mn}\right)_{cpx}}{\left(\frac{Mg}{Fe+Mg}\right)_{amph}\left(\frac{Fe}{Fe+Mg+Ca+Mn}\right)_{cpx}} = \frac{\left(\frac{Mg}{Fe}\right)_{cpx}}{\left(\frac{Mg}{Fe}\right)_{amph}} \qquad (4.8)$$

The Fe/Mg ratios of amphibole and clinopyroxene were calculated assuming all iron is ferrous. As pointed out by Graham & Powell (1984), this assumption is reasonable because it is applied to all amphibole-clinopyroxene pairs and any possible errors that may occur are cancelling each other out. Empirical Fe^{+3} calculation schemes may not provide precise results and, therefore, affect the thermodynamic formulation in a significant way.

In this thermometric formulation, the standard-state differences in enthalpy (Δ_rH°) and entropy (Δ_rS°) of reaction (4.1) will be considered constant. This implies that the difference in heat capacity of the reaction under constant pressure is zero ($\Delta C_P = 0$). This simplification is often used to decrease the complexity of such formulations without introducing much error. In principle, both Δ_rH° and Δ_rS° are a function of temperature and a correct formulation would slightly alter the final form of the thermometric equation. However, accurate inference of Δ_rH° and Δ_rS° at elevated temperatures requires the knowledge of several empirical terms related to the heat capacity of each endmember. Such data are not available for the endmember phases chosen and therefore both Δ_rH° and Δ_rS° must necessarily be considered constant.

The equilibrium of the Fe-Mg exchange reaction between amphibole and clinopyroxene can be expressed in the following way:

$$\Delta_rG^\circ = 0 = \Delta_rH^\circ - T\Delta_rS^\circ + P\Delta_rV^\circ + RT\ln K \qquad (4.9)$$

where Δ_rG°, Δ_rH°, Δ_rS°, and Δ_rV° are the differences in Gibbs free energy, enthalpy, entropy, and volume of the reaction at standard state conditions respectively, and R is the universal gas constant (equal to 8.3145 $J \cdot mol^{-1} \cdot K^{-1}$); Δ_rG° equals zero at equilibrium.

Substituting (4.7) in equation (4.9) gives:

$$\Delta_rH^\circ - T\Delta_rS^\circ + P\Delta_rV^\circ + RT\ln K_D + RT\ln K_\gamma = 0 \qquad (4.10)$$

The $RTlnK_D$ term describes the Gibbs free energy change that is related to the ideal chemical mixing between the constituent phases. In contrast, the $RTlnK_\gamma$ term defines the excess Gibbs free energy change due to non-ideal mixing which is usually referred to as ΔG_{EX}. Therefore, equation (4.10) may be rewritten as:

$$\Delta_r H^\circ - T\Delta_r S^\circ + P\Delta_r V^\circ + RTlnK_D + \Delta G_{EX} = 0 \quad (4.11)$$

Rearranging of (4.11) gives:

$$T(\Delta_r S^\circ - RlnK_D) = \Delta_r H^\circ + P\Delta_r V^\circ + \Delta G_{EX} \quad (4.12)$$

To accurately derive ΔG_{EX}, the activity coefficients (γ) of amphibole and clinopyroxene must be evaluated. This, in turn, requires the development of solid-solution models that describe the non-ideal interactions between endmembers for each phase. Considering, however, the limited amount of experimental data available, it seemed more reasonable to apply a simple regression technique to calculate ΔG_{EX} rather than developing detailed and complex solid-solution models. We approximated ΔG_{EX} by assuming that the observed chemical variations in amphibole and clinopyroxene with pressure reflect energy changes brought about by ionic substitutions in the minerals as the P conditions changed. We assigned the variations with pressure of Al_{tot}^{amph}, Na_{tot}^{amph}, Ca_{tot}^{amph}, Al_T^{cpx}, Na_{tot}^{cpx} and Ca_{tot}^{cpx} to PW_V terms and therefore multiplied each with pressure (subscript '*tot'* stands for total and '*T'* for tetrahedral). The influence of temperature on total Na in both clinopyroxene and amphibole was considered insignificant based on the small values of R^2 and the generally unsatisfactory fitting (Figure 4.2 & 4.3), compared to the profound and large influence of pressure. Following the discussion above, equation (4.12) becomes:

$$T(\Delta_r S^\circ - RlnK_D) = \Delta_r H^\circ + P\Delta_r V^\circ + P\,Al_{tot}^{amph} + P\,Na_{tot}^{amph} + P\,Ca_{tot}^{amph} + P\,Al_T^{cpx} + P\,Na_{tot}^{cpx} + P\,Ca_{tot}^{cpx} \quad (4.13)$$

4.2.4 Calibration Results

Calibration of the thermometer was achieved through linear regression analysis using the calibrant dataset of Table 4.1 and equation (4.13). The term on the left-hand side of equation (4.13) is the dependent variable whereas all parameters on the right-hand side are the independent variables. Up until this point, equation (4.13) contains an unknown ($\Delta_r S^\circ$) in the dependent variable. To overcome this problem,

Δ_rS° was fixed to an empirical value which imposed several advantages to be discussed shortly. Having Δ_rS° fixed, and by substituting the appropriate experimental data values in (4.13), the values of Δ_rH°, Δ_rV° and the statistical coefficients of the six parameters reflecting ΔG_{EX} were regressed.

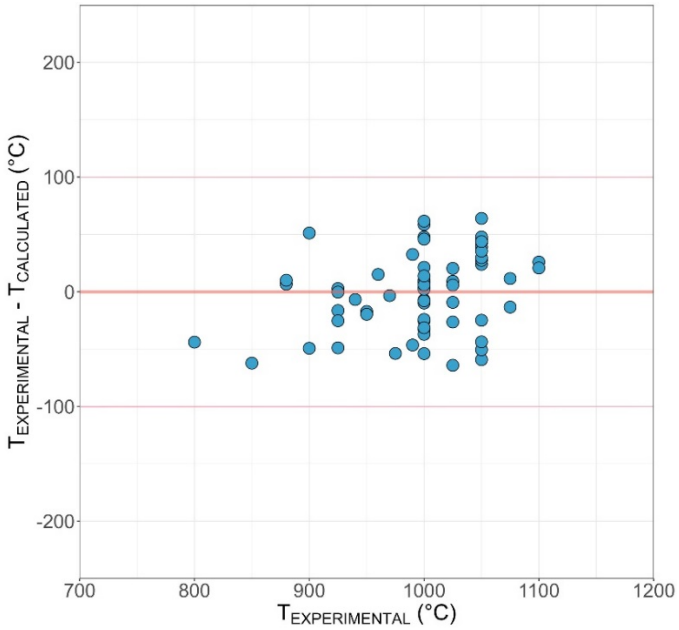

Figure 4.4: T_{exp} vs ΔT plot of the remaining 64 experiments after the calibration of the amphibole-clinopyroxene thermometer (Table 4.1.). All of the experiments fall within 100°C of the zero line without any obvious trend.

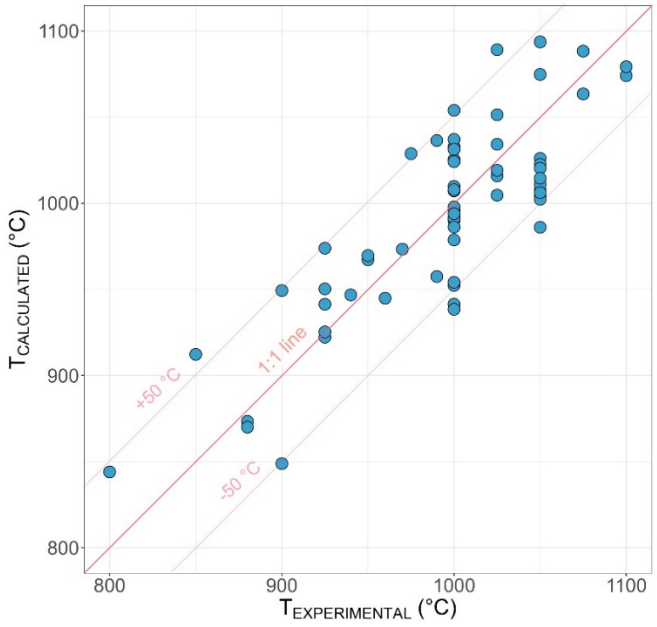

Figure 4.5: T_{exp} vs T_{calc} plot of the remaining 64 experiments after the calibration of the amphibole-clinopyroxene thermometer (Table 4.1.). Notice that all of the experiments fall within 50°C of the 1:1 line.

Setting $\Delta_r S^\circ$ equal to -29 $J \cdot K^{-1} \cdot mol^{-1}$ gave an optimal solution as it effectively produced a horizontal trend in a plot of (T_{exp}–T_{calc}) vs. T_{exp} and concomitantly reduced the standard deviation on the temperature estimate. Experiments with the highest absolute relative deviations $\left(\left|\frac{T_{exp} - T_{calc}}{T_{exp}}\right|\right)$ were then eliminated one at a time until all ΔT values were confined in the ± 100°C interval of Figure 4.4.

Of the initial 84 experiments, 64 remained after the calibration (

Table 4.2). The linear regression analysis yielded a $\Delta_r H^\circ$ value of -39.956 ± 0.72 $kJ \cdot mol^{-1}$ and a $\Delta_r V^\circ$ value of 1.29 ± 0.23 $J \cdot bar^{-1} \cdot mol^{-1}$. The statistical coefficients of the chosen chemical parameters along with their relevant errors are tabulated in Table 4.3. The final form of the amphibole-clinopyroxene thermometer was obtained by substituting the statistically regressed data and rearranging (4.13):

$$T_{amph/cpx}\,(°C) = \left[\left(-39956 + 1.29P - 0.17P\,Al_{tot}^{amph} - 0.15P\,Na_{tot}^{amph} - 0.33P\,Ca_{tot}^{amph} + 0.14P\,Al_{T}^{cpx} - 1.66\,PNa_{tot}^{cpx} - 0.10\,P\,Ca_{tot}^{cpx}\right) \Big/ \left(-29 - R\ln K_D\right)\right] - 273.15 \quad (4.14)$$

where pressure (P) is measured in bar, R is equal to 8.3145 $J \cdot mol^{-1} \cdot K^{-1}$, K_D is calculated by $(Mg/Fe)_{cpx}/(Mg/Fe)_{amph}$ and Al_{tot}^{amph}, Na_{tot}^{amph}, Ca_{tot}^{amph}, Al_{T}^{cpx}, Na_{tot}^{cpx} and Ca_{tot}^{cpx} are measured in atoms per formula unit (apfu). The clinopyroxene formula is calculated on the basis of 6 oxygens while the amphibole formula is derived on the basis of 22 oxygens + 2(OH, F, Cl) following the calculation scheme of Locock (2014). If significant Ti is present in amphibole (more than 4.5 wt % TiO_2, see Chapter 1 for more details), then it must be assumed that (OH, F, Cl) = 2 – 2Ti. As defined by the calibrant dataset, the thermometer should be used for pressures that range from 0.7 to 3.7 GPa and for temperatures that range from 800 to 1100 °C.

Table 4.3: The statistically regressed values of $\Delta_r H^\circ$ and $\Delta_r V^\circ$ and the coefficients of the chemical components used in the formulation. The standard error of each parameter is also given here.

	$\Delta_r H^\circ$ ($J \cdot mol^{-1}$)	$\Delta_r V^\circ$ ($J \cdot bar^{-1} \cdot mol^{-1}$)	PAl_{tot}^{amph}	P Na_{tot}^{amph}	P Ca_{tot}^{amph}	P Al_{T}^{cpx}	PNa_{tot}^{cpx}	P Ca_{tot}^{cpx}
Value	-39956	1.29	-0.17	-0.15	-0.33	0.14	-1.66	-0.10
Error	718	0.23	0.033	0.066	0.072	0.27	0.38	0.19

Table 4.4: Compositional ranges of experimental amphibole and clinopyroxene of our calibrant dataset. The new thermometer should strictly be applied to pairs that fall in the present compositional ranges.

Cation (apfu)	Amphibole	Clinopyroxene
Si	5.88 – 6.80	1.84 – 1.98
Al	1.63 – 2.97	0.084 – 0.28
Mg	3.49 – 4.40	0.81 – 1.21
Fe_{tot}	0.24 – 0.93	0.046 – 0.18
Ca	1.13 – 1.90	0.72 – 0.90
Na	0.49 – 1.20	0 – 0.16

The constructed thermometer reproduces the experimental temperatures with a standard error of ± 34.3°C and shows a satisfactory trend between T_{exp} and T_{calc} (Figure 4.5). It should be applied to natural clinopyroxene-amphibole pairs from ultramafic rocks that fall in the compositional ranges of our calibrant database outlined in Table 4.4.

4.3 Application to natural rocks

In the following section, the new Fe-Mg exchange thermometer was applied to natural amphibole-clinopyroxene pairs in ultramafic rocks from multiple geotectonic settings around the globe that have been previously investigated in the literature. As noted earlier, amphibole is a secondary metasomatic mineral that is incorporated in ultramafic rocks at some point during their geological evolution. The timing of the amphibole formation may therefore affect the calculated temperature of the present thermometer. Clinopyroxenes in mantle rocks are usually primary. Therefore, they may have been formed at completely different P-T-t conditions compared to amphibole and it would therefore be unreasonable to use the two minerals in order to obtain a single temperature. However, if amphibole remains at mantle ambient conditions for time periods long enough, it is possible that it may diffusionally re-equilibrate with the rest of the primary mantle phases such as clinopyroxene. In order to test this hypothesis, the new amphibole-clinopyroxene thermometer was compared to a two-pyroxene thermometer (Brey & Köhler, 1990) which involves two primary mantle phases (clinopyroxene and orthopyroxene). In the case of the two thermometers yielding similar temperatures, it is very likely that amphibole has equilibrated in the mantle. In the opposite scenario, where the two thermometers diverge to a great extent, amphibole is probably in disequilibrium with the clinopyroxene (and the rest of the mantle phases). The comparison between the two thermometers was not always feasible as very often orthopyroxene was not present in the samples under investigation, or it has not been analyzed.

4.3.1 Xenoliths from continental rift-related settings

Figure 4 6 demonstrates the results of the new thermometer against the temperature estimates of the two-pyroxene thermometer of Brey & Köhler (1990) on ultramafic xenoliths from continental rift-related settings. Only cation-normalized pyroxene analyses have been used in the presented calculations. The vast majority of the xenoliths under investigation have been found as inclusions in tholeiites or alkali-basalts. The examined xenoliths mostly comprise of spinel-bearing lherzolites and harzburgites although a few wehrlites are also present in several locations such as in Kandalaksha (Beard et al., 2007), Nógrád Gömör (Liptai et al., 2017), Wilcza Góra (Matusiak-Malek et al., 2017), Spitsbergen (Ionov et al., 2002) and West Eifel (Shaw et al., 2005). A few other thermometric calculatitons were conducted on one xenolithic pyroxenite and two transition zones (grading from lherzolite to pyroxenite) in West Eifel (Witt-Eickschen et al., 1993). Spinel-peridotites are accompanied with the difficulty that, until now, there is no method to accurately determine the equilibration pressure of the samples. Previous calculations in the literature assumed an average pressure of 15 kbar based on the stability field of spinel peridotites. The same pressure was applied for amphibole-clinopyroxene pairs here.

According to Figure 4 6 several localities show exceptionally comparable $T_{amph/cpx}$ and T_{BK90}. For example, in the Eastern Transylvanian Basin, amphibole-clinopyroxene thermometry and two-pyroxene thermometry was applied on porphyroclastic and protogranular grains, respectively. As is evident from Figure 4 6 amphibole-clinopyroxene temperatures (average of 1045 °C) are very similar to two-pyroxene ones (average of 1011 °C). Faccini et al. (2020) showed that clinopyroxenes and amphiboles in xenoliths from the Eastern Transylvanian Basin display similar trace-element patterns which indicates that amphibole has resulted from the hydration of clinopyroxene. Moreover, both Vaselli et al. (1995) and Faccini et al. (2020) agree that amphibole has re-equilibrated at subsolidus conditions, an argument which is accordance with the present thermometric calculations.

Witt-Eickschen & Harte (1994) showed that the primary mantle phases in West Eifel have achieved both textural and chemical equilibrium. They have additionally proven the metasomatic origin of amphibole. Moreover, the new amphibole-clinopyroxene thermometer yields very similar temperatures to two-pyroxene thermometry for matrix amphiboles and pyroxenes (Figure 4 6). This shows that amphibole is also in equilibrium with the primary phases and it remained in the sub-continental mantle at a temperature of ~1000 °C (Figure 4 6) for long enough time

(amphibole formed around 200 Ma according to Stosch, 1987) so as to diffusionally re-equilibrate with the primary phases. Contrastingly, two pairs from West Eifel that involved disequilibrium textures (poikilitic amphibole) plot far away from the 1:1 line of Figure 4 6 giving completely unreasonable temperatures. This shows that the textures of the minerals that are involved in the amphibole-clinopyroxene thermometer are of extreme importance.

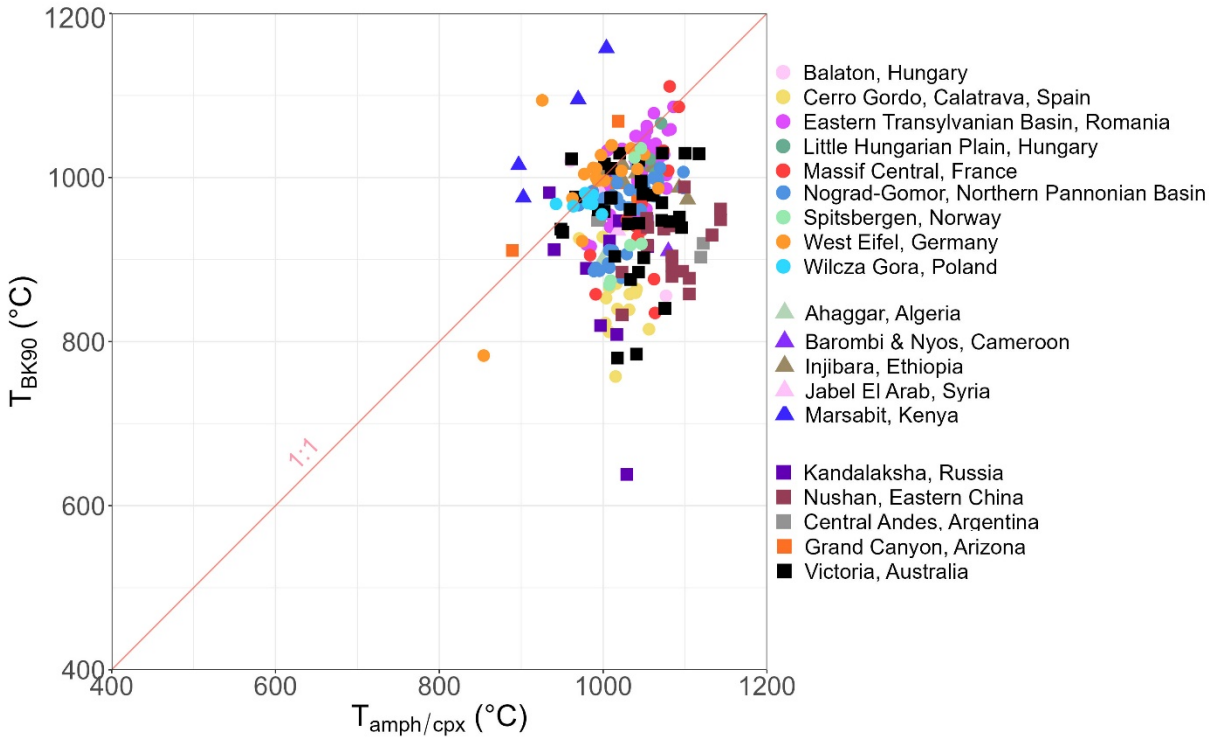

Figure 4 6: $T_{amph/cpx}$ vs T_{BK90} for ultramafic xenoliths that are associated to continental rift-related geotectonic settings. -*Balaton (Hungary)*: Ntaflos e al., 2017 -*Cerro Gordo (Spain)*: Villaseca et al., 2020 -*Eastern Transylvanian Basin (Romania)*: Faccini et al., 2020;Vaselli et al., 1995 -*Little Hungarian Plain (Hungary)*: Szabo et al., 1995 -*Massif Central (France)*: Uenver-Thiele et al., 2014; Denis et al., 2015 -*Nógrád Gömör (Hungary)*: Liptai et al., 2017 -*Spitsbergen (Norway)*: Ionov et al., 1997; Ionov et al., 2002 -*West Eifel (Germany)*: Witt-Eickschen et al., 1993; Witt-Eickschen & Hart, 1994; Ban et al., 2005; Shaw et al., 2005 -*Wilcza Gora (Poland)*: Matusiak-Malek, 2017 1 -*Ahaggar (Algeria)*: Kaczmarek et al., 2016 -*Barombi & Nyos (Cameroon)*: Pinter et al., 2015 -*Injibara (Ethiopia)*: Ferrando et al., 2008; Frezzotti et al., 2010 -*Jabel El Arab (Syria)*: Ismail et al., 2008 -*Marsabit (Kenya)*: Kaeser et al., 2007 -*Kandalaksha (Russia)*: Beard et al., 2007 -*Nushan (China)*: Xu et al., 1997; Xu et al., 1998; Xu & Bodinier, 2004 -*Central Andes (Argentina)*: Lucassen et al., 2005 - Grand Canyon (Arizona): Hunt & Lamb, 2019 -*Victoria (Australia)*: Griffin et al., 1984; Stolz & Davies, 1988; Powell et al., 2004; Bonadiman et al., 2021

Coarse-grained amphibole in xenoliths from Wilcza Góra (Poland) is also expected to be in equilibrium with the rest of the coarse-grained minerals. This is because average $T_{amph/cpx}$ is equal to 977 °C and average T_{BK90} is 969 °C and the

majority of the temperatures fall along the 1:1 line of Figure 4 6. Matusiak-Malek et al. (2017) observed that amphiboles and clinopyroxenes in the studied samples are in equilibrium in texture but also in terms of trace-element composition. The aforementioned authors have predicted that both amphibole and clinopyroxene are metasomatic in origin and derived from a mafic alkaline melt. Succeeding the metasomatic formation, amphibole has probably re-equilibrated and re-crystallized at subsolidus conditions and its major-element composition has been shifted so that amphibole can be stable at ambient mantle conditions.

Another example of equilibrium is evident from fine-grained and disseminated amphiboles and pyroxenes in xenoliths from Injibara (Ethiopia) (Ferrando et al., 2008; Frezzotti et al., 2010). The pairs used here, give an average $T_{amph/cpx}$ equal to 1053 °C and an average T_{BK90} equal to 998 °C. According to Ferrando et al. (2008), a first metasomatic event in the continental lithospheric mantle was related to water-bearing fluids that were derived from a mantle plume. This initial event modally affected the mantle rocks and precipitated amphibole. Subsequently, a second metasomatic event was characterized by a temperature increase to about 1100 °C and caused the recrystallisation of the mantle rocks. Almost all generations of minerals seem to have been affected by the second event and have re-equilibrated. The new amphibole-clinopyroxene thermometer records this higher-T event of re-equilibration as it provides temperatures that range from 998 to about 1100 °C.

Ultramafic xenoliths from Massif Central, are defined by disseminated, re-crystallized amphiboles or fine-grained amphiboles that grow around spinels and they own the same grain size as the coexisting anhydrous primary phases. Using amphibole-clinopyroxene grains that belong to the same texture from Uenver-Thiele et al. (2014) and Denis et al. (2015), temperatures from 984 to 1081 °C were obtained. These temperatures are well within the two-pyroxene temperature range as reported in Uenver-Thiele et al. (2014) but also recalculated in this study (Figure 4 6).

Amphiboles and clinopyroxenes very often do not belong to the same textural group. For example, in Nógrád Gömör, interstitial amphiboles were used along with fine-grained pyroxenes. According to Liptai et al. (2017), clinopyroxene and orthopyroxene are in chemical equilibrium but there is no information about amphibole. On the other hand, the trace-element composition of amphiboles was indicating their formation from fluids or melts at a suprasubduction zone or in an intra-plate setting. Interstitial amphiboles and fine-grained, isometric pyroxenes yield an average $T_{amph/cpx}$ of 1026 °C and a comparable T_{BK90} equal to 962 °C. This observation could be interpreted based on two different scenarios. The first one is that, although textural equilibrium has not been achieved, it is possible that the

amphibole has equilibrated in terms of Fe/Mg exchange through diffusion processes. This could mean that recrystallization processes have been slower compared to the diffusion of chemical species. Another possibility is that the observed agreement of the two thermometric techniques is random and uninterpretable and is not associated with any physical process. Similarly to Nógrád Gömör, the same observations have been made for the Little Hungarian Plain Volcanic Field and Grand Canyon (Arizona).

Disseminated amphiboles in kimberlite-related xenoliths from Kandalaksha (Russia) are a good example of disequilibrium. When they are used along with primary clinopyroxene grains of the same texture, an average temperature of 1011 °C is calculated. On the other hand, two pyroxene thermometry predicts an average of 860 °C (Figure 4 6). This enormous difference in temperatures indicates that amphibole has not attained equilibrium with the rest of the primary mantle phases. According to Beard et al. (2007) the Kandalaksha xenolithic peridotites were firstly subjected to a Devonian carbonatitic metasomatic event. Then, a later metasomatic event resulted in the direct crystallization of the disseminated amphibole. Based on the disequilibrium evidence that is shown here, it is expected that the xenoliths were rapidly transported to the surface from the kimberlite immediately after the amphibole formation during the second metasomatic event. Therefore, amphibole did not remain in the mantle for long enough time to re-equilibrate with the pyroxenes. Because xenoliths are generally transported to the surface rapidly, it is not expected that different closure temperatures could cause this enormous difference in temperatures. This possibility could be plausible in Alpine-type peridotites in which exhumation is much slower compared to xenoliths as will be discussed later. The same scenario is expected for matrix amphibole-clinopyroxene pairs in ultramafic xenoliths from Andes (Argentina), Victoria (Australia) and Nushan (China).

A somewhat different disequilibrium scenario is expected for xenolithic amphibole in Cerro Gordo. Interestingly, according to Villaseca et al. (2020), amphibole in Cerro Gordo was modally formed by metasomatic agents during the Variscan continental collision around 300 Ma ago. However, at 3 Ma ago partial melting occurred in the sub-lithospheric mantle mainly as a result of breakdown reactions that consumed amphibole. It is therefore very possible that the chemical composition of amphibole has been affected by the 3 Ma years old partial-melting event. This could explain the discrepancy observed in Figure 4 6.

Finally, amphiboles from Marsabit (Kenya) are displaying various temperatures depending on the texture that is chosen each time. Two-pyroxene thermometry is, always yielding higher temperatures than the amphibole-

clinopyroxene thermometer. Residual amphibole and metasomatic clinopyroxene show a temperature of 933 °C, whereas residual amphibole and primary clinopyroxene define a temperature equal to 999 °C. Amphiboles in veinlets and metasomatic clinopyroxene are showing an average temperature equal to 900 °C. Finally, amphibole and clinopyroxene that are adjacent to glass yield an average temperature around 985 °C. Marsabit is a good example which shows the large impact the mineral textures have on the calculated temperature.

4.3.2 Alpine-type peridotites

Amphibole-clinopyroxene thermometry in Alpine-type orogenic peridotites is somewhat different compared to ultramafic xenoliths in continental rifting systems. Figure 4.7 shows that the calculated $T_{amph/cpx}$ values are generally lower than those of Figure 4 6. In fact, the majority of the amphibole-clinopyroxene temperatures are plotted in the range between 800 and 1000 °C. Moreover, many of the investigated orogenic peridotites comprise of garnet-bearing lherzolites, pyroxenites and websterites in which the estimation of pressure is totally feasible. If an equilibration pressure has been previously estimated in the literature for the localities present here (Figure 4.7) then the same pressure was used in the thermometric calculations respectively. If the equilibration pressure of the peridotites exceeded that of the maximum pressure of the amphibole stability field (~37 kbar), then an average pressure of 15 kbar was used. Spinel-bearing peridotites have been treated similarly, assuming that the equilibration pressure is 15 kbar.

Only a few localities seem to have attained equilibrium between amphibole and the primary mantle phases and these involve Beni Busera (Morocco), Zabargad Island (Red Sea) and Caussou (France). In more detail, according to El Atrassi et al. (2014) garnet-bearing websterites and clinopyroxenites in Beni Busera have been extensively metasomatized after their initial formation. Coarse-grained amphibole is in textural equilibrium with the rest of the matrix phases in both rocks. However, trace-element equilibrium between amphibole and clinopyroxene has only been achieved in the garnet websterites. Our thermometer shows that amphibole-clinopyroxene pairs have equilibrated, in terms of Mg/Fe exchange, in both types of rock (Figure 4.7). This is in contrast with the findings of El Atrassi et al. (2014) who assumed a general disequilibrium between amphibole and clinopyroxene in the clinopyroxenites. In fact, trace-element disequilibrium between two phases does not necessarily imply that the minerals have not equilibrated in terms of major-elements as well. This difference of equilibration degree between trace and major elements

could be ascribed to cryptic metasomatism which could have affected amphiboles and/or clinopyroxenes at a later stage. But it could also be related to contrasting diffusivities of the compositional species between the minerals. For example, the Fe/Mg exchange could be way faster compared to the exchange of the trace elements between amphibole and clinopyroxene. Similarly to Beni Busera, equilibrium was also found for amphibole-clinopyroxene pairs in Caussou (France). Amphiboles from Caussou are expected to have formed around 103 Ma ago according to Albarède & Vitrac (1978) and show an average $T_{amph/cpx}$ of 984 °C. A comparable T_{BK90} equal to 920 °C has also been calculated.

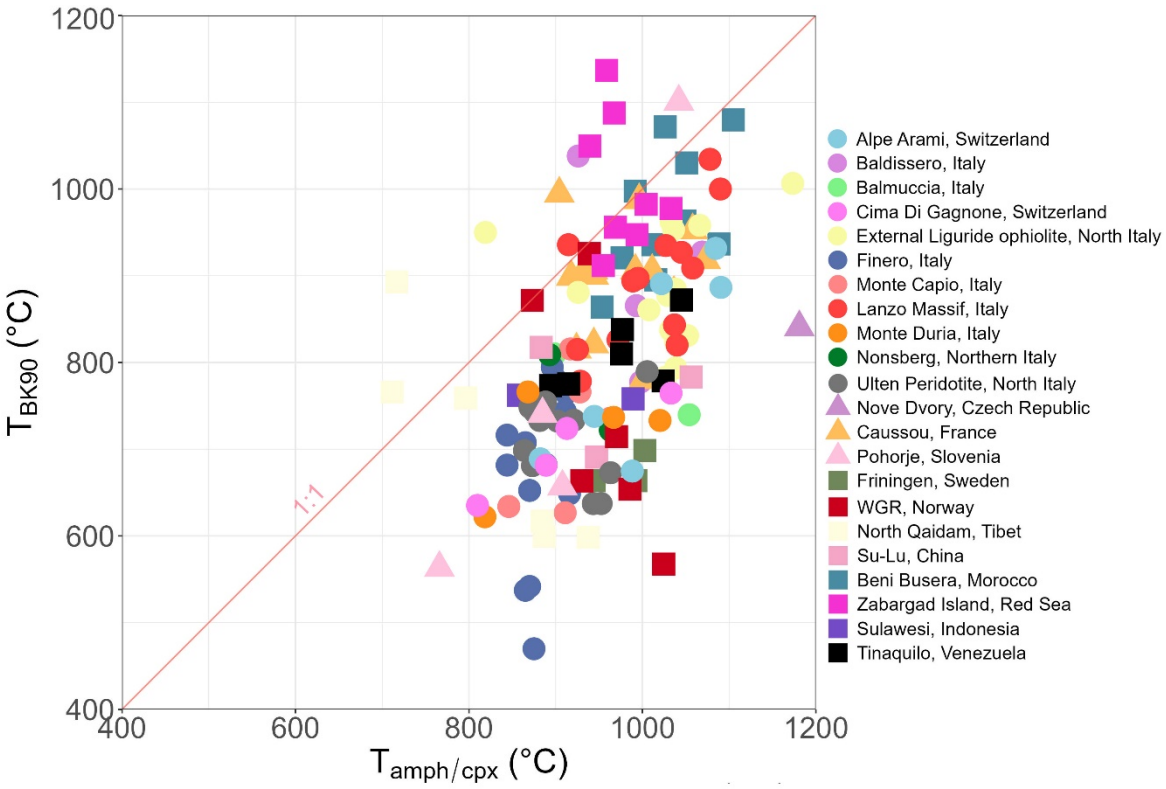

Figure 4.7: $T_{amph/cpx}$ vs T_{BK90} for Alpine-type, orogenic peridotites around the globe. -*Alpe Arami (Switzerland)*: Paquin & Altherr, 2001 -*Baldissero (Italy)*: Mazzucchelli et al., 2010 -*Balmuccia (Italy)*: Mazzucchelli et al., 2009 -*Cima di Gagnone (Switzerland)*: Scambelluri et al., 2014; Hidas et al., 2021; Ferrari et al., 2022 -Finero (Italy): Zanetti et al., 1999; Corvò et al., 2020 -*Monte Capio (Italy)*: Berno et al., 2020 -*Lanzo Massif (Italy)*: Kaczmarek & Muntener, 2008; Duarte et al., 2020 -*Monte Duria (Italy)*: Pellegrino et al., 2020 -*Nonsberg (Italy)*: Obata & Morten, 1987 -*Ulten (Italy)*: Sapienza et al., 2009; Pellegrino et al., 2021; Gudelius et al., 2019 -*Nové Dvory (Czech Republic)*: Muriuki et al., 2020 -*Caussou (France)*: Conquéré, 1971; Fabriès et al., 1989 -*Pohorje (Slovenia)*: Janàk et al., 2006; De Hoog et al., 2009; Vrabec, 2010 -*Friningen (Sweden)*: Gilio et al., 2015 -*WGR (Norway)*: Carswell et al., 1983; Beyer et al., 2006 -*North Qaidam (Tibet)*: Chen et al., 2017 -*Su-Lu (China)*: Ye et al., 2009; -*Beni Busera (Morocco)*: El Atrassi et al., 2014 -*Zabargad Island (Red Sea)*: Bonatti et al., 1986; Piccardo et al., 1988 -*Sulawesi (Indonesia)*: Kadarusman & Parkinson, 2000 -*Tinaquilo (Venezuela)*: Seyler & Mattson, 1989

In Zabargad, amphibole is in textural equilibrium with the primary phases in spinel-lherzolites and a plagioclase-bearing assemblage in pyroxenites. According to Piccardo et al. (1988), pargasites in both types of rocks partially re-equilibrated and re-crystallized during the transition of spinel- to plagioclase-facies. Amphibole-clinopyroxene temperatures show an average of 972 °C while two-pyroxene thermometry yields an average of 993 °C. This agreement in temperatures shows that amphiboles were given enough time and/or temperature to re-equilibrate along with the primary mantle phases. It also implies that the rocks either remained at a stable temperature at some stage of their exhumation path or that the exhumation rates were relatively slow.

In many of the remaining Alpine-type, orogenic peridotites amphiboles have achieved textural equilibrium with clinopyroxene and orthopyroxene. For example, many amphibole grains are found in textural equilibrium with the primary phases in the External Liguride peridotites (Italy), Monte Capio (Italy) and Finero from the Ivrea-Verbano Zone, Lanzo Massif (Italy), Ulten (Italy), Monte Duria (Italy), North Qaidam (Tibet) and Tinaquilo (Venezuela). Orogenic peridotites generally show a very complex history and they are often involved in subduction-zone processes. Additionally they show evidence of partial to full re-equilibration at multiple stages of their geological evolution. They are often infiltrated and affected a variety of metasomatic melts and/or fluids that can either be related to a subducting continental lithorpshere or they may be originated at shallower depths.

For example, the Finero mantle, was affected by a slab-derived silicate melt in a subduction environment and was metasomatized before its incorporation in the continental crust (Zanetti et al., 1999 and references therein). According to Tommasi et al. (2017), Finero experienced a high-T deformation event at around 1050-1080 °C and 20 kbar but then it also experienced another localized deformation event at lower temperatures (~750 °C according to Corvò et al., 2020). The use of interstitial, porphyroclastic and disseminated amphibole along with interstitial, porphryroclastic and granoblastic clinopyroxene, however, yields far higher temperatures (Figure 4.7). This may indicate that the formation of amphibole took place at some non-stable point in the history of Finero. It is also possible that the constantly shifting P-T conditions Finero experienced (maybe associated with corner flow in a mantle wedge environment) did not enable the equilibration of amphibole at a unique temperature and pressure. The higher $T_{amph/cpx}$ values probably represent closure temperatures. This might be a good indication that the Fe/Mg exchange of amphibole and clinopyroxene “freezes” at higher temperatures compared to the other thermometric methods during the exhumation of the peridotite.

Similarly, peridotites from Ulten show evidence of metasomatism by fluids derived from a subducted crust that infiltrated the mantle wedge at conditions of cooling to about ~ 850 °C and elevating pressures (Gudelius et al., 2019 and references therein). The clinopyroxene-orthopyroxene pairs of Gudelius et al. (2019) yield an average T_{BK90} of 740 °C (at 20kbar) which is somewhat lower than the re-equilibration event at 850 °C. However, the new amphibole-clinopyroxene thermometer yields an average value ~885 °C which is closer to that metasomatic event.

Chen et al. (2017) proposed that multiple episodes of metasomatism have affected the North Qaidam mantle peridotites at an advanced exhumation stage. The calculated temperatures for matrix amphibole-clinopyroxene pairs are extremely scattered and non-consistent and span from 711 to 938 °C. This scatter is conceived as an indication of disequilibrium.

The granuloblastic texture in lherzolites, dunites and pyroxenites found in Monte Capio shows the effect of chemical equilibration based on solid-state diffusion and/or recrystallization (Berno et al., 2020). T_{BK90} estimations from Berno et al. (2020) yield temperatures from 733 to 783 °C, however the cations per formula unit of pyroxene are not normalized. When normalized cations are used, the obtained temperatures are from 627 to 816 °C. Berno et al. (2020) have also used the amphibole thermometer of Putirka (2016) on every sample from Monte Capio, however this is a formulation that has only been calibrated for igneous systems and not for ultramafic systems in which solid-state diffusion and re-equilibration plays an important role. On the other hand, amphibole-clinopyroxene temperatures based on granoblastic grains are showing a range from 841 to 963 °C. These slightly higher values may be associated with the higher closure temperatures of the amphibole-clinopyroxene thermometer that were achieved during the exhumation of the peridotite.

Finally, there are multiple localities in which detailed textural data are not available in the literature or that amphibole-clinopyroxene pairs that belong to the same textural group do not coexist in the same sample (e.g. Nové Dvory, Su-Lu, WGR, Balmuccia and Sulawesi). It is observed that the calculated $T_{amph/cpx}$ are generally much higher than two-pyroxene thermometry but the interpretation of them is extremely difficult because of the very complex evolution of the Alpine-type, orogenic peridotites.

4.3.3 Continental-arc xenoliths

Amphibole-clinopyroxene pairs from xenoliths in continental arcs are generally showing signs of chemical equilibration. Xenoliths in volcanic arcs are extremely rare. But additionally to that, pargasitic amphibole in continental rift xenoliths is also not a very commonly found phase. Therefore, there are much fewer localities for the use of the amphibole-clinopyroxene thermometer compared to the previously investigated geotectonic settings. Amphiboles found in xenoliths from the American Cordillera (Deadman Lake, Dish Hill, Kilbourne Hole, San Carlos, Lighting Peak) are all in both textural equilibrium and, based on the new thermometer, chemical equilibrium with the primary mantle phases (Figure 4.8). The same can be said for the Avacha and the Gobernador Gregores xenolithic localities.

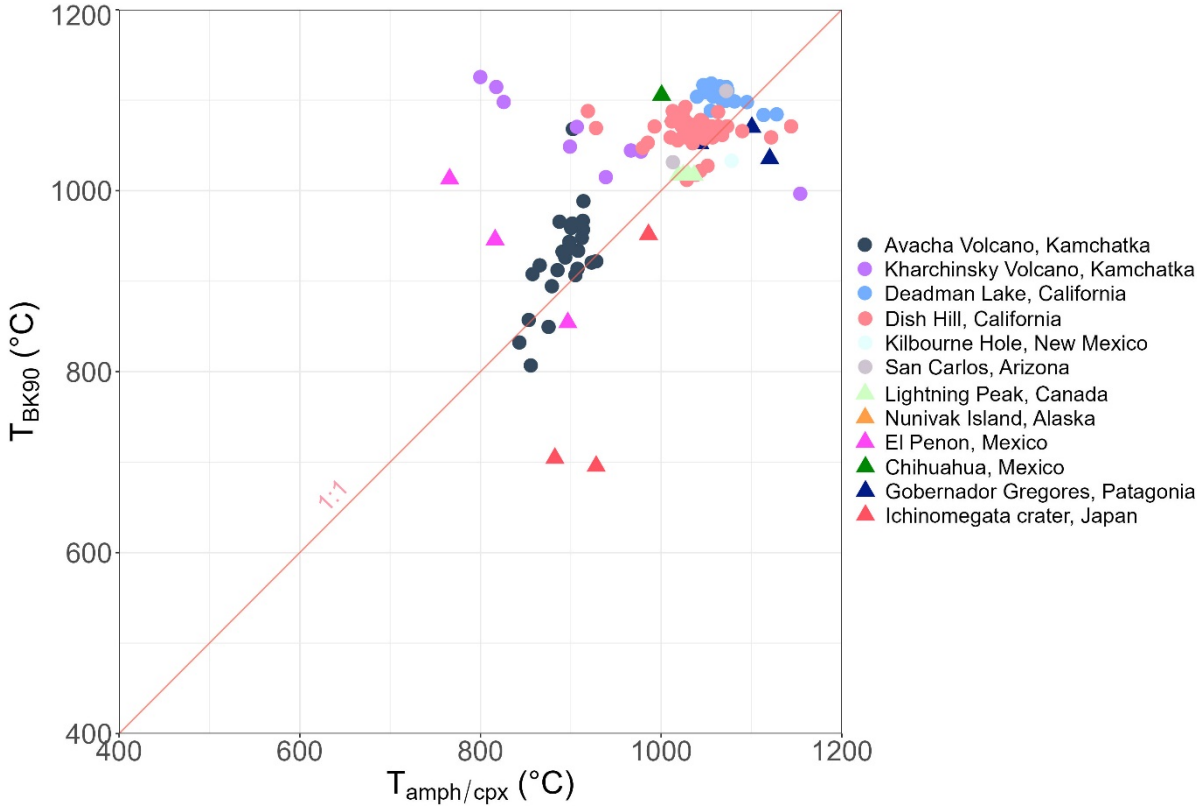

Figure 4.8: $T_{amph/cpx}$ vs T_{BK90} for ultramafic xenoliths in continental arcs around the globe. -Avacha Volcano (Kamchatka): Ishimaru et al., 2007; Ionov, 2010; Bénard & Ionov, 2013 -Kharchinsky Volcano (Kamchatka): Siegrist et al., 2019 -Deadman Lake (California): Wilshire, 1988 -Dish Hill (California): Wilshire, 1988; McGuire et al., 1991; Hunt & Lamb, 2019; -Kilbourne Hole (New Mexico): Hunt & Lamb, 2019; -San Carlos (Arizona): Frey & Prinz, 1978; -Lightning Peak (Canada): Brearley & Scarfe, 1984; -El Peñon (Mexico): Blatter & Carmichael, 1998; -Chihuahua (Mexico): Nimz et al., 1986; -Gobernador Gregores (Patagonia): Laurora et al., 2001; Ichinomegata crater (Japan): Takahashi, 1980

Ionov (2010) based on the values of Mg# of the coexisting clinopyroxene and amphibole supported that the two minerals have achieved chemical equilibration with each other. The author avoided using the two-pyroxene thermometer of Brey & Köhler (1990) as clinopyroxene in Avacha is a late-stage mineral and it could not be fully equilibrated with coarse-grained orthopyroxene. Although, the CaO content in orthopyroxene and the textural association between clinopyroxene and orthopyroxene is proving the opposite. Instead, Ionov (2010), assuming a pressure of 15 kbar, used the Ballhaus et al. (1991) olivine-orthopyroxene-spinel thermometer which yielded temperatures from 895 to 993 °C and the Ca-in-orthopyroxene thermometer of Brey & Köhler (1990) which gave values from 907 to 997 °C. According to the present study, the two-pyroxene thermometer of Brey & Köhler (1990) gives temperatures from 807 to 988 °C which is in total agreement with the rest of the thermometric calculations. Moreover, the amphibole-clinopyroxene thermometer yields values from 843 to 928 °C when using grains in textural equilibrium. By this point, it is clear that all of the thermometric methods that have been adopted agree. This, along with the geochemical data of Ionov (2010) is strong evidence for the equilibration of amphibole in the Avacha sub-continental lithospheric mantle. The new thermometer was also applied to amphibole-clinopyroxene pairs that were found as some intergrowths. The observed temperature was also consistent with the rest (~880 °C).

Similarly to Avacha, matrix amphibole-clinopyroxene pairs from Dish Hill and Deadman Lake are giving consistent temperatures in agreement with the rest of the applicable thermometers. Whenever the majority of available thermometers yield the same temperatures for a locality, it is expected that there is a great degree of equilibrium between the constituent minerals. Equilibrium is also highly expected for amphibole in Kilbourne Hole, San Carlos, Lightning Peak and Gobernador Gregores. However, in the aforementioned localities, there is a lack in numbers of amphibole-clinopyroxene pairs and therefore safe interpretations cannot be made.

Amphiboles in the Kharchinsky volcano xenoliths are of secondary origin and they show an interstitial texture. The calculated T_{BK90} temperatures are ranging from 997 to 1228 °C and $T_{amph/cpx}$ from 795 to 1154 °C with an average of 908 °C when using protogranular pyroxenes in dunites and granuloblastic pyroxenes in harzburgites. Siegrist et al. (2019) noted that the mineral phases in Kharchinsky peridotites are very heterogeneous in terms of composition. Many pyroxene pairs record unreasonably high temperatures. They attributed these temperatures to the abnormal Fe-Mg exchange coefficients between the pyroxenes that exceed the experimental values from the literature. All of the mentioned characteristics here, along with the very variable amphibole-clinopyroxene temperatures (Figure 4.8) are strong evidence that the ultramafic xenoliths from Kharchinsky have not equilibrated.

It is expected that the Kharchinsky xenoliths have been affected by fluid metasomatism, in situ melting and recrystallization, impregnation of mafic melts (Siegrist et al., 2019) along with an immediate and quick transport to the surface that did not enable the equilibration of the minerals at ambient mantle conditions.

Interestingly, the primary mantle phases in xenoliths from Ichinomegata (Japan) are extremely homogeneous and equilibrium has been achieved, according to Takahashi (1980), at about 800 °C. However, both the amphibole-clinopyroxene and the two-pyroxene thermometers yield very inconsistent results (Figure 4.8). The limited data and the lack of detailed textural descriptions for each analyzed mineral do not enable for a consistent interpretation of these temperatures. The same applies for the temperatures calculated for the El Peñon xenoliths.

4.3.4 Oceanic plateaus and core complexes

Abyssal peridotites exposed at slow-spreading mid-oceanic ridges are direct evidence of the composition and the processes that have taken place in the sub-oceanic lithospheric mantle. Abyssal peridotites are usually found along the axis of a mid-oceanic ridge and they are rarely reported from backarc oceanic basins. One exception involves the Godzilla Megamullion which is interpreted as an exhumed footwall of an oceanic detachment fault (for more details see Ohara et al. (2003) and references therein). Harzburgites found in Godzilla Megamullion are extensively serpentinized and the primary texture, wherever preserved, is porphyroclastic. Metasomatic amphibole is rarely present is also found as interstitial, smaller grains between the primary anhydrous minerals. Amphibole in Godzilla Megamullion shows a compositional variability. It can be found as low-temperature, late-stage hornblende and tremolite or as pargasite which is not related to a late-stage hydration of the peridotites. Ohara et al. (2003) supported that pargasite is a product of high-temperature seawater circulation and not related to melt-mantle interaction or to an originally metasomatized mantle domain. However, interstitial amphibole and primary clinopyroxene yield very similar temperatures to two-pyroxene thermometry (Figure 4.9) indicating equilibration between the minerals. On the other hand, there is a difference in texture between them. This implies that amphibole equilibrated in terms of chemical composition but did not recrystallize. This scenario is very similar to the one discussed about Nógrád Gömör in a previous section.

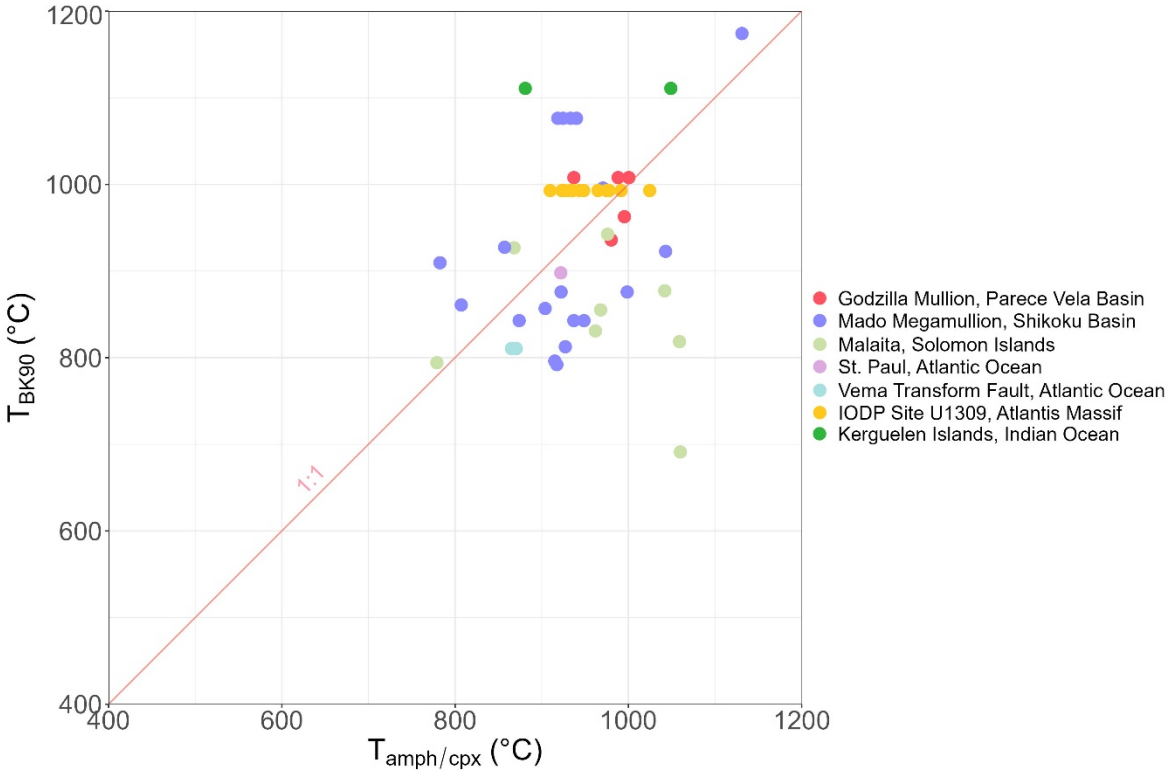

Figure 4.9: $T_{amph/cpx}$ vs T_{BK90} calculated for oceanic plateaus and core complexes around the globe. -*Godzilla Mullion (Parece Vela Basin)*: Ohara et al., 2003 -*Mado Megamullion (Shikoku Basin)*: Akizawa et al., 2021; Sen et al., 2022 -*Malaita (Solomon Islands)*: Neal, 1988 -*St. Paul (Atlantic Ocean)*: Tilley & Long, 1967 -*Vema Transform Fault (Atlantic Ocean)*: Cannat & Seyler, 1995 -*IODP Site U1309 (Atlantis Massif)*: Tamura et al., 2008 -*Kerguelen Islands (Indian Ocean)*: Grégoire et al., 2000.

Amphiboles in the IODP Site U1309 (Atlantis Massif oceanic core complex) belong to a different textural group compared to the two pyroxenes. They are only found as inclusions in anhedral spinel while clinopyroxene and orthopyroxene show protogranular textures. Equilibration is expected based on the calculated temperatures according to Figure 4.9. Tamura et al. (2008) suggested that the chromian spinels and the amphibole inclusions is clear evidence of precipitation by the reaction between melts and the peridotite. Subsequently, Tamura et al. (2014) proved that the inclusions have been formed by a secondary MORB melt that was entrapped in spinel. Tamura et al. (2014) have also supported disequilibrium over equilibrium between pargasite inclusions and the host-rock clinopyroxenes based on trace-element data. Amphibole inclusions may have had enough time to equilibrate in the mantle. However, it is difficult to confirm this scenario because of the textural differences and the lack of direct contact between amphibole and the other primary phases. Therefore the calculated temperatures in Figure 4.9 may be completely uninterpretable.

Mylonitic amphibole, clinopyroxene and orthopyroxene from a peridotite in St. Paul show a $T_{amph/cpx}$ equal to 922 °C and a T_{BK90} equal to 898 °C showing clear

sings of equilibration. However more data are needed as amphibole has not been extensively studied in St. Paul. A larger number of matrix amphibole-clinopyroxene pairs are also needed for peridotites exposed at the Vema Transform Fault which also indicate equilibrium of amphibole in the mantle peridotites (Figure 4.9).

Amphiboles from the Mado Megamullion, which is very approximate to the Godzilla Megamullion, are texturally replacing clinopyroxenes (Akizawa et al., 2021). Both the $T_{amph/cpx}$ and T_{BK90} vary from ~800 to ~1100 °C as shown in Figure 4.9. These values are generally lower compared to the values from Godzilla Megamullion. The scatter observed in Figure 4.9 along with the textural disequilibrium between amphibole and clinopyroxene are difficulties that do not enable a clear interpretation but it is predicted that amphibole has not attained equilibrium with the primary minerals. Amphiboles in alnoite-hosted xenoliths from Malaita but also from the Kerguelen Islands display very variable temperatures (Figure 4.9) based on mineral pairs that belong to different textural groups and disequilibrium is also highly expected.

4.3.4 Ophiolites

Pargasites in ophiolitic peridotites are extremely rare. Moreover, harzburgites comprise the biggest volume of mantle rocks of the ophiolitic mantle sections and therefore clinopyroxene is not always in association with amphibole. It is also immensely difficult to find amphibole-clinopyroxene pairs that fall in the compositional range of the calibrant dataset (Table 4.4). Ophiolites are mostly defined by low-temperature tremolitic amphiboles which are stable at amphibolitic facies conditions in ultramafic rocks. This is the reason why the amphibole-clinopyroxene thermometer was only applicable to one ophiolitic locality. This is the highly deformed and metamorphosed Lizard Ophiolite in England. Thermometry was conducted on pargasitic amphiboles replacing primary clinopyroxene and orthopyroxene. An average $T_{amph/cpx}$ of 913 °C was calculated along with a an average T_{BK90} equal to 856 °C. According to Cook (1999) Ti-rich pargasites have been formed and equilibrated at about 900 to 1000 °C which is in good agreement with the results of the new amphibole-clinopyroxene thermometer.

Conclusions

Amphibole, like phlogopite, is a metasomatic mineral that is incorporated into an ultramafic rock at some point during its geological evolution. For this reason, it is critical to test whether amphibole has remained at the right P-T-t conditions in order to re-equilibrate with the primary mantle phases after its initial formation from a melt or a fluid. This is possible with the use of the newly proposed amphibole-clinopyroxene Fe-Mg thermometer developed in the present study. It is proposed that the amphibole-clinopyroxene thermometer should be used in comparison with one (or multiple) other thermometric methods that is calibrated for ultramafic rocks. If both of the thermometric methods yield approximately the same temperatures, equilibrium between amphibole and the primary mantle phases should be considered. If not, then amphibole has probably not attained equilibrium with the ultramafic rocks.

However, it was shown here that the textures of minerals involved in the thermometric calculations have an extremely critical role on the final interpretation. By applying the proposed method on many localities from different geotectonic settings, two main observations were made: i) The safest results for interpretation are those in which amphibole is in textural equilibrium with the rest of the phases that are involved in the geothermometric methods. For example, matrix or porphyroclastic amphibole should be used along with matrix or porphyroclastic clinopyroxene, respectively. In the case of two-pyroxene thermometry being the chosen method for comparison, then orthopyroxene that belongs to the same textural group must be involved. When the two geothermometric methods yield similar results, equilibrium is highly expected. If the two thermometers yield completely unsimilar results then disequilibrium is the most likely explanation. In such cases, disequilibrium may have resulted for multiple reasons. For example, in Alpine-type peridotites, the differences in temperature may be the result of different diffusivities between cations. It was shown that the amphibole-clinopyroxene thermometer records far higher temperatures compared to the two-pyroxene thermometer of Brey and Köhler (1990). This could mean that the amphibole-clinopyroxene thermometer “freezes” at higher temperatures. In ultramafic xenoliths, the difference between the two thermometric methods might be affected by the relative time of the amphibole formation. Amphiboles that have formed immediately before the transport to the surface may have not had enough time to equilibrate. A third possibility for disequilibrium in ultramafic rocks is when they have been affected by magmatic activity and the

temperature has been raised locally. The local increase in temperature could cause the redistribution of cations between mineral phases and could cause a partial reequilibration. This scenario, for example, is expected for ultramafic xenoliths in Cerro Gordo (Spain); ii) Amphibole and clinopyroxene that belong to completely different textural groups must be treated very carefully. It may be possible that amphibole has managed to diffusionally equilibrate with clinopyroxene although textural equilibrium is not evident. In such cases more geochemical and chronological data should be obtained. On many occasions this complication may be overpassed. It is suggested that amphibole-clinopyroxene pairs that show both equilibrium and disequilibrium textures should be used. If both pairs yield the same temperatures (which are also comparable to two-pyroxene thermometry) it is possible that equilibrium has been achieved.

References

1. Adam J. Green T., 2006, Trace element partitioning between mica- and amphibole-bearing garnet lherzolite and hydrous basanitic melt: 1. Experimental results and the investigation of controls on partitioning behaviour, Contributions to Mineralogy and Petrology, vol. 152, pp. 1-17.
2. Ai Y., 1993, A revision of the garnet–clinopyroxene Fe+2–Mg exchange geothermometer, Contributions to Mineralogy and Petrology, vol. 115, pp. 467–473.
3. Akizawa N., Ohara Y., Okino K., Ishizuka O., Yamashita H., Machida S., Sanfilippo A., Basch V., Snow J.E., Sen A., Hirauchi K.-I., Michibayashi K., Harigane Y., Fujii M., Asanuma H., Hirata T., 2021, Geochemical characteristics of back-arc basin lower crust and upper mantle at final spreading stage of Shikoku Basin: an example of Mado Megamullion, Progress in Earth and Planetary Science, vol. 8, 65.
4. Albarède F., Michard-Vitrac A., 1978, Age and significance of the North Pyrenean metamorphism, vol. 40, pp. 327-332.
5. Ballhaus C., Berry R.F., Green D.H., 1991, High pressure experimental calibration of the olivine-orthopyroxene-spinel oxygen geobarometer: implications for the oxidation state of the upper mantle, Contributions to Mineralogy and Petrology, vol. 107, pp. 27-40.
6. Ban M., Witt-Eickschen G., Klein M., Seck H.A., 2005, The origin of glasses in hydrous mantle xenoliths from the West Eifel, Germany: incongruent break down of amphibole, Contributions to Mineralogy and Petrology, vol. 148, pp. 511-523.
7. Beard A.D., Downes H., Mason P.R.D., Vetrin V.R., 2007, Depletion and enrichment processes in the lithospheric mantle beneath the Kola Peninsula (Russia): Evidence from spinel lherzolite and wehrlite xenoliths, Lithos, vol. 94, pp. 1-24.
8. Bénard A., Ionov D.A., 2013, Melt- and Fluid-Rock Interaction in Supra-Subduction Lithospheric Mantle: Evidence from Andesite-hosted Veined Peridotite Xenoliths, Journal of Petrology, vol. 54, pp. 2239-2378.
9. Berno D., Tribuzio R., Zanetti A., Hémond C., 2020, Evolution of mantle melts intruding the lowermost continental crust: constraints from the Monte Capio-Alpe Cevia mafic-ultramafic sequences (Ivrea-Verbano Zone, northern Italy), Contributions to Mineralogy and Petrology, vol. 175, Issue 2.

10. Bertrand P., Mercier J.-C. C., 1985, The mutual solubility of coexisting ortho- and clinopyroxene: toward and absolute geothermometer for the natural system?, Earth and Planetary Science Letters, vol. 76, pp. 109-122.
11. Beyer E.E., Griffin W.L., O'Reilly S.Y., 2006, Transformation of Archaean Lithospheric Mantle by Refertilization: Evidence from Exposed Peridotites in the Western Gneiss Region, Norway, Journal of Petrologt, vol. 47, pp. 1611-1636.
12. Blatter D.L., Carmichael I.S.E., 1998, Hornblende peridotite xenoliths from central Mexico reveal the highly oxidized nature of subarc upper mantle, Geology, vol. 26, pp. 1035-1038.
13. Bonadiman C., Brombin V., Andreozzi G.B., Benna P., Coltorti M., Curetti N., Faccini B., Merli M., Pelorosso B., Stagno V., Tesauro M., Pavese A., 2021, Phlogopite-pargasite coexistence in an oxygen reduced spinel-peridotite ambient, Scientific Reports, vol. 11, no. 11829
14. Bonatti E., Ottonello G., Hamlyn P.R., 1986, Peridotites from the island of Zabargad (St. John), Red Sea: Petrology and Geochemistry, Journal of Geophysical Research, vol. 91, pp. 599-631.
15. Brearley M., Scarfe C.M., 1984, Amphibole in a spinel lherzolite xenolith: evidence for volatiles and partial melting in the upper mantle beneath southern British Columbia, Canadian Journal of Earth Sciences, vol. 21, pp. 1067-1072.
16. Brey G.P., Köhler T., 1990, Geothermobarometry in Four-phase Lherzolites II. New Thermobarometers, and Practical Assessment of Existing Thermobarometers, Journal of Petrology, vol. 31, pp. 1353-1378.
17. Cannat M., Seyler M., 1995, Transform tectonics, metamorphic plagioclase and amphibolitization in ultramafic rocks of the Vema transform fault (Atlantic Ocean), Earth and Planetary Science Letters, vol. 133, pp. 283-298.
18. Carswell A.D., Harvet M.A., Samman A., The petrogenesis of contrasting Fe-Ti and Mg-Cr garnet peridotite types in the high grade gneiss complex of Western Norway, Bulletin de Minéralogie, vol. 106, pp. 727-750.
19. Chen R.-X., Li H.-Y., Zheng Y.-F., Zhang L., Gong B., Hu Z., Yang Y., 2017, Crust-Mantle Interaction in a Continental Subduction Channel: Evidence from Orogenic Peridotites in North Qaidam, Northern Tibet, Journal of Petrology, vol. 58, pp. 191-226.
20. Conquéré F., 1971, La lherzolite á amphibole du gisement de Caussou (Ariége, France), Contributions to Mineralogy and Petrology, vol. 30, pp. 296-313.
21. Cook C.A., 1999, The tectonic evolution of mantle rocks from the lizardophiolite complex, South-West England, Durham theses, Durham University.
22. Corgne A., Schilling M.E., Grégoire M., Langlade J., 2018, Experimental constraints on metasomatism of mantle wedge peridotites by hybridized adakitic melts, Lithos, vol. 308-309, pp. 213-226.
23. Corvò S., Langone A., Padrón-Navarta J.A., Tommasi A., Zanetti A., 2020, Porphyroclasts: Souce and Sink of Major and Trace Elements During Deformation-Induced Metasomatism (Finero, Ivrea-Verbano Zone, Italy), Geosciences, vol. 10, 196.
24. De Hoog J.C.M., Janàk M., Vrabec M., Froitzheim N., 2009, Serpentinized peridotites from an ultrahigh-pressure terrane in the Pohorje Mts. (Eastern Alps, Slovenia): Geochemical constraints on petrogenesis and tectonic setting, Lithos, vol. 109, pp. 209-222.
25. Denis C.M.M., Alard O., Demouchy S., 2015, Water content and hydrogen behaviour during metasomatism in the uppermost mantle beneath Ray Pic volcano (Massif Central, France), Lithos, vol. 236-237, pp. 256-274.
26. Duarte J.F.V., Kaczmarek M.-A., Vonlanthen P., Putlitz B., Müntener O., 2020, Hydration of a Mantle Shear Zone Beyond Serpentine Stability: A Possible Link to Microseismicity Along Ultraslow Spreading Ridges?, vol. 125, Issue 10.
27. El Atrassi F., Chazot G., Brunet F., Chopin C., Bouybaouene M., 2014, Amphibole genesis in pyroxenites from the Beni Bousera peridotite massif (Rif, Morocco): Evidence for two different metasomatic episodes, Lithos, vol. 208-209, pp. 67-80.

28. Ellis D.J., Green D.H., 1979, An experimental study of the effect of Ca upon garnet-clinopyroxene Fe-Mg exchange equilibria, Contributions to Mineralogy and Petrology, vol. 71, pp. 13-22.
29. Fabriès J., Bodinier J.-L., Dupuy C., Lorand J.-P., Benkerrou C., 1989, Evidence for Modal Metasomatism in the Orogenic Spinel Lherzolite Body from Caussou (Northeastern Pyrenees, France), Journal of Petrology, vol. 30, pp. 199-228.
30. Faccini B., Rizzo A.L., Bonadiman C., Ntaflos T., Seghedi I., Grégoire M., Ferretti G., Coltorti M., 2020, Subduction-related melt refertlisation and alkaline metasomatism in the Eastern Transylvanian Basin lithospheric mantle: Evidence from mineral chemistry and noble gases in fluid inclusions, Lithos, vol. 364-365, 105516.
31. Ferrando S., Frezzotti M.L., Neumann E.-R., De Astis G., Peccerillo A., Dereje A., Gezahegn Y., Teklewold A., 2008, Composition and thermal structure
32. of the lithosphere beneath the Ethiopian
33. plateau: evidence from mantle xenoliths
34. in basanites, Injibara, Lake Tana Province, Mineralogy and Petrology, vol. 93, pp. 47-78.
35. Ferrari E., Montanini A., Tribuzio R., 2022, Rifting evolution of the lithospheric suncontinental mantle: New insights from the External Ligurian ophiolites (Northern Apennine, Italy), Lithos, vol. 410-411, 106571.
36. Frey F.A., Prinz M., 1978, Ultramafic inclusions from San Carlos, Arizona: Petrologic and Geochemical data bearing on their petrogenesis, Earth and Planetary Science Letters, vol. 38, pp. 129-176.
37. Frezzotti M.L., Ferrando S., Peccerillo A., Petrelli M., Tecce F., Perucchi A., 2010, Chlorine-rich metasomatic H_2O-CO_2 fluids in amphibole-bearing peridotites from Injibara (Lake Tana region, Ethiopian plateau): Nature and evolution of volatiles in the mantle of a region of continental flood basalts, Geochimica et Cosmochimica Acta, vol. 74, pp. 3023-3039.
38. Fumagalli P., Zanchetta S., Poli S., 2009, Alkali in phlogopite and amphibole and their effects on phase relations in metasomatized peridotites: a high-pressure study, Contributions to Mineralogy and Petrology, vol. 158, pp. 723-737.
39. Gilio M., Clos F., Roermund H.L.M., 2015, The Frininggen Garnet Peridotite (central Swedish Caledonides). A good example of the characteristic PTt path of a cold mantle wedge garnet peridotite, Lithos, vol. 230, pp. 1-16.
40. Graham C.M., Powell R., 1984, A garnet-hornblende geothermometer: calibration, testing and application to the Pelona Schist, Southern California, Journal of Metamorphic Geology, vol. 2, pp. 13-31.
41. Green D.H., 1973, Experimental melting studies on a model upper mantle composition at high pressure under water-saturated and water-undersaturated conditions, Earth and Planetary Science Letters, vol. 19, pp. 37-53.
42. Green D.H., Hibberson W.O., Kovács I., Rosenthal A., 2010, Water and its influence on the lithosphere-asthenosphere boundary, Nature, vol. 467, pp. 448-451.
43. Green D.H., Hibberson W.O., Rosenthal A., Kovács I., Yaxley G.M., Falloon T.J., Brink F., 2014, Experimental Study of the Influence of Water on Melting and Phase Assemblages in the Upper Mantle, Journal of Petrology, vol. 55, pp. 2067-2096.
44. Grégoire M., Lorand J.P., O'Reilly S.Y., Cottin J.Y., 2000, Armalcolite-bearing, Ti-rich metasomatic assemblages in harzburgitic xenoliths from the Kerguelen Islands: Implications for the oceanic mantle budget of high-field strength elements, Geochimica et Cosmochimica Acta, vol. 64, pp. 673-694.
45. Griffin W.L., Wass S.Y., Hollis J.D., 1984, Ultramafic Xenoliths from Bullenmerri and Gnotuk Maars, Victoria, Australia: Petrology of a Sub-Continental Crust-Mantle Transition, Journal of Petrology, vol. 25, pp. 53-87
46. Grove T.L., Chatterjee N., Parman S.W., Médard E., 2006, The influence of H_2O on mantle wedge melting, Earth and Planetary Science Letters, vol. 249, pp. 74-89.

47. Gudelius D., Aulbach S., Braga R., Höfer H.E., Woodland A.B., Gerdes A., 2019, Element Transfer and Redox Conditions in Continental Subduction Zones: New Insights from Peridotites of the Ulten Zone, North Italy, Journal of Petrology, vol. 60, pp. 231-268.
48. Harley S.L., 1984, An experimental study of the partitioning of Fe and Mg between garnet and orthopyroxene, Contributions to Mineralogy and Petrology, vol. 86, pp. 359-373.
49. Hidas K., Borghini G., Tommasi A., Zanetti A., Rampone E., 2021, Interplay between melt infiltration and deformation in the deep lithospheric mantle (External Liguride ophiolite, North Italy), Lithos, vol. 380-381, 105-855
50. Higgins O., Sheldrake T., Caricchi L., 2022, Machine learning Thermobarometry and chemometry using amphibole and clinopyroxene: a window into the roots of an arc volcano (Mount Liamuiga, Saint Kitts), Contributions to Mineralogy and Petrology, vol. 177, 10.
51. Hunt L.E., Lamb W.M., 2019, Application of mineral equilibria to estimate fugacities of H_2O, H_2, and O_2 in mantle xenoliths from the southwestern U.S.A., American Mineralogist, vol. 104, pp. 333-347
52. Ionov D.A., Griffin W.L., O'Reilly S.Y., 1997, Volatile-bearing minerals and lithophile trace elements in the upper mantle, Chemical Geology, vol. 141, pp. 153-184
53. Ionov D.A., Bodinier J.-L., Mukasa S.B., Zanetti A., 2002, Mechanisms and Sources of Mantle Metasomatism: Major and Trace Element Compositions of Peridotite Xenoliths from Spitsbergen in the Context of Numerical Modelling, Journal of Petrology, vol. 43, pp. 2219-2259.
54. Ionov D.A., 2010, Petrology of Mantle Wedge Lithosphere: New Data on Supra-Subduction Zone Peridotite Xenoliths from the Andesitic Avacha Volcano, Kamchatka, Journal of Petrology, vol. 51, pp. 327-361.
55. Ishimaru S., Arai S., Ishida Y., Shirasaka M., Okrugin V.M., 2007, Melting and Multi-stage Metasomatism in the Mantle Wedge beneath a Frontal Arc Inferred from Highly Depleted Peridotite Xenoliths from the Avacha Volcano, Southern Kamchatka, Journal of Petrology, vol. 48, pp. 395-433.
56. Ismail M., Delpech G., Cottin J.-Y., Grégoire M., Moine B.N., Bilal A., 2008, Petrological and geochemical constraints on the composition of the lithospheric mantle beneath the Syrian rift, northern part of the Arabian plate, in Coltorti M., Grégoire M. (eds), Metasomatism in Oceanic and Continental Lithospheric Mantle, Geological Society London, Special Publications, vol. 293, pp. 223-251.
57. Janák M., Froitzheim N., Vrabec M., Krogh Ravna E.J., De Hoog J.C.M., 2006, Ultrahigh-pressure metamorphism and exhumation of garnet peridotite in Pohorje, Eastern Alps, Journal of Metamorphic Geology, vol. 24, pp. 19-31.
58. Kadarusman A., Parkinson D., 2000, Petrology and P-T evolution of garnet peridotites from central Sulawesi, Indonesia, Journal of Metamorphic Geology, vol. 18, pp. 193-209.
59. Kaeser B., Kalt A., Pettke T., 2007, Crystallization and Breakdown of Metasomatic Phases in Graphite-bearing Peridotite Xenoliths from Marsabit (Kenya), Journal of Petrology, vol. 48, pp. 1725-1760.
60. Kaczmarek M.-A., Müntener O., 2008, Juxtaposition of Melt Impregnation and High-Temperature Shear Zones in the Upper Mantle; Field and Petrological Constraints from the Lanzo Peridotite (Northern Italy), Journal of Petrology, vol. 49, pp. 2187-2220.
61. Kaczmarek M.-A., Bodinier J.-L., Bosch D., Tommasi A., Dautria J.-M., Kechid S.A., 2016, Metasomatized Mantle Xenoliths as a Record of Lithospheric Mantle Evolution of the Northern Edge of the Ahaggar Swell, In Teria (Algeria), Journal of Petrology, vol. 57, 345-382.
62. Krogh E.J., 1988, The garnet-clinopyroxene Fe-Mg geothermometer- a reinterpretation of existing experimental data, Contributions to Mineralogy and Petrology, vol. 99, pp. 44-48.
63. Kushiro I., 1969, Compositions of magmas formed by partial zone melting of the Earth's upper mantle, Journal of Geophysical Research, vol. 73, pp. 619-634.

64. Ravna E.K., 2000, Distribution of Fe^{+2} and Mg between coexisting garnet and hornblende in synthetic and natural systems: an empirical calibration of the garnet-hornblende Fe-Mg geothermometer, Lithos, vol. 53, pp. 265-277.
65. Laurora A., Mazzucchelli M., Rivalenti G., Vannucci R., Zanetti A., Barbieri M.A., Cingolani C.A., 2001, Metasomatism and Melting in Carbonated Peridotite Xenoliths from the Mantle Wedge: The Gobernador Gregores Case (Southern Patagonia), Journal of Petrology, vol. 42, pp. 69-87.
66. Lee H.Y, Ganguly J., 1988, Equilibrium Compositions of Coexisting Garnet and Orthopyroxene: Experimental Determinations in the System $FeO-MgO-Al_2O_3-SiO_2$ and Applications, Journal of Petrology, vol. 29, pp. 93-113.
67. Liptai N., Patkó L., Kovács I.J., Hidas K., Pintér Z., Jeffries T., Zajacz Z., O'Reilly S.Y., Griffin W.L., Pearson N.J., Szabó C., 2017, Multiple Metasomatism beneath the Nógrád-Gömör Volcanic Field (Northern Pannonian Basin) Revealed by Upper Mantle Peridotite Xenoliths, Journal of Petrology, vol. 58- pp. 1107-1144.
68. Lucassen F., Franz G., Viramonte J., Romer R.L., Dulski P., Lang A., 2005, The late Cretaceous lithospheric mantle beneath the Central Andes: Evidence from phase equilibria and composition of mantle xenoliths, Lithos, vol. 82, pp. 379-406.
69. McGuire V., Dyar M.D., Nielson E., 1991, Metasomatic oxidation of upper mantle peridotite, Contributions to Mineralogy and Petrology, vol. 109, pp. 252-264.
70. Mallik A. Nelson J., Dasgupta R., 2015, Partial melting of fertile peridotite fluxed by hydrous rhyolitic melt at 2-3 GPa: implications for mantle wedge hybridization by sediment melt and generation of ultrapotassic magmas in convergent margins, Contributions to Mineralogy and Petrology, vol. 169, 48.
71. Mandler B.E., Grove T.L., 2016, Controls on the stability and composition of amphibole in the Earth's mantle, Contributions to Mineralogy and Petrology, vol. 171, no. 68.
72. Matusiak-Malek M., Puziewicz J., Ntaflos T., Grégoire M., Kukula A., Wojtulek P. M., 2017, Origin and evolution of rare amphibole-bearing mantle peridotites from Wilcza Góra (SW Polang), Central Europe, vol. 286-287, pp. 302-323.
73. Mazzucchelli M., Rivalenti G., Brunelli D., Zanetti A., Boari E., 2009, Formation of Highly Refractory Dunite by Focused Percolation of Pyroxenite-Derived Melt in the Balmuccia Peridotite Massif (Italy), Journal of Petrology, vol. 50, pp 1205-1233.
74. Mazzucchelli M., Zanetti A., Rivalenti G., Vannucci R., Correia C.T., Tassinari C.C.G., 2010, Age and geochemistry of mantle peridotites and diorite dykes from the Baldissero body: Insights into the Palaeozoic-Mesozoic evolution of the Southern Alps, Lithos, vol. 119, pp. 485-500
75. Mengel K., Green D.H., 1989, Stability of amphibole and phlogopite in metasomatized peridotite under water-saturated and water-undersaturated conditions, Kimberlites and related rocks, vol. 1, pp. 571-581.
76. Millhollen G.L., Irving A.J., Wyllie P.J., 1974, Melting interval of peridotite with 5.7 per cent water to 30 kilobars, Journal of Geology, vol. 82, pp. 575-587.
77. Muriuki J., Nakamura D., Hirajima T., Svojtka M., 2020, Mineralogical heterogeneity of UHP garnet peridotite in the Moldanubian Zone of the Bohemian Massif (Nové Dvory, Czech Republic), Journal of Mineralogical and Petrological Sciences, vol. 115, pp. 1-20.
78. Mysen B.O., Boettcher A.L. 1975, Melting of a Hydrous Mantle: I. Phase Relations of Natural Peridotite at High Pressures and Temperatures with Controlled Activities of Water, Carbon Dioxide, and Hydrogen, Journal of Petrology, vol. 16, pp. 520-548.
79. Nakamura D., 2009, A new formulation of garnet-clinopyroxene geothermometer based on accumulation and statistical analysis of a large experimental data set, Journal of Metamorphic Geology, vol. 27, pp. 495-508.
80. Neal C.R., 1988, The Origin and Composition of Metasomatic Fluids and Amphiboles beneath Malaita, Solomon Islands, Journal of Petrology, vol. 29, pp. 149-179.

81. Niida K., Green D.H., 1999, Stability and chemical composition of pargasitic amphibole in MORB pyrolite under upper mantle conditions, Contributions to Mineralogy and Petrology, vol. 135, pp. 18-40.
82. Nimis P., Grütter H., 2010, Internally consistent geothermometers for garnet peridotites and pyroxenites, Contributions to Mineralogy and Petrology, vol. 159, pp. 411-427.
83. Nimz G.J., Cameron K.L., Cameron M., Morris S.L., 1986, The petrology of the lower crust and upper mantle beneath southeastern Chihuahua, Mexico: A progress report, Geof. Int. Vol., vol. 25-1, pp. 85-116.
84. Ntaflos T., Bizimis M., Abart R., 2017, Mantle xenoliths from Szentbékálla, Balaton: Geochemical and petrological constraints on the evolution of the lithospheric mantle underneath Pannonian Basin, Hungary, Lithos, vol. 276, pp. 30-44.
85. Obata M., Morten L., 1987, Transformation of Spinel Lherzolite to Garnet Lherzolite in Ultramafic Lenses of the Austridic Crystalline Complex, Northern Italy, Journal of Petrology, vol. 28, pp. 599-623.
86. Ohara Y., Fujioka K., Ishii T., Yurimoto H., 2003, Peridotites and gabbros from the Parece Vela backarc basin: Unique tectonic window in an extinct backarc spreading ridge, Geochemistry, Geophysics, Geosystems, vol. 4, no. 7.
87. O'Neill H.St.C., Wood B.J., 1979, An experimental study of Fe-Mg partitioning between garnet and olivine and its calibration as a geothermometer, Contributions to Mineralogy and Petrology, vol. 70, pp. 59-70.
88. Oxburgh E.R., 1964, Petrological Evidence for the Presence of Amphibole in the Upper Mantle and its Petrogenetic and Geophysical Implications, Geological Magazine, vol. 101, pp. 1-19.
89. Paquin J., Altherr R., 2001, New Constraints on the P-T Evolution of the Alpe Arami Garnet Peridotite Body (Central Alps, Switzerland), Journal of Petrology, vol. 42, pp. 1119-1140.
90. Pellegrino L., Malaspina N., Zanchetta S., Langone A., Tumiati S., 2020, High pressure melting of eclogites and metasomatism of garnet peridotites from Monte Duria Area (Central Alps, N Italy): A proxy for melt-rock reaction during subduction, Lithos, vol. 358-359, 105391.
91. Pellegrino L., Menegon L., Zanchetta S., Langenhorst F., Pollok K., Tumiati S., Malaspina N., 2021, Reaction-Induced Mantle Weakening at High-Pressure Conditions: An example From Garnet Pyroxenites of Ulten Zone (Eastern Alps, N Italy), Journal of Geophysical Research: Solid Earth, vol. 126, e2021JB022584.
92. Piccardo G.B., Messiga B., Vannucci R., 1988, The Zabargad peridotite-pyroxenite association: petrological constraints on its evolution, Tectonophysics, vol. 150, pp. 135-162.
93. Pintér Z., Foley S.F., Yaxley G.M., Rosenthal A., Rapp R.P., Lanati A.W., Rushmer T., 2021, Experimental investigation of the composition of incipient melts in upper mantle peridotites in the presence of CO_2 and H_2O, Lithos, 106224
94. Powell R., 1985, Regression diagnostics and robust regression in geothermometer/geobarometer calibration: the garnet-clinopyroxene geothermometer revisited, Journal of Metamorphic Geology, vol. 3, pp. 231-243.
95. Powell W., Zhang M., O'Reilly S.Y., Tiepolo M., 2004, Mantle amphibole trace-element and isotopic signatures trace multiple metasomatic episodes in lithospheric mantle, western Victoria, Australia, Lithos, vol. 75, pp. 141-171.
96. Putirka K., 2016, Amphibole thermometers and barometers for igneous systems and some implications for eruption mechanisms of felsic magmas at arc volcanoes, American Mineralogist, vol. 101, pp. 841-858.
97. Ridolfi F., 2021, Amp-TB2: An Updated Model for Calcic Amphibole Thermobarometry, Minerals, vol. 11, 324
98. Ringwood A.E., 1962, A model for the upper mantle, Journal of Geophysical Research, vol. 67, pp. 857-867.

99. Sapienza G.T., Scambelluri M., Braga R., 2009, Dolomite-bearing orogenic garnet peridotites witness fluid-mediated carbon recycling in a mantle wedge (Ulten Zone, Eastern Alps, Italy), Contributions to Mineralogy and Petrology , vol. 158, pp. 401-420.
100. Scambelluri M., Pettke T., Rampone E., Godard M., Reusser E., 2014, Petrology and Trace Element Budgets of High-pressure Peridotites Indicate Subduction Dehydration of Serpentinized Mantle (Cima di Gagnone, Central Alps, Switzerland), Journal of Petrology, vol. 55, pp. 459-498
101. Seckendorff V., O'Neill H.St.C., 1993, An experimental study of Fe-Mg partitioning between olivine and orthopyroxene at 1173, 1273 and 1423 K and 1.6 GPa, Contributions to Mineralogy and Petrology, vol. 113, pp. 196-207.
102. Sen A., Snow J.E., Ohara Y., Hirauchi L., Kouketsu Y., Sanfilippi A., Basch V., Harigane Y., Fujii M., Okino M., Akizawa N., 2022, Melting and evolution of amphibole-rich back-arc abyssal peridotites at the Mado Megamullion, Shikoku Basin, Geochemistry, Geophysics, Geosystems, vol. 22, Issue 12.
103. Seyler M., Mattson P.H., 1989, Petrology and thermal evolution of the Tinaquilo peridotite (Venezuela), Journal of Geophysical Research, vol. 94, pp. 7629-7660.
104. Shaw C.S.J., Eyzaguirre J., Fryer B., Gagnon J., 2005, Regional Variations in the Mineralogy of Metasomatic Assemblages in Mantle Xenoliths from the West Eifel Volcanic Field, Germany, vol. 46, pp. 945-972.
105. Siegrist M., Yogodzinski G., Bizimis M., Fournelle J., Churikova T., Dektor C., Mobley R., 2019, Fragments of Metasomatized Forearc: Origin and Implications of Mafic and Ultramafic Xenoliths From Kharchinsky Volcano, Kamchatka, Geochemistry, Geophysics, Geosystems, vol. 20, pp. 4426-4456.
106. Stolz A.J., Davies G.R., 1988, Chemical and Isotopic Evidence from Spinel Lherzolite Xenoliths for Episodic Metasomatism of the Upper Mantle beneath Southeast Australia, Journal of Petrology, Special Lithosphere Issue, pp. 303-330.
107. Szabó Cs., Vaselli O., Vannucci R., Bottazzi P., Ottolini L., Coradossi N., Kubovics I., 1995, Ultramafic xenoliths from the Little Hungarian Plain (Western Hungary): a petrologic and geochemical study, Acta Vulcanologica, vol. 7, pp. 249-263.
108. Takahashi E., 1980, Thermal history of lherzolite xenoliths-I. Petrology of lherzolite xenoliths from the Ichinomegata crater, Oga peninsula, northeast Japan, Geochimica et Cosmochimica Acta, vol. 44, pp. 1643-1658.
109. Tamura A., Arai S., Ishimaru S., Andal E.S., 2008, Petrology and geochemistry of peridotites from IODP Site U1309 at Atlantis Massif, MAR 30°N: micro- and macro-scale melt penetrations into peridotites, Contributions in Mineralogy and Petrology, vol. 155, pp. 491-509.
110. Tamura A., Morishita T., Ishimaru S., Arai S., 2014, Geochemistry of spinel-hosted amphibole inclusions in abyssal peridotite: insight into secondary melt formation in melt-peridotite reaction, 2014, Contributions in Mineralogy and Petrology, vol. 167, 974.
111. Taylor W.R., 1998, An experimental test of some geothermometer and geobarometer formulations for upper mantle peridotites with application to the Thermobarometry of fertile lherzolite and garnet websterite, Neues Jahrbuch für Mineralogie, vol. 172, pp. 381-408.
112. Tilley C.E., Long J.V.P., 1967, The Porphyrocalst Minerals of the Peridotite-Mylonites of St. Paul's Rocks (Atlantic), Geological Magazine, vol. 104, pp. 46-48.
113. Tommasi A., Langone A., Padrón-Navarta J.A., Zanetti A., Vauchez A., 2017, Hydrous melts weaken the mantle, crystallization of pargasite and phlogopite does: Insights from a petrostructural study of the Finero peridotites, southern Alps, Earth and Planetary Science Letters, vol. 477, pp. 59-72.
114. Uenver-Thiele L., Woodland A.B., Downes H., Altherr R., 2014, Oxidation State of the lithospheric mantle below the Massif Central, France, Journal of Petrology, vol. 55, pp. 2457-2480.

115. Vaselli O., Downes H., Thirwall M., Dobosi G., Coradossi N., Seghedi I., Szakacs A., Vannucci R., 1995, Ultramafic Xenoliths in Plio-Pleistocene Alkali Basalts from the Eastern Transylvanian Basin: Depleted Mantle Enriched by Vein Metasomatism, Journal of Petrology, vol. 36, pp. 23-53.
116. Villaseca C., Serrano J.G., Pérez-Soba C., 2020, Subduction-related metasomatism in the lithospheric mantle beneath the Calatrava volcanic field (central Spain): constraints from lherzolite xenoliths of the Cerro Gordo volcano, International Geology Review
117. Vrabec M., 2010, Garnet peridotites from Pohorje: Petrography, geothermobarometry and metamorphic evolution, Geologija, vol. 53/1, pp. 21-36.
118. Wallace M.E., Green D.H., 1991, The Effect of Bulk Rock Composition on the Stability of Amphibole in the Upper Mantle: Implications for Solidus Positions and Mantle Metasomatism, Mineralogy and Petrology, vol. 44, pp. 1-19.
119. Wang C., Liang Y., Xu W., 2021, Formation of Amphibole-Bearing Peridotite and Amphibole-Bearing Pyroxenite Through Hydrous Melt-Peridotite Reaction and In Situ Crystallization: An experimental Study, Journal of Geophysical Research: Solid Earth, vol. 126, e2020JB019382
120. Wells P.R.A., 1977, Pyroxene thermometry in simple and complex systems, Contributions to Mineralogy and Petrology, vol. 62, pp. 129-139
121. Wells P.R.A., 1979, P-T conditions in the Moines of the Central Highlands, Scotland: Journal of the Geological Society London, vol. 136, pp. 663-671.
122. Wilshire H.G., Meyer C.E., Nakata J.K., Calk L.C., Shervais J.W., Nielson J.E., Schwarzman E.C., 1988, Mafic and ultramafic xenoliths from volcanic rocks of the western United States: U.S. Geological Survey Professional Paper, vol. 1443 pp. 179-576.
123. Witt-Eickschen G., Seck H.A., Reys C., 1993, Multiple Enrichment Processes and their Relationships in the Subcrsutal Lithosphere Beneath the Eifel (Germany), Journal of Petrology, vol. 34, pp. 1-22.
124. Witt-Eickschen G., Harte B., 1994, Distribution of trace elements between amphibole and clinopyroxene from mantle peridotites of the Eifel (western Germany): An ion-microprobe study, Chemical Geology, vol. 117, pp. 235-250.
125. Wu C.M., Zhao G.C., 2007, A recalibration of the garnet-olivine geothermometer and a new geobarometer for garnet peridotites and garnet-olivine-plagioclase-bearing granulites, Journal of Metamorphic Geology, vol. 25, pp. 497-505.
126. Xu Y., Mercier J.C., Chuanyong L., Amphibole-bearing peridotite xenoliths from Nushan, Anhui Province: Evidence for melt percolation process in the Upper mantle and lithospheric uplift, Chinese Journal of Geochemistry, vol. 16, no. 3.
127. Xu X., O'Reilly S.Y., Griffin W.L., Zhou X., Huang X., 1998, The Nature of the Cenozoic Lithosphere at Nushan, Eastern China, Mantle Dynamics and Plate Interactions in East Asia, vol. 27, pp. 167-195.
128. Xu Y.G., Bodinier J.L., 2004, Contrasting Enrichments in High- and Low-Temperature Mantle Xenoliths from Nushan, Eastern China: Results of a Single Metasomatic Event during Lithospheric Accretion?, Journal of Petrology, vol. 45, pp. 321-341.
129. Ye K., Song Y.R., Chen Y., Xu H.J., Liu J.B., Sun M., 2009, Multistage metamorphism of orogenic garnet-lherzolite from Zhimafang, Sulu UHP terrane, E. China: Implications for mantle wedge convection during progressive oceanic and continental subduction, Lithos, vol. 109, pp. 155-175.
130. Zanetti A., Mazzucchelli M., Rivalenti G., Vannucci R., 1999, The Finero phlogopite-peridotite massif: An example of subduction-related metasomatism, Contributions to Mineralogy and Petrology, vol. 134, pp. 107-122

CHAPTER 5
Novel 3D geochemical discrimination diagrams: A new method to infer the genesis of amphibole in ultramafic rocks

Introduction

For at least 40 years geochemical databases on rocks and minerals have been crucial in the field of petrology but also in geochemistry, geophysics and tectonics. Igneous and metamorphic phase equilibria, thermobarometric formulations, thermodynamic modelling, partial melting calculations, statistical analyses and comparisons are only a few of the applications in which geochemical databases have been useful. Because of the enormously large amount of data present in geochemical datasets and also the wide variety of possible applications, they have a collective impact on the solution of large-scale geological and, more specifically, petrological problems. PetDB (Lehnert et al., 2000), GEOROC (Schramm et all., 2006). SedDB (Lehnert et al., 2007), NAVDAT (Carlson et al., 2001), CHRONOS (Cox & Richard, 2005) and LEPR (Hirschmann et al., 2008) are only a few examples of databases that have been extensively used in the literature throughout the years. Moreover, databases are also necessary for the development of artificial intelligence models (AI) which have been of petrological interest in recent years. The amount of data involved in a petrological dataset can immediately affect the applicability range and quality of the AI formulation. In the present and final chapter, a new database will be presented that involves major-element chemical analyses of amphiboles from a wide variety of natural and experimental rock compositions as well as from the majority of geotectonic settings. The database is aiming to shed light on the processes that are involved in the formation of amphibole in ultramafic rocks around the globe. It will additionally provide information on the nature of the metasomatic agent that was involved during its crystallization.

5.1 The compiled database

An extensive database has been compiled using published major-element analyses of amphibole. The database consists of natural amphiboles occurring in

ultramafic rocks from various geotectonic settings around the globe but also in felsic to mafic igneous rocks. Moreover, a large number of amphibole analyses from a wide compositional spectrum of experiments has been included. However, this study will be focused on amphiboles that are related to ultramafic rocks. A total number of 9501 amphiboles was initially involved in the database. Subsequently, their stoichiometry was tested by making sure that the sums of cations for each crystallographic site (T, C, B and A) were within ±0.2 a.p.f.u. of the expected value (based on the general amphibole formula). A total number of 100 amphiboles were found non-stoichiometric and were excluded. The remaining 9401 amphibole analyses in the dataset cover a time range in bibliography from 1963 to 2022 with most of them having been published from 1990 and thereafter. Amphiboles found in natural rocks define the majority of the database (with a total number of 7953 analyses) whereas 1448 amphiboles have been selected from existing experimental works.

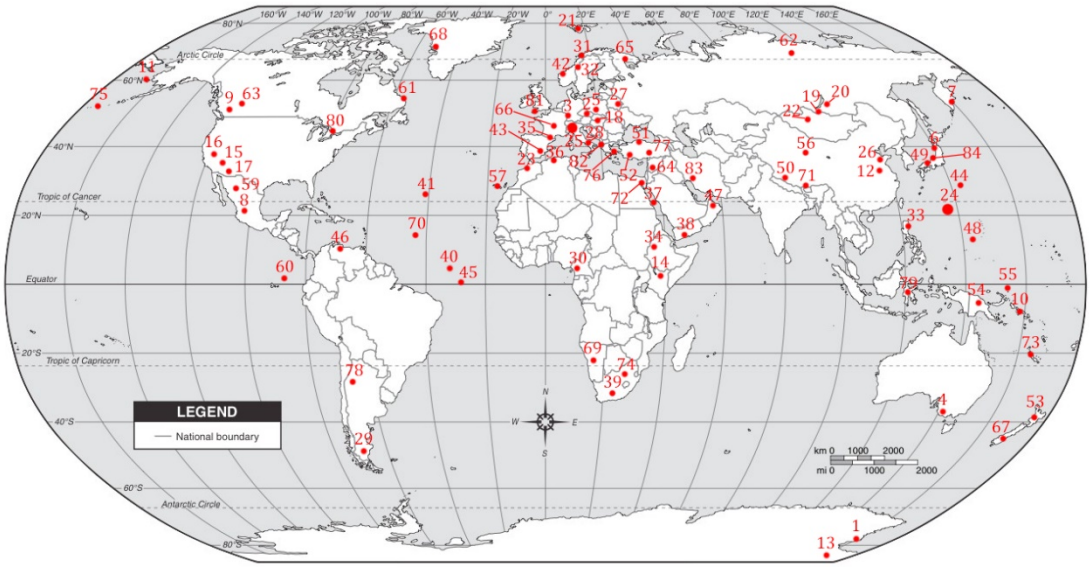

Figure 5.1: World map showing the localities from which amphiboles in ultramafic rocks have been accumulated for the database. 1. Victoria Land (Antarctica); 2. Nové Dvory (Czech Republic), Eastern Transylvanian Basin (Romania); 3. West Eifel (Germany 4. Victoria (Australia); 5. Wilcza Góra (Poland); 6. Ichinomegata (Japan); 7. Avacha, Kharchinsky, Valovayam, Shiveluch (Russia); 8. El Peñon (Mexico); 9. Lightning Peak (Canada); 10. Malaita, San Jorge (Solomon Islands); 11. Nunivak (Alaska); 12. Nushan (China); 13. Foster Crater (Antarctica); 14. Marsabit (Kenya) 15. Grand Canyon, San Carlos, Cima, Black Rock, Vulcan's Throne (U.S.A.); 16. Dish Hill, Deadman Lake (U.S.A.); 17. Kilbourne Hole, Chino Valley, Coliseum, Cleator, Soda Springs, Peridot (U.S.A.); 18. Nógrád Gömör (Hungary), Szentbekalla (Hungary), Szigliget (Hungary), Little Hungarian Plain (Hungary, Pohorje (Slovenia); 19. Bartoy (Russia); 20. Vitim (Russia); 21. Spitsbergen (Norway); 22. Shavaryn (Mongolia); 23. Beni Busera (Morocco); 24. Mado Megamullion, Godzilla Megamullion (Parece Vela Basin); 25. External Ligurides, Ulten, Finero, Balmuccia, Baldissero, Lanzo, Sesia (Italy), Alpe Arami, Monte Duria, Cima di Gagnone (Switzerland); 26. Su-Lu, Raobazhai (Tibet); 27. Pripyat rift (Belarus); 28. Mt. Vulture (Italy); 29. Gobernador Gregores, Cerro del Mojon (Patagonia); 30. Barombi, Nyos (Cameroon); 31.Svartberget (Norway); 32. Friningen (Sweden); 33. Dinapigui, Iraya, Monglo, Pinatubo, Sabtang (Philippines); 34. Injibara (Ethiopia); 35. Caussou, Lherz (France); 36. Ahaggar (Algeria); 37. Zabargad (Red Sea); 38. Ataq, Bir Ali (South Arabia); 39. Jagersfontein (South Africa); 40. Vema Transform Fault (Atlantic Ocean); 41. Atlantis Massif (Atlantic Ocean); 42. West Gneiss Region (Norway); 43. Cerro Gordo (Spain); 44. Hahajima (Izu-Bonin arc); 45. St. Paul (Atlantic Ocean); 46. Tinaquilo (Venezuela); 47. Semail Ophiolite (Oman); 48. Mariana Trench;

49.Oeyama, Ohsa-yama (Japan); 50. Yungbwa, Purang (Tibet); 51. Küre, Kizilirmak (Turkey); 52. Lycian Ophiolite (Turkey); 53. Anita (New Zealand); 54. Bismarck (Papua New Guinea); 55. TUBAF (Papua New Guinea); 56. Qaidam (Tibet); 57. La Palma (Canary Islands); 58. Sierra Nevada (U.S.A.); 59. Chihuahua (Mexico); 60. Hess Deep (Pacific Ocean); 61. Newfoundland (Canada); 62. Birekte (Russia); 63. Craven Lake (Canada); 64. Jabel El Arab, Shamah (Syria); 65. Kandalaksha, Pechenga (Russia); 66. Massif Central (France); 67. Kakanui (New Zealand); 68. Qaarsut (Greenland); 69. Damara (Namibia); 70. 15°20′ N Fracture Zone (Atlantic Ocean); 71. Xigaze (Tibet); 72. Wadi Natash, Hagar Dungash, Sinai, Gerf, Daha (Egypt); 73. Tiebaghi, Massif du Sud (New Caledonia); 74. Kaapval (South Africa); 75. Kadak, Moffett, Kanaga (Aleutian Arc); 76. Ochi (Greece); 77. Berit (Turkey); 78.Central Andes (Argentina); 79. Sulawesi (Indonesia); 80. Mt. Albert (Canada); 81. Lizard (United Kingdom); 82. Mirdita (Albania); 83. Zagros (Iran); 84. Miyamori (Japan)

More specifically, natural amphiboles in lherzolites, harzburgites, dunites, chromitites, wehrlites, websterites and serpentinites form 40.8 % of the dataset, a number which is equivalent to 3835 analyses in total (Table 5.1). These ultramafic rocks are either defined by the spinel or garnet stability field conditions or are igneous in origin (e.g. chromitites). The amphiboles have been collected from multiple localities around the globe (Figure 5.1) and represent all of the possible geotectonic settings where amphibole can possibly exist in ultramafic rocks. The ultramafic part of the database may be split into two parts: one that involves amphiboles found in continental settings and one in oceanic settings.

Those that are found in continental settings can further be divided, based on the geotectonic setting, into amphiboles in Alpine-type peridotites, continental rift-related settings and continental arcs. An exact number of 416 amphiboles from Alpine-type peridotites has been derived from bibliography (Table 5.1). The vast majority of them comes from works conducted on the Italian and Swiss Alps. However, the database also involves amphiboles in orogenic peridotites from New Zealand, Morocco, France, Norway, Sweden, the Czech Republic, Slovenia, China, Venezuela and Indonesia (Figure 5.1) that display similar characteristics to the Alpine peridotites. Amphiboles in ultramafic xenoliths from continental rift-related systems are 610 in total (Table 5.1). The vast majority of them has been derived from localities from Central Europe (e.g. West Eifel). Localities that are currently on an intra-continental rifting tectonic regime but may have been affected by a subduction zone in their geological history, are also included in this category (e.g. Eastern Transylvanian Basin). Localities from the African rifting system have also been included (e.g. Injibara). Xenolithic amphiboles in continental rifts from Australia (Victoria), China (Nushan), Russia (Kandalaksha), Antarctica (Foster Crater), Siberia (Bartoy and Birekte), South Arabia (Ataq and Harrat Hutaymah), Syria (Jabel El Arab) and Argentina (Central Andes) are also present in the database. Xenolithic amphiboles from active continental-arc settings comprise two dominant groups. The first group consists of amphiboles from the American Cordillera (e.g. Dish Hill and Deadman Lake) and is made of 201 amphibole analyses. The second important group

in the database is defined by amphiboles found in ultramafic xenoliths from Kamchatka (e.g. Avacha) and consists of 195 amphiboles. Several more xenolithic continental-arc and back-arc localities have also been involved including volcanoes from the Aleutian arc (e.g. Moffett), the back-arc setting of Patagonia (e.g. Gobernador Gregores), the Ichinomegata crater in Japan and Kakanui in New Zealand. Finally, amphiboles in crustal ultramafic rocks are 250 in number and are exclusively represented by the Pechenga ultramafic rocks (Russia) (Fiorentini et al., 2008).

Amphiboles in ultramafic rocks from oceanic settings are 376 in total (Table 5.1) and have mainly been derived from core complexes, plateaus and fracture zones that expose the rocks on the surface. Some of the most important localities involve the Godzilla and Mado megamullions in the Pacific ocean, the Atlantis Massif, the Vema Transform Fault and the St. Paul rocks in the Atlantic ocean and finally the Kerguelen Islands in the Indian ocean. In this category, amphiboles in serpentinites from the Newfoundland passive margin have also been included. Amphiboles, from oceanic arcs and back-arcs are 641 in number (Table 5.1) and they are mostly related to xenoliths trapped in mafic melts. The most crucial localities are found in Papua New Guinea (e.g. Bismarck and Lihir), Philippines (e.g. Batan and Mt. Pinatubo) and Solomon islands (e.g. San Jorge). Two small ultramafic masses from Sinai (Egypt) have also been considered in this category, although they show a complex origin at an older suprasubduction zone (Maurice et al., 2021). Ophiolitic amphiboles are 589 in number and the majority of them have been collected from Turkey (e.g. Lycian Ophiolite), Tibet (e.g. Yungbwa), Egypt (e.g. Gerf), Albania (Mirdita), New Caledonia and England (Lizard). Several more localities have been included such as Mt. Kalnik in Croatia, Ochi ophiolite in Greece and finally Oeyama and Ohsa-yama in Japan. We considered ophiolitic chromitites as a separate category in this study so as to separately investigate the formation of amphibole in these rocks. Amphiboles in ophiolitic chromitites are 219 in total and have been found in multiple localities from South Arabia (Al Ays complex), Turkey (Lycian Ophiolite) to New Caledonia (Tiebaghi and Massif du Sud), Albania (Mirdita), Oman (Semail), Japan (Miyamori) and Iran (Neyriz and Zagros). Amphiboles in dunites from the Semail ophiolite (248 in number) have also been considered as a separate category to reduce their influence on the interpretation of ophiolitic harzburgites.

Table 5.1: Table presenting the number of amphiboles in each geotectonic setting and type of rock involved in the database.

Category	Number of amphiboles
Natural ultramafic rocks	

Continental rift	573
Continental arc	523
Alpine-type	416
Crustal Ultramafics	250
Oceanic core complexes and plateaus	376
Oceanic arc	641
Ophiolite	589
Ophiolitic Chromitite	219
Semail Dunite	248
Natural mafic to felsic rocks	
Basalt	153
Gabbro	410
Dacite	816
Andesite-Diorite	993
Hornblendite	97
Monzonite	36
Dolerite	15
Rhyolite	958
Lamprophyre	33
Basanite	25
Kimberlite	478
Eclogite	105
Experimental database	
Peridotite	117
Basalt	410
Gabbro	50
Dacite	309
Andesite-Diorite	341
Dunite	12
Tonalite	52
Phonolite	9
Trachyte	16
Rhyolite	16
Carbonatite	3
Granite	26
Lamproite	5
Pyroxenite	9
Basanite	73

The constructed database in this study also involves natural amphiboles in mafic to felsic rocks that have been previously studied (4119 in number). While the majority of them are of igneous origin, 105 amphiboles in eclogites have also been involved. Similarly to ultramafic rocks, the amphiboles in mafic to felsic rocks have been accumulated from multiple regions around the globe. For example natural amphiboles in basalts have been acquired from studies in Italy (Etna), the Mariana Trench and Germany (Rhön) and amphiboles from natural andesites to basaltic-andesites have been derived from China (Awulale), Russia (Bezymianny), the Carpathian-Pannonian region, Tibet (Comei), Indonesia (Mt. Merapi), Japan (Shikanoshima), Russia (Shiveluch) and Peru (Yanacocha).

In a similar manner, amphiboles from a wide spectrum of experiments spanning from ultramafic to felsic compositions have been incorporated in the

database (1448 in number). LEPR has been considered here (Hirschmann et al., 2008) but was updated to involve new experimental works from 2009 and thereafter. Amphiboles from experimental ultramafic compositions are identical to the ones used in Chapter 4 for the calibration of the thermometer. However, disequilibrium amphiboles (e.g. Shaw, 2009) have also been involved. Amphiboles formed from all of the possible experimental techniques have been included in the database. These techniques involve experiments using fused, homogeneous glasses as starting materials brought in sub-liquidus conditions so that new phases can crystallize (e.g. Adam & Green, 1994; Pichavant et al., 2002; Costa et al., 2004; Holtz et al., 2005; Feig et al., 2006; Irving & Green, 2008; Bonechi et al. 2020). Moreover, experiments in which starting materials were exposed to super-liquidus conditions and then were cooled down to the desired sub-liquidus equilibrium temperatures have also been considered (crystallization experiments) (e.g. Klein et al., 1997; Cannao et al., 2022). There is also experimental work in which the sub-solidus behavior of the starting materials has been explored (e.g. Ernst & Liu, 1998; Forneris & Holloway, 2003). These studies were aiming to investigate the metamorphic evolution of metabasalts or other rock types and the relevant phase transformations. Finally, experiments involving interactions between two starting materials (such as peridotite and basaltic melt) have also been considered (e.g. Wang et al., 2021). The compositions of the experiments used in the present study are shown in Table 5.1.

5.2 Classification and geochemical characteristics of amphiboles in the database

5.2.1 Distribution of amphibole species between geotectonic settings

Similarly to previous chapters, the classification of amphiboles in the database was performed by applying the nomenclature of Hawthorne et al. (2012) and the Microsoft excel spreadsheet of Locock (2014). As discussed in Chapter 4, Fe^{+3} in amphibole cannot be precisely estimated with empirical calculation methods. Moreover, the calibration of the amphibole-clinopyroxene thermometer did not require the derivation of Fe^{+3} as this problem was treated in a different manner. However, in the statistical analysis of the present chapter, Fe^{+3} is needed for the inference of the amphibole species and formula. The Fe^{+3} content was calculated by constraining the sum of a set of cations to a particular value and assuming electroneutrality (Hawthorne et al., 2012; Locock, 2014). Nevertheless, the Fe^{+3} values will only be considered as indicative. Finally, whenever TiO_2 exceeded 4.5 wt

%, the (OH, F, Cl) = 2 -2Ti estimation was considered to enable the classification of kaersutitic amphiboles.

Calcic amphiboles (pargasite, Mg-hornblende, hastingsite, tschermakite, edenite, tremolite, actinolite and sadanagaite) form the most dominant group in ultramafic rocks from every geotectonic setting around the globe (Figure 5.2). Moreover they are the most widespread type of amphibole in mafic to felsic rocks of experimental or natural origin. As is evident from Figure 5.2, pargasite (n = 2806) and Mg-hornblende (n = 2738) represent 60 % of the total number of amphiboles in the database. Hastingsite is the third most common composition in the database with a total number of 1337 analyses. Tremolite, sadanagaite, actinolite form minor groups but they seem to be important at several geotectonic settings.

Pargasite is the most abundant calcic amphibole in ultramafic rocks from continental rift-related settings, continental arcs and Alpine-type peridotites (Figure 5.2). However, a small number of Mg-hornblendes, hastingsites an sadanagaites are also observed in all of the aforementioned settings. Tremolitic and actinolitic amphiboles completely lack from any of the continental settings except from a few Alpine-type localities (West Gneiss Region, Pohorje, Anita, Cima di Gagnone). Another interesting observation is that amphiboles from continental rift-related settings do not show any signs of Mg-hornblende, with the exception of Zabargad island. A small amount of sadanagaites in rift-related settings is also found in Grand Canyon and Injibara whereas in continental arcs they are observed in localities from the American Cordillera (e.g. Deadman Lake, Dish Hill, La Olivina, San Carlos and Toroweap). Hastingsite in continental settings is more common in continental arcs. Adak Island, Ichinomegata and Kharchinsky ultramafic xenoliths show large concentrations of hastingsites.

Ophiolites are dominated by the existence of Mg-hornblende, tremolite and actinolite. These end-member compositions are all found in almost every ophiolitic locality. Although pargasite is not a regular mineral in ophiolitic rocks, it seems to have an important role in ultramafic rocks from Lizard, Kure, the Gerf, Lycian and the New Caledonian ophiolites. Minor numbers of hastingsites have also been observed in the Lizard complex but also in Mirdita and in the Purang dunitic rocks. Interestingly, amphiboles in the Semail dunites are exclusively pargasitic. Amphiboles in ophiolitic chromitites are primarily tremolitic in origin but there is also an important number of pargasites. Amphiboles from oceanic arcs are mainly tremolites and Mg-hornblendes. A few pargasites are found in a wide variety of localities from Philippines and Papua New Guinea and 8 fine-grained edenites have been located in TUBAF (Papua New Guinea). In contrast to ophiolites and oceanic

arcs, ultramafic rocks from oceanic plateaus and core complexes show a significant content in pargasites. Only a minor amount of Mg-hornblendes, tremolites and actinolites are present in a few oceanic plateaus. Two ultramafic bodies from Sinai (Egypt) seem to contain important amounts of anthophyllite as well as tremolite.

The oxo-amphibole group is entirely represented by kaersutite which forms a relatively large fraction of the database (n = 547). Kaersutites seem to be associated to continental rather than oceanic settings. Kaersutite in Alpine-type peridotites has only been observed in the External Ligurides Ophiolite (Ferrari et al., 2022). In continental rift-related settings kaersutite is present in multiple localities from Victoria Land (Antarctica) to Zabargad in the Red Sea and Marsabit in Kenya. On the other hand, localities from continental arcs that show crucial amounts of kaersutite are located in the American Cordillera (e.g. Deadman Lake, Black Rock Summit, Black Canyon, Lunar Craters) but also in Kakanui (New Zealand). A very small number of kaersutites in ophiolitic ultramafic rocks are located at the Lizard complex in England and at the Ochi ophiolite in Greece. Finally, the crustal ultramafic rocks from Pechenga (Russia) are almost entirely represented by kaersutite.

Multiple end-member compositions of the sodium-calcium group have been observed (e.g. winchite, barroisite, katophorite, taramite), although in insignificant numbers. A few katophoritic grains have been collected from Marsabit, Kaapvaal, Jagersfontein, Shamah, Birekte, Teria and Jabel El Arab. Richterite is generally associated with kimberlitic rocks or deep-seated ultramafic xenoliths in kimberlites (e.g. Kaapval) (Figure 5.2).

Experimental amphiboles in dacitic, andesitic and basaltic compositions are also dominated by the presence of pargasite. However, hastingsite, sadanagaite, Mg-hornblende and kaersutite have been formed on many occasions. Tremolite is absent in the experimental dacites, andesites and basalts. Finally, glaucophane and barroisite in experimental basalts are only present in sub-solidus experiments (e.g. Forneris & Holloway, 2003).

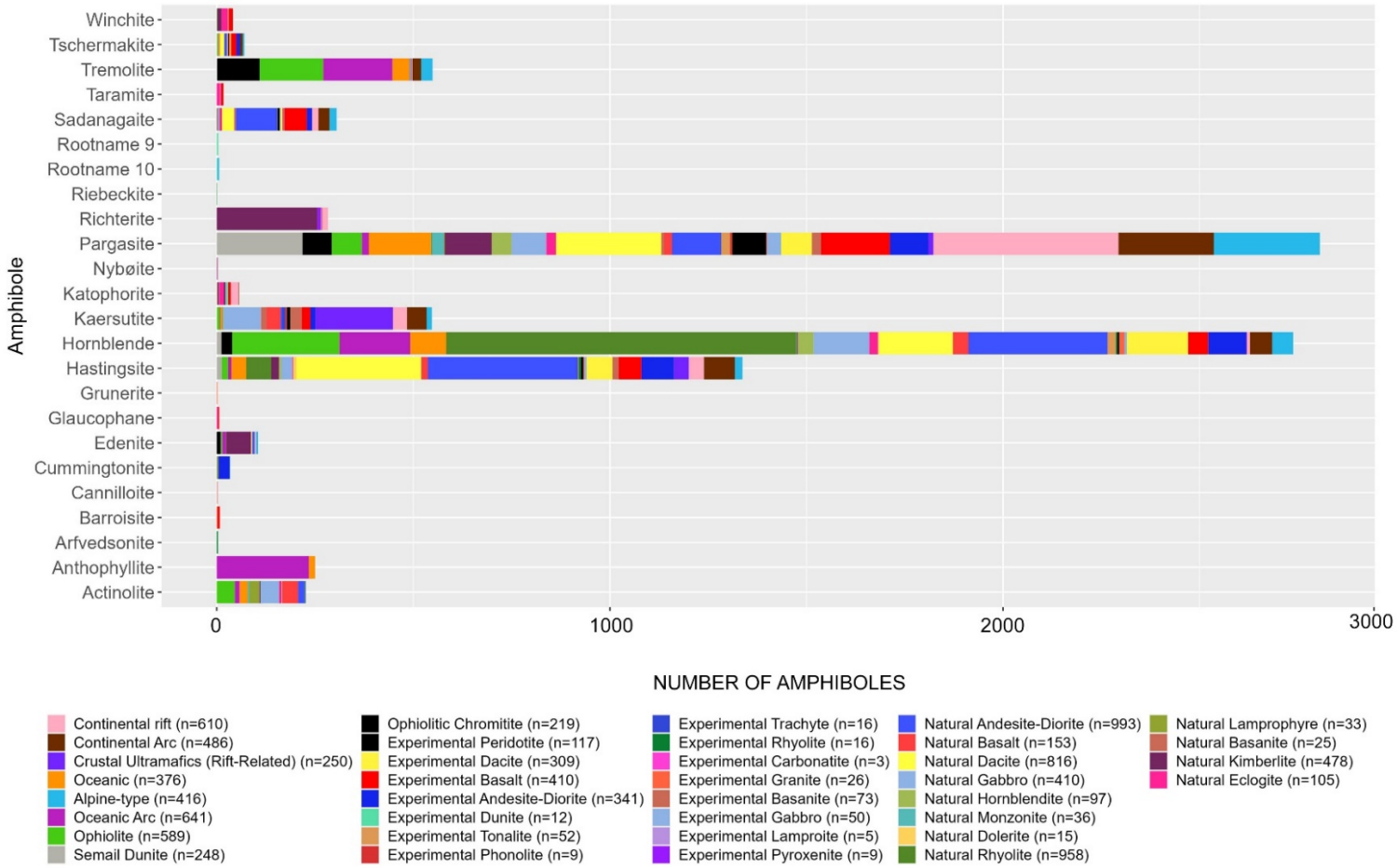

Figure 5.2: Bar plot demonstrating the distribution of each amphibole species between geotectonic settings. Amphibole prefixes have been avoided for simplification reasons.

5.2.2 The $^{C}(Al + Fe^{+3} + 2Ti)$ vs $^{A}(Na + K + 2Ca)$ classification diagrams

The previously discussed amphiboles from the compiled dataset were plotted in the classification diagrams of Hawthorne et al. (2012) (Figure 5.3). These may be useful to detect the chemical differences between amphiboles from each geotectonic setting. For example, Figure 5.3a shows that pargasitic amphiboles from continental rift-related xenoliths are systematically plotted at the top-most part of the pargasite compositional field. This is in great contrast with the amphiboles from Alpine-type peridotites and continental arcs. The vast majority of the latter are plotted at the bottom part of the pargasitic field with a large number of them also falling in the Mg-hornblende field. The exact reason why this difference occurs will be discussed shortly.

In Figure 5.3b, amphiboles from different oceanic settings are compared. Those that originate from oceanic plateaus and core complexes are mostly plotted in the pargasitic field compared to amphiboles from ophiolites and oceanic arcs which are mostly defined by the tremolitic and Mg-hornblenditic fields. Amphiboles from the Semail dunites are systematically plotted at the top part of the pargasitic field showing completely different and unique characteristics compared to the rest of the oceanic amphiboles. Moreover, several trends are observed in amphiboles from oceanic and ophiolitic settings that extend from tremolite to Mg-hornblende.

Three different generations of amphibole exist in ophiolitic chromitites. The first one is concentrated at the bottom left corner of the tremolitic field, almost resembling the end-member composition. Another generation of amphiboles is pargasitic in composition and the third one is located within the edenite compositional field.

Amphiboles in experimental peridotitic compositions are clearly plotted in the middle of the pargasitic field but a few Mg-hornblendes also exist (Figure 5.3c). Although amphiboles in experimental basalts and andesites are predominantly plotted in the pargasite field, they show a general tendency to higher $^{C}(Al + Fe^{+3} + 2Ti)$ values compared to natural amphiboles but also to amphiboles from experimental peridotitic compositions.

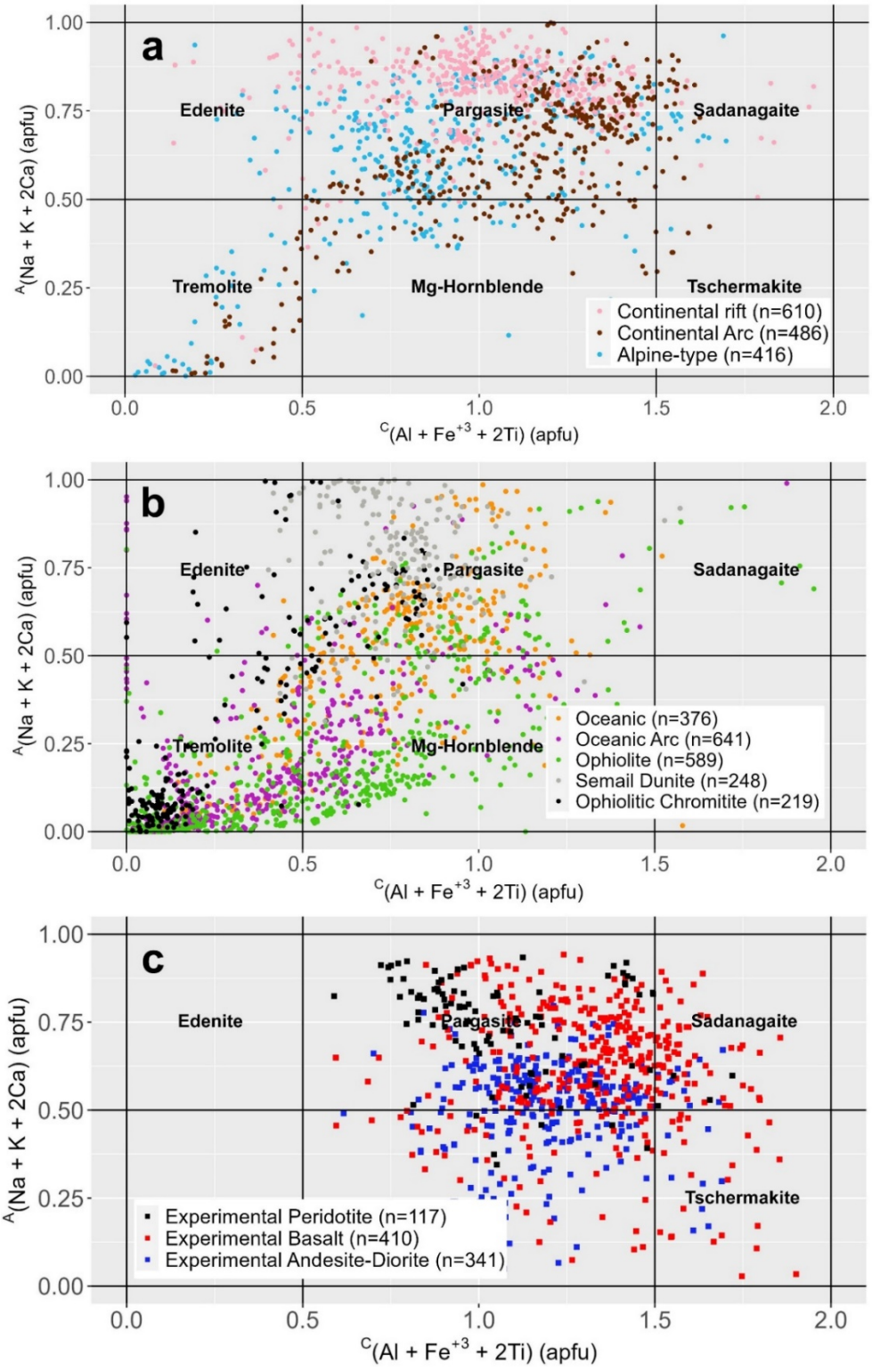

Figure 5.3: The $^{C}(Al + Fe^{+3} + 2Ti)$ vs $^{A}(Na + K + 2Ca)$ classification diagram proposed by Hawthorne et al. (2012) applied to natural and experimental amphiboles from the database. a. Continental Settings b. Oceanic Settings d. Experimentally-produced amphiboles in peridotitic, basaltic and andesitic compositions. The labels of each field are only applicable for the classification of the calcic amphibole group. However, amphiboles from other compositional groups can be plotted in this diagram as well.

5.2.3 Major-element differences

Figure 5.4a shows that the, previously mentioned, difference in composition between amphiboles in continental rifts and other continental settings is the result of increased Na in the crystallographic site A. In Chapter 4, it was shown that Na in amphibole is greatly increasing with increasing pressure. This could possibly indicate that the amphiboles in continental rifts systematically form at greater depths. Increased Na content in site A was also observed for amphiboles in Alpine-type peridotites from North Qaidam (Tibet), Su-Lu (China), Tinaquillo (Venzuela) and the External Ligurides Ophiolite (Italy). In continental arcs, amphiboles with significant amount of Na in site A are found in Nunivak (Alaska), Kakanui (New Zealand) and Dish Hill (U.S.A.). Interestingly, the highest Na in site A is contained in amphiboles from the Semail dunites which are found as inclusions in chromite but based on Rospabé et al. (2020), the pargasitic amphiboles in Semail are clearly of magmatic origin. Figure 5.4a additionally demonstrates that amphiboles from continental settings and oceanic arcs generally show variable amounts of K whereas amphiboles from oceanic plateaus, core complexes and ophiolites (including ophiolitic chromitites and Semail dunites) are almost absent of K.

In terms of total Mg and Fe^{+2} (Figure 5.4b) there is no significant distinction between geotectonic settings. Anthophyllites from Sinai and other oceanic localities stand out because of their high Mg content. To the contrary, a very low Mg content in amphibole (2-3 a.p.f.u.) has been observed in megacrysts collected by King et al. (1999). The megacrysts have been sampled from multiple localities in the American Cordillera (Lunar Crater, Peridot, Soda Springs, Hopi Buttes and Cleator) and are kaersutitic in composition (Ti-rich). This increase of Ti and large decrease in Mg could be associated with mainly two substituions ($^{C}Ti^{+4} + 2^{T}Al \Leftrightarrow {}^{C}Mg + 2^{T}Si$ or $^{C}Ti^{+4} + 2^{W}O^{-2} \Leftrightarrow {}^{C}Mg + 2^{W}OH$) that have previously been discussed by Hawthorne et al. (2012). When amphiboles from all geotectonic settings are considered together, a very profound trend is visible between total Mg and Fe^{+2} in which the increase in Mg, imposes a decrease in Fe^{+2}. This trend is also thought to result from a substitution between Fe^{+2} and Mg. Amphiboles in ophiolitic chromitites are generally showing the highest values of Mg and the lowest values of Fe^{+2}.

Fe^{+3} does not indicate any major dissimilarities in amphiboles between geotectonic settings (Figure 5.4c). It has only been observed that the amphiboles from the Semail dunite are almost devoid of Fe^{+3}. On the other hand, Ti is generally extremely low in amphiboles related to ophiolitic rocks (harzburgites and chromitites) but also in oceanic arcs. Amphiboles from continental settings but also oceanic

plateaus and core complexes show variable amounts of Ti spanning from 0.1 to 0.45 atoms per formula unit. These findings will be discussed thoroughly in the following section.

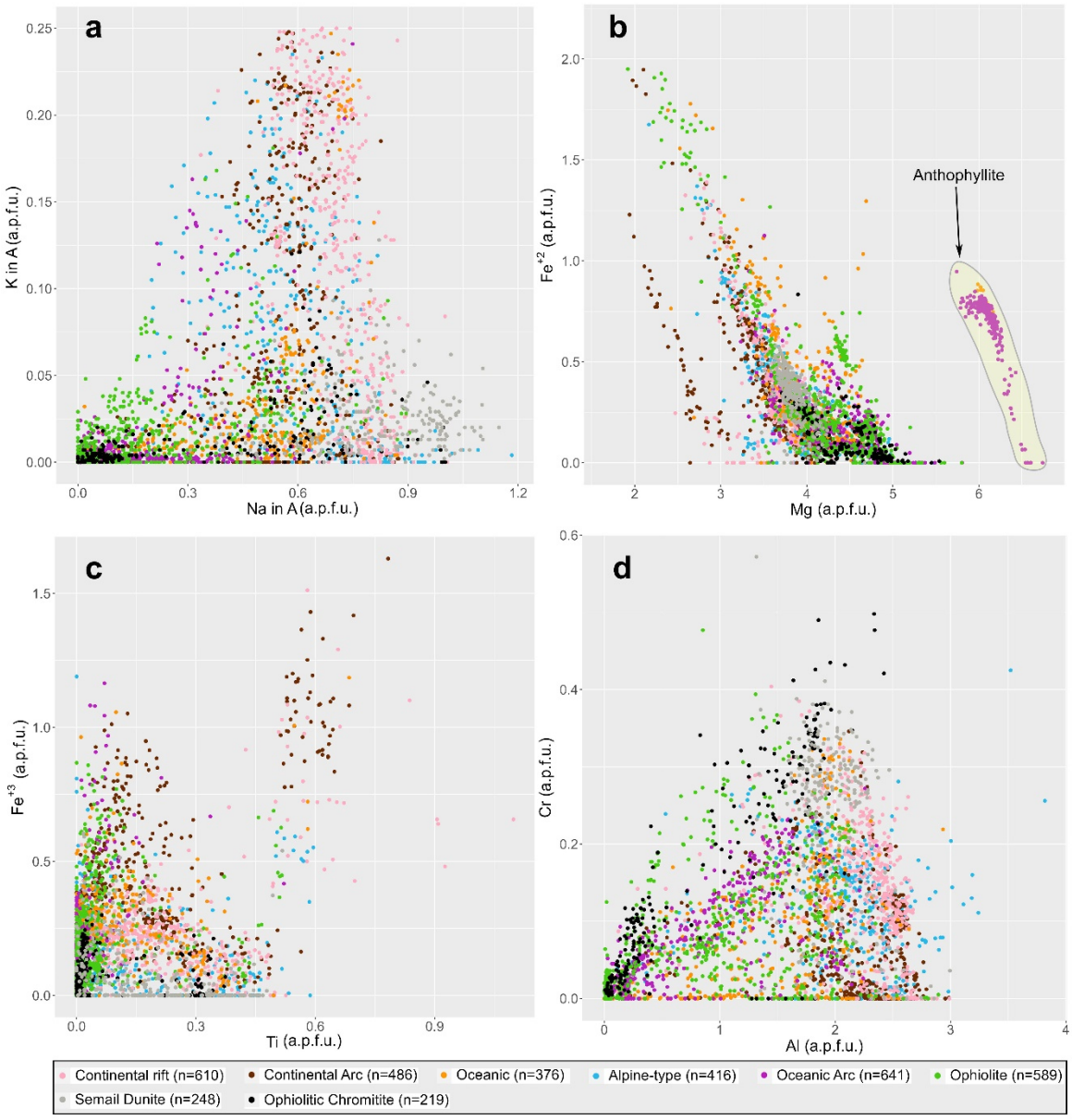

Figure 5.4: Major-element variations in amphiboles from the natural, ultramafic database. The cations are measured as atoms per formula unit. a. Na in A vs K in A b. Total Mg vs Total Fe^{+2} c. Total Ti vs Total Fe^{+3} d. Total Al vs Total Cr.

The total Al vs total Cr diagram displays several important characteristics (Figure 5.4d). Tremolites in ophiolitic chromitites are Cr-poor whereas pargasites in ophiolitic chromitites form some of the most Cr-rich amphiboles among every geotectonic setting (0.3 to 0.5 a.p.f.u.). The implications of these characteristics will

also be discussed shortly. The total amount of Al in amphiboles of continental settings seems to range from 2.1 to 2.6 a.p.f.u. whereas amphiboles from oceanic settings are showing more variable and far lower total Al content, ranging from 0 to 2.1 a.p.f.u.. Several positive trends, between Al and Cr, can also be observed for amphiboles from oceanic arcs and ophiolites.

5.3 Novel 3D geochemical diagrams

5.3.1 The rationale

The texture of amphibole is generally helpful to understand the processes of its formation. For example, amphiboles that are growing at the expense of pyroxenes are indisputable evidence of pyroxene hydration and reaction with a melt or fluid. However, on many occasions textural evidence is not enough on its own. For example, it is difficult to predict how a matrix amphibole, in an ultramafic rock, was initially formed. This is because matrix amphiboles have experienced recrystallization and reequilibration processes and their original signatures have been lost. For this reason, additional techniques have been developed to predict the nature of the metasomatic agent and the process that led to the formation of amphibole. One of the most well-established techniques involves using the trace-element compositions of the constituent minerals. For example, Powell et al. (2004) conclude that amphiboles in Victoria are related to a silicate-rich or a carbonatitic fluid by investigating the REE and HFSE content of amphibole, clinopyroxene and the bulk-rock composition. Similarly, in the Eastern Transylvanian Basin two metasomatic agents have been detected based on the trace-element compositions of xenolithic minerals (Faccini et al., 2020). However, the trace-element data can also be complicated to interpret or hard to acquire.

In this chapter, a series of major-element proxies are proposed aiming at the discrimination between different formation processes and tectonic settings. The first proxy is the Cr content in amphibole, measured in atoms per formula unit, and is aiming to predict the influence of the mantle source. It is generally accepted that the mantle is rich in Cr which is mostly hosted in the primary mantle phases such as spinel and pyroxene. On the other hand melts and fluids are almost entirely depleted in Cr. Based on the work of Kostopoulos (1989), basaltic lavas in oceanic settings could contain 100 ppm of Cr on average. According to Tiepolo et al. (2007) the partitioning coefficient of Cr, between amphibole and a silicate melt ($^{Amph/L}D_{Cr}$), ranges from 3.56 to 53. For the purposes of the present study, an average $^{Amph/L}D_{Cr}$

value of 10 was assumed. Therefore, an amphibole crystallizing from a silicate melt could contain up to 1000 ppm of Cr. This equals to 0.1 wt% of Cr_2O_3, an amount which is hardly even detectable during routine microprobe techniques. This behaviour is also illustrated in Figure 5.5. Notice that amphiboles in rocks of dacitic, andesitic and basaltic composition are almost devoid of Cr in their crystal structure. In fact, the average content of Cr_2O_3 is exactly 0.1 wt% and the median is 0.02 wt% for the amphiboles depicted in Figure 5.5. As a consequence, amphiboles that are found in ultramafic rocks and are Cr-rich are only expected to have acquired their Cr from the primary mantle phases such as mantle spinel, clinopyroxene and orthopyroxene but not from melts. Therefore, Cr can be used as a proxy to detect the interaction of a melt or a fluid with an ultramafic primary phase leading to the formation of amphibole.

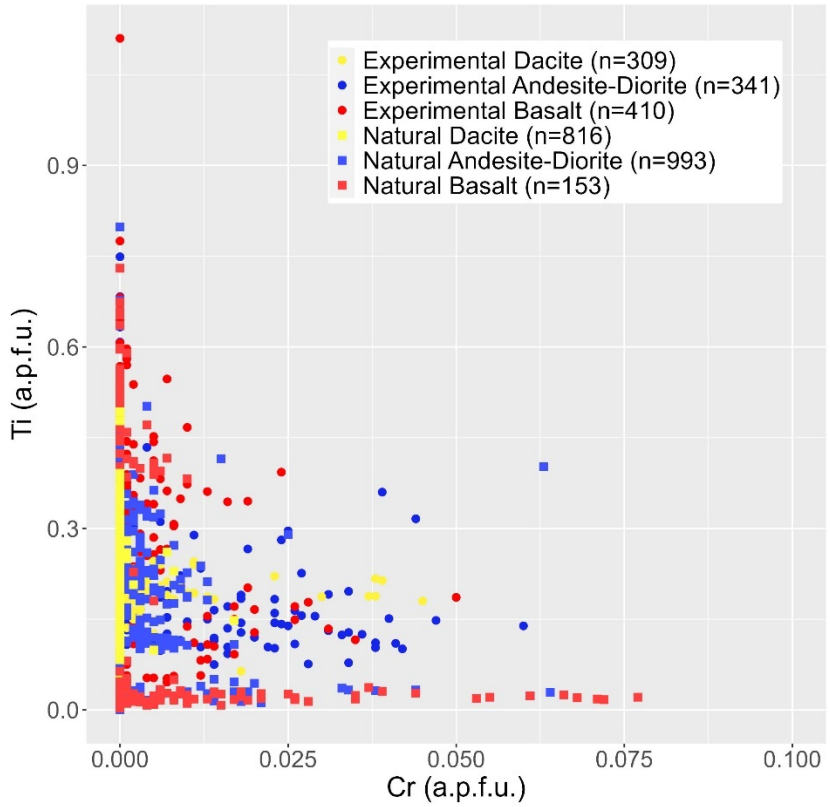

Figure 5.5: Total Cr vs total Ti for amphiboles present in mafic to felsic natural rocks and experimental runs.

The second proxy assumed here is the total Ti content in amphibole. This proxy is going to be used to distinguish a melt from a fluid. According to Audétat & Keppler (2005) and Adam et al. (2014) , at relatively low P-T conditions, aqueous fluids do not have the capacity to transport incompatible elements such as Ti. In contrast, silicate melts show a much more important ability to do so. For example, it was shown that at a temperature of 1050 °C and a pressure of 1.0 GPa, the $^{fluid/melt}D_{Ti}$

value is equal to ~0.05. This means that a silicate melt can carry significant amounts of Ti compared to a H_2O-fluid at these P-T conditions. As temperature and pressure increase, the Ti partition coefficient between a fluid and a melt increases. For instance, At 1200 °C and 2.0 GPa, the partition coefficient has increased to 0.2. However, even at these high P-T conditions, the silicate melt can transport more Ti compared to an H_2O-fluid.

Average TiO_2 contents for andesitic and basaltic melts were calculated using the GEOROC databases (https://georoc.eu/, downloaded on the 1st of November, 2022). An average of 1.95 wt% TiO_2 was measured for natural basaltic melts. This value is in concordance with the work of Gale et al. (2013) who calculated the mean composition of ocean ridge basalts. A value of 0.90 wt% TiO_2 for andesitic melts was also acquired from GEOROC. According to Tiepolo et al. (2007), the average $^{Amph/L}D_{Ti}$ is equal to 3.1. This value is also in agreement with the ones estimated by Pearce & Norry (1979). However, based on the previous works, it must be noted that the Ti partition coefficient can vary a lot depending on the amphibole and melt composition. For simplification reasons, however, the previous value has been chosen. Therefore, amphiboles crystallizing from basaltic melts could contain up to 6 wt% TiO_2 whereas those from andesitic melts could contain up to 2.79 wt% TiO_2. These calculations show that amphiboles related to melts are expected to be Ti-rich. On the other hand peridotitic compositions are extremely depleted in Ti. For example, based on the GEOROC database, the average value of TiO_2 in lherzolites is 0.14 wt%. All of the previously mentioned points lead to the conclusion that Ti can be used as a proxy for silicate melts.

The alkali content in ultramafic rocks, melts and fluids is generally variable and can be affected by multiple natural processes. Adam et al. (2014) showed that, in contrast to Ti, alkalis can easily be transported by H_2O-rich fluids. Their data also agree with findings from earlier works (Pearce & Norry, 1979; Adam et al., 1997; Ayers et al., 1997). Therefore, amphiboles that are Cr-rich and Ti-poor and contain variable amounts of alkalis (Na + K) are expected to have formed from alkali-rich, hydrous fluids.

Based on the aforementioned criteria, several different types of amphiboles can be distinguished: a) Those that are Ti-rich, Cr-poor and contain variable amounts of alkalis have been directly precipitated from melts (*Type-I*) b) Amphiboles that are Ti-rich, Cr-rich and contain variable amounts of alkalis are reactive amphiboles that have resulted from the interaction of melts with primary mantle phases (*Type-II*) c) Ti-poor, Cr-rich and alkali-rich amphiboles have originated from the reaction between a fluid and the primary mantle phases (*Type-III*) d) Amphiboles that contain neither

Ti, Cr nor alkalis have most likely precipitated from shallow hydrothermal fluids (*Type-IV*) (Manning & Frezzotti, 2020).

5.3.2 Ti vs Cr vs (Na + K) three-dimensional diagrams

5.3.2.1 Continental-rift related settings

The previously described proxies were used as the key parameters of three-dimensional Ti vs Cr vs (Na + K) diagrams. The diagrams may be used to infer the processes of amphibole formation and also the nature and the composition of the metasomatic agent that was involved. For these diagrams, any amphiboles from ultramafic rocks in which Cr was not initially analyzed, were excluded. On the other hand, amphiboles in which the Cr content was not detectable from routine microprobe techniques were set to contain no Cr.

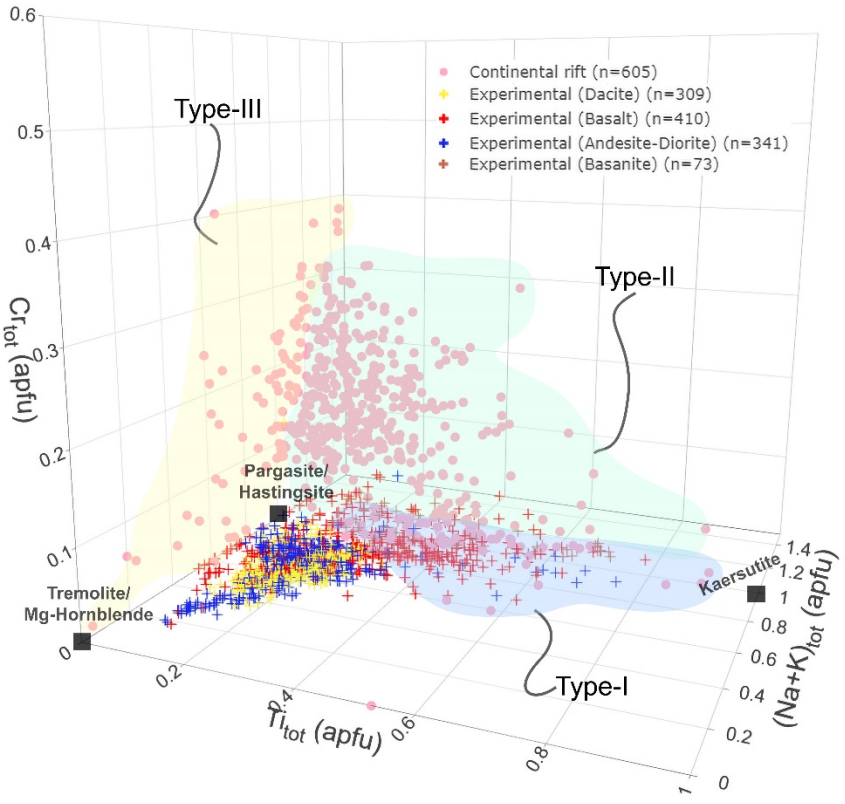

Figure 5.6: Ti vs Cr vs (Na + K) diagram demonstrating the different origins of amphibole in continental rift-related settings. Type-I amphiboles have been directly precipitated from silicate-melts. Type-II amphiboles are the result of interaction between a silicate melt and primary mantle phases (e.g. clinopyroxene and spinel). Type-III amphiboles have formed by the reaction of fluids with the primary mantle phases. See main text for more details.

Experimental amphiboles from the database are Cr-poor and contain variable amounts of Ti and alkalis (Figure 5.6). Therefore, they are plotted at the bottom of the three-dimensional diagram. A large number of amphiboles in ultramafic xenoliths from continental rifts are also devoid of Cr but contain reasonable amounts of Ti and alkalis (Figure 5.6). These amphiboles are mainly matrix pargasites and according to the rationale presented earlier, they seem to have directly precipitated from silicate-melts (Type-I). Notice that they are compositionally very similar to experimental amphiboles from basalts and basanites and not dacites or andesites. This is a strong indication that they have directly crystallized from intra-plate melts of basaltic composition. In fact, according to Figure 5.7, the most possible melt composition is alkali-basaltic and basanitic. It was additionally noted that the majority of kaersutitic amphiboles are generally formed due to direct crystallization from alkali-basaltic melts (Type-I). This behavior has been previously observed in the literature. For example, Tatsumoto et al. (1992) supported the close relation of alkali-basalts and kaersutites from multiple localities in China.

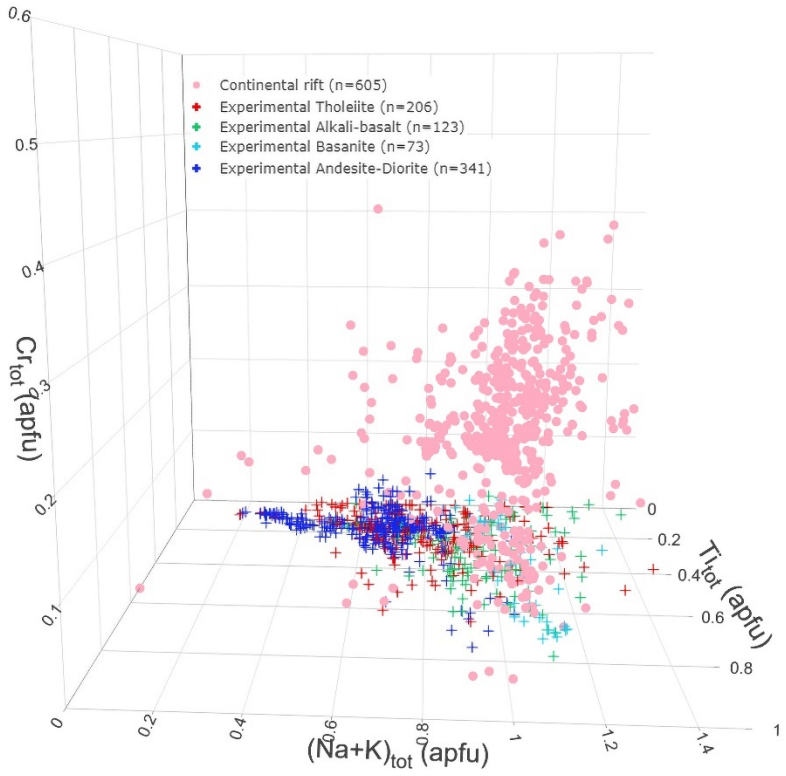

Figure 5.7: In this diagram experimental amphiboles from basalts of different alkalinity have been plotted along with amphiboles from continental rifts and experimental andesites.

Type-II amphiboles are plotted directly "above" Type-I, in the three-dimensional space, because of their higher Cr content (Figure 5.6). These amphiboles are thought to be the result of interaction between alkali-basaltic or basanitic melts

and primary mantle phases such as clinopyroxene, orthopyroxene and spinel. Matrix, interstitial or replacive textures are the most common in this group. Type-III amphiboles in continental rift-related settings comprise a smaller group and they are expected to have formed from fluids reacting with primary mantle phases.

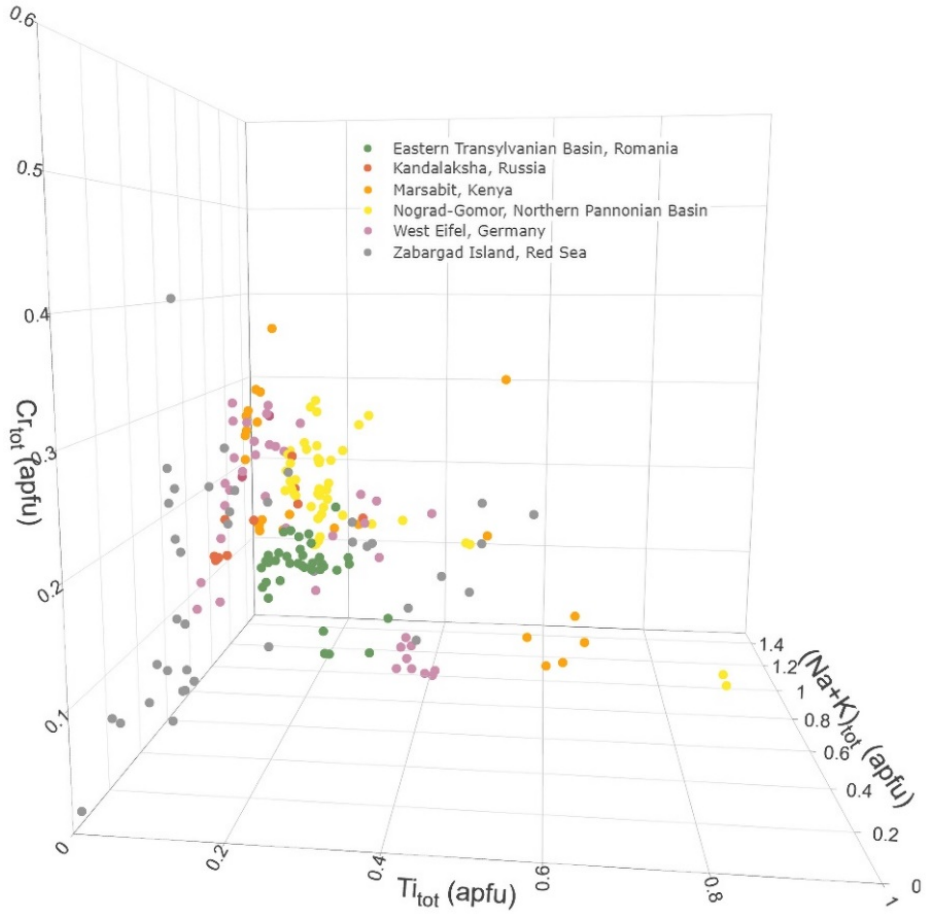

Figure 5.8: The discrimination of amphiboles in a few selected localities from rift-related settings (see text for more details).

The results from the new three-dimensional diagrams largely agree with previous studies. A few demonstrative examples from important localities are presented here. According to Figure 5.8, amphiboles from the Eastern Transylvanian Basin have formed from basaltic melts reacting with clinopyroxene (Type-II). This is in great agreement with the findings of Faccini et al. (2020). Similarly, Liptai et al. (2017) attributed the formation of amphibole from Nógrád Gömör to basaltic melts related to decompressional melting. The rationale presented here, confirms this hypothesis but it additionally shows that the amphiboles are the result of basalt interaction with primary mantle phases. Two generations of amphibole have been identified in Kandalaksha (Russia). The first generation is Ti-poor and belongs to Type-III and the second one is Ti-rich and belongs to Type-II. These findings agree

with Beard et al. (2007) who also anticipated the effect of two metasomatic events. A large number of amphiboles from Zabargad belong to the Type-III group, having been formed from a fluid reacting with peridotites. These results are in total concordance with Piccardo et al. (1988) and Agrinier et al. (1993) who supported that pargasite in Zabargad has formed from H_2O-rich fluids. However, Type-II amphiboles also exist in Zabargad. Amphiboles from Marsabit were thought to have originated from the replacement of clinopyroxene (Kaeser et al. 2007). Marsabit amphiboles belong to Type-II and Type-III. It is therefore expected that two different metasomatic agents (a basaltic melt and a hydrous fluid) have reacted with clinopyroxenes during different metasomatic events. In West Eifel amphiboles are mostly defined as Type-II and Type-III and are related to basaltic melts. However, five pargasitic grains seem to belong to Type-I. These results agree with the work of Shaw et al. (2005) and that of Witt-Eickschen & Hart (1994).

5.3.2.2 Continental arcs

Amphiboles from continental arcs indicate the influence of more differentiated melts. This is evident from Figure 5.9 as the majority of amphiboles are similar, in terms of Ti and alkalis, to amphiboles from dacites and andesites. This is especially true for amphiboles that originate from localities in Kamchatka. On the other hand, amphiboles from the American Cordillera contain higher amounts of alkalis, making them similar to those from basaltic compositions. This geotectonic setting is also defined by Type-I,-II and -III amphiboles similarly to continental rifts.

Amphiboles from Avacha (Kamchatka) are exclusively Type-III interstitial Mg-hornblendes and pargasites, that according to Figure 5.9, have formed when hydrous fluids reacted with primary mantle phases. Ionov (2010) showed that tectonic activity shortly before the transport of the Avacha xenoliths to the surface induced fracturing and recrystallization. This tectonic activity enabled the infiltration of hydrous fluids and the precipitation of amphibole. Therefore, the results of Ionov (2010) closely resemble those of the present study. The fluids in Avacha are expected to own a subduction-zone origin and be silicate- and alkali-rich (Manning & Frezzotti, 2020). According to Shu et al. (2022) they are most likely deriving from the progressive dehydration of serpentine, lawsonite and phengite.

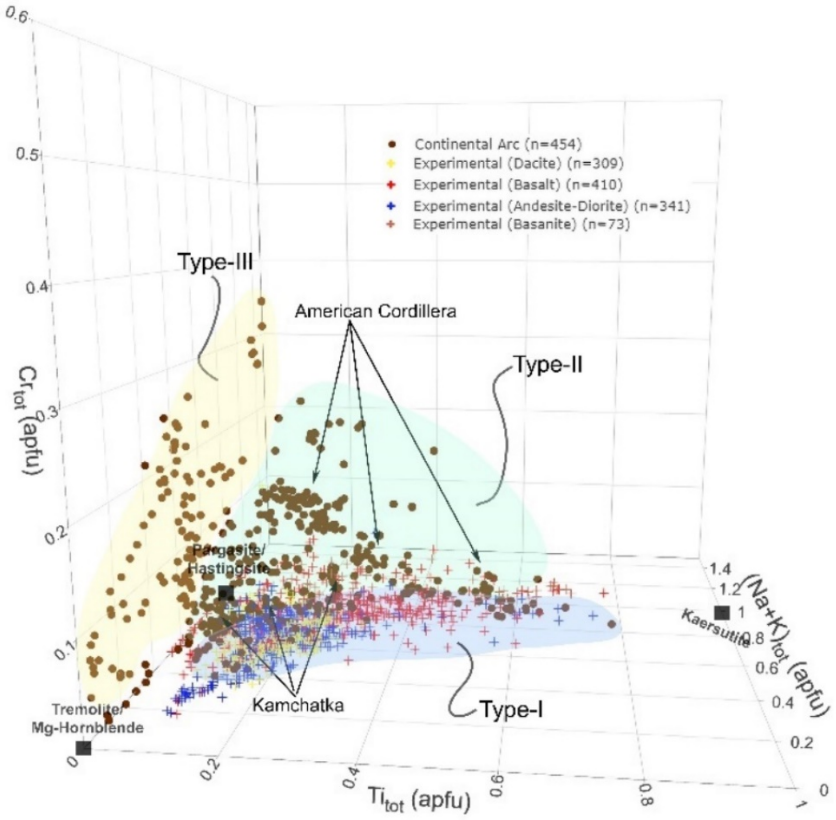

Figure 5.9: Ti vs Cr vs (Na + K) diagram demonstrating the different origins of amphibole in ultramafic rocks from continental arcs.

Amphiboles from the American Cordillera are found in mantle xenoliths that have been divided into the Al-augite group and the Cr-diopside group (Wilshire & Shervais, 1975). Matrix and replacive pargasites from Dish Hill (U.S.A.) belong to Type-II and are clearly magmatic in origin. Type-I amphiboles in Dish Hill are solely kaersutites (more than 0.5 Ti atoms per formula unit). Based on their alkalinity, both Type-I and Type-II amphiboles from Dish Hill are probably related to basalts. Our results agree with McGuire et al. (1991) and Wilshire et al. (1988). Amphiboles from Deadman Lake are identical to those from Dish Hill. Pargasites have formed from the interaction of basaltic melts with pyroxenes whereas kaersutites are direct precipitates from basalts.

The majority of localities in continental arcs around the globe seem to be related with calc-alkaline activity and more precisely with andesitic or dacitic magmatic activity. However, this is not true for amphiboles in localities from the American Cordillera (e.g. the previously mentioned Dish Hill and Deadman Lake) which they seem be affected by basaltic melts of medium to high-alkalinity. These results are confirmed by the work of Ben Othman et al. (1990) who showed that

amphiboles from the Western United States have been predominantly derived from basaltic melts of MORB or Oceanic Island Basalt affinity.

Amphiboles from Kakanui (New Zealand) are also Type-I kaersutites and Ti-rich pargasites. According to Siegrist et al. (2019), interstitial pargasites in ultramafic xenoliths from the Kharchinsky volcano were crystallized from melts and fluids or by fluid-rock interactions. This is also confirmed by the present study. More specifically, almost half of the amphiboles from the Kharchinsky volcano belong to Type-I and the other half to Type-II. It is expected late-stage pargasites in Kharchinsky have been formed by andesitic melts.

5.3.2.3 Alpine-type peridotites

The majority of amphiboles in Alpine-type peridotites are related to hydrous fluids reacting with primary mantle phases (Type-III) (Figure 5.10). It is generally considered that Alpine-type peridotites are involved in subduction zones, although their exact geological evolution is still not well constrained. Therefore, the amphibole-forming fluids could be dehydration products of subducted lithosphere which, subsequently, hydrate the mantle wedge. These subduction-related fluids are expected to be rich in alkalis (e.g. Keppler, 1996; Adam et al., 2014; Manning & Frezzotti, 2020) and form amphiboles which also contain variable amounts of Na and K. Type-IV amphiboles related to late-stage hydrothermal fluid activity are also observed. They are tremolitic in composition and their lack of alkalis and Ti positions their generation at shallower depths during exhumation and retrogression/hydrothermal alteration. Finally, Type-II, reactive amphiboles from percolating hydrous melts and Type-I precipitative magmatic amphiboles do also form on many occasions.

Type-III amphiboles in Alpine-type localities are matrix, interstitial or replacive in texture and are mainly observed in Alpe Arami, Cima di Gagnone, Finero, Monte Duria, Mount Albert, Nonsberg, Pohorje, Portet d'Aspet, Su-Lu and Ulten (see Figure 5.1 for the exact locations). In many of these occasions, amphibole is considered a prograde, primary phase and the metasomatic agent which initially formed it is unknown as for example in Alpe Arami (Nimis & Trommsdorff, 2001). Amphiboles in Cima di Gagnone and Monte Duria have resulted from the interaction between fluids and the primary mantle phases. This is accordance with the works of Scambelluri et al. (2014) and Pellegrino et al. (2020), respectively, who predicted the infiltration of an alkali-rich fluid of crustal origin. A similar origin is also expected for the Pohorje peridotitic body in Slovenia (Janàk et al., 2006; Vrabec, 2010). Type-IV

amphiboles are also present in Pohorje but also in Cima di Gagnone. It is expected that a late-stage hydrous fluid penetrated the ultramafic bodies and crystallized tremolite. Amphiboles from the Anita peridotite are mainly Type-III. These amphiboles, however, contain minimum amounts of Ti from 0.03 to 0.06 atoms per formula unit. These values are not entirely indicative of a melt. The present results, however, partly disagree with the trace-element work of Czertowicz et al. (2016). These authors showed that although amphibole grew at the expense of clinopyroxene and plagioclase through the interaction with a basalt. Therefore, it is expected that a fluid/melt mixture might have existed during their crystallization.

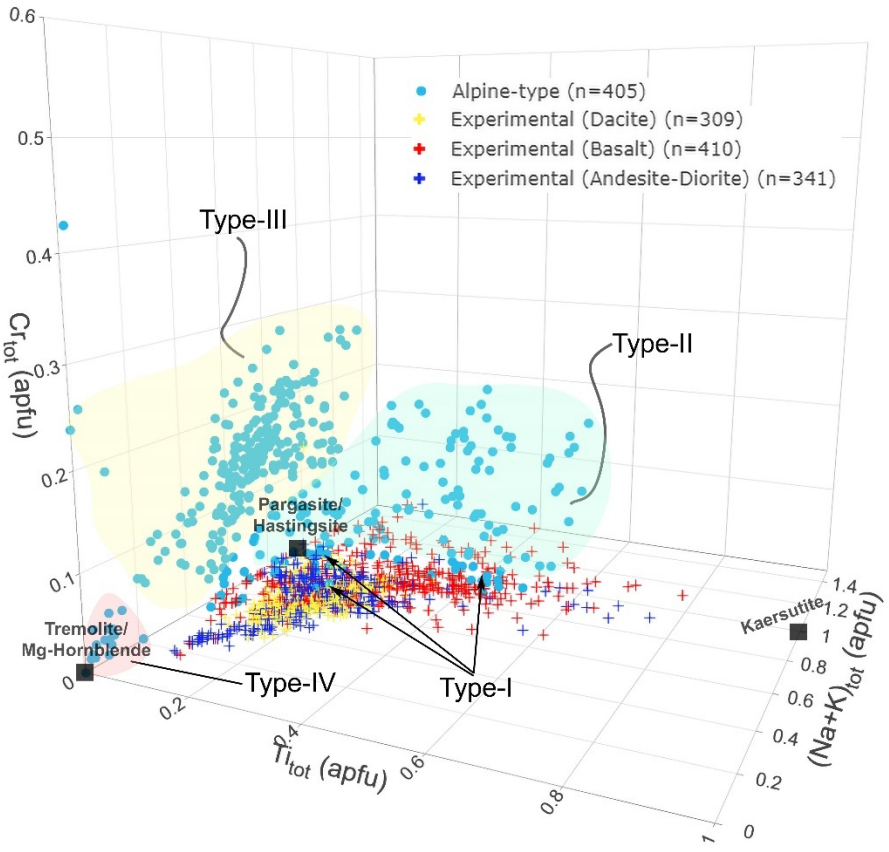

Figure 5.10: Ti vs Cr vs (Na + K) diagram demonstrating the different origins of amphibole in ultramafic rocks from Alpine-type peridotites.

Type-I precipitative amphiboles from a silicate melt have only been located in Beni Bousera, Fen, Lherz, Nové Dvory and Raobazhai. Melts of basaltic composition directly precipitated amphiboles in Beni Bousera. These results are in perfect agreement with the work of Et Atrassi et al. (2014). No information, from the literature, for the formation of Type-I amphiboles in the remaining localities is available.

Type-II, reactive amphiboles from a silicate-melt are present in Baldissero, Balmuccia, Caussou, the External Liguride Ophiolite and Tinaquillo. Fabriès et al. (1989) proposed that under upper lithospheric mantle conditions, a basaltic melt infiltrated the Caussou peridotitic rocks and percolated through a grain-boundary process reacting with the original, primary mantle minerals and forming Ti-rich pargasite. This is in accordance with the present study. Similarly, Seyler & Mattson (1989) attributed the formation of amphibole to mafic melts infiltrating the Tinaquillo peridotites. Melt infiltration has also been expected for the External Liguride Ophiolite according to Hidas et al. (2021).

5.3.2.4 Oceanic plateaus and core complexes

Figure 5.11 shows that amphiboles in ultramafic rocks from oceanic plateaus and core complexes are usually related to aqueous fluids (Type-III and -IV) and less frequently to melts reacting with primary mantle phases (Type-II). Magmatic precipitative amphiboles (Type-I) can also be present on several occasions. The 15°20'N Fracture Zone area in the Mid-Atlantic Ridge is defined by Type-I, -III and -IV amphiboles forming almost a trend from tremolitic/actinolitic to Mg-hornblenditic and pargasitic compositions (Figure 5.12). The type-I amphiboles are similar to amphiboles from tholeiitic basalts. It is therefore proposed that the rocks have experienced complex metasomatic processes from basaltic melts directly precipitating Mg-hornblendes to aqueous fluids reacting with the host peridotites along the walls of the detachment fault. Strikingly, Albers et al. (2019) proposed the interaction of magmatic activity and hydrothermal alteration at the detachment fault of this area. Mado Megamullion (back-arc oceanic core complex) is very similar to the 15°20'N Fracture Zone as amphiboles of multiple types coexist (Figure 5.12). However, this time, Type-I tremolites are very scarce and Type-II amphiboles are also present. Sen et al. (2022) assumed that pargasitic amphiboles in veins and as replacement of a clinopyroxene have crystallized from a hydrous melt. This study confirms this hypothesis but also shows that many other generations of amphiboles that are either related to fluids of melts coexist with the precipitative ones. Replace amphiboles after clinopyroxene in serpentinites from the Newfoundland passive margin (Canada) are entirely of Type-IV, meaning that they have formed from aqueous, hydrothermal fluids, completely lacking alkalis (Figure 5.12). The present results are in accordance with Kodolányi et al. (2012) who also attributed the formation of amphiboles to hydrothermal fluids.

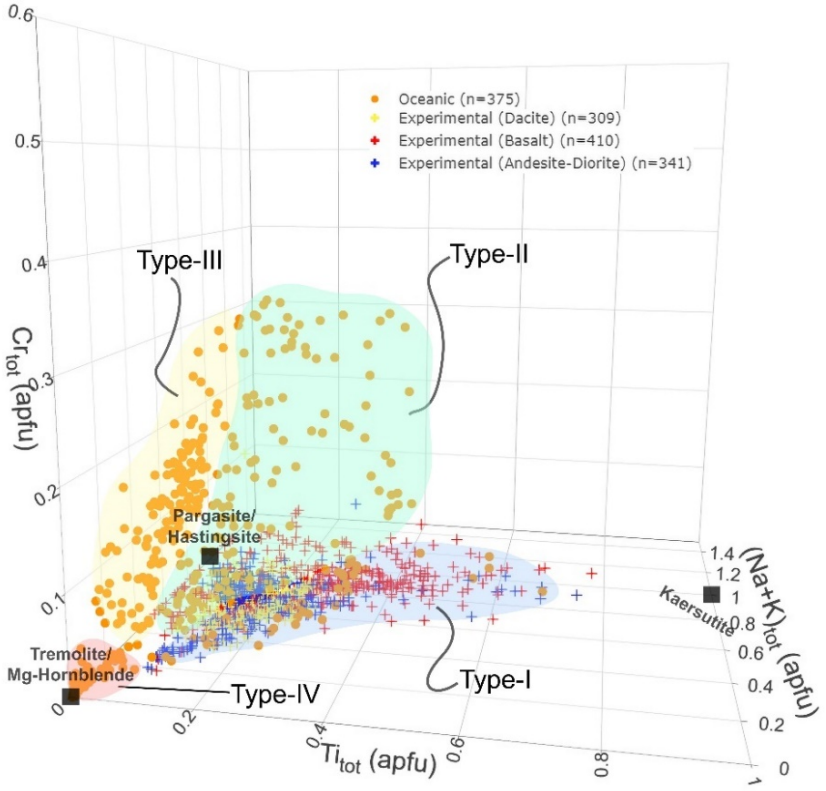

Figure 5.11: Ti vs Cr vs (Na + K) diagram demonstrating the different origins of amphibole in ultramafic rocks from oceanic plateaus and core complexes.

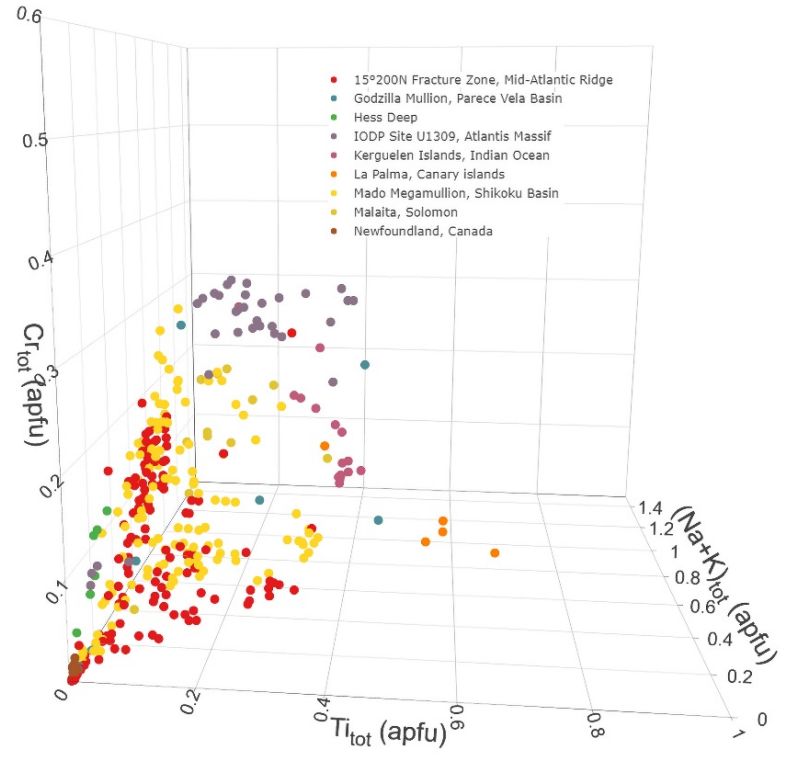

Figure 5.12: Amphiboles from a few representative localities in oceanic settings. See text for full description.

It was previously discussed that amphibole inclusions in spinels from the IODP Site in the Atlantis massif represent trapped melts (Tamura et al., 2008; Tamura et al., 2014). This hypothesis is now confirmed as the amphiboles are Ti-rich, indicating the existence of a basaltic melt but also Cr-rich showing the interaction with a primary phase (spinel) (Figure 5.12). Neal (1988) supported the reaction of a fluid with primary mantle phases for Malaitan xenoliths. The present study supports that the Malaitan amphiboles have indeed formed from a reaction process but with a melt of basaltic composition.

5.3.2.5 Oceanic arcs

Amphiboles in ultramafic xenoliths from oceanic arcs are mostly reactive in origin and related to subduction-zone or late-stage hydrothermal fluids (Type-III and Type-IV). Mt. Pinatubo contains mostly Type-III amphiboles related to alkali-rich, subduction zone fluids but a few Type-I amphiboles have also been observed (Yoshikawa et al., 2016; Payot et al., 2018). However, their low Ti content from 0.05 to 0.1 a.p.f.u. could be indicative of a melt/fluid mixture. Contrastingly, one hastingsite from Batan is clearly Type-I. Type-III amphiboles have been identified in Bismarck, the Hahajima seamount, the Mariana Trench and the TUBAF in New Ireland. The findings here are congruent with the results of the relevant studies for each locality respectively (Franz et al., 2002; Okamura et al., 2006; Ohara & Ishii, 1998; Bénard et al., 2021). However, Bismarck does also contain Type-II amphiboles. Type-II also is observed in Sinai and Lihir. Finally, anthophyllites and tremolites from Sinai have been crystallized from alkali-depleted hydrous melts at low temperatures (Type-IV). This has probably occurred at a subduction-zone environment as also proposed by Maurice et al. (2021).

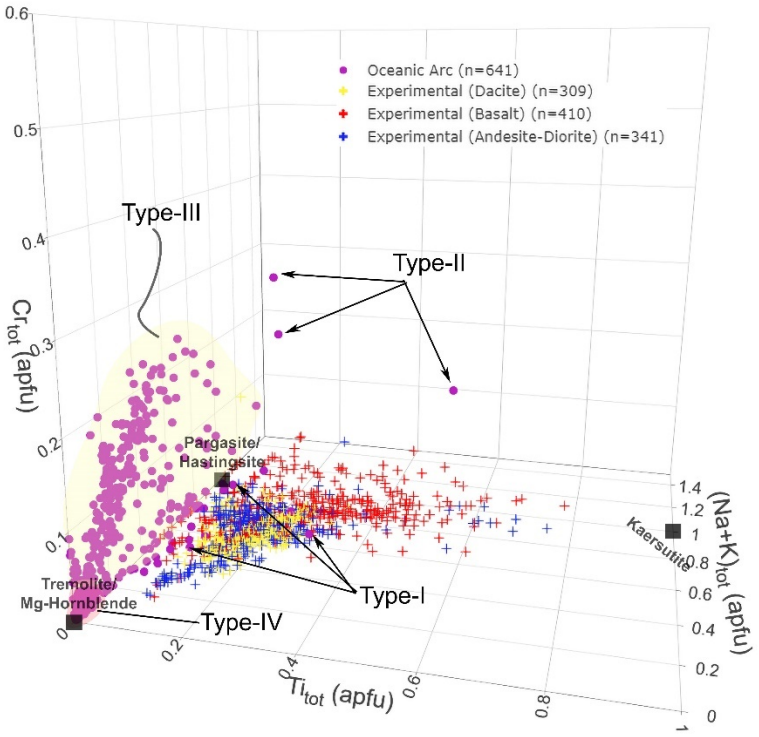

Figure 5.13: Ti vs Cr vs (Na + K) diagram demonstrating the different origins of amphibole in ultramafic xenolithic rocks from oceanic arcs.

5.3.2.6 Ophiolites

Tremolites, actinolites and Mg-hornblendes in ophiolitic harzburgites and dunites are mostly Type-III and Type-IV and have formed from the interaction of fluids with clinopyroxene and spinel. Subduction-zone, alkali-rich fluids are the most possible metasomatic agents that have affected the rocks. The Purang, Yungbwa, Lycian, Ochi, Hagar Dungash, Mirdita, New Caledonian, Oeyama, Ohsa-yama and Xigaze ophiolites are all defined by the two aforementioned categories of amphibole. Kaersutites from Ochi as well as pargasites and Mg-hornblendes from the Küre, Mt. Kalnik, Lizard, Dinapigui and Gerf ophiolites are either Type-I or Type-II.

Amphiboles in ophiolitic mantle peridotites show variable contents of alkalis which are portrayed by trends visible in the Ti vs Cr vs (Na + K) space (Figure 5.14). It is, therefore, expected that the nature (alkalinity) of aqueous fluids released by dehydrating lithologies in subduction zones can affect the composition of amphiboles found in ophiolitic harzburgites, lherzolites and dunites. However, Figure 5.14 shows that the extent of depletion, reflected in the spinel Cr#, can also affect the composition of amphiboles dramatically. For example, tremolitic to Mg-hornblenditic amphiboles in harzburgites and dunites from the Lycian Ophiolite (Turkey) clearly display the interaction between a moderately depleted mantle and water-rich alkaline fluids.

Amphiboles in harzburgites from the Yungbwa Ophiolite (Tibet) require interaction between less depleted mantle compositions and a hydrous Ti-bearing fluid/melt. This is because spinels in the Lycian Ophiolite contain much more Cr compared to Yungbwa. Therefore, the amphiboles crystallized after more Cr-rich spinels will also be more enriched in Cr (Figure 5.14).

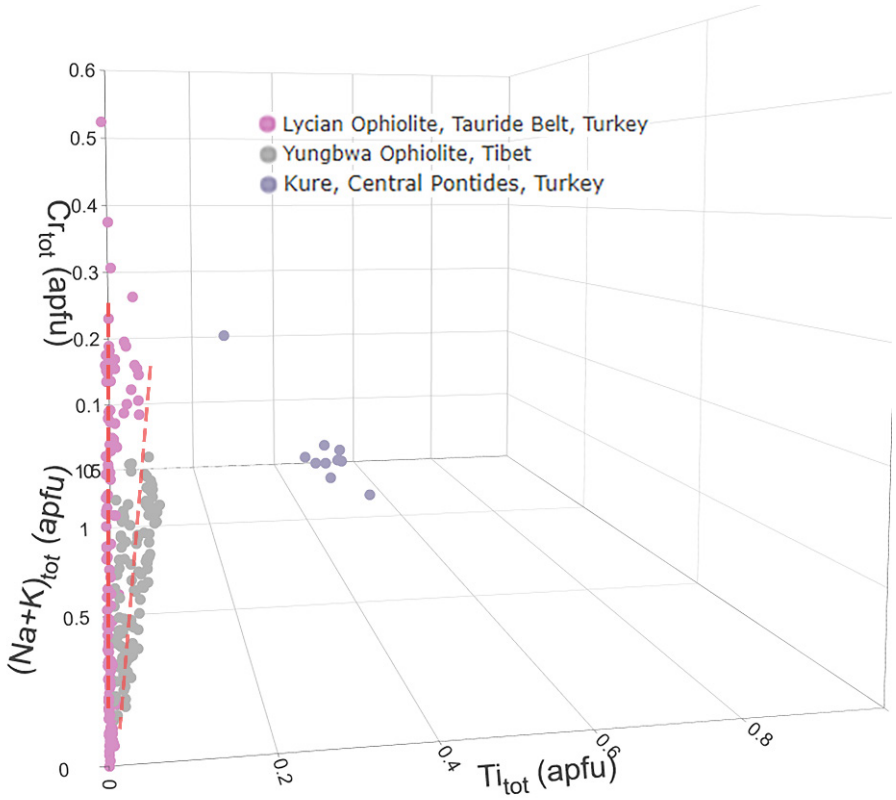

Figure 5.14: Amphiboles from the Lycian and the Yungbwa ophiolites form two distinct trends. These trends are thought to be the result of the alkalinity of the metasomatic fluid but also the degree of depletion of the mantle harzburgites or dunites.

Amphibole is often found in ophiolitic chromitites as inclusions in chromitites. Interstitial amphibole grains have rarely been reported in ophiolitic chromitites (Melcher et al., 1997; Rollinson, 2008). A new suite of amphiboles forming inclusions in chromite but also interstitial grains in chromitites has been discovered in the Lycian Ophiolite. According to Pan et al. (2022), the amphibole inclusions in chromites from the Lycian chromitites coexist with other silicate mineral inclusions (pyroxene) and represent trapped melts that reacted with fluids along the surfaces of chromite. These fluids were subsequently released into the surround lithologies forming interstitial amphibole grains. However, based on Figure 5.15, the tremolites and pargasites in the Lycian chromitites seem to be unaffected by melts as they contain no Ti at all. Based

on the newly proposed rationale, they belong to Type-III and Type-IV, being mostly related to aqueous fluids reacting with chromite. Therefore, it is proposed that amphibole inclusions in Lycian chromite have crystallized from residual silica-rich fluids that were separated from the melt which crystallized chromite. The lack of a Ti imprint indicates that the fluid/melt ratio was very high during the crystallization of amphibole. The fluids were subsequently gathered on chromite surfaces (Matveev & Ballhaus, 2002) and were released to the surrounding lithologies forming interstitial Ti-poor amphiboles.

Similarly to the Lycian ophiolite, amphibole inclusions in ophiolitic chromitites from multiple localities around the globe (Figure 5.15) are only related to fluids. Usually in the literature, amphibole inclusions in chromites are mostly interpreted as trapped melts during the crystallization of the chromites. The absence of Ti, however, is a strong indicator of a fluid phase. Arai & Miura (2016) supported that a combination of magmatic and hydrothermal processes can lead to the formation of chromitites. In fact, they proved that hydrothermal fluids could dissolve and precipitate chromite at high temperatures. Recently, this hypothesis has been confirmed by Johan et al. (2017) who showed that chromite may precipitate from a reducing fluid phase at a temperature less than 1050 °C. In their proposed theory, a large volume of harzburgites is hydrothermally altered by a large amount of fluids which they become enriched in Cr. These fluids can then reprecipitate chromite under reducing conditions. Therefore, in such a fluid-dominant environment, Cr-rich, Ti-poor amphiboles are also expected to crystallize. This hypothesis seems to hold true for the fluid-related amphiboles depicted in Figure 5.15. However, chromitites from the literature have usually been associated with magmatic processes. A magmatic origin is expected for pargasitic amphibole inclusions in chromitites from the Semail ophiolite which have been crystallized by trapped basaltic melts reacting with the primary chromites (Type-II) (Figure 5.15). This is in accordance with the works of Borisova et al. (2012) and Rospabé et al. (2020).

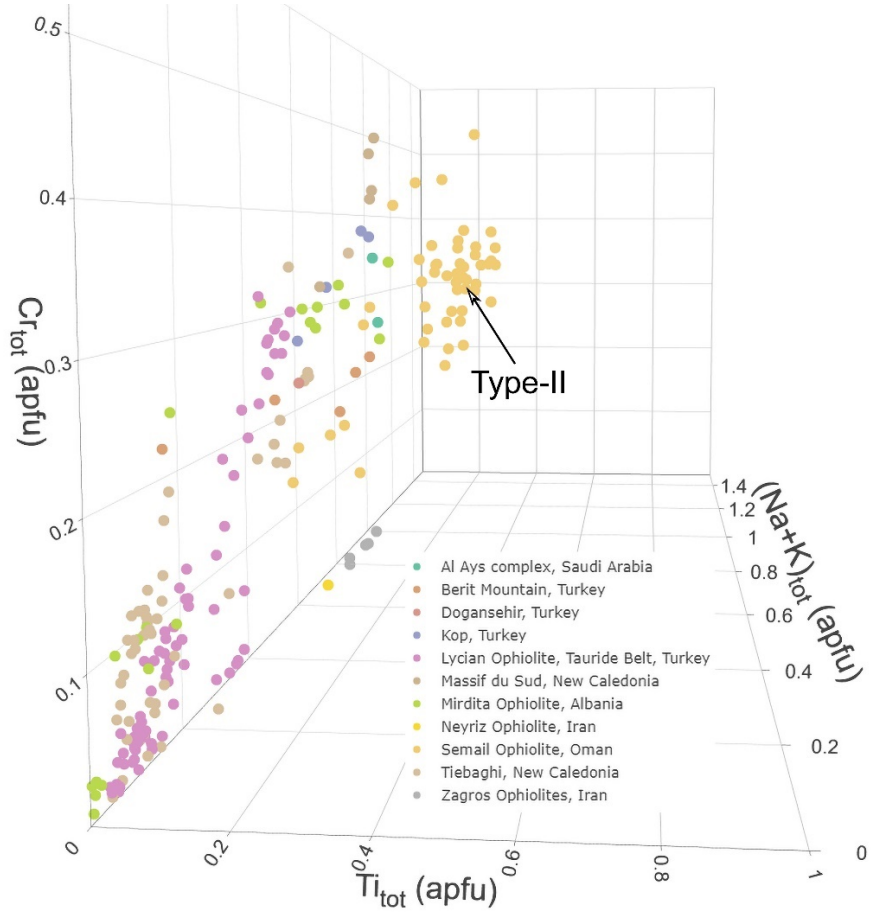

Figure 5.15: Ti vs Cr vs (Na + K) diagram demonstrating the origin of amphibole in ophiolitic chromitite. Fluids seem to have an important role on the genesis of such amphiboles (see text for more details).

5.3.3 Mg# vs Si vs Ti three-dimensional diagrams

In Chapter 4, a new method to decide whether an amphibole is in equilibrium with the primary mantle phases was developed. Here, a simple Mg# vs Si vs Ti three-dimensional diagram is proposed to confirm the results from Chapter 4. The amphibole Mg# $\left(\frac{Mg}{Mg+Fe_{tot}}\right)$ is used to empirically derive how equilibrated an amphibole in the mantle. Results are shown in Figure 5.16. Magmatic amphiboles in equilibrium with basaltic and andesitic melts are generally characterized by Mg# values in the range 0.40-0.85 whereas amphiboles in equilibrium with natural ultramafic compositions are characterized by Mg# in the range 0.62 to 0.98. Experimental amphiboles formed in equilibrium with mantle peridotite display Mg# values in the range 0.90-0.98. It is, therefore, proposed that amphiboles in ultramafic

rocks with Mg# values smaller than about 0.90-0.85, have not reached chemical equilibrium, in terms of Mg and Fe, with their surrounding mantle phases. Natural amphiboles with Mg# ranging from 0.85 to 0.98 are expected to be in chemical equilibrium with the primary mantle phases. Note that the amphiboles under investigation must also contain Si in the range from 5.5 to 7 a.p.f.u. so that they are similar to the pargasites from the ultramafic experiments. Figure 5.16 shows that the majority of amphiboles from continental rifts are in equilibrium with the mantle rocks in which they were formed. On the other hand, amphiboles from oceanic arcs are generally in disequilibrium with the mantle rocks except from a few localities. The results here, are perfectly concordant with those from Chapter 4.

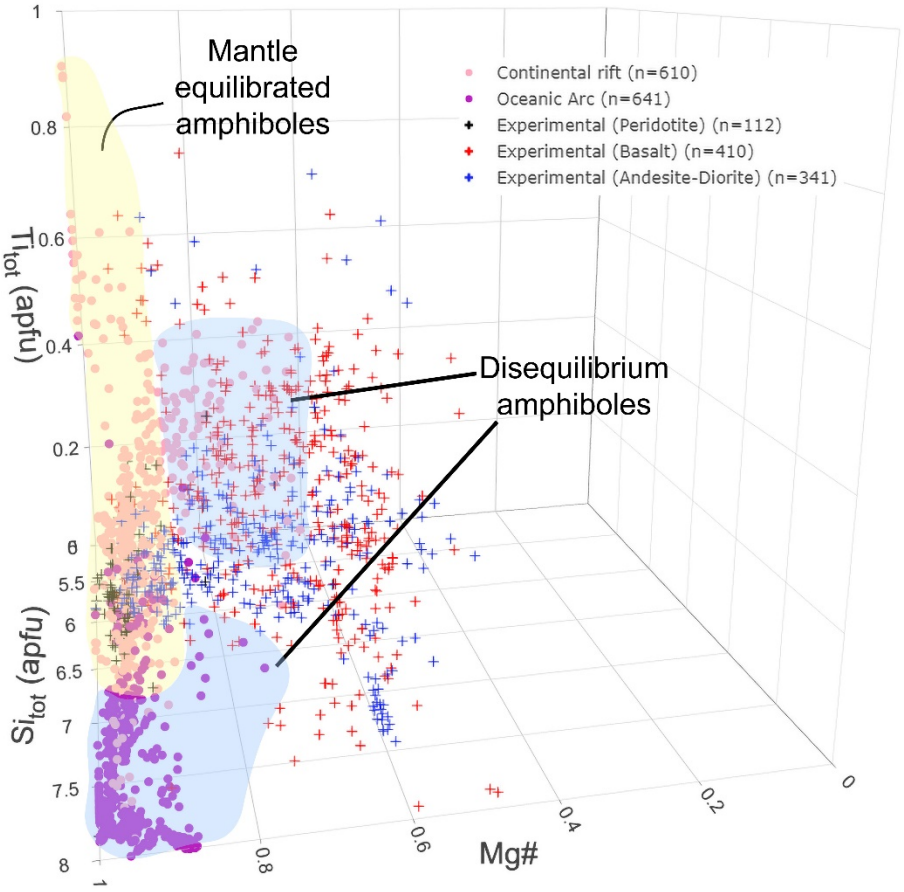

Figure 5.16: Mg# vs Si vs Ti diagram used to empirically predict if amphibole has equilibrated in mantle rocks. Amphiboles from continental rifts and oceanic arcs are shown as examples.

Conclusions

In Chapters 4 and 5 of the present study it was shown that, by using several simple methods, the exact processes which contributed to the formation of amphibole in ultramafic rocks can be derived. More specifically, after the obtainment of a

microprobe major-element analysis, the chemical composition of amphibole can be plotted in a simple Ti vs Cr vs (Na + K) three-dimensional diagram. This diagram will enable the identification of the metasomatic fluid that formed amphibole as well as the process that was initially involved (reaction or direct crystallization). Then, the amphibole-clinopyroxene thermometer can be used to estimate the temperature of equilibration. This thermometer should only be used for amphiboles falling in the compositional range of the calibrant dataset (see Chapter 4). It is pointed out that the amphibole-clinopyroxene thermometer does not yield magmatic temperatures as it is exclusively calibrated based on equilibrium ultramafic experiments. Therefore, a single amphibole-clinopyroxene temperature might not be as useful. It is proposed that the amphibole-clinopyroxene temperatures should be compared to other thermometric methods (e.g. two-pyroxene, garnet-clinopyroxene etc.). If the thermometric results from the two methods yield comparable temperatures then it is highly expected that amphibole is in equilibrium with the pyroxenes. In future work, it would be very useful to experimentally derive the diffusion rates of cation species in the crystal structure of amphibole depending on temperature. We could then compare the diffusivities of cations such as Mg and Fe^{+2} in amphibole with other mineral phases (e.g. pyroxenes). These data could be valuable to interpret amphibole-clinopyroxene temperatures more thoroughly.

The previously mentioned methods have been applied to amphiboles in ultramafic from different geotectonic settings. Amphibole equilibrium has been located in a wide variety of localities from multiple geotectonic settings but mostly in continental-rift related settings. On the other hand, amphiboles in Alpine-type peridotites seem to be governed by a large degree of disequilibrium. Moreover, the presently proposed three-dimensional diagrams seem to confirm studies which are based on trace-element analyses or other techniques. Strikingly, the three-dimensional diagrams showed that amphiboles in ophiolitic chromitites are almost exclusively related to a fluid phase. This is a point which is greatly supported by recent experimental work and shows that chromitites can indeed be formed in chemically open, fluid-rich systems. The results of the present work show that the three-dimensional diagrams are an extremely simple and efficient tool which can be used to predict the formation of amphibole in ultramafic rocks with great detail.

References

1. Adam J., Green T.H., 1994, The effects of pressure and temperature on the partitioning of Ti, Sr and REE between amphibole, clinopyroxene and basanitic melts, Chemical Geology, vol. 117, pp. 219-233.

2. Adam J., Green T.H., Sie S.H., Ryan C.R., 1997, Trace element partitioning between aqueous fluids, silicate melts and minerals, European Journal of Mineralogy, vol. 9, pp. 569-584.
3. Adam J., Locmelis M., Afonso J.C., Rushmer T., Fiorentini M.L., 2014, The capacity of hydrous fluids to transport and fractionate incompatible elements and metals within the Earth's mantle, Geochemistry, Geophysics, Geosystems, vol. 15, pp. 2241-2253.
4. Agrinier P. Mével C., Bosch D., Javoy M., 1993, Metasomatic hydrous fluids in amphibole peridotites from Zabargad Island (Red Sea), Earth and Planetary Science Letters, vol. 120, pp. 187-205.
5. Albers E., Schroeder T., Bach W., 2019, Melt Impregnation of Mantle Peridotite Facilitates High-Temperature Hydration and Mechanical Weakening: Implications for Oceanic Detachment Faults, Geochemistry, Geophysics, Geosystems, vol. 20, pp. 84-108.
6. Arai S., Miura M., 2016, Formation and modification of chromitites in the mantle, Lithos, vol. 264, pp. 277-295.
7. Audétat A., Keppler H., 2005, Solubility of rutile in subduction zone fluids, as determined by experiments in the hydrothermal diamond anvil cell, Earth and Planetary Science Letters, vol. 232, pp. 393-402.
8. Ayers J.C., Dittmer S.K., Layne G.D., 1997, Partitioning of elements between peridotite and H_2O at 2.0-3.0 GPa and 900-1100°C, and application to models of subduction zone processes, Earth and Planetary Science Letters, vol. 150, pp. 381-398.
9. Beard A.D., Downes H., Mason P.R.D., Vetrin V.R., 2007, Depletion and enrichment processes in the lithospheric mantle beneath the Kola Peninsula (Russia): Evidence from spinel lherzolite and wehrlite xenoliths, Lithos, vol. 94, pp. 1-24.
10. Bénard A., Müntener O., Pilet S., Arculus R.J., Nebel O., 2021, Silica-ricj spinel harzburgite residues formed by fractional hybridization-melting of the intra-oceanic supra-subduction zone mantle: New evidence from TUBAF seamount peridotites, Geochimica et Cosmochimica Acta, vol. 293, pp. 477-506.
11. Ben Othman D., Tilton G.R., Menzies M., 1990, Pb, Nd, Sr isotopic investigations of kaersutite and clinopyroxene from ultramafic nodules and their host basalts: The nature of the subcontinental mantle, Geochimica et Cosmochimica Acta, vol. 54, pp. 3449-3460.
12. Bonechi B., Perinelli C., Gaeta M., Tecchiato V., Fabbrizio A., 2020, Amphibole growth from a primitive alkaline basalt at 0.8 GPa: Time-dependent compositional evolution, growth rate and competition with clinopyroxene, Lithos, 354-355, 105272.
13. Borisova A.Y., Ceuleneer G., Kamenetsky V.S., Arai S., Béjina F., Abily B., Bindeman I.N., Polvé M., De Parseval P., Aigouy T., Pokrovski G.S., 2012, A New View on the Petrogenesis of the Oman Ophiolite Chromitites from Microanalyses of Chromite-hosted Inclusions, vol. 53, pp. 2411-2440.
14. Cannao E., Tiepolo M., Borghini G., Langone A., Fumagalli P., 2022, The influence of oxygen fugacity and chlorine on amphibole-liquid trace element partitioning at upper-mantle conditions, European Journal of Mineralogy, vol. 34, pp. 35-57.
15. Carlson R.W., Walker D., Black R., Glazner A., Farmer L., Grossman J., 2001, NAVDAT: A western North American volcanic and intrusive rock geochemical database, Geological Society of America Abstract Programs, vol. 33, pp. 175.
16. Czertowicz T.A., Scott J.M., Waight T.E., Palin J.M., Van der Meer Q.H.A., LeRoux P., Münker C., Piazolo S., 2016, The Anita Peridotite, New Zealand: Ultra-depletion and Subtle Enrichment in Sub-arc Mantle, Journal of Petrology, vol. 57, pp. 717-750
17. DIGIS Team, 2022, "2022-09-2JETOA_BASALT_part1.csv", GEOROC Compilation: Rock Types, https://doi.org/10.25625/2JETOA/RCWTHS, GRO.data, V4.
18. DIGIS Team, 2022, "2022-09-2JETOA_ANDESITE_part1.csv", GEOROC Compilation: Rock Types, https://doi.org/10.25625/2JETOA/UTZUYB, GRO.data, V4.

19. DIGIS TEAM, 2022, "2022-09-2JETOA_LHERZOLITE.CSV", GEOROC COMPILATION: ROCK TYPES, HTTPS://DOI.ORG/10.25625/2JETOA/EUVQ7D, GRO.DATA, V4.
20. El Atrassi F., Chazot G., Brunet F., Chopin C., Bouybaouene M., 2014, Amphibole genesis in pyroxenites from the Beni Bousera peridotite massif (Rif, Morocco): Evidence for two different metasomatic episodes, Lithos, vol. 208-209, pp. 67-80.
21. Ernst W.G., Liu J., 1998, Experimental phase-equilibrium study of Al- and Ti-contents of calci amphibole in MORB- A semiquantitative thermobarometer, American Mineralogist, vol. 83, pp. 952-969.
22. Holtz F., Sato H., Lewis J., Behrens H., Nakada S., 2005, Experimental Petrology of the 1991-1995 Unzen Dacite, Japan. Part I: Phase Relations, Phase Composition and Pre-eruptive Conditions, Journal of Petrology, vol. 46, pp. 319-337.
23. Costa F., Scaillet B., Pichavant M., 2004, Petrological and Experimental Constraints on the Pre-eruption Conditions of Holocene Dacite from Volcan San Pedro (36°C, Chilean Andes) and the importance of Sulphur in Silicic Subduction-related Magmas, Journal of Petrology, vol. 45, pp. 855-881.
24. Cox S.J.D., Richard S.M., 2005, A formal model for the geologic time scale and global stratotype section and point, compatible with geospatial information transfer standards, Geosphere, vol. 1, pp. 119-137.
25. Fabriès J., Bodinier J.-L., Dupuy C., Lorand J.-P., Benkerrou C., 1989, Evidence for Modal Metasomatism in the Orogenic Spinel Lherzolite Body from Caussou (Northeastern Pyrenees, France), Journal of Petrology, vol. 30, pp. 199-228.
26. Faccini B., Rizzo A.L., Bonadiman C., Ntaflos T., Seghedi I., Grégoire M., Ferretti G., Coltorti M., 2020, Subduction-related melt refertlisation and alkaline metasomatism in the Eastern Transylvanian Basin lithospheric mantle: Evidence from mineral chemistry and noble gases in fluid inclusions, Lithos, vol. 364-365, 105516.
27. Feig S.T., Koepke J., Snow J., 2006, Effect of water on tholeiitic basalt phase equilibria: an experimental study under oxidizing conditions, Contributions to Mineralogy and Petrology, vol. 152, pp. 611-638.
28. Ferrari E., Montanini A., Tribuzio R., 2022, Rifting evolution of the lithospheric suncontinental mantle: New insights from the External Ligurian ophiolites (Northern Apennine, Italy), Lithos, vol. 410-411, 106571.
29. Fiorentini M.L., Beresford S.W., Deloule E., Hanski E., Stone W.E., Pearson N.J., 2008, The role of mantle-derived volatiles in the petrogenesis of Palaeoproterozoic ferropicrites in the Pechenga Greenstone Belt, Northwestern Russia: Insights from in-situ microbeam and nanobeam analysis of hydromagmatic amphibole, Earth and Planetary Science Letters, vol. 268, pp. 2-14.
30. Forneris J.F., Holloway J.R., 2003, Phase equilibria in subducting basaltic crust: implications for H_2O release from the slab, Earth and Planetary Science Letters, vol. 214, pp. 187-201.
31. Franz L., Becker K.-P., Kramer W., Herzig P.M., 2002, Metasomatic Mantle Xenoliths from the Bismarck Microplate (Papua New Guinea)-Thermal Evolution, Geochemistry and Extent of Slab-induced Metasomatism, Journal of Petrology, vol. 43, pp. 315-343.
32. Gale A., Dalton C.A., Langmuir C.H., Su Y., Schilling J.-G., 2013, The mean composition of ocean ridge basalts, Geochemistry, Geophysics, Geosystems, vol. 14, pp. 489-518.
33. Hawthorne F.C., Oberti R., Harlow G.E., Maresch W.V., Martin R.F., Schumacher J.C., Welch M.D., 2012, Nomenclature of the amphibole supergroup, American Mineralogist, vol. 97, pp. 2031-2048.
34. Hidas K., Borghini G., Tommasi A., Zanetti A., Rampone E., 2021, Interplay between melt infiltration and deformation in the deep lithospheric mantle (External Liguride ophiolite, North Italy), Lithos, vol. 380-381, 105-855.

35. Hirschmann M.M., Ghiorso M.S., Davis F.A., Gordon S.M., Mukherjee S., Grove T.L., Till C.B., 2008, Library of Experimental Phase Relations (LEPR): A database and Web portal for experimental magmatic phase equilibria data, Geochemistry, Geophysics, Geosystems, 9(3).
36. Ionov D.A., 2010, Petrology of Mantle Wedge Lithosphere: New Data on Supra-Subduction Zone Peridotite Xenoliths from the Andesitic Avacha Volcano, Kamchatka, Journal of Petrology, vol. 51, pp. 327-361.
37. Irving A., Green D.H., 2008, Phase Relationships of Hydrous Alkalic Magmas at High Pressures: Production of Nepheline Hawaiitic to Mugearitic Liquids by Amphibole-Dominated Fractional Crystallization Within the Lithospheric Mantle, Journal of Petrology, vol. 49, pp. 741-756.
38. Janàk, M., Froitzheim N., Vrabec M., Krogh Ravna E.J., De Hoog J.C.M., 2006, Ultrahigh-pressure metamorphism and exhumation of garnet peridotite in Pohorje, Eastern Alps, Journal of Metamorphic Geology, vol. 24, pp. 19-31.
39. Johan Z., Martin R.F. Ettler V., 2017, Fluids are bound to be involved in the formation of ophiolitic chromite deposits, European Journal of Mineralogy, vol. 29, pp. 543-555.
40. Kaeser B., Kalt A., Pettke T., 2007, Crystallization and Breakdown of Metasomatic Phases in Graphite-bearing Peridotite Xenoliths from Marsabit (Kenya), Journal of Petrology, vol. 48, pp. 1725-1760.
41. Keppler H., 1996, Constraints from partitioning experiments on the composition of subduction-zone fluids, Nature, vol. 380, pp. 237-240.
42. King P.L., Hervig R.L. Holloway J.R., Vennemann T.W., Righter K., 1999, Oxy-substitution and dehydrogenation in mantle-derived amphibole megacrysts, Geochimica et Cosmochimica Acta, vol. 63, pp. 3636-3651.
43. Klein M., Stosch H.-G., Seck H.A., 1997, Partitioning of high field-strength and rare-earth elements between amphibole and quartz-dioritic to tonalitic melts: an experimental study, Chemical Geology, vol. 138, pp. 257-271.
44. Kodolányi J., Pettke T., Spandler C., Kamber B.S., Gméling K., 2012, Geochemistry of Ocean Floor and Fore-arc Serpentinites: Constraints on the Ultramafic Input to Subduction Zones, Journal of Petrology, vol. 53, pp. 235-270.
45. Kostopoulos D., 1989, Geochemistry, Petrogenesis and Tectonic Setting of the Pindos Ophiolite, NW Greece, University of Newcastle-upon-Tyne, England
46. Lehnert K., Su Y., Langmuir C.H., Sarbas B., Nohl U., 2000, A global geochemical database structure for rocks, Geochemistry, Geophysics, Geosystems, 1(5).
47. Lehnert K., Goldstein S., Johansson A., Murray R.W., Pisais N., Vinayagamoorthy S., Djapic B., 2007, SedDB-A new information system to facilitate use of marine sediment geochemistry in science and education, MARGINS Newsl., vol. 18, pp. 9-11.
48. Liptai N., Patkó L., Kovács I.J., Hidas K., Pintér Z., Jeffries T., Zajacz Z., O'Reilly S.Y., Griffin W.L., Pearson N.J., Szabó C., 2017, Multiple Metasomatism beneath the Nógrád-Gömör Volcanic Field (Northern Pannonian Basin) Revealed by Upper Mantle Peridotite Xenoliths, Journal of Petrology, vol. 58- pp. 1107-1144.
49. Locock A.J., 2014, An Excel spreadsheet to classify chemical analyses of amphiboles following the IMA 2012 recommendations, Computers & Geosciences, vol. 62, pp. 1-11.
50. Manning C.E., Frezzotti M.L., 2020, Subduction-Zone Fluids, Elements, vol. 16, pp. 395-400.
51. Matveev S., Ballhaus C., 2002, Role of water in the origin of podiform chromitite deposits, Earth and Planetary Science Letters, vol. 203, pp. 235-243.
52. Maurice A.E., Azer M.K., Asimow P.D., Basta F.F., Helmy H.H., Shibata T., 2021, The Kabr el-Bonaya peridotites, southeastern Sinai, Egypt: Petrology, Geochemistry, and metamorphism of Neoproterozoic arc ultramafic cumulates, American Journal of Science, vol. 321, pp. 1445-1496.
53. McGuire V., Dyar M.D., Nielson E., 1991, Metasomatic oxidation of upper mantle peridotite, Contributions to Mineralogy and Petrology, vol. 109, pp. 252-264.

54. Melcher F., Grum W., Simon G., Thalhammer T.V., Stumpfl E.F., 1997, Petrogenesis of the ophiolitic giant chromite deposits of Kempirsai, Kazakhstan: A study of solid and fluid inclusions in chromite, Journal of Petrology, vol. 38, pp. 1419-1458.
55. Neal C.R., 1988, The Origin and Composition of Metasomatic Fluids and Amphiboles beneath Malaita, Solomon Islands, Journal of Petrology, vol. 29, pp. 149-179.
56. Nimis P., Trommsdorff V., 2001, Revised Thermobarometry of Alpe Arami and other Garnet Peridotites from the Central Alps, Journal of Petrology, vol. 42, pp. 103-115.
57. Ohara Y., Ishii T., 1998, Peridotites from the southern Mariana forearc: Heterogeneous fluid supply in mantle wedge, The Island Arc, vol. 7, pp. 541-558.
58. Okamura H., Arai S., Kim Y.-U., 2006, Petrology of forearc peridotite from the Hahajima Seamount, the Izu-Bonin arc, with special reference to chemical characteristics of chromian spinel, Mineralogical Magazine, vol. 70, pp. 15-26.
59. Pan Q.-Q., Xiao Y., Su B.-X., Liu X., Robinson P.T., Uysal I., Zhang P.-F., Sakyi P.A., 2022, Amphibole as a witness of chromitite formation and fluid metasomatism in ophiolites, American Mineralogist, vol. 107, pp. 294-305.
60. Payot B.D., Arai S., Yoshikawa M., Tamura A., Okuno M., Rivera D.J.V., 2018, Mantle Evolution from Ocean to Arc: The Record in Spinel Peridotite Xenoliths in Mt. Pinatubo, Philippines, Minerals, vol. 8, 515.
61. Pearce J.A., Norry M.J., 1979, Petrogenetic Implications of Ti, Zr, Y and Nb Variations in Volcanic Rocks, Contributions to Mineralogy and Petrology, vol. 69, pp. 33-47.
62. Pellegrino L., Malaspina N., Zanchetta S., Langone A., Tumiati S., 2020, High pressure melting of eclogites and metasomatism of garnet peridotites from Monte Duria Area (Central Alps, N Italy): A proxy for melt-rock reaction during subduction, Lithos, vol. 358-359, 105391.
63. Piccardo G.B., Messiga B., Vannucci R., 1988, The Zabargad peridotite-pyroxenite association: petrological constraints on its evolution, Tectonophysics, vol. 150, pp. 135-162.
64. Pichavant M., Martel C., Bourdier J.-L., Scaillet B., 2002, Physical conditions, structure, and dynamics of a zoned magma chamber: Mount Pelée (Martinique, Lesser Antilles Arc), Journal of Geophysical Research, vol. 107, no. B5 2093.
65. Powell W., Zhang M., O'Reilly S.Y., Tiepolo M., 2004, Mantle amphibole trace-element and isotopic signatures trace multiple metasomatic episodes in lithospheric mantle, western Victoria, Australia, Lithos, vol. 75, pp. 141-171.
66. Rollinson H., 2008, The geochemistry of mantle chromitites from the northern part of the Oman ophiolite: inferred parental melt compositions, Contributions to Mineralogy and Petrology, vol. 156, pp. 273-288.
67. Rospabé, M., Ceuleneer G., Benoit M., Kaczmarek M.-A., 2020, Composition gradients in silicate inclusions in chromites from the dunitic mantle-crust transition (Oman ophiolite) reveal high temperature fluid-melt-rock interaction controlled by faulting, Ofioliti, vol. 45, pp. 103-114.
68. Sen A., Snow J.E., Ohara Y., Hirauchi L., Kouketsu Y., Sanfilippo A., Basch V., Harigane Y., Fujii M., Okino M., Akizawa N., 2022, Melting and evolution of amphibole-rich back-arc abyssal peridotites at the Mado Megamullion, Shikoku Basin, Geochemistry, Geophysics, Geosystems, vol. 22, Issue 12.
69. Scambelluri M., Pettke T., Rampone E., Godard M., Reusser E., 2014, Petrology and Trace Element Budgets of High-pressure Peridotites Indicate Subduction Dehydration of Serpentinized Mantle (Cima di Gagnone, Central Alps, Switzerland), Journal of Petrology, vol. 55, pp. 459-498.
70. Seyler M., Mattson P.H., 1989, Petrology and thermal evolution of the Tinaquilo peridotite (Venezuela), Journal of Geophysical Research, vol. 94, pp. 7629-7660.
71. Shaw C.S.J., Eyzaguirre J., Fryer B., Gagnon J., 2005, Regional Variations in the Mineralogy of Metasomatic Assemblages in Mantle Xenoliths from the West Eifel Volcanic Field, Germany, vol. 46, pp. 945-972.

72. Shaw C.S.J., 2009, Textural development of amphibole during breakdown reactions in a synthetic peridotite, Lithos, vol. 110, pp. 215-228.
73. Shramm B., Jochum K.P., Sarbas B., Nohl U., 2006, GEOROC and GeoReM-Linking the information of two geological databases, Geochimica et Cosmochimica Acta, suppl., vol. 70, A565.
74. Shu Y., Nielsen S.G., Le Roux V., Wörner G., Blusztajn J., Auro M., 2022, Sources of dehydration fluids underneath the Kamchatka arc, Nature Communications, vol. 13, 4467.
75. Siegrist M., Yogodzinski G., Bizimis M., Fournelle J., Churikova T., Dektor C., Mobley R., 2019, Fragments of Metasomatized Forearc: Origin and Implications of Mafic and Ultramafic Xenoliths From Kharchinsky Volcano, Kamchatka, Geochemistry, Geophysics, Geosystems, vol. 20, pp. 4426-4456.
76. Tamura A., Arai S., Ishimaru S., Andal E.S., 2008, Petrology and geochemistry of peridotites from IODP Site U1309 at Atlantis Massif, MAR 30°N: micro- and macro-scale melt penetrations into peridotites, Contributions in Mineralogy and Petrology, vol. 155, pp. 491-509.
77. Tamura A., Morishita T., Ishimaru S., Arai S., 2014, Geochemistry of spinel-hosted amphibole inclusions in abyssal peridotite: insight into secondary melt formation in melt-peridotite reaction, 2014, Contributions in Mineralogy and Petrology, vol. 167, 974.
78. Tatsumoto M., Basu A.R., Wankang H., Junwen W., Guanghong X., 1992, Sr, Nd and Pb isotopes of ultramafic xenoliths in volcanic rocks of Eastern China: enriched components EMI and EMII in subcontinental lithosphere, Earth and Planetary Science Letters, vol. 113, pp. 107-128.
79. Tiepolo M., Oberti R., Zanetti A., 2007, Trace-Element Partitioning Between Amphibole and Silicate Melt, Reviews in Mineralogy & Geochemistry, vol. 67, pp. 417-452.
80. Vrabec M., 2010, Garnet peridotites from Pohorje: Petrography, geothermobarometry and metamorphic evolution, Geologija, vol. 53/1, pp. 21-36.
81. Wang C., Liang Y., Xu W., 2021, Formation of Amphibole-Bearing Peridotite and Amphibole-Bearing Pyroxenite Through Hydrous Melt-Peridotite Reaction and In Situ Crystallization: An experimental Study, Journal of Geophysical Research: Solid Earth, vol. 126, e2020JB019382.
82. Wilshire H.G., Shervais J.W., 1975, Al-augite and Cr-diopside ultramafic xenoliths in basaltic rocks from western United States, Physics and Chemistry of the Earth, First International Conference on Kimberlites, Cape Town, 1975, pp. 257-272.
83. Wilshire H.G., Meyer C.E., Nakata J.K., Calk L.C., Shervais J.W., Nielson J.E., Schwarzman E.C., 1988, Mafic and ultramafic xenoliths from volcanic rocks of the western United States: U.S. Geological Survey Professional Paper, vol. 1443 pp. 179-576.
84. Witt-Eickschen G., Harte B., 1994, Distribution of trace elements between amphibole and clinopyroxene from mantle peridotites of the Eifel (western Germany): An ion-microprobe study, Chemical Geology, vol. 117, pp. 235-250.
85. Yoshikawa M., Tamura A., Arai S., Kawamoto T., Payot B.D., Rivera D.J., Bariso E.B., Mirabueno M.H.T., Okuno M., Kobayashi T., 2016, Aqueous fluids and sedimentary melts as agents for mantle wedge metasomatism, as inferred from peridotite xenoliths at Pinatubo and Iraya volcanoes, Luzon Arc, Philippines, Lithos, vol. 262, pp. 355-368.